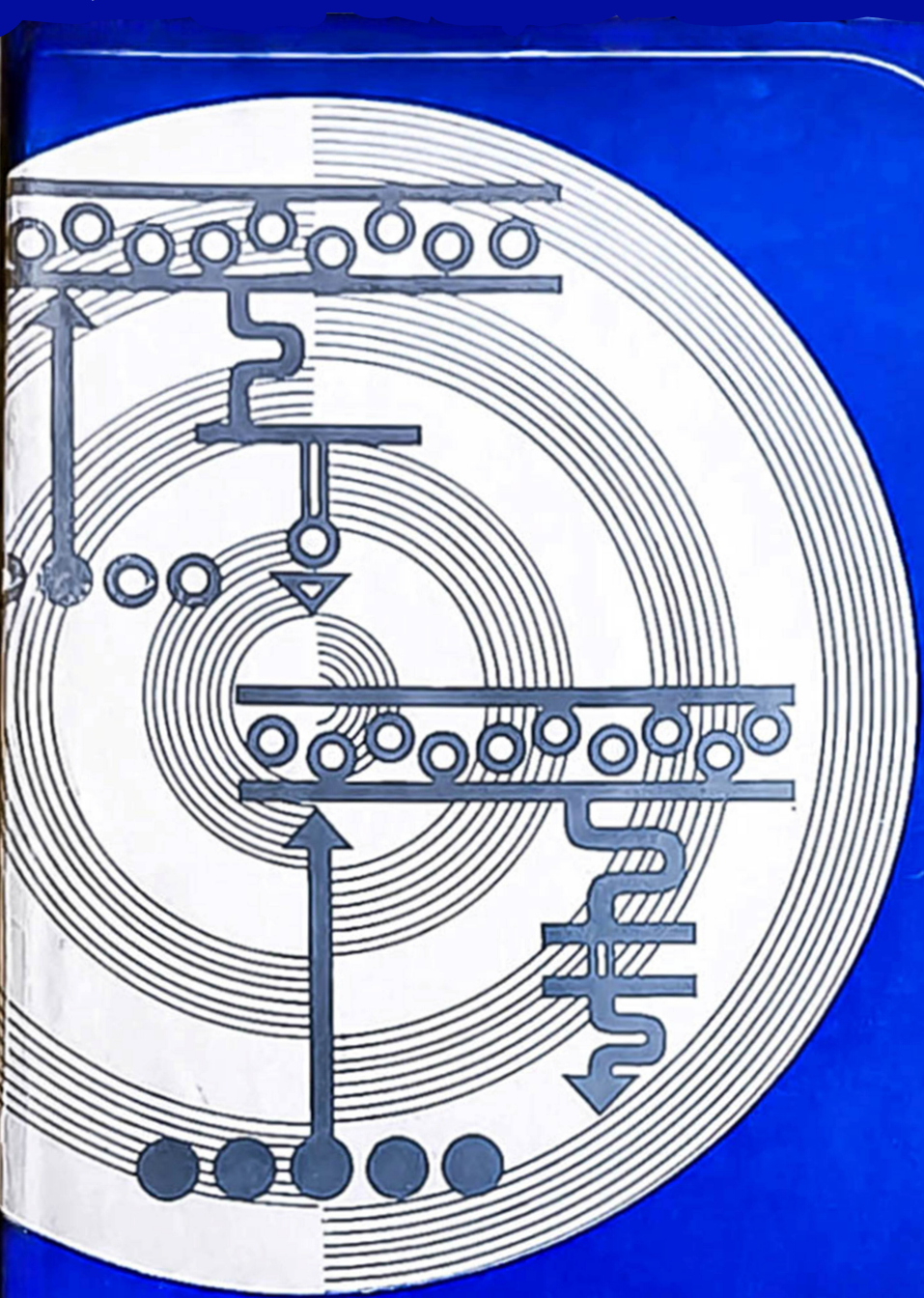

Yu. LYUBAVSKY
V. OVCHINNIKOV

SOLID-STATE LASER TECHNOLOGY

MIR PUBLISHERS

Yu. LYUBAVSKY
V. OVCHINNIKOV

SOLID-STATE LASER TECHNOLOGY

Yu. LYUBAVSKY
V. OVCHINNIKOV

SOLID-STATE LASER TECHNOLOGY

ИЗДАТЕЛЬСТВО МИР

Ю. В. ЛЮБАВСКИЙ, В. М ОВЧИННИКОВ

ТВЕРДОТЕЛЬНЫЕ ЛАЗЕРЫ

Под редакцией академика *А. М. Прохорова*

МОСКВА

Yu. LYUBAVSKY, V. OVCHINNIKOV

SOLID-STATE LASER TECHNOLOGY

Translated from the Russian
by Boris KUZNETSOV

MIR PUBLISHERS
MOSCOW

First published 1975
Revised from the 1972 Russian edition

The Greek Alphabet

Αα	Alpha	Ιι	Iota	Ρρ	Rho
Ββ	Beta	Κκ	Kappa	Σσ	Sigma
Γγ	Gamma	Λλ	Lambda	Ττ	Tau
Δδ	Delta	Μμ	Mu	Υυ	Upsilon
Εε	Epsilon	Νν	Nu	Φφ	Phi
Ζζ	Zeta	Ξξ	Xi	Χχ	Chi
Ηη	Eta	Οο	Omicron	Ψψ	Psi
Θϑθ	Theta	Ππ	Pi	Ωω	Omega

TO THE READER

Mir Publishers welcome your comments on the content, translation, and design of the book.

We would also be pleased to receive any suggestions you care to make about our future publications.

Our address is:

USSR, 129820, Moscow, I-110, GSP, Pervy Rizhsky Pereulok, 2, Mir Publishers

На английском языке

© *English translation, Mir Publishers, 1975*

CONTENTS

Editor's Foreword 6
Preface 8
Notation 9
Introduction. Principles of Laser Engineering 11

Chapter One. OPTICAL ELEMENTS OF LASERS 19
1.1. Laser Pumps 19
1.2. Laser Rods 34
1.3. Optical Elements 43
1.4. Laser Optical Cavities 54
1.5. Optico-Mechanical Shutters 72
1.6. Phototropic Shutters 79
1.7. Electro-Optic Shutters 90
1.8. Controlled Electro-Optic Reflectors 105
1.9. Electrically Exploded Film Shutters 112
1.10. Optical Isolators 115

Chapter Two. OPTICAL SYSTEMS OF PULSED LASER OSCILLATORS 120
2.1. Systems Using Optico-Mechanical Shutters 120
2.2. Systems Using Phototropic Shutters 126
2.3. Electro-Optic Control of the Laser Cavity 132
2.4. Optical Systems Using Electrically Exploded Film Shutters . . . 140
2.5. Mode Selection Systems 141
2.6. Laser Amplifiers 150
2.7. Optical Systems for Second-Harmonic Generation 162
2.8. Alignment of Optical Systems 171

Chapter Three. ELECTRICAL COMPONENTS OF LASER OSCILLATORS 181
3.1. Optical Pumping Tubes 181
3.2. Energy Storage Circuits 188
3.3. Pulsed Power Supply 191
3.4. Flash Tube Trigger Circuit 194
3.5. High-Voltage Pulse Generator 198

Chapter Four. LASER INSTABILITIES AND DISTORTIONS 200
4.1. Thermal Processes in Optical Elements 200
4.2 Optical Distortions in Laser Components 211
4.3. Propagation of Laser Light in a Medium with a Nonuniform Distribution of Refractive Index 218
4.4. Measurement of Thermal Distortions in Laser Elements 226
4.5. Correction of Laser Light Distortions 235
4.6. Temperature Stability of Laser Oscillators 246

References 262
Index 279

EDITOR'S FOREWORD

Since the announcement of the first laser, quite a number of books have appeared, describing lasers to a different degree of sophistication. Among them have been thorough monographs on specialized topics, text-books, and popular publications. In all of them, main emphasis is placed on the physical aspects of the laser (the materials used for lasing action, population inversion, mode generation, kinetics of the lasing action, dependence of laser emission on operating conditions, principles of laser light amplification and conversion, etc.). Little, if at all, has been done to examine the engineering aspects of laser technology. Yet, these aspects deserve an all-round and deep examination in view of the growing field of application for quantum electronics.

Research and industrial centres have accumulated a wealth of experience in the development of a multitude of laser components, circuits and systems. Pooling this experience on a systematic basis will undoubtedly promote the selection and dissemination of the most attractive designs and configurations. This book is in effect the first attempt to do this with special reference to solid-state (crystal and glass) lasers. It is a fact that precisely these types of lasers have been widely employed in research and practical applications owing to their high power output over a wide range of pulse durations. No attempt is made to take up other types of lasers (liquid, gas, semiconductor, etc.), since each may be the subject of a separate discussion.

The reader will find a fairly complete coverage of practical components for both laser oscillators and amplifiers. Separate sections are devoted to the use of these components for the generation of laser emission having specific characteristics (milli-, nano-, and picosecond pulses, single-mode emission, etc.).

No doubt, the book will be useful in the development of lasers in industry, and also in experimental applications in the laboratory.

November 1973

A. Prokhorov Academician
Lenin and Nobel Prize winner

PREFACE

This book covers the engineering aspects of optical quantum generators, or lasers.

Engineering data accumulated to date on this subject may be useful to a large number of workers concerned with the development and application of lasers. The authors are aware that the book does not cover all the problems encountered in laser engineering in their entirety.

Main emphasis is placed on the present state of the art as regards solid-state pulsed lasers. The material has been gathered from special journals and from the authors' own work in the field.

Chapters 1 and 2 discuss laser components and optical systems. Chapter 3 describes the electric circuits supporting operation of the optical elements. Chapter 4 covers instabilities in laser operation and laser beam distortions caused by the interaction of laser components with laser output emission and pump light.

Chapters 1 and 2 have been written by V. Ovchinnikov (Introduction, Sections 1.4, 1.6-1.10, 2.2-2.7) and Yu. Lyubavsky (Sections 1.1-1.3, 2.1, 2.8). Chapter 3 has been written by V. Ovchinnikov.

Chapter 4 has been written by A. Bugayev and V. Ovchinnikov.

The authors wish to express their gratitude to A. Prokhorov for his constant support in and consideration for their work on the book. The authors feel it their duty to thank A. Manenkov who read the manuscript and made valuable suggestions which were incorporated in the final draft. The authors are sincerely thankful to V. Korobkin, P. Pashinin, V. Fedorov, G. Shipulo, Ye. Dianov, M. Stelmakh and V. Dmitriyev for their reviews.

NOTATION

C = capacitance
d = specific heat
E = electric field strength, electric intensity
F = number of photons per pulse, passing through unit section
H = magnetic field strength, magnetic intensity
L = laser cavity length
M = magnification of an optical system
n = refractive index; relative population inversion
n_o, n_e = refractive indexes of the ordinary and extraordinary waves
N_1, N_2 = population density of the 1st and 2nd levels
N_0 = active centre density
N_F = Fresnel number
P_k = polarization vector components
P = pressure; emission power
r = coefficient of refraction
R_t = tube resistance
T = temperature; transmission of an optical system
t_p = pulse duration
t_d = delay time
t_{cav} = photon lifetime in the cavity
t_1 = photon transit time through the cavity
V = voltage; volume
α_T = coefficient of heat exchange
α_0 = absorption coefficient at the maximum of the fluorescence line
β = phase shift
ε = permittivity, dielectric constant
E = emission energy
E_p = pump energy

E_S = emission energy surface density
η = efficiency
θ_{match} = phase-matching angle
Θ = dimensionless temperature
Λ = number of flash tubes
λ = wavelength
ν = frequency
Π = polarizability
ρ = density of a material; non-saturable (lump) loss coefficient
ρ_t = tube resistivity
σ = absorption cross-section
τ = relaxation time
φ = relative photon density

INTRODUCTION

PRINCIPLES OF LASER ENGINEERING

Physical basis of laser engineering. The physical basis of optical-quantum generators, or lasers, is the amplification of light by stimulated emission of radiation. In systems in a state of thermal equilibrium, stimulated absorption of light is predominant, because lower-energy states are more numerous. For stimulated emission of radiation to be predominant, the thermal equilibrium should be shifted so that there will be more higher-energy than lower-energy states. Then the electromagnetic field will cause excited active centres (which may be atoms, ions, excitons, or molecules) to jump from the higher to the lower energy states, and in the ensuing interaction with the atomic systems the radiation will gain in intensity, provided the number of excited energy states is sufficient for the emission of quanta to exceed their absorption. The difference in density between the excited and ground states of an amplifying medium (the population inversion density, or the population inversion, or the inverted population) is the key factor deciding whether the amplification or generation of light by stimulated emission of radiation is possible at all.

Population inversion can be obtained in several ways. In solid-state lasers (those using crystals or glass), the active atoms are usually excited by optical pumping, that is, by exposing the material to high-intensity light. Optical pumping causes the material to absorb energy with the result that the atoms are raised to excited energy states and undergo radiative or non-radiative transitions to produce the desired population inversion. The materials having absorbing centres with an appropriate set of discrete energy levels suitable for population inversion are called active media.

A laser is a source of self-sustained vibrations which are due to electromagnetic-field oscillators. These oscillators may be the natural modes of the electromagnetic field contained between the mirrors of an optical cavity or resonator, having the shape of three-dimensional standing waves (the cavity or resonator modes). The active centres located at the loops of a mode lose their excitation at the highest rate as they interact with the photons of that mode and jump to a lower level. Conversely, the centres located at the nodes undergo no stimulated transitions in the field of the

mode. However, the nodes of one mode may be located at the loops of others. Therefore, a self-sustained energy source in a solid-state laser maintains modes according to their spatial field distribution. This explains why lasers can oscillate in many modes to the detriment of beam coherence and angular spread. The coherence and angular spread of the laser beam are improved by selecting the dominant mode during the lasing action.

Many of the most important characteristics of the laser beam (duration and intensity of light pulses, distribution of radiation in space, etc.) depend on the kinetics of the lasing action in the cavity. It affects both the rise in the intensity of the individual modes and their coupling. Therefore, varying electromagnetic losses in the laser cavity, one can control the lasing action. Methods of loss control widely differ, depending on the space and time characteristics sought in the output laser light.

For example, in the generation of nanosecond light pulses, it is usual to spoil the Q-factor of the cavity (Q-spoiling or Q-switching) so that the lasing action is held off as long as optical pumping continues and until a considerable inversion of the appropriate energy levels is built up. When the population inversion is a maximum, the cavity Q is suddenly switched to a high value, and a very strong laser pulse with a duration of about 10 ns is coupled out. A different example is offered by laser systems which emit a spectrum of closely spaced frequencies. In such cases, the output laser pulse depends on the amplitudes and phases of the individual modes. If nothing is done to keep them in a proper relationship, random fluctuations and non-linearities might produce all kinds of changes in the laser beam with time. If, on the other hand, the frequency spacing and phase relationships between adjacent modes are properly maintained, the output laser pulse will change in time in a precisely predictable manner. This is called mode locking. In the general case, the shape of the output laser beam will depend on the modes utilized and also on the phase relations between them.

Thus, from an engineering point of view, designing a workable laser reduces to obtaining a population inversion, controlling the modes, and guiding energy transfer between the laser material and the electromagnetic emission from the laser cavity.

Existing lasers have limited capabilities as regards the generation of high-power pulses or the control of the laser beam frequency spectrum. High-power pulses can be obtained by boosting the laser beam in a laser amplifier. Laser amplifiers may use either a simple population-inversion medium or a modified laser oscillator operating below the lasing-action threshold. The frequency control of the laser beam (modulation, demodulation, tuning, etc.) involves the use of various processes of non-linear optics, notably

Raman scattering, second-harmonic generation (SHG), and parametric phenomena.

Practical methods used to engineer laser oscillators and amplifiers, and means for laser spectrum control constitute the subject-matter of laser engineering. Since these matters can be tackled from widely different angles for different types of lasers, the subsequent discussion will be limited to solid-state lasers adopted for a variety of laboratory applications. Specifications for this class of instruments are mainly decided by the requirements of a particular application. These requirements also influence the design of the elements, assemblies and circuits intended to obtain population inversion, to control modes, lasing action, and beam emission, and also to amplify, modulate or demodulate the laser beam.

Population inversion in solid-state lasers is obtained by optically pumping the laser material with a gas-discharge flash tube. The light produced by the flash tube is concentrated onto the laser rod by the chamber enclosing the pumping system, or simply the pump. Flash tubes are energized by banks of storage capacitors charged from a.c. mains via step-up transformers and rectifiers. Optical pumping is started (that is, the flash tube is caused to fire) by a suitable trigger circuit. The actual configuration of supply circuits for flash tubes depends to a great extent on the energy storage required and the repetition frequency of firing cycles. A specific feature of all supply circuits for flash tubes is the use of high-voltage capacitors, semiconductor devices, relays and other components designed for heavy-current pulses.

The key element in the conversion of electrical energy into the energy of excited atoms is the laser rod. Although a population inversion can be obtained in a great number of solid-state materials, the most frequently used ones at present are ruby, neodymium-doped glass, yttrium-aluminium garnet, and dysprosium-doped fluorite. Other active materials are not practically used because of lack of know-how or low efficiency.

Optical pumping to obtain a population inversion is accompanied by the liberation of a large amount of heat in the laser rod. Since the physical characteristics of the laser rod depend sensitively on temperature, it is important to abstract the heat it generates during optical pumping by a cooling system. For the class of lasers discussed in this book only liquid cooling systems are of practical interest.

Mode control. A variety of open optical cavities or resonators are used to shape the laser beam. Each type has merits of its own and each may serve as the basis for the optical system of a laser. Apart from the end reflectors, the optical system of a laser cavity may comprise different selecting, polarizing, and beam controlling elements. Any inhomogeneities in the material of optical elements,

surface irregularities, or maladjustment might produce distortions in the wave fronts within the optical cavity and in the mode set-up of the output radiation. This is why one cannot overestimate the importance of the quality of materials, the finish of surfaces, and the alignment of cavity elements.

A specific feature of solid-state lasers is the generation of a considerable amount of heat during the lasing action. This heat may bring about changes in the geometry of the laser elements, thermal stresses and distortions, birefringence, etc. Depending on operating conditions and the set-up of the optical system, heat liberation may affect the characteristics of the laser beam in a variety of ways and in an unpredictable manner. One of the major factors that can heavily distort the wave front of the output radiation is abberation due to the non-uniform heating of the laser rod. To maintain the temperature of the laser within the tolerable limits, it is important to cool the optical elements during lasing action or to bring them back to the original temperature before the start of a next lasing cycle. Since these goals cannot always be achieved, it is practically important to determine the actual temperature conditions for the optical elements and their effects on the properties of the laser beam, although this is a difficult problem defying solution in many cases. We still lack correction methods for laser systems which would compensate thermal distortions in optical elements, although it would be feasible in some cases.

Lasing action control. This form of control is mainly accomplished by means of shutters and reflectors. Most often, use is made of optico-mechanical, phototropic (reversibly bleachable) and electro-optic shutters, electrically-exploded and bleachable film shutters, electro-optic and optico-mechanical reflectors. The fact that laser engineering uses multiplicity of shutters and reflectors stems from the simple reason that lasing action control poses a multitude of problems which cannot be successfully solved by a single type of such devices. For example, optico-mechanical Q-switches are used in cases where their inherent time lag is not an obstacle. Piezo-acoustical Q-switches are convenient for high-rate operation. Phototropic (reversibly bleachable) shutters are used not only to switch the Q of the optical cavity, but also to isolate amplifier stages and to select a single mode in the Q-switched lasers. Besides, the non-linear relationship between the transmission of a phototropic (bleachable) shutter and light intensity may be utilized as a means for maintaining proper phase relationship between the individual resonator modes. This property provides a basis for obtaining picosecond light pulses by the mode self-locking method. Phototropic (bleachable) film shutters hold out special promise for the control of large-diameter laser beams. Still more promising are electro-optic shutters and reflectors that will trans-

mit or reflect light in a particular direction, according to the magnitude of the applied voltage; because of this, they can be used as Q-switches. In contrast to the methods described above, these switches can be controlled by an external signal. By using high-frequency light-beam modulation, it is possible to lock the individual resonator modes in phase and to obtain picosecond pulses. Last but not least, the ability of electro-optic devices to control light polarization makes them suitable for control of path-switched laser systems which are of special importance as sources of nanosecond pulses, for coupling nanosecond pulses out of the optical cavity, for control of the output beam, polarization and the like.

For their operation, electro-optic shutters and reflectors require electronic circuits to generate the requisite electric pulses. With Q-switching, the control voltage source is a nanosecond high-voltage pulse generator triggered by an external signal and synchronized with the trigger pulse of the flash tube. The generation of picosecond pulses involves the use of high-rate Q-switches. In some cases, electro-optic shutters may be controlled by nanosecond high-voltage pulse generators triggered by light-controlled spark gaps in which the break-down is brought about by the action of a light pulse. In multi-path optical cavities, the paths are switched by circuits which generate electric pulses of elaborate waveforms.

Electrically exploded film shutters are metal films deposited on a transparent polyethylene film and made transparent by a strong electric pulse. An electrically exploded film shutter is specially convenient in the control of large-diameter beams in cases where the shutter should be opened externally by signals from other devices.

Laser beam amplification. In engineering terms, the construction of a laser amplifier reduces to obtaining a population inversion and to guiding the laser beam through the inverted population. There are several types of laser amplifiers, differing in the size of the amplifying medium and in the method for guiding the laser beam through that medium. Among them are single-pass travelling-wave amplifiers, multipass amplifiers, controlled cavity amplifiers and regenerative amplifiers. Single-pass travelling-wave amplifiers incorporate an extended inverted-population medium through which the laser beam to be amplified is allowed to travel once and in one direction only. In this type of amplifier, the beam has to be expanded as amplification progresses, since otherwise the beam density may reach saturation or even exceed the damage threshold of the laser material. High-gain amplifying media entail a number of difficulties caused by super-fluorescence which depletes the inverted population and gives rise to noise. To avoid superfluorescence, the amplifying medium is distributed between the amplifier stages, each with a relatively low gain, isolated from

one another by shutters. An amplifier stage is a laser rod optically pumped by a flash tube in much the same way as in laser oscillators. In fact, the supply circuits for the flash tubes and the method of cooling the laser rod are the same as those used in laser oscillators. A main distinction of laser amplifiers is the larger size of laser rods. Because of this, use has to be made of special methods for the suppression of super-fluorescence, and this may in turn greatly affect the shape of the active elements, the type of pump cavity, the composition of cooling agent, and some other design features. The beam to be amplified is expanded by a telescopic system. The reflected laser light is suppressed by magneto-optic isolators which pass light in one direction only. The suppression of reflected amplified light prevents the destruction of the laser elements at the amplifier input. In fact, optical isolators may sometimes be necessary in laser oscillators to obtain single-pass travelling-wave operation.

Multi-pass amplifiers make a better use of the laser material than single-pass travelling-wave amplifiers. In them, plane-parallel or curvilinear mirrors cause the beam to take different paths in going through the laser rod in the forward and backward directions. The choice of amplifier stages, shutters and optical isolators poses practically the same problems as with single-pass travelling-wave amplifiers. It is advantageous to use plane-parallel mirrors within the linear region of amplification, while curvilinear mirrors should preferably be employed when amplification approaches the saturation or damage threshold of the laser material, because they expand the beam as it passes through the laser material. Multi-pass amplifiers can do the same jobs as single-pass travelling-wave amplifiers, but with a smaller count of optical elements and with a lower level of pumping energy. The spectrum width of a single pass travelling-wave amplifier and of a multi-pass amplifier is determined by the fluorescence spectrum of the laser material.

Controlled-cavity amplifiers provide maximum amplification for short light pulses with a minimum size of the laser rod. The beam is admitted inside the cavity and allowed to be multiply reflected between the 100% reflecting mirrors of the cavity for amplification, after which the amplified beam is coupled out of the cavity. Controlled-cavity amplifiers are advantageous where light pulses should be boosted to energies below the damage threshold of the cavity elements. The spectrum width is decided by the cavity parameters.

Regenerative amplifiers are remarkable for the small size of the laser rod and for their ability to amplify long pulses or CW emission. The beam to be amplified is guided through the laser material by an optical cavity with semitransparent mirrors. In effect, a regenerative amplifier is a laser oscillator operating below the

threshold energy required for lasing action. Its spectrum width is likewise determined by the cavity parameters.

Laser frequency control. This is based on the utilization of non-linear optical processes (optical frequency multiplication and mixing, parametric frequency conversion, etc.). The manner in which non-linear processes take place is determined by the phase relationships between the interacting electromagnetic fields. In all of these processes, the decisive factor is the dispersion of the medium. The effectiveness with which these processes are applied to lasers is due to the high power, high monochromaticity and negligible divergence of the laser beam.

In practice, the most commonly used method is harmonic generation. More specifically, the second harmonic is generated by causing the laser beam to interact with a non-linear element placed inside the laser cavity. With this arrangement, a major problem is that of separating the primary beam and the second harmonic. When a non-linear element is placed externally to the optical cavity, the need arises to enhance its effectiveness. One approach is to project the laser beam onto the non-linear element by cylindrical optical elements.

A further non-linear process of special value to laser frequency control is parametric oscillations with which the wavelength of the laser beam can be controlled continuously. In this case, too, a non-linear element must be placed inside the optical cavity. The optical cavities used in parametric oscillators do not materially differ from those used in solid-state laser oscillators. The relatively low efficiency of parametric oscillators and a number of difficulties in their manufacture have impeded their wider use in laser engineering. This is why laser frequency control by parametric techniques has not been included in this book.

Another class of non-linear optical processes well investigated and well adapted for laser frequency control includes stimulated Raman scattering (SRS). Raman scattering occurs when light of a particular wavelength passes through a material and is scattered by the molecular fields. When a Raman-active material is placed within an optical cavity and pumped with a laser beam, the result is a stimulated Raman emission at frequencies of the corresponding Raman scattering.

The beam of a Raman laser may be boosted by a Raman amplifier. It should be noted that Raman laser oscillators and amplifiers may well use the same elements and circuits to control lasing action, to guide the laser beam, etc. as conventional solid-state lasers.

Still another class of materials well adapted for laser frequency control are organic dyes. A dye laser optically pumped with a beam from a solid-state laser may emit radiation over a wide con-

tinuous spectrum. Like Raman lasers, dye lasers differ from solid-state lasers only in the manner of obtaining a population inversion.

To extend the range of laser frequency control, use may be made of a combination of optical non-linear processes and optical cavities incorporating dispersive elements. By this arrangement, it is possible to control the frequency of Raman, dye, and solid-state lasers within the spectrum of the generated radiation.

Because of fundamental differences in their physical aspects, Raman and dye lasers lie outside the scope of this book.

Chapter One

Optical Elements of Lasers

1.1. Laser Pumps

In solid-state lasers, a population inversion is obtained by optical pumping with a flash tube or a continuous lamp. For better efficiency, the flash tube and the laser rod are combined in a laser pumping cavity, or simply the pump which is, as a rule, a closed optical system where the light emitted by the flash tube is focused by reflectors onto the laser rod.

The configuration of a pumping cavity is determined by the type of flash tube and laser rod used, their relative position, and operating conditions. In turn, the pump geometry greatly affects the efficiency of light transmission and the distribution of absorbed energy in the laser rod and, through them, the angular spread and energy distribution and level of the resultant laser beam.

In a laser pump, light energy is concentrated in a manner far from ideal. Coupled with the low efficiency with which electrical energy is converted to light (35-50%) [1], and the incomplete utilization of energy absorbed by the laser rod (6-15%) [1], the losses in the laser pump (30-70%) [2] are a major factor determining the low efficiency of solid-state lasers (0.1-5%).

The choice of a laser pump depends on the requirements that the associated laser should meet. For example, in a single-mode laser it is important that the pumping energy be distributed uniformly and symmetrically across the diameter of the laser rod. In other cases, the main criterion is the maximum efficiency of light transfer. In high-output laser systems, use is made of multi-tube pumps which ensure the requisite radiant flux despite the relatively low efficiency. Some of the most commonly used laser pumps are shown in Fig. 1.1.

Laser pumps with condensers and cylindrical laser rods. In [3], a CW laser beam was obtained by using a laser condenser such as shown at I*c* in Fig. 1.1, consisting of a truncated sapphire cone and a laser rod bonded to it. Light from an arc-lamp was directed by a system of mirrors onto the conical part which focused the pumping light into the laser rod. A straight-cone condenser with a sapphire sphere (at I*a* in Fig. 1.1) and a chisel shaped condenser (at I*b* in Fig. 1.1) were also used in CW lasers [4]. The lowest threshold value for lasing action and the more uniform distribution

Tube location relative to laser rod	Pump configuration
Cylindrical laser rod	
I. Tube removed from laser rod	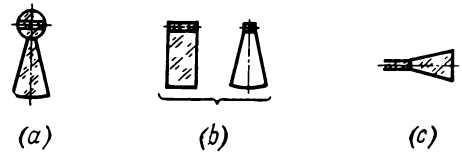 (a) (b) (c)
II. Tube on rod axis	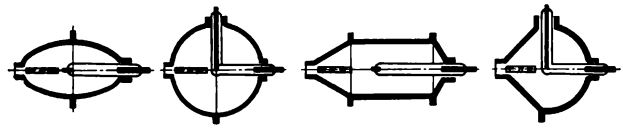 (a) (b) (c) (d)
III. Tube parallel with rod axis	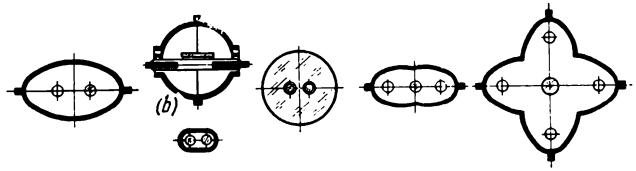 (a) (b) (c) (d) (e) (f)
IV. Tube concentric with laser rod	(a) (b)
Flat laser rod	
V. Tube parallel with rod side	(a) (b)

Continued

Tube location relative to laser rod	Pump configuration
	Laser disc
VI. Tube opposite disc face	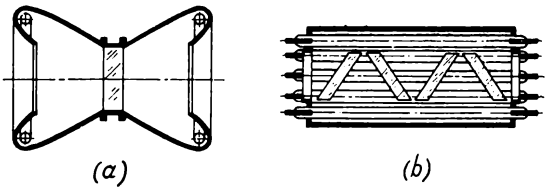 (*a*) (*b*)

Fig. 1.1. Classification of laser pump units

of pumping energy were obtained with the straight-cone laser condenser.

Laser pumps in which the flash tube is arranged along the axis of the laser rod are discussed in [5] through [10]. They distribute the absorbed energy uniformly across the laser rod.

In elliptical laser pumps (at II*a* in Fig. 1.1), the reflecting surfaces are formed by rotating an ellipse about an axis passing through the flash tube and the laser rod. Calculations and experiments have shown that a high efficiency can be obtained by using filamentary flash tubes [5], the efficiency of the laser pump being a maximum when the flash tube and the laser rod are on the major axis of the ellipsoid between its vertex and focus, and the ratio of the rod length to the semi-major axis is close to unity.

The efficiency of a spherical laser pump (at II*b* in Fig. 1.1) is somewhat lower than that of the ellipsoidal one. For a case where the diameter of the flash tube is equal to that of the laser rod and the reflectivity of the walls is 70%, the efficiency of the spherical laser pump is about 56%.

In choosing the relative position of the laser rod and the flash tube, it should be remembered that in spherical pumps with the flash tube and laser rod arranged axially, the threshold value for lasing action is somewhat higher than it is when the two elements are arranged in parallel, while the output energy rises with pumping at a faster rate, as is seen in Fig. 1.2. With the parallel arrangement of the flash tube and the laser rod, the separation between them should be kept to a minimum. Spherical and elliptical pumps may be used in CW lasers [6]. In axicon pumps (at II*c* in Fig. 1.1) and sphericon pumps (at II*d* in Fig. 1.1), light is allowed to pass

the laser rod on several passes before it leaves the system [7 through 11]. Although with an optimal choice of parameters, they may have a light efficiency of about 50%, sphericon pumps have been used on a limited scale because high reflectivity is difficult to secure in this pumping configuration. Axicon laser pumps have a still lower efficiency. It appears that the replacement of metal mirrors with glass mirrors silvered on the outside surface may substantially improve the efficiency of this type of laser pump. Axially symmetrical laser pumps are effective when used in conjunction with relatively short laser rods whose diameter is 1 to

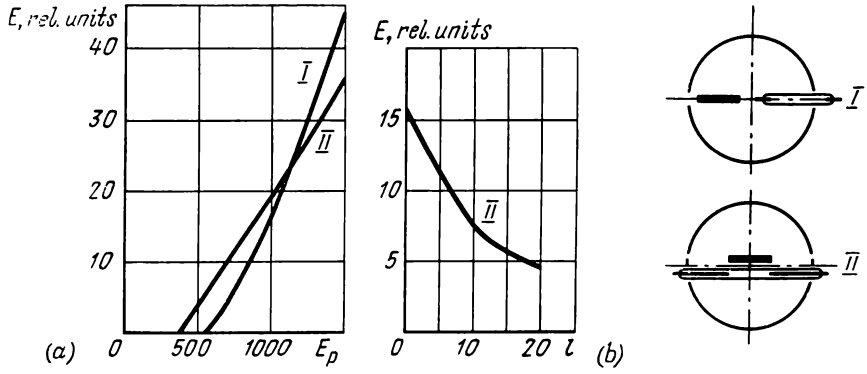

Fig. 1.2. Emission energy, E, as a function of (*a*) pump energy and (*b*) separation between the flash tube and the laser rod for a spherical pump cavity.

1.5 mm greater than that of the flash tube. This type of laser pump may be especially advantageous where the laser rod and the flash tube are cooled by a single stream of coolant in a common axial cooling system (Fig. 1.3).

In solid-state lasers, use is most widely made of pump units in which the flash tube is arranged parallel with the axis of the laser rod, and the reflector is the shape of an elliptical cylinder, with the flash tube and the laser rod placed on its focal axes (as III*a* in Fig. 1.1). Single-lamp elliptical cylinders have a very high efficiency — about 75% [2]. Besides, with them, the flash tube and the laser rod may be cooled separately, and the laser rod is pumped rather uniformly across the diameter, if it is only a fraction of the lateral dimension of the reflector.

When the focal axes of a pump unit are properly aligned (the eccentricity tends to zero), the magnification of an elliptical mirror approaches unity, and the light efficiency tends to 100%. Since, however, an elliptical pump is a variable-magnification system, while the flash tube and the laser rod have finite dimensions, only

a fraction of the flash tube energy is utilized in it. Besides, a considerable proportion of non-absorbed light passing through the rod and multiply reflected from the walls fails to fall upon the rod again because the lateral dimensions of the reflector are many times the diameter of the laser rod. Yet, multiple reflections may improve the efficiency, provided the flash tube is closely wrapped round the laser rod and the two are very close in cross-section (at

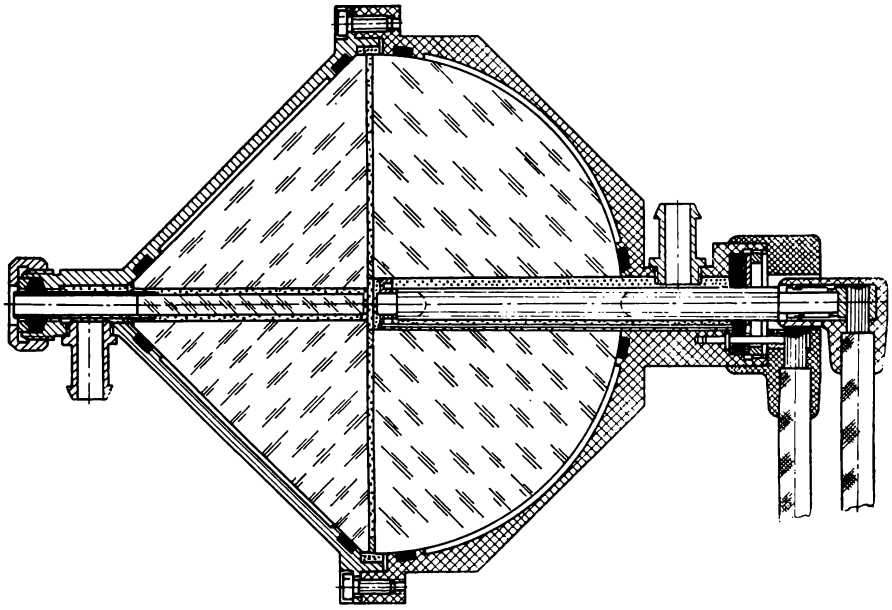

Fig. 1.3. Laser oscillator with a sphericon pump cavity

III*c* in Fig. 1.1). In such cases, the shape of the reflector is immaterial — it may be round or oval, while its internal surface may be regularly or diffusely reflecting. The efficiency of a diffusely reflecting laser pump may be found by the equation $\eta = r_w S_a / S_p$, where η is the efficiency of the laser pump, r_w is the reflectivity of the walls, S_a is the side surface area of the laser rod, and S_p is the surface area of the pump.

Tightly coupled laser pumps show high energy performance, but suffer from a non-uniform distribution of pumping energy across the cross-sectional area of the laser rod.

Cylindrical laser pumps (at III*d* in Fig. 1.1) have a lower light efficiency than elliptical ones, but they are simpler to make. This type of laser pump may be fabricated from glass or quartz tubes chemically silver-plated on the outside.

In high-output lasers, the laser element has the shape of a rod whose diameter exceeds that of the flash tube. In such cases, in order to increase the pumping density, use is made of multiple laser pumps (at III*e* and *f* in Fig. 1.1) in which the reflecting surfaces are the shape of elliptical cylinders. The laser rod is located on the common focal axis, while the flash tubes are arranged at the conjugate focuses. The relative amount of energy striking the laser rod in this case increases with the number of flash tubes, but the total efficiency of the system is reduced. The plots in Fig. 1.4 show that the light intensity within the laser rod increases mainly due to the increase in its cross-sectional area [12]. In some multiple

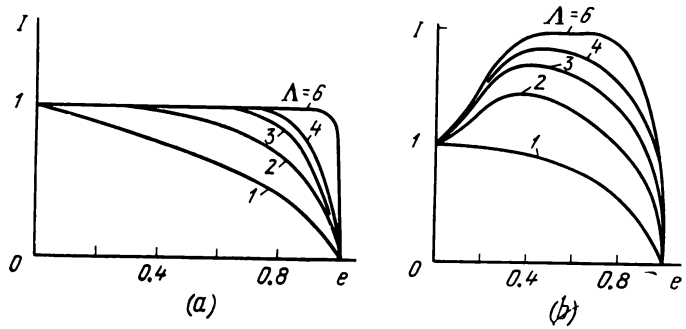

Fig. 1.4. Relative light intensity, *I*, in the laser rod bulk as a function of the eccentricity, *e*, of the ellipse and the number of flash tubes
(*a*) $r_m/r_t=1$; (*b*) $r_w/r_t=2$

laser pumps, the flash tubes are enclosed in glass semicylinders [13]. The optimum number of flash tubes for multiple pumping cavities is given by $\Lambda_{opt} = R_a n/R_t$, where R_a is the radius of the laser rod, R_t is the radius of the flash tube, and n is the refractive index of the medium surrounding the laser rod.

Laser pumping cavities for wide-bore and helical flash tubes (at II*a* and *b* in Fig. 1.1) are enclosures with a heavy coating of magnesium oxide. With wide-bore flash tubes, a coating of magnesium oxide is deposited on the outer surface of the flash tube. Although the light efficiency of wide-bore flash tubes is 30% below that of tubular flash tubes [14], they give a higher overall efficiency in some applications. This is especially true of high-energy pumping where laser rods with a diameter of over 30 mm are employed. At pumping energies under 1000 J, wide-bore flash tubes are less effective than tubular ones.

For laser pumps using wide-bore flash tubes, the threshold energy for lasing action is higher, while the output energy rises with increasing pumping energy at a faster rate than in laser pumps using tubular flash tubes. In choosing the relative dimen-

sions of a laser pump, it should be remembered that the light efficiency of the optical system rises in direct proportion to the ratio R/R_e where R_e is the radius of the enclosure. At the ratio $l_t/R_e > 5$ (l_t is the length of the flash tube) the light efficiency of the optical system changes little with increasing length of the enclosure. Theoretically, the light efficiency of wide-bore flash tubes is evaluated in [15].

Laser pumps with wide-bore flash tubes give the highest concentration and uniform distribution of energy in the laser rod. If the clearance between the laser rod and the flash tube is small and filled with a cooling agent, the light efficiency of this system may be increased and the overall efficiency may be as high as 5% [16]. Wide-bore flash tubes have been used on a limited scale because they have a shorter service life than tubular flash tubes.

Laser pumps for laser rods of rectangular cross-section. In some cases, use is made of laser rods of rectangular cross-section [18, 19]. The dimensions of a rectangular laser rod are chosen to ensure a uniform distribution of pumping energy across its diameter. One such laser pump is shown at V*a* in Fig. 1.1. It may be fabricated from a cylindrical metal or glass tube split along its axis, or from a cylindrical glass block with an opening to accommodate a flash tube. This type of reflector is predominantly used in intermittently fired lasers because it is convenient for the effective cooling of the flash tube. The laser pump shown at V*b* in Fig. 1.1 may be used in high peak-power pulsed laser oscillators and amplifiers.

Disc laser systems. In high-power lasers, the energy output is decided by the ability of the laser materials to stand up to the action of the laser beam. If the active element is to operate for a long time, it is important that the power density be one third to one fourth of the critical power density, that is, one at which the first flash would destroy the rod end face [17]. Light pulses with a greater output energy can be obtained by increasing the cross-sectional area of the active element. With cylindrical rods, however, there is a limit to the increase in the rod diameter because pumping energy tends to be distributed non-uniformly. Besides, it may be undesirable to employ cylindrical laser rods because they are susceptible to thermal stresses. The axial temperature gradient may be reduced and output energy raised without the risk of destroying the end face by using laser disc systems (at VI*b* in Fig. 1.1) [20]. Disc systems provide a promising approach to lasers fired at a high repetition frequency and a high average power. In these laser systems, the discs are face-pumped and tilted at an angle close to the Brewster angle.

In order to minimize the effect of spontaneous fluorescence on population inversion, the cylindrical surface of the disc should have a minimum reflectivity. To keep to a minimum the radiation

reflected from the glass-liquid interface, it is important that the refractive index of the cladding liquid be as close to that of the glass as practicable.

The pump shown at VI*a* in Fig. 1.1 is intended for use in conjunction with laser discs and tubular flash tubes bent in a circle [21].

The flash tubes are installed on each side of the disc in an elliptical tore changing into a truncated cone. With this arrangement,

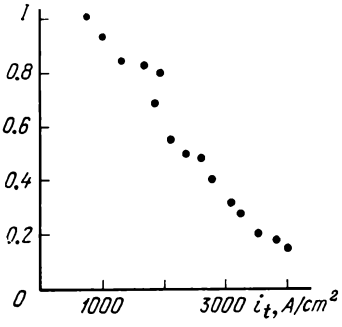

Fig. 1.5. Light intensity (at λ = = 5500 Å) transmitted through 1 cm of the plasma as a function of the current density in the flash tube

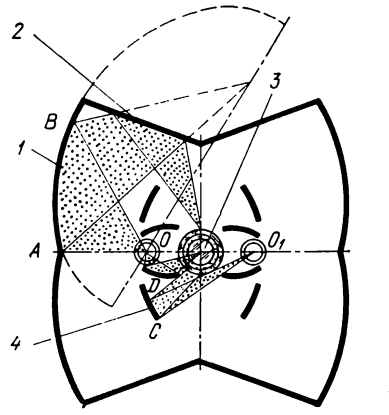

Fig. 1.6. Two-cavity pump unit

the gain of the system can be controlled by installing laser discs in a sort of chain.

The choice of a laser pumping configuration materially depends on the operating conditions of the flash tube. With a pronounced gradient in the discharge, the plasma will absorb a great proportion of its own radiation. A plot relating the opacity of the xenon plasma to the electrical gradient is shown in Fig. 1.5 [22]. On the other hand, in order to raise the brightness temperature, it is necessary to increase the density of the current flowing through the flash tube to a limiting value determined by the strength of the flash tube. This can be done by using a double-pulsed flash tube (see Sec. 4.5). Then the flash tube will operate as a surface radiator, and the laser rod will be illuminated only by those parts of the flash tube that can be seen from the centre of the rod. A type of laser pumping cavity for flash tubes with an increased brightness temperature is shown in Fig. 1.6 [23]. In this pump configuration, all of the flash tube is seen from the centre of the laser rod,

without vignetting. The radiant flux subtending the angle AOB, on being reflected from the elliptical cylinder *1*, by a plane mirror *2*, is directed onto the laser rod *3*. In a double elliptical laser pumping cavity, this part of radiant flux is absorbed by the tube discharge. The cylindrical mirrors *4* throw the radiant flux subtending the angle CO_1D back onto the laser rod.

The type of laser pumping cavity shown in Fig. 1.7 is best adapted for small electrical gradients [24]. In this type of laser pump, part of the radiant flux reflected from the cylinder *1*, passes through the plasma of the flash tube *2*, and, on being reflected from the elliptical cylinder *3*, strikes the laser rod *4*.

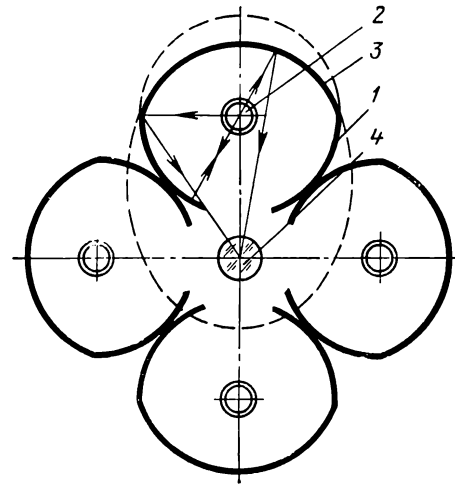

Fig. 1.7. Four-cavity pump unit

So that the efficiency of a particular pump configuration can be evaluated in quantitative terms one should know optimum relationships for its elements and also the absorbed pump energy density distribution in the laser-rod bulk. The problem is greatly complicated by processes occurring in the laser pumping cavity, such as release of absorbed radiation by the plasma, an increase in the transmission of the laser rod, multiple traverses of the laser beam through the rod, and also the fact that the system tends to focus off-axis rays. Different types of laser pumps can be compared in terms of light-trapping (geometric) efficiency,* assuming that the flash tube operates as a uniform Lambert radiator, that all light striking the laser rod is absorbed that the rays missing the rod will not be turned back on it, and also that the flash tube and the laser rod are long.

Analytically, the efficiency of a laser pump with different degrees of approximation to real conditions is examined in [25-28]. With an accuracy sufficient for most practical purposes, the efficiency of a laser pump can be obtained by finding the limiting angles within which light from the flash tube will strike the rod either directly

* Leaving out the release of absorbed energy by the plasma, an increase in the transmission of the laser rod, and the pump energy distribution in the rod, it is defined as the ratio of the pump radiant flux collected by the rod to the total radiant flux.

or after a single reflection, with allowance for the assumptions made earlier [27].

Taking a dual pumping cavity as an example, the following is an analytical analysis of the light-trapping efficiency of the laser pump:

$$\eta_0 = f(a, b, d_a, d_t, e, \Lambda, r_m)$$

where η_0 is the light-trapping efficiency; a is the semi-major axis of the cross-sectional ellipse; b is the semi-minor axis of the cross-sectional ellipse; d_a is the diameter of the laser rod; d_t is the diameter of the flash tube; e is the ellipticity of the ellipse; Λ is the

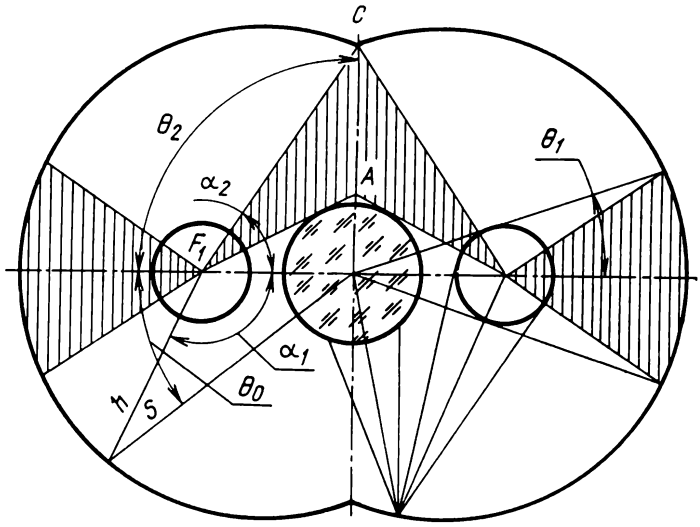

Fig. 1.8. Explaining the calculation of a two-cavity pump unit (the shaded areas are proportional to the radiant flux loss)

number of flash tubes (or partial elliptical cavities) used; and r_m is the reflectivity of mirror surfaces.

Each element on the surface of the elliptical cavity forms an image of the flash lamp at the laser rod. This image is magnified or demagnified as the ratio of the image distance to the object distance h/s (Fig. 1.8). An image of the flash tube at the conjugate focus will have the size $d_t h/s$. The fraction of the total radiated energy striking the laser rod will be equal to $(d_a/d_t)(s/h)$. This product may not exceed unity because the laser rod cannot collect more energy than is radiated by the flash tube. That portion of the elliptical reflector nearer the flash lamp forms a magnified image of the flash tube at the laser rod, and some of the energy liberated by the tube will not reach the laser rod. The other portion of the

elliptical reflector nearer the laser rod is more efficient, because it forms a reduced image of the flash tube, and all of its energy will reach the rod.

The light-trapping efficiency of the laser pumping cavity is given by

$$\eta_0 = \int_0^{\pi} (d_a/d_t)\,(s/h)\,d\alpha = \frac{100}{\pi}\left[\alpha_1 + \int_{\alpha_1}^{\pi} (d_a/d_t)\,(s/h)\,d\alpha\right] \qquad (1.1)$$

where α_1 describes the angle within which the radiant flux from the flash tube exactly fills the diameter of the laser rod or, which is the same, within which an image of the tube is less than or equal to the diameter of the laser rod.

Since $(s/h)\,d\alpha = d\theta$ (see Fig. 1.8), equation (1.1) reduces to the form

$$\eta_0 = \frac{100}{\pi}\left[\alpha_1 + (d_a/d_t)\,\theta_0\right] \qquad (1.2)$$

The angle α_1 is such that

$$\cos\alpha_1 = \frac{1}{e}\left[1 - \frac{1-e^2}{2}(1 + d_a/d_t)\right] \qquad (1.3)$$

Some of the reflective surface of the ellipse back of the flash tube is screened by the tube which may be regarded as an opaque body, and so the angle α_1 should be reduced by an angle θ_1 such that

$$\sin\theta_1 = d_t/4\ ae \qquad (1.4)$$

Besides, the laser rod fails to collect the flux proportional to CF_1A, and so the angle α_1 should further be reduced by an angle α_2 such that

$$\cos\alpha_2 = \frac{(2e/1+e^2) - \cos\theta_2}{1 - (2e/1+e^2)\cos\theta_2} \qquad (1.5)$$

where $\theta_2 = \pi/\lambda$.

Noting the above expressions and allowing for the reflectivity, we obtain the following expression for the light-trapping efficiency of a dual elliptical laser pumping cavity:

$$\eta_0 = \frac{100}{\pi}\left[(\alpha_1 - \alpha_2)\,r_m + (d_a/d_t)\,r_m\,(\theta_0 - \theta_1) + \arcsin\,(d_a/4ae)\right] \qquad (1.6)$$

The term $\arcsin\, d_a/4ae$ describes the proportion of the total radiant flux collected by the laser rod without reflections from the ellipse walls.

The above procedure can readily be adapted to calculate both single and multiple elliptical laser cavities, while its accuracy is quite acceptable for practical selection of an optimum configuration.

An increase in the number of flash tubes used in a laser pump is not the only way to raise the density of energy collected by the

laser rod. For example, the light transfer efficiency and the intensity of the output beam can markedly be enhanced by giving the laser rod a coat of dielectric [29]. The thickness of the dielectric cladding can readily be found from simple relations that can be derived from the construction shown in Fig. 1.9. As is seen, the radius, R_{im} of the cladding should be such that the ray tangent to the outer cylinder will be tangent to the circle of radius R_a after refraction.

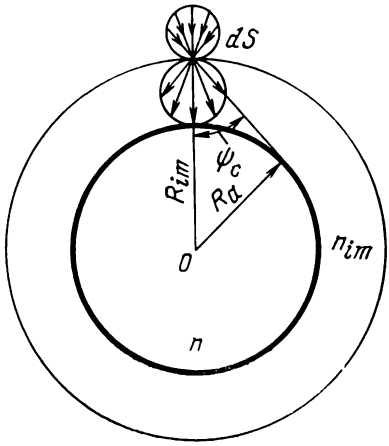

Fig. 1.9. Laser rod in a dielectric cladding

Still another way of enhancing the light transfer efficiency is to immerse the laser rod in a liquid. Analysis shows that with a transparent laser rod of refractive index n, immersed in a cladding liquid and optically pumped by an isotropic diffuse light source, the energy density varies with radius. The ratio of the maximum energy density inside the laser rod to that outside the rod is approximately n^2, the maximum value being observed inside a core of radius $R_{im} = R_a/n_{im}$ (where R_a is the radius of the laser rod). It is an easy matter to show that the resultant pump flux can exceed that radiated by the isotropic source. The proof is as follows. According to Fig. 1.9 [30], the pump flux incident on a surface element dS comes in from all directions within an angle of 2π steradians, while the refracted rays are bounded by a cone with a vertex angle of $2\psi_c$. The solid angle within the cone is:

$$\Omega = 2\pi (1 - \cos \psi_c)$$

The ratio of the solid angles of the incident and reflected rays is

$$2\pi/\Omega = \frac{n_{im}}{n_{im} - (n_{im}^2 - 1)^{1/2}} \tag{1.7}$$

where n_{im} is the refractive index of the immersion cladding. For values of n_{im} in the range 1.3 to 1.7, an approximate value of the ratio is given by

$$2\pi/\Omega = 1.49 n_{im}^{2.37} \tag{1.8}$$

As a rule, immersion liquids are simultaneously used as a cooling agent for the laser rod and a filtering medium. In such cases immersion liquids should have a high refractive index, stand up well to the effects of strong light, do not absorb the radiation of

the pumping source and have a low viscosity and a high thermal conductivity. If the primary objective is to obtain a maximum concentration of the radiant flux within the laser rod, the depth of the immersion liquid should be about $R_a(n_{im} - 1)$, where n_{im} is the refractive index of the immersion liquid, and R_a is the radius of the laser rod.

Apart from the light efficiency of the laser pump, a good deal of importance is attached to a uniform pumping energy distribution within the laser rod, because it is a major factor affecting the uniformity of population inversion. For example, when the flash tube is operating at a level only slightly exceeding the threshold value for lasing action, oscillations will be excited only by some areas of the rod rather than by its entire area. With an increase in excitation, the oscillating area expands until it fills the entire cross-section of the rod at a certain definite value [31, 32]. Because of a non-uniform distribution of pumping energy within the laser rod, it is heated differently at different parts, a factor which leads to thermally induced strains.

The non-uniform distribution of pumping energy will affect the laser rod of any cross-section. When the laser rod is arranged symmetrically with respect to the flash tube, non-uniform absorption will give rise to a radial temperature gradient varying both during and after the pumping period. The manner in which the pumping energy is distributed within the laser rod depends on the focusing properties of the cylindrical surface, its finish, and also on absorption of light as it passes from the periphery to the centre of the rod. The pump energy distribution may be described in terms of the product $\varkappa R_a$ where $\varkappa$ is the absorption coefficient for the pump energy in the laser rod.

The relative pump energy density distribution in cylindrical laser rods, both polished- and rough-sided, for a number of values of $\varkappa R_a$ is illustrated in the plots of Fig. 1.10. With various assumptions, they are computed, for example, in [25, 29, 33, 34].

As is seen from the plot for a polished-sided rod, the pump energy distribution is most uniform when $\varkappa R_a = n$. With increasing $\varkappa R_a$, the pump energy density in the centre of the rod decreases. In a rough-sided specimen, no increase in the pump energy density near the axis is observed, because the side surface shows no focusing action.

Neodymium-doped glass rods (especially, of large cross-section) are sometimes made rectangular, as this promotes a more uniform distribution of pump energy. In a polished-sided cylindrical rod at $\varkappa R_a = 0.1$ the relative pump energy density varies by a factor of more than 2 over the cross-section. For a rectangular rod under the same conditions this change does not exceed 10%. The pump energy density is a maximum in the corners of the rod.

The plots of Fig. 1.10 apply to rods with uniformly illuminated sides. In practical laser pump units with mirror reflectors, the pump energy distribution in the rod differs markedly from that described above. It is extremely difficult to calculate the pump energy density distribution for laser rods. With different degrees of approximation, this can be done on a computer.

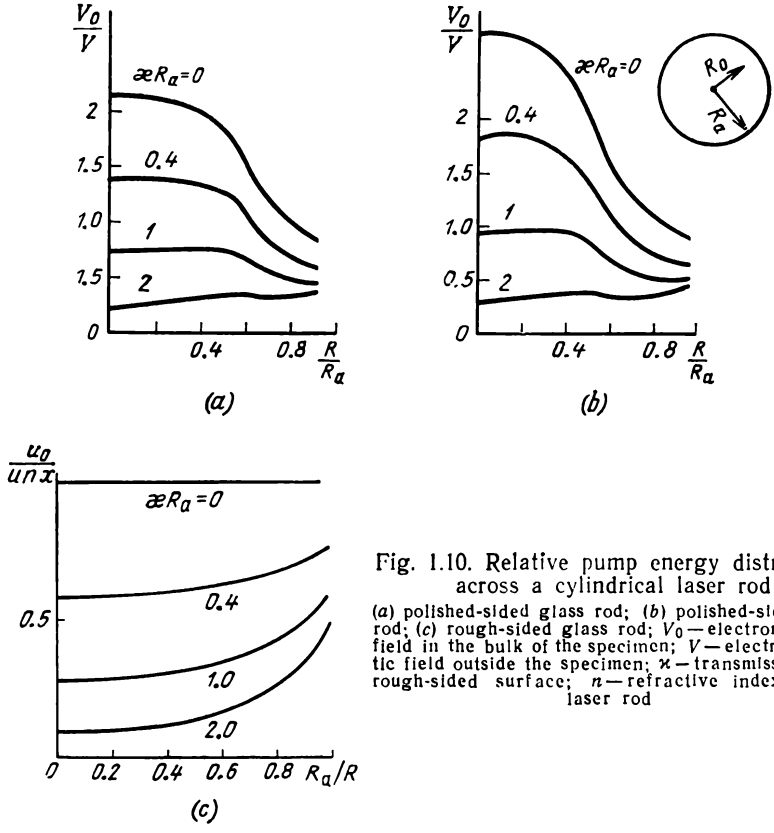

Fig. 1.10. Relative pump energy distribution across a cylindrical laser rod

(*a*) polished-sided glass rod; (*b*) polished-sided ruby rod; (*c*) rough-sided glass rod; V_0 — electromagnetic field in the bulk of the specimen; V — electromagnetic field outside the specimen; $\varkappa$ — transmission of a rough-sided surface; n — refractive index of the laser rod

Since the efficiency of a laser pump sensitively depends on the reflectivity of the mirror surfaces [5], an important feature in a good pump configuration, the reflector should combine a high reflectivity with the ability to stand up to the action of radiation. Several types of mirror reflectors are shown in Fig. 1.11. The elliptical mirrors (Fig. 1.11*a*) are fabricated from sheet brass 0.5 mm thick by cold stamping followed by buffing with soft wheels to a surface finish of Class 12 or 13. The heavy silver deposit (0.1 mm thick), also highly polished, gives a reflectivity of about 90%; the polished surface may be reconditioned two or three times to re-

move silver oxide. The reflectors fabricated from aluminium and its alloys lack in mechanical strength and have a reflectivity of 70 to 75%. Vacuum-aluminized steel or brass reflectors (at II*b* in Fig. 1.1) additionally protected with silicon monoxide have a reflectivity of 84 to 90%.

In direct contact with water, the silver plating on the mirror is rapidly oxidized by atomic oxygen given up by water under the action of strong light from the flash tube. The silver plating tarnishes, absorbs an excessive amount of light, overheats, and fails rather soon [35].

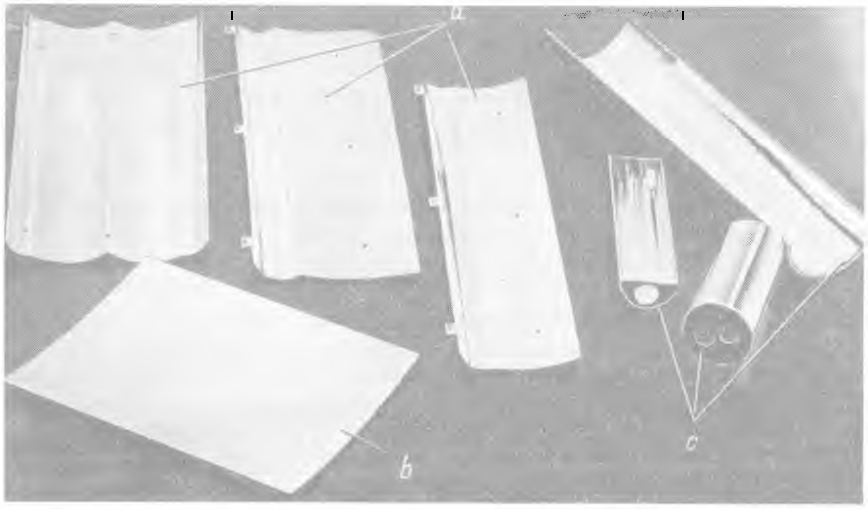

Fig. 1.11. Reflector geometries

Reflectors fabricated from glass or fused-quartz tubes (at II*c* in Fig. 1.1) have an outer layer of chemically deposited silver reinforced by a layer of electroplated silver 150 to 200 μm thick. The silver deposit is protected by a layer of nickel topped by a heavy layer (0.1 mm thick) of copper. The intervening nickel deposit minimizes the diffusion of copper into the silver. Glass or fused quartz can readily be polished to a surface finish of Class 14. Silver deposited on a transparent glass substrate protects the mirror coating against direct exposure to air or water, thereby ensuring a high mechanical strength and high reflectivity (93-96%). These reflectors can endure from 60,000 to 100,000 flashes with an average power of 6 kW without a marked impairment in reflectivity.

When the pump energy density exceeds 50-80 J/cm^2, the silver plating tends to peel off the glass substrate after 50 to 200 flashes.

In some cases, a glass or fused-quartz tube may be given a dielectric coating on its external or internal surface. Reflectors with dielectric coating have improved reflection within the absorption bands of the laser rod and, as a result, enhanced transmission in the remaining region of the spectrum. The net effect of this technique is an increase in the pumping efficiency and a reduction in harmful heating of the laser rod. The stability of pump units with dielectric coating has been investigated under conditions of pulsed pumping at energies up to 1000 J, pulse repetition frequencies of up to 20 Hz and an average power of 4 to 6 kW [36]. No changes have been noted in the spectral characteristics of the dielectric-coated reflectors after 10^6 shots.

1.2. Laser Rods

The laser materials used in solid-state lasers may be solid or ionic crystals, glass, or organic compounds doped with suitable elements. The dopants most often used are the ions of transition-group metals, rare-earth metals, and actinides. In most cases, a dopant ion is introduced through isomorphic substitution of a host ion. The energy level structure of active centres is above all determined by dopant atoms. A very extensive list of the laser materials employed to-day, along with their physical and chemical properties and growing methods will be found in [37, 233, 234]. Over a hundred laser materials based on inorganic ionic materials that can be excited to a negative absorption state are known to-day. However, only a few have been widely used. This is because laser materials should have a high efficiency, low beam divergence, and stability of emission with time. A very important property of a laser material is its ability to operate at room temperature. The main spectral requirements that a prospective laser material should meet are listed in [2, 73, 96, 234]. The laser materials most often used at present are ruby, different glasses doped with trivalent neodymium, neodymium-doped yttrium-aluminium garnet (YAG), and neodymium-doped calcium tungstate. At liquid-nitrogen temperature, an acceptable performance, energy-wise, has been shown by laser materials based on fluorites doped with divalent dysprosium [37]. The spectral properties of doped laser crystals are examined in [234]. In lasers with high output energy and high pulse power use is predominantly made of ruby crystals and neodymium-doped glass.

Apart from the quality of the laser material, the emission characteristics of a laser may be affected by some other aspects in the rod geometry or mounting.

In good-quality laser rods of a substantial size, spontaneous laser action may take place even at a relatively low pumping level because of reflections from the rod ends, before a high population inversion is built up. To minimize reflections from the ends of the laser rod, they must be either made anti-reflecting or immersed in a liquid [76] as shown in Fig. 1.12.

Using an immersion liquid with a refractive index as close to that of the laser rod as practicable, feedback may be reduced to zero.

With this type of mounting, the rod end is better preserved at high power levels and more conveniently illuminated by the pump source. The angle of tilt, ψ_t, of the window is given by

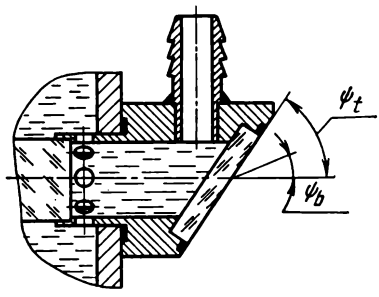

Fig. 1.12. Laser rod immersed in a liquid

$$\psi_t = \arccos\left(\frac{n_g}{n_{lm}}\sqrt{1+n_{lm}^2}\right) \tag{1.9}$$

where n_g is the refractive index of glass.

The angle of deflection for the output beam will then be

$$\psi_b = \arcsin\frac{n_g\left(\sqrt{n_{lm}^2 - n_g^2 - n_{lm}n_g} - 1\right)}{n_{lm}\left(1+n_g^2\right)} \tag{1.10}$$

However, the methods examined above have found a limited use because of the low stability of anti-reflection coatings (of the order of 100 J/cm^2) and absorption losses in the immersion liquid. At high energy densities, it is more advantageous to employ laser rods whose ends are bevelled at a small angle (2° to 5°) or at the Brewster angle.

Ruby. At present, Soviet makers turn out laser rods fabricated from synthetic ruby to Soviet State Standards OST 3-24-70 and OST 3-25-70. Under these Standards, ruby rods may have the configurations listed in Table 1.1.

The designation of a ruby rod consists of a type code (Table 1.1) and its dimensions (for example, РЛ1Б 10 × 120). Ruby rods come in diameters from 3.5 to 16 mm and in lengths from 45 to 240 mm, with the optical axis oriented from 60 to 90°. The side surfaces are ground to a surface finish of Class 5 to 10, mechanically polished to a surface finish of at least Class 12, and finally chemically polished. When mechanically polished, the diameter of a

laser rod is a sliding fit of Class 4; with all other types of working, it is a sliding fit of Class 5.

Table 1.1

Type designation	Laser rod sketch
Р	
РЛ	
РЛ1Б	
РЛ2Б	
РЛС	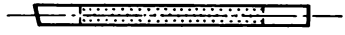
РЛО	
РЛОЛ	
РЛОЛ1Б	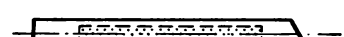
РЛОЛ2Б	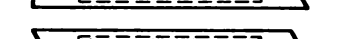

The ends of rod types Р, РЛ, and РЛ2Б are parallel to within 10″. By chromium concentration, change of refractive index, number of bubbles and other imperfections, and fringe count, ruby rods are classed into three categories according to Table 1.2.

The energy level diagram of the dopant, the plots relating the life of the metastable level, the wavelength and bandwidth of laser light as functions of temperature, the absorption spectrum, and main physical constants of ruby will be found in [2, 73].

Ruby rods have come to be widely used in laser technology because ruby emits in the visible region of the spectrum, can operate at room temperature, and has high mechanical strength and high damage threshold. Unfortunately, ruby crystals usually suffer from marked optical inhomogeneity. This inhomogeneity can be traced back to lattice defects (dislocations, blocks, slip planes), foreign inclusions, variations in chromium ion concentration throughout the sample. Lattice defects give rise to internal stresses in the crystal. Variations in the distribution of trivalent chromium ions in a crystal entail marked variations in the refractive index and lattice distortion, which leads to anomalous birefringence [38].

The effects of optical inhomogeneity in laser rods on laser light have been studied by several workers, for example [39-42].

The wave front is mostly affected by mechanical stresses and non-uniform distribution of chromium across the diameter [43].

Table 1.2

Category	Ruby rod diameter, mm	Average chromium concentration, % (by weight)	Refractive index change, $\times 10^5$	Number of imperfections and bubbles		Fringe count
				max 0.2 mm	max 0.3 mm	
1	8	0.013-0.017	0.6	9	—	0.3
2	8	0.018-0.025	0.9	16	—	0.5
3	8	0.026-0.036	2.7	—	—	—
1	—	—	0.7	15	—	0.3
2	10	0.20-0.028	1.1	25	—	0.5
3	10	0.29-0.040	4.0	—	—	—
1		—	1.2	—	20	0.3
2	16	0.024-0.037	1.6	—	30	0.5
3		—	9.0	—	—	—

Existing crystal-growing techniques cannot ensure a uniform distribution of chromium across the rod. The core of a specimen has a lower chromium concentration and, as a consequence, a lower refractive index n, than at its periphery. The radial refractive-index gradient may range from several units in the fifth decimal place to unity in the fourth decimal place. Besides, the refractive index may undergo a sudden change at the boundaries of some crystal areas. Also, crystal growth brings about internal strains. Because of this, a rod with perfectly parallel ends, may optically behave like a diverging lens. On passing through such a rod, a plane wave is markedly distorted because of the radial changes in the refractive index caused by strains and the non-uniform distribution of chromium concentration. This entails an increased beam divergence of, and a non-uniform energy distribution in, the laser beam. The studies conducted by [44] have shown, among other things, that the internal mechanical strains in a rod affect most of all the beam divergence, light intensity distribution, and mode selection,

The distribution and magnitude of stresses in crystals can be determined from the positions of fringes in the birefringence pattern. The fringe positions are decided by the change of optical path length for the ordinary and extraordinary rays according to the

relation:

$$\Delta (n_o - n_e) l_a = m_{in}\lambda \tag{1.11}$$

where n_o and n_e are the refractive indexes of the ordinary and extraordinary rays; l_a is the length of the rod; and m_{in} is the order of interference.

The magnitude of stress ξ can be found from

$$\Delta (n_o - n_e) = B_{ph}\xi \tag{1.12}$$

where B_{ph} is the photo-elasticity constant.

For an average value of photo-elasticity constant, $B_{ph} = 0.9 \times \times 10^{-7}$ cm^2/kg [45], the stresses are $\xi = 100$ kg/cm^2 for low-quality specimens and under 30 kg/cm^2 for high-quality specimens. The magnitude of internal stresses in ruby rods is a convenient criterion for the selection of ruby rods for single-mode (TEM_{00}) operation. High-quality specimens (with $\xi < 30$ kg/cm^2) oscillate in a single transverse mode over a sufficiently wide range of pump energies (25% above the threshold energy) [44].

The magnitude of mechanical stresses in a ruby rod depends on the density and distribution of dislocations in the rod. Dislocations are formed and accumulated not only while a crystal is grown, but also when it is machined. Mechanical stresses give rise to double refraction, and the ruby crystal becomes biaxial [46]. The non-uniform distribution of stresses in the crystal promotes a further distortion of the spherical wavefront. Unfortunately, crystal flaws vary widely from specimen to specimen both qualitatively and quantitatively.

The performance of a ruby rod can be improved by annealing. The optical inhomogeneity of a ruby rod can be corrected by shaping one of the rod ends to a sphere [47], or by adding a positive lens to the optical resonator [48], or by using a spherical mirror [49], or by attaching a sphere to one of the sides of the reflector prism [50].

How effective any of these correction methods actually is can only be determined in each specific case by testing the laser rod in operation.

One of the factors setting a limit to the maximum energy that can be handled by a laser rod is its stability towards strong laser light. The point is that at a certain definite energy density, the laser rod begins to give in at the ends or in the bulk. The first to be damaged are of course the rod ends. According to [51] the destruction of the rod ends may be explained by the mechanism of thermal damage as local surface flaws such as minute cracks, boundaries between blocks, etc. absorb light. As a result, the local surface flaws rapidly rise to a temperature at which irreversible events take place (such as fusion, crazing, etc.). The surface da-

mage threshold of a ruby rod depends on the duration of the white light pulse, the flaws and structure of the rod end surface.

The surface damage threshold for single-crystal ruby rods is several times the value for ruby rods with an amorphous surface structure. A carefully polished surface will usually be more stable [52]. With short light pulses, the surface-damage threshold, P_{th}, is proportional to $1/t_p$, where t_p is the light pulse duration. It is seen from the plot of Fig. 1.13 that for long light pulses the surface-damage threshold is fixed and independent of t_p. With long light pulses, the surface-damage threshold is about 10^6 W/cm^2. For short light pulses of about 50 ns, the threshold is about 280 MW/cm^2 [53].

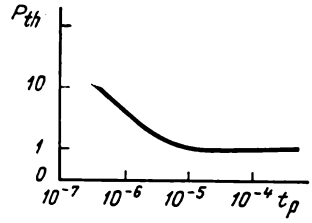

Fig. 1.13. Surface damage threshold as a function of laser pulse duration

The bulk strength of a ruby rod is considerably greater than its surface strength, and is 3×10^{10} W/cm^2 [54].

Neodymium-doped glass. The types, sizes and technical characteristics of laser rods fabricated in the USSR from neodymium-doped glass are established by State Standards OST 3-31-70 and OST 3-30-70.

The type designations of rods according to their cross-sectional area and the tilt of rod ends are listed in Table 1.3.

Table 1.3

Type designation	*Laser rod sketch*	*Laser rod cross-section*
ЭНЦ-90		
ЭНЦ-φ		
ЭНЦ-Б		
ЭНП-90		
ЭНП-φ		

The designation of a neodymium-doped glass rod consists of a type designation according to Table 1.3 and its dimensions in brackets. For example, ЭНЦ-90 (8×100). Neodymium-doped glasses are classed according to their refractive index at a wavelength of $\lambda = 586$ nm, as presented in Table 1.4.

Standard neodymium-doped glass rods come in several sizes from 80 to 1200 mm in length and from 5 to 60 mm in diameter.

Except the mounting bosses, the side surfaces of a neodymium-doped glass rod are etched with a mixture of hydrofluoric and sulphuric acids and treated for protection with an acid-and-wax mixture. The mounting bosses are machined to a sliding fit of Class 4. Rod ends at right angles to the axis are lapped parallel to 10″, while rod ends arranged at other angles are lapped parallel to 2′. The quality of neodymium-doped glass is evaluated in terms of non-active absorption, or non-saturable loss, (at $\lambda = 1060$ nm), the size and number of bubbles, and also by the amount of solid non-metallic inclusions. According to these factors, neodymium-doped glasses are classed into categories according to Table 1.5.

Table 1.4

Glass type	Refractive index, mm, at λ=586 nm
ГЛС-1	0.190
ГЛС-1П	0.190
ГЛС-2	0.185
ГЛС-3	0.47
ГЛС-4	0.41
ГЛС-4П	0.41

The properties of neodymium ions in different types of glass, absorption spectra, and fluorescence intensity as a function of time for different neodymium concentrations will be found in [55] and [73].

Table 1.5

Category	Absorption index, cm^{-1}, at λ=1060 nm	Max. bubble diameter in boule, mm	Average number of bubbles greater than 0.1 mm (in 1 kg of glass)	Number of stones and crystals from 0.06 to 0.5 mm (per kg of glass)
1	0.002	—	—	None
2	0.004	—	—	10
3	0.006	0.2	—	—
4	—	0.3	—	—
5	—	0.5	—	—
6	—	0.7	—	—
7	—	1.0	—	—
A	—	—	10	—
Б	—	—	30	—
В	—	—	100	—

With glass used as a host, laser rods can be fabricated in any size and with a sufficiently high optical homogeneity. This property of glass makes it a preferred material for high-power laser oscillators and amplifiers.

Unfortunately, glass lacks in thermal stability and thermal conductivity. In operation at high pulse repetition frequencies, stresses are produced in the laser rods, which may cause the glass to shatter. The large amount of heat liberated in the course of pumping due to the non-active absorption (non-saturable loss) stresses the laser rod, thereby impairing its original properties and the characteristics of the laser beam. The non-uniform distribution of pumping energy throughout the rod produces a temperature gradient and causes the population inversion to be distributed non-uniformly with the result that the optical path length is changed and double refraction takes place [58]. This behaviour, so characteristic of solid-state laser materials, is especially pronounced in glass, because, when not excited, the glass has extremely high optical properties and shows a nearly complete absence of anisotropy. In turn, induced double refraction affects the intensity distribution across the beam and beam polarization.

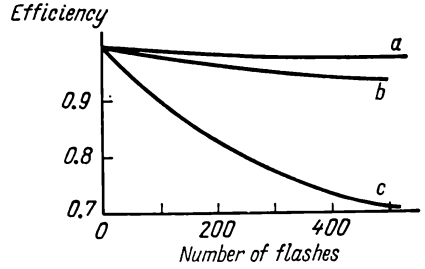

Fig. 1.14. Effect of pump-energy filtering on laser efficiency
(*a*) ТФ-105 filter; (*b*) ЛК-318 filter; (*c*) without a filter

The effect of thermal distortions is greatly dependent on the geometry of the laser rod. In [57] it is shown that rectangular glass rods can be made free from thermal distortions for plane-polarized emission, because in them the temperature gradient is predominantly linear. Accordingly, laser amplifiers intended to produce a high-power, plane-polarized beam should preferably use rectangular glass rods as less susceptible to induced double refraction [58].

In neodymium-doped glass rods, flash-tube light and the laser beam may cause scaling on the side surface, damage to the rod ends and to the bulk of the rod. The point is that the surface layer of a glass rod 20 to 60 μm thick absorbs half the ultra-violet component at $\lambda \leqslant 330$ μm [59], which accounts for 10% of the total flash-tube energy [60]. In the absence of cooling, heat liberation in the surface layer suddenly rises up to 10^3 J/cm^3, the surface layer rises to a temperature of 800 °C and this causes scaling.

Another weakness of neodymium-doped glass is photo-chemical instability. The ultra-violet rays reaching into the laser rod reduce the trivalent iron to divalent, and this absorbs radiation at a wavelength of 1.06 μm. As a result, the laser material "ages", that is, the glass rod gradually loses its ability to generate electro-magnetic waves, until this ability disappears altogether. These changes in the performance of glass rods due to ultra-violet rays (Fig. 1.14)

[62] can be minimized to a great extent through the use of dye-solution filters [61] or glass filters which absorb wavelengths shorter than 400 μm.

Among the factors limiting the power of the laser beam are the absorption of laser emission by microimpurities in the bulk and on the surface of the rod, and also the effects of self-focusing [65-67]. Microinclusions of platinum diffusing into the glass during manufacture absorb laser emission, and a rapid and highly localized heat build-up takes place which gives rise to thermo-elastic strains and causes crazing in the rod. The threshold energy required for microinclusions to cause damage in the bulk depends on their orientation and size and also on the energy and duration of light pulses. For light pulses with a duration of about 50 ns, this threshold energy is 4 to 6 J/cm^2 [68].

In the absence of microinclusions, the strength of glass is improved by a wide margin, and now an increase in the energy density is limited by the effects of self-focusing. Due to self-focusing, the radiant flux density may run as high as 3×10^{12} W/cm^2, which may prove sufficient to cause damage to a uniform glass such as type K-8 [69].

Fluorite. Fluorite crystals doped with divalent dysprosium are a suitable material for lasers operating continuously or at high pulse repetition frequencies, because of low threshold energies, high gain, and satisfactory thermal stability. The energy level diagrams, absorption bands, and some physical properties of fluorite crystals can be found, for example, in [2, 37, 73].

Table 1.6

Laser material	Dopant concentration	Emission wavelength, μm	Laser emission spectrum width, cm^{-1}		Efficiency, % (free emission)	Refractive index	References
			T = 300K	T = 77K			
Ruby	0.03-0.05 mole	0.69	21	0.3	2	1.76	[2, 73]
Neodymium-doped glass	2-6 (by weight)	1.06	44.2-88.5	—	6	1.55	[2, 73]
Yttrium-aluminium garnet	3 moles	1.06	6.5	1-1.5	2	1.83	[73, 74]
Fluorite	0.02 mole	2.36	—	0.01	1.3	1.42	[2]
Calcium tungstate	2 moles	1.058	—	0.2-0.5	1.7	1.92	[75]

With time, the lasing threshold of fluorite crystals increases until no lasing action occurs at all.

Yttrium-aluminium garnet. The spectrum properties and main physical and chemical constants of this material are given in [37]. YAG crystals have a low threshold for lasing action at room temperature, high mechanical strength, and good thermal conductivity. Because of this, they are well suited as laser material for CW and high PRF lasers. Reference [22] reports a CW laser oscillator with a power output of 220 W and an efficiency of about 2%, while reference [71] reports a YAG laser operating at a frequency of 5 kHz with an average power output of 1 W. The use of yttrium-aluminium garnet in high power lasers is limited by the low damage threshold of the material.

Some of the characteristics of the above listed laser materials are summarized in Table 1.6.

1.3. Optical Elements

Spatial distribution, spectral make-up, beam divergence and other characteristics of laser emission are to a great extent determined by the optical elements that make up the laser optical cavity or resonator. These optical elements may be mirrors, resonant reflectors, prisms and aperture stops or their equivalents.

Mirrors. Obviously, the mirrors of a laser optical cavity should have low absorption and scattering losses, be stable to laser emission, mechanical and environmental influences, and have in some cases a high reflectivity. Besides, mirrors for parametric laser oscillators should have a broad-band response. In laser engineering, use is made of flat, cylindrical, spherical and aspherical mirrors with metallic and dielectric coatings.

Mirrors with metal coatings suffer from a number of important disadvantages. The reflectivity of aluminium and silver is 90 and 95%, respectively. The aluminium deposit on a glass surface is mechanically weak, and it has to be protected by a transparent dielectric film. In mirrors fabricated by the chemical precipitation of silver from solution, this protective layer is provided by the glass substrate. Such mirrors are stronger mechanically and more stable towards strong emissions. Yet, absorption losses in the metallic coating are rather high (10 to 15%) and this causes their damage in lasers emitting strong light pulses.

With dielectric coatings, mirrors may have a reflectivity of nearly 100% and an absorption of a fraction of one per cent.

Dielectric mirrors are prepared by depositing alternating layers with high and low refractive indexes on a substrate. The substrate may be glass, fused quartz, or any other material transparent to laser emission. Dielectric mirrors are mainly fabricated by thermal

evaporation in a high vacuum, by centrifuging of suitable solutions, and by cathode sputtering in an oxygen atmosphere. The number of materials suitable as mirror coatings is rather limited. At present, use is made of coatings from zinc sulphite as a highly refractive material, in conjunction with magnesium fluorite or strontium fluorite as a low-refractive material [77, 75, 78].

The stability of mirrors is to a great extent determined by the surface finish of the substrate. As is shown in [79], all of the advantages offered by dielectric coatings may be utilized only if the substrate is of high quality and prepared thoroughly.

Among other things, the surface finish of the substrate affects the reflectivity of multilayer reflectors. For example, in order to obtain a reflectivity of above 99% at $\lambda = 0.7$ μm, the height of microscopic irregularities on the reflecting surface should not exceed 50 Å, that is, $1/150\lambda$. Before the deposition of a coating material, the substrate should be thoroughly cleaned by rinsing and subjected to electron or ion bombardment in a vacuum [80]. For better adhesion of the coating to the substrate, the latter is worked with jewelers rouge immediately before deposition.

Table 1.7

Type of coating	Deposition process	Threshold power density, MW/cm²
Sapphire, polished and coated with SiO_2	Cathode sputtering	230
Dielectric mirror, 15 layers	Vacuum evaporation	90
Same	Cathode sputtering	180

When exposed to laser emission, the dielectric coatings either burn out or peel off the substrate. The threshold power densities for the mirrors of ruby lasers are listed in Table 1.7 [53]. It should be noted that the power density averaged over the cross-sectional area of a laser rod is one-forth of the power density given in the Table. The stability and strength of coatings depend on the number of layers deposited, the temperature of the substrate at the time of deposition, the purity of source materials, the flaws present in the film, and the orientation of the crystallites in the deposit [82]. The damage threshold energy is the highest for a single-layer coating. With increasing number of layers, the crystallites grow in size and the damage threshold is brought down, being a minimum for five- or six-layer coatings. Any further increase in the number of layers does not produce any marked reduction in the

damage threshold. Some materials, such as lead oxide, have a greater refractive index than zinc sulphide. With these materials, mirrors may have a high reflectivity with a smaller number of layers.

The experimentally found threshold energy densities for lead oxide and cryolite coatings exposed to the continuous emission of a ruby laser are listed in Table 1.8 [83].

Table 1.8

Number of layers	Reflectivity	Density threshold, * J/cm²	Reflectivity	Density threshold, ** J/cm²
1	40	680	44	2100
5	86	500	90	1400
7	95	360	97	1300
9	97	320	99	1040

* Coatings were deposited at a substrate temperature of 20° C.
** Coatings were deposited at a substrate temperature of 200° C.

The lowest stability of the lead-oxide and cryolite coatings appears to be due to the fact that lead oxide has a lower melting point (888 °C) than zinc sulphide.

No marked difference has been found in the stability of dielectric coatings when exposed to laser emission from the substrate side or from the outside. Most strongly, the damage threshold energy of dielectric coatings depends on the duration of the laser pulse. With a pulse duration of about 600 μs, the threshold energy density for vacuum-deposited dielectric-coated mirrors is about 2000 J/cm² at a wavelength of $\lambda = 1060$ nm. For a pulse duration of about 30 ns, the threshold power density is 30 MW/cm².

The increase in the duration of laser pulses from a few tens of nanoseconds to hundreds of microseconds is equivalent to an increase of three orders of magnitude in the threshold energy density.

Resonant reflector. In some cases, the output mirror of a laser optical cavity is a resonant reflector which is a succession of identical uncoated, transparent dielectric plates separated by an equal air gap. The interference taking place when light is multiply reflected from the plates in this reflector makes its reflectivity dependent on the frequency of laser emission. According to [85], the maximum reflectivity of a system consisting of m_p plates of equal thickness which, like the identical air gap, is equal to a certain odd integer, $\lambda_0/4$ (where λ_0 is the wavelength of the emission in a

vacuum) is given by

$$r_{\max} = \left(\frac{1 - n^{2m_p}}{1 + n^{2m_p}}\right)^2 \tag{1.13}$$

A plot of the reflectivity as a function of the number of plates and refractive index is shown in Fig. 1.15*a*. The dependence of the

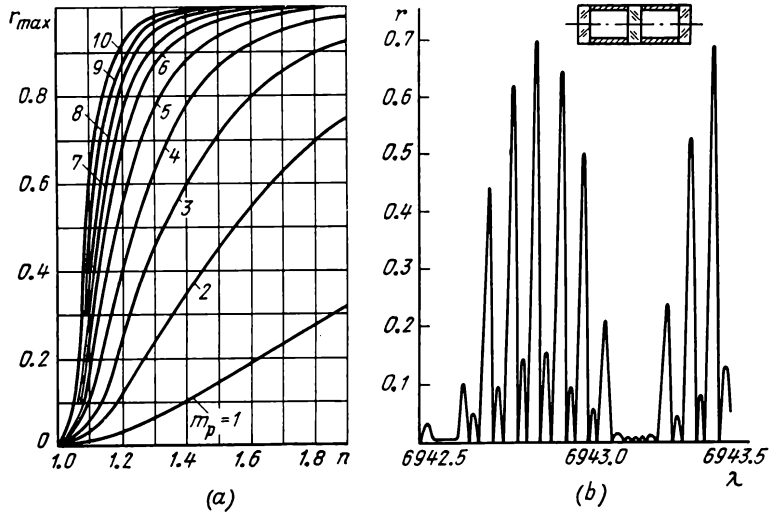

Fig. 1.15. Maximum reflection coefficient of a resonant reflector as a function of reflective index and number of plates (*a*) and the reflection coefficient of a 3-plate resonant reflector as a function of emission wavelength (*b*)

reflectivity of a single plate of thickness D with the same reflectivity on both sides ($r_1 = r_2 = r$) on the frequency, ν, of incident light is described by the following expression

$$R(\nu) = \frac{4r \sin^2(2\pi nD\nu)}{(1 - r)^2 + 4r \sin^2(2\pi nD\nu)} \tag{1.13a}$$

and is a periodic function of emission frequency. The frequency interval $\Delta\nu_p$ between adjacent reflection maxima is

$$\Delta\nu_p = (2nD)^{-1} \tag{1.14}$$

The frequency dependence of the reflectivity of a multi-plate reflector is a complex function whose behaviour depends on the number of plates and can be evaluated, using either the theory of cascaded two-ports [86] or the usual equations from thin-film theory, solved on a computer [227].

The frequency interval between the reflection maxima of a multiplate reflector is decided by the minimum thickness in the system

Glass type	Emission wavelength, μm	Damage threshold with continuous emission		Damage threshold in single-pulse operation		Reference
		energy density, J/cm²	power density, W/cm²	energy density, J/cm²	power density, W/cm²	
Fused quartz	0.69	—	—	220	1.4×10^{10}	[230]
Crown glass	0.69	—	—	133	0.89×10^{10}	[230]
White crown glass	0.69	—	—	350	50×10^{10}	[231]
Boron-silicate crown glass	0.69	—	—	500	71×10^{10}	[231]
Heavy barite crown glass	0.69	—	—	500	71×10^{10}	[231]
Superheavy flint glass	0.69	—	—	40	0.56×10^{10}	[231]
Crown glass	1.06	15,000	16.5×10^{6}	—	—	[232]
Barite crown glass	1.06	13,500	14×10^{6}	—	—	[232]
Heavy crown glass	1.06	7000	8.7×10^{6}	—	—	[232]
Heavy flint glass	1.06	10,000	11.7×10^{6}	—	—	[232]
Flint glass	1.06	9200	11.5×10^{6}	—	—	[232]
Light flint glass	1.06	7500	9.5×10^{6}	—	—	[232]

(that of a plate or an air gap) and, as is the case with a single plate, is equal to $\Delta\nu_p = (2D)^{-1}$. The relationship between the reflectivity of a resonant reflector using three 2.5-mm glass plates ($n \simeq 1.51$) and wavelength, determined by the methods of thin-film optics, is shown in Fig. 1.15*b* [226].

It should be noted that for a two-plate reflector frequency intervals may be evaluated approximately. For example, for a reflector using two plates of thickness $D_1 = 2.0$ mm ($n \approx 1.79$) and an air gap of width $D_2 = 25$ mm, the frequency interval between the major maxima at $\lambda = 6943$ Å is equal to $\Delta\nu_1 = (2D_1)^{-1} = 0.67$ Å, while the frequency interval between minor maxima is $\Delta\nu_2 = (2nD_2)^{-1} = 0.069$ Å [132]. The last figure differs from the one obtained by precise methods [226] by about 10%.

A resonant reflector may be assembled from plates differing in thickness or with air gaps differing in width. However, theoretical analysis has shown that this type of reflector offers no material advantages [226], while the difficulties in its fabrication would limit its large-scale use.

In order to secure the desired reflectivity in a resonant reflector, the difference in thickness between its plates should not exceed $\lambda/8$. Otherwise, the reflection would decrease at the major maxima and increase at the minor maxima. An equal change in plate thickness or in air-gap width across the diameter (due to, say, a change in temperature) would shift the frequency at which a reflectivity maximum occurs. If the difference in thickness between the plates or ring spacers exceeds $\lambda/4$, the reflectivity of the resultant system would be equal to the sum of the Fresnel reflection coefficients of all surfaces.

Table 1.10

Material	Surface finish	Surface damage threshold, J/cm²
Glass K-8	Super-high polish	190±25
Glass K-8	Regular mechanical polish	87±8
Glass K-8	Grinding	9±0.6

This stack arrangement is used as the output reflector of a laser optical cavity in cases where mode selection is not required. Stacked reflectors are highly stable to strong emission limited only by the damage threshold of the plate material. The damage threshold energies for some materials are summarised in Table 1.9. Table 1.10 gives the surface strength of glass as a function of surface finish [152] when exposed to the principal transverse mode from a Q-switched ruby laser.

In some cases, the end reflector of a laser optical cavity takes the form of a set of plane-parallel glass plates which are equal in thickness but differ in cross-section. In this type of reflector, optical transmission varies across the diameter of the laser rod [88], a feature that may be utilized in lasers to compensate to some degree for the non-uniform distribution of population inversion by appropriately matching the gain and loss across the rod. Another advantage of this type of reflector is a reduced spread between the instants when laser action is initiated in the various areas of the rod section, reduced pulse duration, and reduced beam divergence.

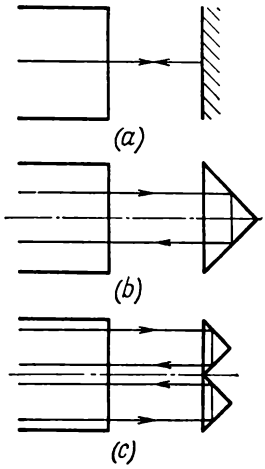

Fig. 1.16. Optical cavity elements
(a) mirror; (b) roof prism; (c) two roof prisms

Prisms. When used in a low-divergent beam, a roof prism enables one to dispense with reflecting coatings and utilize total internal reflection from the prism sides. Because of this, the power density threshold of the laser optical cavity may be raised while the prism itself is insensitive to misalignment in one direction due to an even number of reflections. This is the reason why roof prisms are widely used in Q-switched lasers where the power density in the optical cavity is particularly high and the optical components are subjected to intense light emission. Above all, a roof prism equalizes the laser emission density across the diameter of the rod. In a cavity with a mirror, the beam traverses the same path in the rod several times (Fig. 1.16*a*), because of which the non-uniformity of the emission field is accentuated and the beam acquires a filamentary structure of a high local density likely to cause damage to the reflecting layer. In cavity with a roof prism (Fig. 1.16*b*), each ray in the laser rod traverses different paths in the forward and reverse directions. If, instead of one, use is made of two roof prisms [88], it is seen from Fig. 1.16*c* that the rays emitted by the rod core will, after reflection from the prism, pass in the peripheral part of the rod. The net result is that the energy density is made to be the same across the rod and the regular component of optical non-uniformity is cancelled out.

In a roof prism in which the roof edge is not parallel to the hypotenuse face, some emission will be lost upon reflection from the hypotenuse face. The magnitude of loss depends on the prism material and may be as high as 8 or 9%. This disadvantage may be avoided by using a prism in which the hypotenuse face is

oriented at the Brewster angle (Fig. 1.17). Such a prism also has selective properties. The reflected ray will coincide with the incident ray only if, after refraction at the entrance face, the rays are propagated in a plane perpendicular to the prism edge, and this condition can be satisfied only by a certain wavelength. Any other wavelength after reflection from the side faces will emerge from the prism at an angle to the original direction and will not be built up.

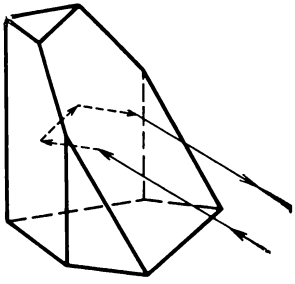

Fig. 1.17. Roof prism with a Brewster-angled entrance window

A very important requirement for prisms used in laser optical cavities is that the reflected ray should travel in the same path as the incident ray. In a prism with the roof edge not parallel to the hypotenuse face, the reflected ray will be shifted in a plane passing through the roof edge. In a prism not precisely right-angled, the ray will be shifted in a plane perpendicular to its edge. If the error in the right angle is δ, the emerging ray will be deflected through an angle $\Delta\psi$ [89]:

$$\Delta\psi = 2\left(n\frac{\cos i'_{refr}}{\cos i_{incid}} - 1\right)\delta + 2\delta \qquad (1.15)$$

where i_{incid} and i'_{refr} are the angles of incidence and refraction of the ray at the entrance face of the prism, and n is the refractive index If the ray strikes the entrance face at right angles, then

$$\Delta\psi = 2n\delta \qquad (1.16)$$

For a Brewster-angled prism, $i'_{refr} + i_{incid} = 90°$, and so

$$\Delta\psi = 2n^2\delta \qquad (1.17)$$

The limit of a negative error in the right angle is

$$\delta \leqslant d_a/8n^2\sqrt{2}L \qquad (1.18)$$

where d_a is the rod diameter, L is the cavity length, and n is the refractive index of the prism.

A negative tolerance should be specified for the right angle of a prism; it may be greater than the positive tolerance, and is independent of the number of reflections, m_{refl}.

According to [90] the total number of reflections, m_{refl}, of a ray before it emerges from the laser optical cavity consisting of a mirror and a prism is:

$$m_{refl} = d_a/L\delta \qquad (1.19)$$

For an optical cavity made up of two plane mirrors, the number of reflections for a ray striking the mirror at an angle i_{incid} can be found by

$$m_{refl} = d_a / 2Li_{incid} \tag{1.20}$$

A plot of m_{refl} as a function of i_{incid} is shown in Fig. 1.18. The dotted curve represents an optical cavity using plane mirrors, and the solid line a cavity with a plane mirror and a prism. As is seen, at $i_{incid} = \delta, 2\delta, \ldots$, closed paths are formed in the prism cavity, so that the rays cannot pass through the side walls of the cavity. It is also seen that the rays travelling at an angle less

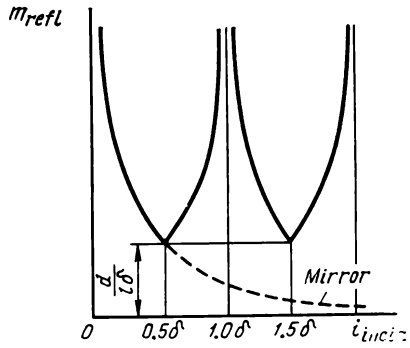

Fig. 1.18. Number of beam reflections in an optical cavity as a function of the angle between the beam and the cavity axis

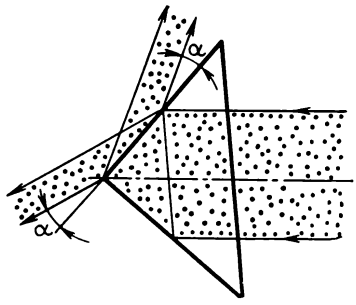

Fig. 1.19. Variable-reflectivity roof prism

than 2δ will make about three times more passes before they emerge from the prism cavity than in the cavity using plane mirrors.

The lack of parallelism between the roof edge and its hypotenuse face will cause the ray emerging from the prism to deviate through an angle

$$\gamma = 2(m_{refl} - 1)\delta_{par} \tag{1.21}$$

The limit for the lack of parallelism is

$$\delta_{par} \leqslant d_a / 2\sqrt{2}(n-1)(m_{refl}+1)^2 Lm_{refl} \tag{1.22}$$

where m_{refl} is the number of passes completed by the ray.

The behaviour of the roof prism as the end reflector of a laser optical cavity is investigated in [92]. This configuration (Fig. 1.19) utilizes the change in the reflectivity of glass near the angle of total internal reflection.

The reflectivity of such a prism undergoes a sudden change as it is turned about its edge. With a change of a few degrees in the angle of incidence, the reflectivity may change by an amount from a few to 100%. Since, however, the reflection coefficient changes gradually, an optimum value can conveniently be obtained under any operating conditions.

The two light beams emerging from the roof prism have the same intensity, but are propagated in opposite directions. The intensity distribution within the beam is compressed in a direction normal to the roof edge by an amount proportional to tan α.

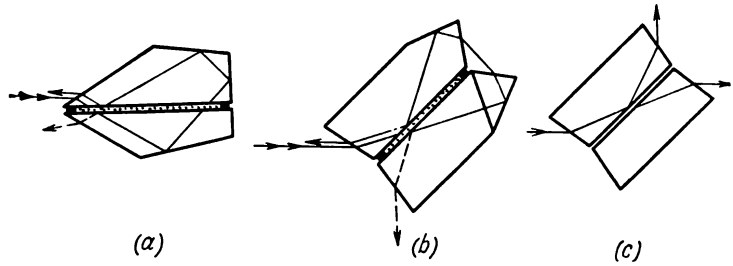

Fig. 1.20. Variable-reflectivity composite prisms
(*a*) the reflected ray travels in parallel with the incident ray after an odd number of reflections and (*b*) same, after an even number of reflections; (*c*) a beam-splitting prism

In TIR prisms operating at high densities of the reflected radiant flux, the first to be damaged are the surfaces where total internal reflection takes place. In [228] it is shown that the early damage to the prism may be avoided by placing it appropriately in the light beam. The incident and reflected beams produce standing waves near the plane of reflection. At loops, the field intensities **E** of the incident and reflected beams will be combined vectorially. If the vector **E** of the incident wave makes an angle of about 45° with the side face of the prism (in the plane of incidence), the field intensity at a loop will be $\sqrt{2}\,|\mathbf{E}|$. If the vector **E** is parallel with the side face, the field intensity at a loop will be $2\,|\mathbf{E}|$.

The angular spread of the laser beam can be reduced through the use of prism reflectors utilizing critical internal reflection (CIR). The behaviour of a rhombic prism in which the beam is reflected four-fold at a nearly critical angle is investigated in [229]. The rays striking the reflecting plane at an angle less than the critical one are drastically attenuated by four-fold reflection. Another feature of a rhombic prism in the laser optical cavity is a marked increase in the radiant flux density within the solid angle.

Composite prisms such as shown in Fig. 1.20 may likewise be used as reflectors in a laser optical cavity [91]. They have a high reflectivity, stand considerable power densities (up to 1 GW/cm^2),

and enable the reflection coefficient to be continuously adjusted from 0 to 1 to suit emissions over a wide spectral range. A composite reflector consists of two prisms separated by a thin layer (about 2 μm) of couplant (such as water or methanol). Now that total internal reflection cannot take place at the interface, the beam entering the prism is split up into two beams which are caused to travel in opposite directions and are again combined immediately before they emerge from the prism. The beam emerging from the prism in parallel with the entering beam may undergo either an odd number (Fig. 1.20*a*) or an even number (Fig. 1.20*b*) of reflections. This difference in the behaviour of composite prisms determines their properties. With an even number of reflections, the reflected beam will not be split up in a transverse direction. With an odd number of reflections, the reflected beam will be split up transversely, which may be utilized to select transverse modes.

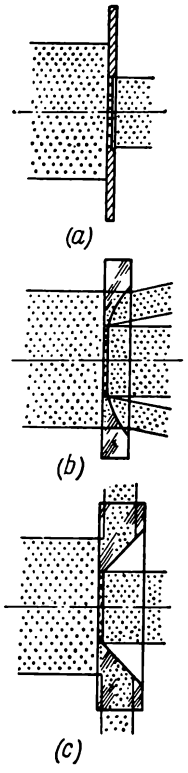

Fig. 1.21. Aperture stops

The reflection coefficient may be controlled either by using a liquid having an appropriate refractive index or by varying the angle of incidence for the incoming ray. This type of reflector calls for utmost care in the manufacture of prism elements. Additional difficulties are posed by the need to seal in the couplant.

The composite prism shown in Fig. 1.20*c* may be used as the end reflector in, say, a ring cavity. In this type of reflector, the prisms are separated by a fine air gap whose width (on the order of a few fractions of the emitted wavelength) is determined by the required transmission. The ray enters the composite prism at the Brewster angle and is split up at the interface into two rays, one of which, on being reflected, emerges from the prism at right angles to the incident ray, while the other passes through the air gap and leaves the prism in a direction parallel to the incident ray.

Aperture stops. The optical cavities of lasers operating at a relatively low power level use aperture stops fabricated from opaque metals (Fig. 1.21*a*). A high-power beam might destroy the material at the aperture edges. To avoid this, the aperture edges may be given the shape of a spherical or conical surface which is polished for high reflectivity. High stability towards strong laser emission has been shown by an aperture stop fabricated from a

transparent material (such as glass or fused quartz) in which the aperture has a sharp edge on the entrance side and a spherical or conical chamfer on the exit side (Fig. 1.21*b* and *c*). The "stopped-down" beam passes through the sharp-edged aperture, while the spherical chamfer deflects the remainder from the initial direction through an angle determined by the radius of curvature. The conical chamfer reflects the incident radiation at the total internal reflection angle (Fig. 1.21*c*).

1.4. Laser Optical Cavities

One type of the laser optical cavity is arranged along the lines of the Fabry-Perot interferometer, which has the advantage of producing a directional and coherent beam [93]. Apart from the plane-parallel Fabry-Perot resonator, there are cavities using spherical, parabolic and other surfaces.

Theoretical analysis of the electromagnetic field in different laser cavities [94, 95] shows that it may be described by an expansion of a system of functions of three indexes. Each term represents a particular mode designated TEM_{mnq}. The first two indexes represent the functions describing a transverse mode, TEM_{mn}. For each transverse mode, there are several longitudinal modes differing in the number of half-waves that can be accommodated over the length of the cavity. These modes are marked by the index q. For any mode, there is a specific frequency, ν_{mnq}. The number of longitudinal modes that can actually exist in a laser oscillator is decided by the fluorescence line width of the rod and the type of cavity. A detailed examination of laser cavities and an extensive bibliography on the subject will be found in [73, 96 through 98]. What follows is only a brief outline of the principal factors determining the existence of transverse and longitudinal modes in laser cavities.

The transverse modes are related to the diffraction of laser light as it is reflected from the mirrors, diffraction losses on the elements limiting the beam aperture, etc.

The effect of diffraction on the distribution of the electromagnetic field in a laser cavity was for the first time investigated on the basis of the Huygens-Fresnel principle in [94]. According to [94], the alternate reflections of the beam from the mirrors in the cavity may be likened to the propagation of a wave through a medium containing an infinite set of coaxial and identical apertures in equi-distant, parallel and absolutely absorbing black screens (Fig. 1.22). This analogy holds, if the mirror is large in comparison with the wavelength, and the electromagnetic field is very close to the transverse one and uniformly polarized in one direction. Then the field u_p in the Fresnel zone due to the illuminated

aperture A can be described by a surface integral of the form

$$u_p = \frac{jk}{4\pi} \int_A u_a \frac{e^{-jkR}}{R} (1 + \cos \chi)\, dS \qquad (1.23)$$

where u_a is the field at the aperture, k is the propagation constant for the medium in question, R is the distance of a point on the aperture to the observer, and χ is the angle between the radius vector R and the normal to the plane of the aperture. When the wave undergoes a reflection from the cavity mirrors, at any instant the field at one mirror is related to the field at the other by expression (1.23). After multiple reflections, the field distribution at

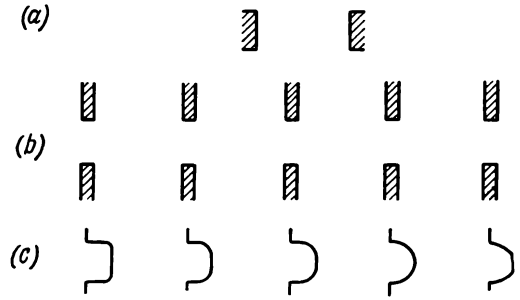

Fig. 1.22. (*a*) Fabry-Perot interferometer; (*b*) analogy of a transmitting medium; (*c*) change in transverse field distribution with the number of traverses between mirrors

the mirrors will change but little from reflection to reflection, becoming stationary with time. The manner in which a plane wave approaches a stationary condition is diagrammatically shown in Fig. 1.22*c*. With reflections, the field changes at the edges at a faster rate than in the central parts. After some reflections, the field at the edges becomes so small that the diffraction losses near the edges are reduced considerably and become comparable to the losses in the centre of the mirror. In the general case, a stationary condition is attained, after a number, g, of passes and the field distributions on the mirrors become the same up to the complex constant, and we may write

$$u_p = (1/Z_c)^g\, v(R) \qquad (1.24)$$

where $v(R)$ is the distribution function which does not change from reflection to reflection and represents the normal cavity mode, and Z_c is the complex constant independent of space coordinates. Substituting (1.24) into (1.23) gives an integral expression of the form

$$v = Z_c \int_A kv\, dS \qquad (1.25)$$

whose kernel has the form

$$K = \frac{jk}{4\pi R}(1 + \cos\chi)\, e^{-jkR} \tag{1.26}$$

Analysis of the above equation shows that at $(r_m^2/\lambda L) \ll (L/r_m)^2$, where r_m is the mirror radius, L is the separation between the mirrors, and λ is the emission wavelength, the mirror size and separation are essential only in a specific combination and the only parameter of importance is the Fresnel number, $N_F = (r_m^2/\lambda L)$ which is approximately equal to the number of Fresnel zones seen in one mirror from the centre of the other. The solution of equation (1.25) for several cavity configurations, along with a more general analysis and some simplified methods of investigation, will be found in [94 through 98]. Therefore, the subsequent discussion will be solely concerned with the findings of interest to design work on the optical systems of laser oscillators.

Of all multitude of laser cavity configurations those of practical interest are cavities with spherical and plane mirrors. Spherical mirrors periodically focus the beam which is reflected from the mirrors in turn. A similar effect takes place in a periodic sequence of lenses which may be utilized as an optical transmission link. Any type of laser cavity may be approximated by an equivalent sequence of lenses. Tracing the travel of rays through equivalent optical systems provides an insight into many properties of these devices, including system stability and the losses of an unstable cavity. The travel of rays through different optical systems may be described in terms of a transfer matrix. At present, the matrix analysis of optical systems is a well developed technique, and a more detailed exposition of associated problems may be found in monographs and original publications (see for example [98]). A few points bearing on the stability and losses of spherical cavities are taken up below.

Resonators using spherical mirrors of arbitrary radii of curvature, R_1 and R_2, spaced a distance L apart may make up a stable or an unstable system. In a stable system, the beam reflected from the mirrors in turn is periodically focused, while in an unstable system the beam broadens more and more with each reflection. The condition for the system stability derived from the travel of rays through a periodic sequence of lenses which is an analogue of the laser cavity has the form

$$0 < (1 - L/R_1)(1 - L/R_2) < 1 \tag{1.27}$$

In graphic form, the stability of different cavities with arbitrary spherical mirrors is shown in the plot of Fig. 1.23, with the terms $1 - (L/R_1)$ and $1 - (L/R_2)$ laid off on the g_1 and g_2 axes. The

stability regions (shown unshaded) are bounded in the plot by a hyperbola described by the following equation

$$(1 - L/R_1)(1 - L/R_2) = 1 \qquad (1.28)$$

The mode fields for stable cavities are concentrated near the axis of the system more than the fields for unstable cavities. Because of this, diffraction losses for unstable cavities are many times

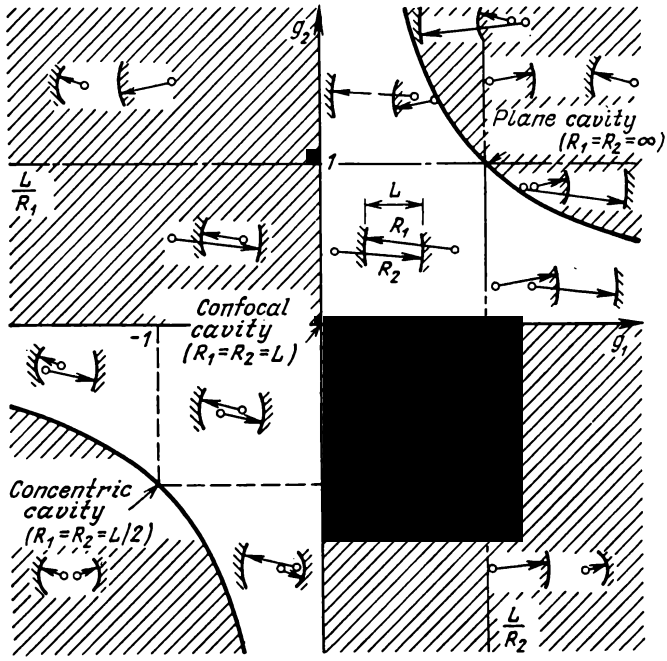

Fig. 1.23. Stability diagram of a laser cavity (the shaded areas represent instability regions)

those for stable cavities. Mirrors of the same configuration make up a stable or an unstable system, depending on the separation between them. The transition from a stable to an unstable condition (near the boundaries) becomes more sudden with increasing Fresnel number. A gradual transition is only possible in cavities with very small Fresnel numbers. As a cavity changes to an unstable condition, a sudden increase is observed in the absolute value of diffraction losses and in the difference in loss between the modes of different orders. The origin of coordinates in the stability diagram represents a confocal system using mirrors of equal curvature. In this case, diffraction losses for a given Fresnel num-

ber are a minimum. A concentric cavity ($R_1 = R_2 = L/2$) and a plane cavity ($R_1 = R_2 = \infty$) lie at the stability boundary.

Two concave mirrors or a concave and a convex mirror may make up both a stable and an unstable system, depending on the mirror curvature and mirror separation. In a hemispherical cavity made up of a plane and a spherical mirror, the natural mode field has the same structure as in a cavity using spherical mirrors spaced a distance $2L$ apart. Two convex mirrors may form only an unstable system.

As regards the spectral and spatial mode structure of the laser beam, the most important characteristics of the laser cavity are the

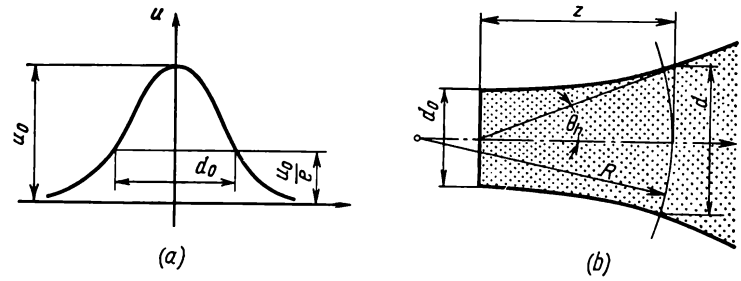

Fig. 1.24. (*a*) Electromagnetic field distribution and (*b*) beam parameters of the dominant mode

distribution spectrum of all possible modes, the difference in loss between the individual modes, and the volumes occupied by the various modes inside the cavity. There is a good deal of difference between stable and unstable cavities as regards all of these three factors.

Stable cavities. The intensity distribution of the light emission is affected by the modes excited in a laser cavity in a very complex manner. For example, the intensity distribution over the cross-section and the beam divergence widely differ for different orders of modes. In the lowest (dominant) mode, the beam intensity is purely Gaussian over the cross-section. The diameter, d_0, of such a beam is taken to be the distance over which the intensity falls off to $1/e$ of its maximum value. The Gaussian beam is contracted to its minimum diameter d_0 in a certain definite plane (the beam neck) where the phase front is plane (Fig. 1.24). The envelope of the beam is a hyperbola with asymptotes making with the axis the angle

$$\theta_h = 2\lambda/(\pi d_0) \qquad (1.29)$$

This angle is equal to the angle of diffraction in the far zone for the dominant mode. In sketch form, a stable cavity using mirrors

of different curvatures, R_1 and R_2, is shown in Fig. 1.25. In this cavity, the mirror surface coincides with the phase wavefront of the cavity modes. The diameters, $2d_1$ and $2d_2$, of the dominant

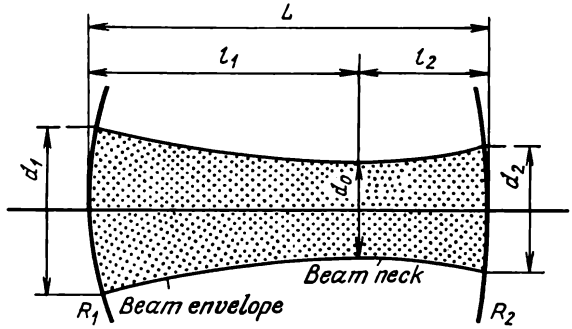

Fig. 1.25. Mode parameters in a cavity using mirrors of different curvatures

mode beam on the mirrors and the minimum diameter inside the cavity are defined as follows

$$d_1^4 = 4\left(\frac{\lambda R_1}{\pi}\right)\frac{R_2 - L}{R_1 - L}\,\frac{L}{R_1 + R_2 - L} \tag{1.30}$$

$$d_2^4 = 4\left(\frac{\lambda R_2}{\pi}\right)\frac{R_1 - L}{R_2 - L}\,\frac{L}{R_1 + R_2 - L} \tag{1.31}$$

$$d_0^4 = 4\left(\frac{\lambda}{\pi}\right)^2 \frac{L(R_1 - L)(R_2 - L)(R_1 + R_2 - L)}{(R_1 + R_2 - 2L)^2} \tag{1.32}$$

The distances l_1 and l_2 between the plane where $d = d_0$ and the mirrors (the "+" sign at l_1 and l_2 applies to the case shown in Fig. 1.25) are given by

$$l_1 = L(R_2 - L)/(R_1 + R_2 - 2L) \tag{1.33}$$

$$l_2 = L(R_1 - L)/(R_1 + R_2 - 2L) \tag{1.34}$$

The spectrum of resonant frequencies for low total losses in a cavity is given by

$$\nu/\nu_0 = (q + 1) + \beta/\pi \tag{1.35}$$

where ν is the resonant frequency of the respective mode and β is the phase shift depending on the cavity configuration.

For circular mirrors over a sufficiently wide range of values of N_F, g_1 and g_2 (except where they are very close to unity), the phase shift is

$$\beta = (2m + n + 1)\arccos\sqrt{g_1 g_2} \tag{1.36}$$

For other values of N_F and q, the phase shift is described by more complex expressions.

The loss γ depends on the Fresnel number, N_F, and the mode order, the dependence varying with type of cavity configuration. For a confocal cavity, the frequency spectrum may be described by

$$\nu/\nu_0 = (q+1) + \frac{1}{2}(m+n+1) \tag{1.37}$$

The dependence of losses for modes of different orders on the Fresnel number has the form

$$\gamma = \frac{2\pi (8\pi N_F)^{2m+n+1} e^{-4\pi N_F}}{\Gamma(m+1)\Gamma(m+n+1)} [1 + 0(1/2\pi N_F)] \tag{1.38}$$

where $\Gamma(m+1)$ and $\Gamma(m+n+1)$ are gamma-functions.

The beam diameters on the mirrors and inside the confocal cavity are small and independent of mirror size: $d_1 = d_2 = \sqrt{\lambda L}/\pi$, $d_0 = \sqrt{\lambda L}/2\pi$. Obviously, confocal cavities are unattractive because they are wasteful of laser rod volume with any reasonable cavity length.

In a plane cavity, the beam diameter may in principle be made equal to that of the mirrors, and this is why in a plane cavity the volume of the laser rod is utilized to advantage. The phase shift and losses for different modes are given by

$$\beta = (M_F/4\delta)\gamma \tag{1.39}$$

$$\gamma = 8K_{mn} \frac{8(M_F + \delta)}{[(M_F + \delta)^2 + \delta^2]^2} \tag{1.40}$$

where $\delta = 0.824$, $M_F = \sqrt{8\pi N_F}$, K_{mn} is the $(m+1)$st zero of the Bessel function of the nth order. As with the losses for confocal cavities, this expression is not valid at small Fresnel numbers where the losses are insignificant. Plane mirror cavities are simple to design and build, and they may conveniently be used where the presence of a great number of modes is of minor importance.

A plot of diffraction losses for the two lowest modes, TEM_{00} and TEM_{10}, as a function of the Fresnel number for the values of g applicable to a stable hemispherical cavity using circular mirrors [99] is shown in Figs. 1.26 and 1.27. The respective plots for the phase shifts are shown in Figs. 1.28 and 1.29.

The plots of Figs. 1.30 and 1.31 relate the losses for the TEM_{00} and TEM_{10} modes to the Fresnel number for a hemispherical and a spherical cavity using similar mirrors. The dotted curves represent the absolute losses for the dominant modes. It is seen from Fig. 1.30 that, although in a plane-parallel cavity the loss-versus-Fresnel number relation for these two modes yields a slightly inclined straight line, the absolute losses for large Fresnel numbers exceed those for cavities with a smaller g (especially in a hemispheric cavity). As will be recalled, in order to suppress higher

modes, it is essential that their absolute loss be greater than the gain of the laser material. In a plane-parallel cavity the absolute losses for the various modes are comparable with the gain of the

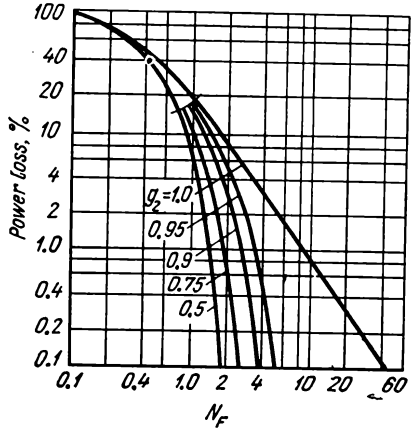

Fig. 1.26. Diffraction losses per pass for TEM_{00} mode in a stable hemispherical cavity with round mirrors ($g_1 = 1.0$)

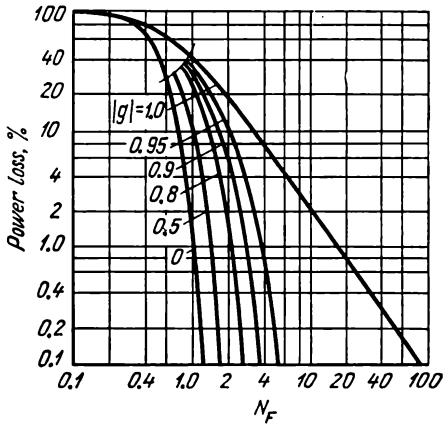

Fig. 1.27. Diffraction losses per pass for TEM_{10} mode in a stable hemispherical cavity with round mirrors

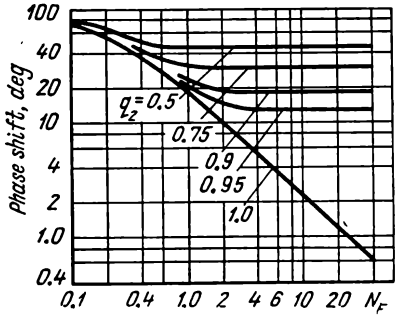

Fig. 1.28. Phase shift per pass for TEM_{00} mode in a stable hemispherical cavity with round mirrors ($g_1 = 1.0$)

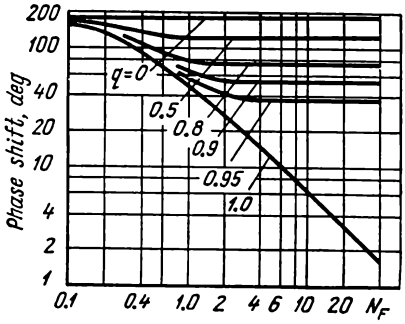

Fig. 1.29. Phase shift per pass for TEM_{10} mode in a stable hemispherical cavity with round mirrors

solid-state laser media. This is the reason why a plane-parallel cavity may advantageously be used for transverse mode selection by choosing a suitable Fresnel number for the cavity and a suitable gain for the laser material. Besides, the selected mode occupies a much greater volume in a plane-parallel cavity than in other cavities, a feature important from the viewpoint of utilization of the population inversion.

Unstable cavities. The stable cavities discussed above can be moved into an unstable state near the stability boundary (see Fig. 1.32) by suitably changing the separation between, or the curvature of, the reflecting mirrors. So that the output beam can be coupled out of such cavities, one of the mirrors is made partly

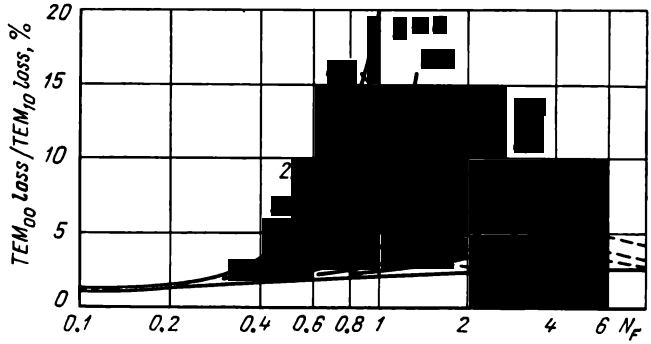

Fig. 1.30. Ratio of losses per pass for two lowest-order modes in a stable hemispherical cavity with round mirrors ($g_1 = 1.0$) (the dotted lines represent the constant-loss curves for the TEM_{00} mode)

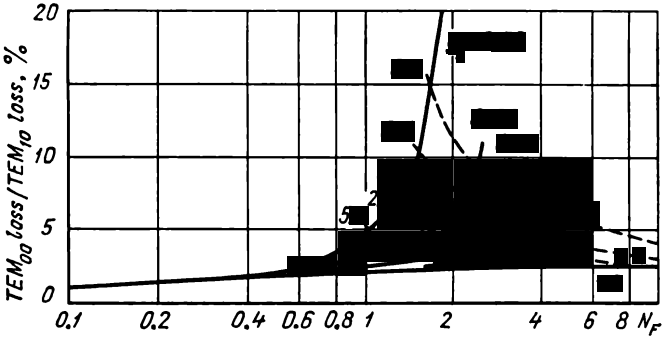

Fig. 1.31. Ratio of losses per pass for two lowest-order modes in a stable spherical cavity with round mirrors (the dotted lines represent the constant-loss curves for the TEM_{00} mode)

transparent. In cavities driven into an unstable state, the difference in diffraction loss between the various modes increases markedly [100].

Of considerable interest are cavities which show heavy diffraction losses and in which the spherical wavefront greatly increases in curvature on passing through the cavity (Fig. 1.31). The latter feature is the basis of the so-called annular output coupling, in which emission is coupled out of the cavity because during the final passes the beam diameter exceeds that of one of the mirrors.

Annular output coupling is often referred to as diffraction output coupling, although this name is not precise; it only brings out the fact that laser light is coupled out and diffraction losses occur over the same paths [101].

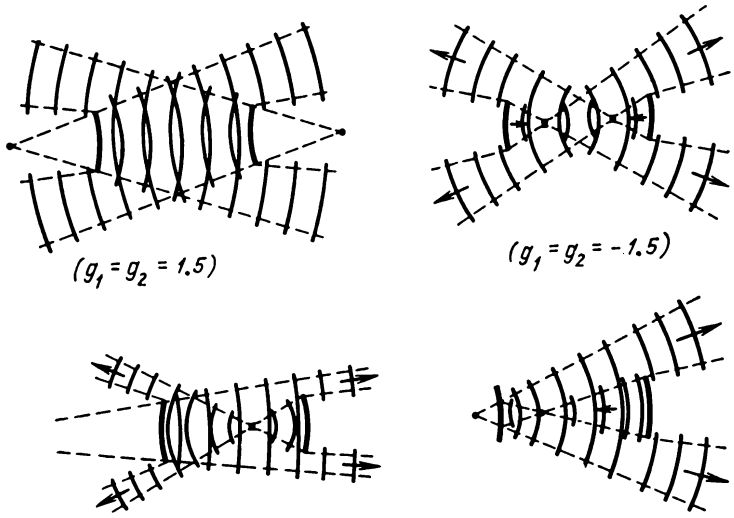

Fig. 1.32. Typical distribution of the emission field for unstable cavities in the various regions of the stability diagram

A very important characteristic of an unstable cavity is the linear magnification, M, of the spherical wave in the transverse direction as it passes from one mirror to another (in asymmetrical cavities, it is more convenient to consider the magnification for a round trip through a cavity). In the ray approximation, the linear magnification of a spherical wave determines the losses in a cavity. For a two-dimensional cavity these losses are $\gamma = 1 - (1/M)$, and for a threedimensional cavity, $\gamma = 1 - (1/M^2)$. An idea about the various modes existing in an unstable cavity (Fig. 1.33) can be gleaned from the ray consideration given with some rather rough approximations in [102]. The distribution function and attenuation constant obtained there for different modes have the form

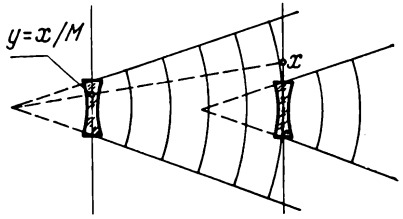

Fig. 1.33. Geometric construction for an analysis of wavefronts in an unstable cavity (an equivalent-lens system)

$$u_n(x) = x^n, \quad \gamma_n = 1/M^{n+1/2} \tag{1.41}$$

The distribution for the first four modes is shown in Fig. 1.34. As is seen, every next reflection from the mirrors causes the higher modes to lose more energy than the dominant mode.

In a first ray approximation, the average loss of energy per path for the lowest mode in an unstable cavity (in contrast to a stable cavity) is independent of mirror size or shape [98]

$$\gamma = 1 \pm \frac{1 - \sqrt{1 - (g_1 g_2)^{-1}}}{1 + \sqrt{1 - (g_1 g_2)^{-1}}} \tag{1.42}$$

In expression (1.42) the "+" sign is taken for the values of g lying in the first and third quadrants of the stability diagram, and the "—" sign for those lying in the remaining two quadrants.

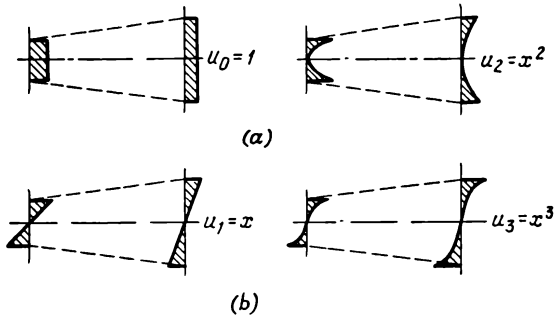

Fig. 1.34. Field distribution for the first four modes in an unstable cavity (ray approximation)
(*a*) symmetrical; (*b*) antisymmetrical

Loss calculations based on the ray approximation yield results differing greatly from the numerical solutions found by the Prony method for the matrix equation of the eigenvector describing the mode field distribution and the eigenvalue determining the losses of a given mode [103]. It is noteworthy that the mode losses are oscillatory with changes in the equivalent Fresnel number, $N_{ef} = N_F (g^2 - 1)^{1/2}$ and, as a consequence, one of the higher modes may well dominate the emission. On the other hand, it is difficult to choose a Fresnel number such that the lowest mode would be dominant, because we lack a precise analytical method for calculating the losses of an unstable cavity.

Unstable cavities include a telescopic cavity [104] consisting of a convex mirror ($R_2 > 0$) and a concave mirror ($R_2 = -[2L + R_2]$) arranged confocally. The linear magnification, M, for this cavity is $1 + (2L/R_2)$. In sketch form, a telescopic cavity along with its equivalent diagram is shown in Fig. 1.35. While in a plane-parallel cavity multiple reflections from the mirrors lead to an accumulation of disturbances in the wavefront because of edge diffraction,

in a telescopic cavity the emission field spreads only after several traverses because the beam core has a small diameter and the mirror edges have at first a very insignificant disturbing effect on the emission field. It is only when the beam diameter approaches the mirror size that diffraction comes to markedly affect the transverse structure of the emission. A special feature of telescopic cavities is that a convergent light wave with a periodic curvature may develop. In passing repeatedly through the cavity, the convergent waves which appear due to light scattering may grow in intensity by several orders of magnitude. The accompanying field

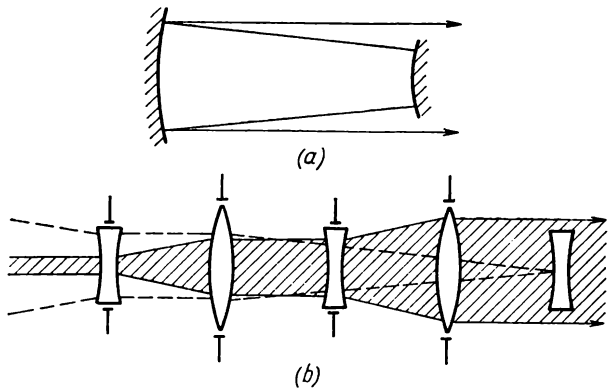

Fig. 1.35. (*a*) Telescopic cavity and (*b*) equivalent diagram

build-up near the cavity axis may redistribute a considerable number of excited atoms across the laser rod and change the emission pattern as a consequence.

Apart from the telescopic cavity configuration discussed above, there may be telescopic cavities of ring geometries.

Optical cavities in laser oscillators. The optical cavity of a practical laser oscillator differs from an unfilled optical cavity in several important respects, namely: (1) the laser rod and other elements are optically non-uniform because of imperfections in the material, residual strains, scattering centres, etc; (2) the laser material may further be made optically non-uniform by non-uniform optical pumping; (3) the population inversion may be distributed across the rod diameter likewise non-uniformly; (4) the operation of the cavity may be affected by saturation and by the excitation of several modes; and (5) the cavity elements may be improperly adjusted and aligned.

In the final analysis, these factors may combine to produce a greater angular spread and several longitudinal modes. The increase in angular spread may be due to both a great number of

transverse modes and the wave-front distortion caused by an optically non-uniform laser material, with the result that the wave-front of the emission associated with the highest-Q modes may strongly differ from a plane one. Many workers refer to this as "mode deformation". The relevant problems are reviewed in [105].

Of the elements making up a laser optical cavity, it is the laser rod that shows the highest optical non-uniformity. Incidentally, ruby crystals show a considerable non-uniformity because of blocks, slip planes and stress gradients (in contrast to neodymium-doped glass which has a very high uniformity). When a plane wave with a diffraction-induced spread is allowed to pass through a ruby crystal, the output emission shows appreciable amplitude and phase distortion and a marked increase in the beam divergence mainly traceable to the presence of microstresses [43]. If this optically non-uniform crystal be used as a laser material, the beam divergence will be determined not so much by the mode structure of the cavity, as by the optical non-uniformity of the crystal. In fact, the optical non-uniformity of the laser material greatly affects the mode structure of the emission, notably transverse mode selection [44]. For example, a plane-parallel reflector cavity using an optically uniform ruby crystal will consistently generate a single mode (the lowest TEM_{00} mode) with the pump power exceeding the threshold by a considerable amount (up to 70%), while in the same cavity using a crystal of low optical uniformity the single-mode operation can be maintained consistently only within a very narrow range of pump power (not more than 5% above the threshold). The effects of various light scaterring sources (slip planes) are examined in [43, 44]; it is also shown that macroscopic imperfections mainly affect the core of the distribution, while light scattering by microscopic imperfections affect the "wings" of the distribution.

In plane-parallel cavities, the various optical inhomogeneities are most strongly felt across the beam diameter. Practically, it often happens that higher transverse modes are excited, which mask the losses due to the optical non-uniformity of the laser material.

Most readily, this type of optical distortion occurs in laser rods because, in contrast to other laser components, they are exposed to both output emission and pump energy. Even in single-pulse operation this may cause a marked increase in the beam divergence. Cases have been reported where the beam divergence angle towards the end of the pump cycle doubled in a laser using a neodymium-doped glass rod [112] or increased three to five times in a ruby laser [123]. Thermally induced optical distortions still more strongly felt in the rods of lasers operating on a periodic basis [117-120] or continuously [124]. In these cases, however, the

distribution of optical distortions does change with time and can readily be compensated for by adding an appropriate element (say, a lens) to the cavity. It is likewise possible to correct the wavefront in Q-switched lasers where the pump-induced temperature distribution cannot practically change during the generation of a light pulse. Thermal distortions are mainly responsible for aberrations even in neodymium-doped glass normally showing a high optical uniformity. The possibilities of fully correcting thermal distortions are rather limited. Among other things, thermal distortions in the polarized light can be corrected by using flat rods and through a careful selection of temperature and optical constants for laser materials [18, 105, 122].

The effect of variations in the distribution of pump energy in polished cylindrical rods on the mode structure of the emission is discussed in [126, 127].

In cylindrical rods with a rough surface around the diameter, the pump energy is usually distributed symmetrically, being in the centre of the crystal 1.5 to 2 times that at the edges. The concurrence of transverse modes under conditions of a non-uniform pump energy distribution is discussed in [128]. If the ratio of pump intensity to losses, I/ρ, may be approximated by a sum of intensities of the lowest modes, then the oscillations will be excited in precisely these modes. Under such conditions, both mode deformation and overall angular spread will be small. Most often, this situation occurs when the ratio I/ρ gradually falls off in going from the centre to the edge of the cavity. The intensity of the lowest mode in this case is much higher than it is with a uniform pump energy distribution (provided there are no thermal strains). When I/ρ is a minimum at the axis of the laser rod, the beam divergence is usually noticeable and increases with increasing asymmetry in the pump energy distribution, being affected by both multi-modal operation and mode deformations [105].

The gain saturation of a laser rod in the free-running operation does not entail any marked deformation of the dominant transverse mode, provided the variations in the gain are small (15% between the axis and periphery of the rod). In the Q-switched operation, however, that is, at high values of gain, the gain saturation brings about considerable inhomogeneities in the mode profile, increasing with increasing Fresnel number [129].

The effect of gain saturation is especially noticeable on longitudinal modes. As the inverted population at the loops of a sustained mode is depleted, this mode may die out to give way to modes which can readily be sustained by a region with an "undepleted" inverted population [130].

The accuracy with which the mirrors are adjusted for parallelism is likewise a major factor. Should the mirrors be out of paral-

lelism, the light spot may be pulled out in the far zone, or it may even break up into several spots if the mirrors are out of parallelism by a large amount. Laser cavities with a uniform laser material are especially susceptible to lack of parallelism.

Selection of axial modes. Given a large Fresnel number and, as a consequence, small diffraction losses, the Fabry-Perot cavity is prone to favour the resonance of uniform plane waves propagated in both directions along and at some angle to the axis. As a result, standing waves appear in the cavity, satisfying the condition of resonance

$$q\lambda = 2L \cos \theta_i \tag{1.43}$$

where q is an integer and θ_i is the angle between the beam and the cavity axis. At $\cos \theta_i = 1$, these modes are called axial. The frequency spacing between axial modes is $\Delta\nu = (2L)^{-1}$. The same frequency spacing exists for axial modes in a cavity using spherical mirrors. A multitude of axial modes can be excited in a Fabry-Perot cavity because the field of a standing wave is spatially non-uniform relative to the active centres of the rod. The active centres at the loop of a mode readily lose excitation through interaction with the mode photons, while the centres at the nodes undergo no induced transitions in the field of that mode. These centres are sources of energy for other modes. Axial modes can most effectively be selected with tilted Fabry-Perot etalons used either as a frequency filter placed internal to the laser [131] or as the end, or resonant, reflector [132]. Because of convenience the latter has come into widest use (see for example [87]). The frequency spacing between adjacent reflectivity maxima or minima is $\Delta\nu_p = (2nD)^{-1}$ (see Sec. 1.2). The value of D is chosen such that the constant of one of the etalons, say, the plate, be close to the fluorescence line width, and that of the other will ensure a sufficient difference in reflectivity to suppress the cavity mode adjacent to the axial mode located at the maximum of the fluorescence line [134]. A cavity incorporating a resonant reflector is in effect a complex cavity.

Axial modes can be suppressed and the separation between them can be controlled in other types of complex cavities. One variety of a complex cavity is the so-called coupled cavity in which there is at least one more reflecting surface (for example, the ends of the optical elements) between the end reflectors. In this system the natural frequencies are not equidistant, and the gain for the various modes depends on the cavity configuration [73]. In such complex cavities, the maximum Q is obtained at frequencies which are the same for different arms. By adjusting the cavity length and the transmission coefficient of the middle mirror, it is possible

to obtain oscillation at one coincident frequency and to attenuate appreciably or suppress altogether the remaining ones.

Still another variety of the coupled cavity is that built along the lines of the Michelson interferometer (Fig. 1.36). The coincident frequencies of the resonators $L_2 + L_1$ and $L_2 + L_3$ suffer no losses at the beam splitter. According to [135], the system losses at non-coincident frequencies, equal the transmission coefficient of the beam splitter, with one amplifying medium placed in the arm L_2

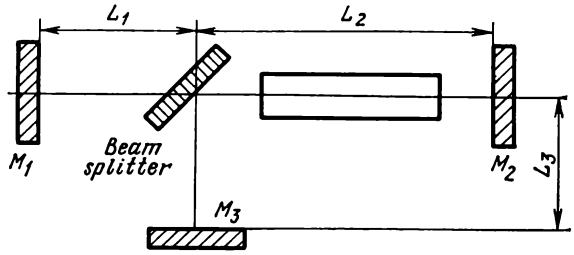

Fig. 1.36. Complex cavity of the Michelson interferometer type
M_1, M_2, M_3 — mirrors

or two amplifying media of about the same gain in the arms L_1 and L_2, such that $L_1 = L_3$, are given by

$$T_{splitter} \approx \sin^2(\pi/m) \approx (\pi/m)^2 \qquad (1.44)$$

where m is the number of axial modes in the longer cavity. When an amplifying medium is placed in the arm L_1 or the arm L_3 and if the shortest length is associated with the cavity $L_2 + L_3$ or $L_1 + L_2$, the losses become

$$T_{splitter} = 4\frac{\sin^2(\pi/m)}{1 + (4\pi/m)^2} \approx \frac{4(\pi/m)^2}{1 + 4(\pi/m)^2} \qquad (1.44a)$$

As is seen, the selectivity of such systems is increased three or four times. The beam splitter may be a polarizing prism [136] whose transmission axis makes an angle of 45° with the plane of polarization of the laser light (Fig. 1.37). The losses in this case are likewise given by expression (1.44).

The spatial non-uniformity of mode fields can be eliminated by replacing standing waves with a unidirectional propagation of emission in a travelling-wave cavity. According to [137], in travelling-wave operation, the emission spectrum width for ruby can be reduced from 1 cm^{-1} down to one axial mode, with only a small amount (not over 20%) above the threshold energy required for lasing action.

As an alternative, the spatial non-uniformity of the mode field can be eliminated by causing the active centres to move relative

to the standing waves along the cavity axis [106]. This can be done in two ways, namely either by mechanically shifting the laser rod [125], or by modulating the refractive index in the cavity in antiphase on each side of the rod, while keeping the optical path of the cavity unchanged. As a result, the nodes and loops of the modes will vibrate about active centres [133].

In [57, 81] it is reported that the emission spectrum of a laser has been reduced in the pump energy range from 1 to 1.2 $E_{threshold}$ by shifting the condenser and ruby rod assembly along the cavity axis at a rate of 40 cm/s.

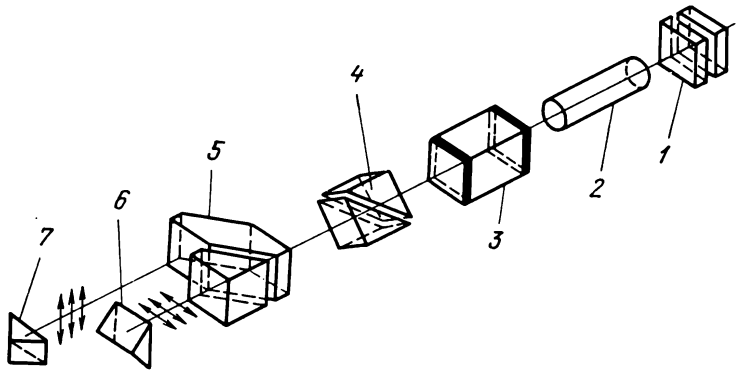

Fig. 1.37. Optical schematic of a split-cavity laser oscillator
1—resonant reflector; *2*—ruby rod; *3*—KDP electro-optic shutter; *4*—Glan-Foucault prism; *5*—polarizing beam-splitter; *6, 7*—roof prisms

Transverse mode selection. In order to reduce the angular spread of the laser beam, resort is made to different methods for minimizing the number of transverse modes and their deformations. With an ideal laser material and a uniform pump energy distribution, mode deformations are small, and the number of modes mainly depends on the relative magnitudes of diffraction and non-selective losses. To improve angular mode selection under the circumstances, it is necessary to increase diffraction losses for off-axis modes.

The simplest and most natural method for angular mode selection is to reduce the Fresnel number through the use of pinholes. A pinhole in the cavity, along with an increase in diffraction loss for off-axis modes, leads to an increase in absolute losses. With pinholes chosen by trial and error, effective mode selection is feasible, even though the laser material and other cavity elements may be inhomogeneous [100]. Pinholes or physical apertures also remove the possibility of distortions in the pulse waveform and the mode structure of the laser emission caused by gain saturation

in a Q-switched laser [129]. A pinhole can select one transverse mode in a cavity of any configuration, including those using parallel-plane mirrors [138]. Instead of pinholes or physical apertures, use may be made of attenuating filters whose transmission varies with radius in the same manner as the emission distribution in the mode being selected. Of special interest from this point of view are controlled stops utilizing the piezo-optic effect as in electro-optic shutters [139]. In a controlled piezo-optic stop the transmission over the cross-section may be adjusted to vary according to, say, the dominant transverse mode. This stop can be turned on by energizing the electro-optic shutter with a periodic voltage which will set the crystal into mechanical vibrations.

Another approach to improving the utilization of the laser rod is to place a pinhole at the common focus of two lenses arranged in front of a mirror in a plane-parallel cavity [140] or in the central plane of a coaxial cavity [141]. In this case, however, the limit to the generated power will be set by spontaneous air breakdown in the pinhole. In [142] the mode filter was a bleachable absorbing dye solution. The action of this dye "pinhole" is based on the non-linear relationship between the transmission coefficient and the emission density. In the case of a non-uniform distribution in the population inversion the conditions for oscillations may be quite different at the various points across the beam.

Still another method for angular mode selection based on a reduction in the Fresnel number is to increase the cavity length [143]. However, under conditions of heavy aberrations, an increase in the cavity length leads to a marked increase in diffraction losses, and this in turn results in a decrease in laser power output. A still more serious roadblock to the practical employment of this method for mode selection is the relationship existing between the cavity length and the clear diameter of the output beam. The cavity length increases in proportion to the square of the radius of the laser beam and becomes practically unfeasible with a radius of 0.5 cm.

Angular mode selection may advantageously utilize Fabry-Perot etalons tipped at an angle to the axis of the laser. For its operation, this type of mode selector depends on the fact that in a Fabry-Perot etalon the transmission is a function of not only wavelength but also of the direction of emission. Angular mode selection, or beam angle narrowing, in two planes will require the use of two Fabry-Perot etalons [131].

A further method of angular mode selection, called the CIR (critical internal reflection) technique, is based upon the sensitive dependence of reflectivity on the incidence angles near the critical angle [144]. This purpose may be served by single- or multiple-reflection prisms, such as Lummer-Gehrcke plates or composite

prisms [144, 145]. According to [146], a rhombic prism can halve the beam divergence in comparison with a plane-mirror cavity.

Still more attractive are end reflectors having a variable reflection corresponding to the emission distribution of a given mode. Variable-reflection end reflectors may be built as mirrors with a multi-layer dielectric coating deposited in such a manner that only one transverse mode is reflected [147], or as stacks of plates (Lummer-Gehrcke plates) with a variable diameter, owing to which the angular spread can be brought down by a factor of 1.2 to 1.5 [148].

Diffraction losses for the unwanted modes can effectively be increased by reducing the stability of the laser cavity. This can be done either by suitably adjusting the separation between the mirrors in spherical and hemispherical cavities, or by including in a (say, plane-parallel) cavity an element that would shift the cavity into an unstable region (see Fig. 1.23).

Shifting the cavity into an unstable region improves the effectiveness of the above discussed methods for angular mode selection. For example, where angular mode selection utilizes pinholes, shifting the cavity into an unstable region makes it possible to increase the pinhole diameter [149].

Cavities with diffraction-coupled output use no selective elements, and their selectivity is solely due to the marked difference in losses between the various modes because of cavity instability. These cavities utilize large-size homogeneous laser rods. In order that the angular beam spread can be held to a minimum in unstable cavities, the laser material must be extremely homogeneous optically and pumped uniformly [105]. Besides, as experiments with a telescopic cavity have shown, the diffraction divergence angle encompasses not all of the energy; a greater proportion of energy is distributed over a range of angles up to several minutes of arc [150]. This factor limits the use of a telescopic cavity laser as a single-mode master oscillator in an amplifying system of high power output, brightness and contrast *.

1.5. Optico-Mechanical Shutters

To obtain short and strong light pulses, solid-state lasers employ special devices which control losses in the cavity. These devices, known as shutters, may be classed into several types according to the method of control. Optico-mechanical shutters control the reflection or transmission of light either by shifting the optical elements of the cavity or by mechanically deforming the elastic medium in which the emission is propagated.

* By "contrast" is meant the ratio of the maximum pulse energy to the background energy.

Shutters which intercept the light beam are made as thin metal discs (with an aperture on its periphery) mounted on the shaft of a high-speed motor [151]. In a plane-parallel cavity, the rotating disc is located in the focal plane of two confocal lenses which reduce the beam diameter to a few tenths of a millimetre, while in a spherical cavity the disc is mounted at the narrowest point of the beam. The switching time of this shutter is usually at least several microseconds and is determined by the rotational speed of the disc, the beam diameter, and the distance from the aperture to the axis of rotation. In this type of shutter, strong light pulses may damage the edges of the aperture and also set off a spark

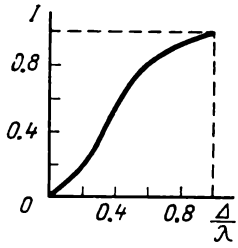

Fig. 1.38. Reflected light intensity as a function of air gap (in units of λ)

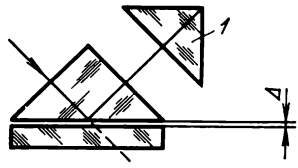

Fig. 1.39. Sketch of an optico-mechanical contact shutter

breakdown in the air. For these reasons, disc shutters have so far been used on a limited scale.

Light control may be based on the relationship that exists between total internal reflection and the gap between two dielectrics separated by a distance comparable with the wavelength. The reflectivity of a thin air layer at the interface between two media is illustrated in Fig. 1.38, and may range from 0 to 1. The operating principle of this type of shutter will be clear from reference to Fig. 1.39. The control voltage applied to a piezo-electric slab causes its thickness and, as a consequence, the air gap, Δ, to change. The air gap and the control voltage are chosen such that the air gap between the slab and prism reduces to zero when the voltage is applied. Depending on the position of the end roof prism *1*, the shutter may be caused to open either when the voltage is applied or when it is removed. A similar type of shutter is described in [153]. It should be noted that the shutter opens slowly, the switching time being from 5 to 10×10^{-6} s, and also experiences considerable molecular forces at the optical contact. It takes a force of 20 to 50 kg/cm^2 to separate two glass plates. Contact shutters have not found use in laser oscillators, either.

In some cases, it is convenient to use a shutter in the form of a mirror oscillating about a middle position at its natural frequency of mechanical resonance under the action of an alternating magnetic field. This type of shutter may be a mirror mounted on the free end of a tapering cantilever rod. To make up for reaction, the root end of the rod is made fast to a solid base. The system is caused to vibrate by the interaction of the alternating magnetic field with two levers fabricated from a magnetic material and arranged near the embedded end of the tapering rod. Utilizing mechanical resonance, the mirrors in such systems may be twisted through angles up to several degrees by small forces. Over a single oscillation, the mirror will take up the middle position corresponding to the maximum Q twice, and so the pulse repetition frequency will be equal to twice the resonant frequency of the oscillating mirror. The maximum rate of oscillations is limited by the strength of the material from which the tapering rod is fabricated, and also by the distortion of the mirror surface due to the high centrifugal acceleration. This type of shutter can be employed in lasers operating at high pulse repetition frequencies and small beam apertures. In [154], for example, this method was used to switch the Q of a garnet laser continuously pumped at 5000 Hz.

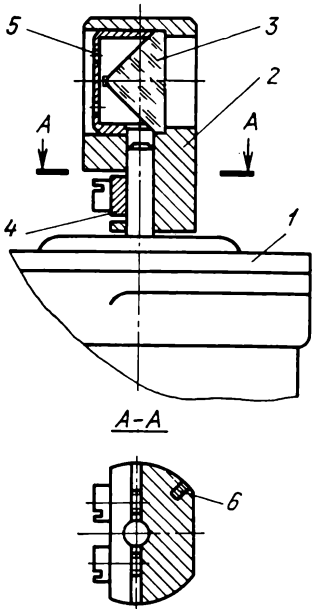

Fig. 1.40. Optico-mechanical shutter using a spinning prism

In Q-switches, widest use has been made of spinning-prism or spinning-mirror shutters.

These optico-mechanical shutters mainly use roof prisms because of their low sensitivity to the wobbling of the motor shaft and high stability to the action of strong radiation.

In sketch form, the arrangement of an optico-mechanical shutter using a roof prism is shown in Fig. 1.40. The shaft of a high-speed motor *1* carries a total internal reflection (TIR) prism *3* set up in a mount *2*. The mount is attached to the motor shaft by a clamp *4*. The prism *3* and the cover *5* of the mount are held in place with ЭД6-8 cement. The depth of the bore which locates the prism is chosen such that the centre of gravity of the prism lies on the axis of rotation. Then the centrifugal forces acting on the prism will be kept to a minimum. By rotating the cover *5*, the prism edge is

positioned to be at right angles to the axis of motor rotation. The firing time of the flash tube is controlled by a magnet *6* press-fitted into the mount.

The prism is fabricated from K-8 glass or fused quartz, with the hypotenuse and side faces highly diamond-polished to impart them a better stability towards radiation. The tolerances for the physical dimensions of the prism and the requirements for its material are listed in Fig. 1.41. It is important to keep the chamfer on the right-angle side to a minimum. The prism mount, especially the part beyond the chamfer, must be thoroughly polished and have

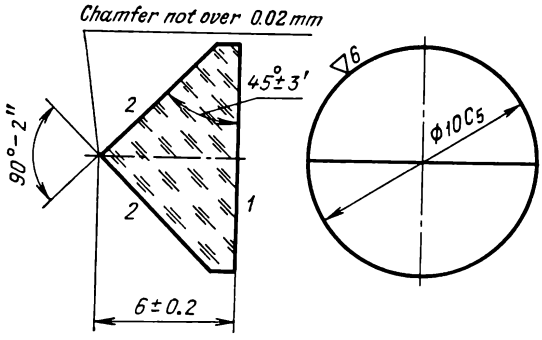

Material specifications	Δn_D	–
	$\Delta(n_F - n_C)$	–
	Homogeneity	1
	Birefringence	1
	Light absorp.	00
	Striae	15
	Bubbles	1
Manufacture specifications	N_1	0.2
	ΔN_1	0.1
	N_2	0.1
	ΔN_2	0.1
	π	1'
	P	IV
	cl. dia.	9

Fig. 1.41. Drawing of, and specifications for, a roof prism

a high reflectivity so that the emission passing through the prism chamfer will not destroy the mount.

This type of shutter calls for an utmost care in manufacture, assembly, and the balancing of the spinning prism together with the motor rotor. Lack of balance, especially at high speeds, will inevitably reduce the service life of the bearings, give rise to fatigue failure of the structural members, and increase vibration and noise. Among other things, lack of balance may be due to the axial or radial wobbling of the parts mounted on the rotating shaft. In designing an optico-mechanical shutter, it is important to specify appropriate tolerances on residual unbalance and to provide for its compensation.

Lack of balance may be due to misalignment between the axis of inertia and the axis of rotation. Unbalance may be static and dynamic. Static unbalance occurs when the centre of gravity of a rotating member is shifted relative to the axis of rotation. The axis of rotation is parallel with the axis of inertia (Fig. 1.42*a*), and the separation between them, or eccentricity (*e*), represents the off-set of the centre of gravity. A purely static unbalance can be revealed by mounting the assembly on knife edges. A poorly

balanced assembly will rotate on the knife edges until the centre of gravity takes up the lowest position.

Dynamic unbalance occurs when the axis of inertia revolves around the axis of rotation, with the centre of gravity lying on the axis of rotation (Fig. 1.42*b*). Dynamic unbalance manifests itself only during rotation. As rotational speed increases, the dynamic load on the supports due to the centrifugal forces of the unbalanced masses increases in proportion to the square of the speed, and so the assemblies of an optico-mechanical shutter must be

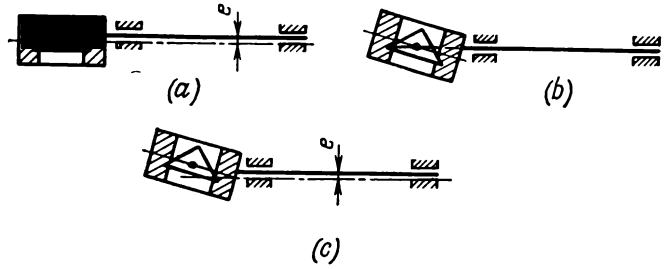

Fig. 1.42. Types of unbalance
(*a*) static unbalance; (*b*) dynamic unbalance; (*c*) overall unbalance

balanced dynamically. A quantitative estimate of unbalance is given [155] by

$$F_c = m_w R_w \omega_w^2 \tag{1.45}$$

where F_c is the centrifugal force, m_w is the mass of a counterweight, R_w is the radius of the point where the counterweight is installed

$$m_w = G_w / g; \quad F_c = (G_w / g) R_w \omega_w^2 = (\omega_w^2 / g)(G_w R_w) \tag{1.46}$$

where G_w is the counterweight, g is the acceleration due to the pull of gravity, $\omega_w = \pi n_w / 30$ is the angular frequency of rotation, and n is the number of revolutions per second.

For a comparison between rotating assemblies differing in weight, use may be made of specific unbalance, that is, the amount of unbalance $G_w R_w$ per kilogram of a rotating member (this quantity has the dimensions of length and is expressed in μm). The limit of residual unbalance for the rotating part of a spinning-prism shutter may be 0.3 to 0.8 μm. In high-speed assemblies, the residual unbalance can be compensated for by drilling holes or soldering drops of solder in planes located near the supports.

The prism or mirror may be mounted on the motor shaft in cantilever fashion (see Fig. 1.40), if the rotational speed does not exceed 30,000 rpm and the clear diameter is not over 10 mm. With

rotational speeds exceeding 30,000 rpm and with clear diameters exceeding 10 mm, preference should be given to the design shown in Fig. 1.43 where use is made of Class C radial-axial bearings, with a stiff distance sleeve between the outer races of the ball bearing and with an axial interference of 5 to 8 kg. For normal operation of the assembly over a wide temperature range and in order to minimize wobbling, the ball-bearings should be mounted on the shaft with a clearance of 0.001 to 0.004 mm. The bearings

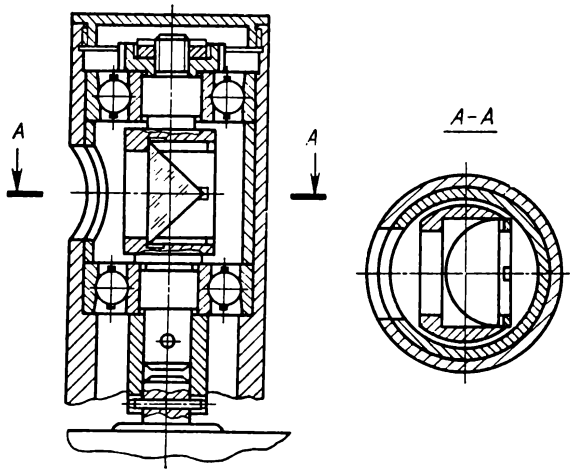

Fig. 1.43. Spinning prism mounted on two bearings

should be made a sliding fit, because even a slight amount of interference would drastically increase run-out. The outer race of the bearing should be a guaranteed fit with a clearance anywhere between 0.002 and 0.008 mm. In order to satisfy these requirements, each location should be adjusted individually to the actual size of a ball-bearing.

The prism may be rotated by high-speed turbines or electric motors. Some of the motor types suitable for this application are listed in Table 1.11.

When an optico-mechanical shutter is employed as a Q-switch, an optimum position for the prism which ensures a maximum power output is that in which the apex of the prism divides the diameter of the laser rod into two parts equal in area. The shift of the prism apex by 10% of the rod diameter would decrease power output by as much as 20% [156]. The main requirements for this type of shutter is high switching speed and low losses in the open condition [157].

Synchronization between the shutter and the flash tube in a laser oscillator can be provided by photoelectric, electromagnetic,

and electric-spark devices. With a photoelectric device, the rotor that carries the prism also mounts a mirror which illuminates the photo-electric detector in a definite position of the prism. The mirror is in turn illuminated by a low-power light source. The time by which the electric signal leads the operating position of the spinning prism can be adjusted by varying the position of the photo-electric detector. With an electromagnetic device, the motor rotor carries a permanent magnet which, just as it passes near the air gap, completes the circuit of a solenoid, and a current pulse is induced in its winding. With an electric-spark device, the electric pulse is generated in a high-voltage circuit by a spark discharge which is set off when a metal vane attached to the mount of the spinning prism moves through the spark-gap.

Table 1.11

Motor type	Rpm	Torque, gram-cm	Service life, hours	Temperature range, °C	Operating voltage, V
ДИД-1 Та two-phase induction motor	18,000	9	1500	−60 to +100	36
ДИД-2 Та two-phase induction motor	18,000	18	1500	−60 to +100	36
ДП-13	14,500	50	300	−60 to +50	27
ДП-33	14,500	50	300	−60 to +50	
АВС-1000/2А three-phase induction motor	60,000	20	250	±50	27
АВС-1000/4 three-phase induction motor	30,000	20	250	±50	40
Д-16 d.c. two-pole motor	13,750	100	70	50	27
АДП-124Б	12,000	125	50	−40 to +70	110
МГ-30-400А	11,000	270	500		115
ДИД-1Т4 two-phase induction motor	20,000	14		−60 to +100	36
ДИД-2Т4 two-phase induction motor	20,000	27		−60 to +100	36

Despite the "wandering" of the beam axis, low efficiency, motor noise and vibration, optico-mechanical shutters incorporating a spinning prism have come into wide use in controlled-action lasers owing to simplicity of design and adjustment, reliability, and capability to operate over a wide temperature and spectral range.

For its operation, an optico-acoustical shutter depends on changes in the refractive factor of a medium due to the propagation of an ultrasonic wave. The controlled-loss media may be optical elements fabricated from fused silicon [158] or fused quartz [159] which are set in oscillation by means of a piezo-optical transducer. In a fused-quartz block, this transducer sets up a travelling axial sound wave, with the result that the laser beam is deflected by the discontinuities produced by periodical changes in the refractive index.

An optico-acoustical quartz shutter is convenient in YAG lasers. It shows low losses because of high transmittance at $\lambda = 1.06$ μm and good reproducibility at frequencies up to several kilohertz, owing to which the emission amplitude varies by not more than 1%. In order to change from Q-switching to continuous operation, it will suffice to remove the high frequency from the transducer. The upper limit of the Q-switching rate in this type of shutter for continuously pumped YAG lasers is only limited by the properties of the laser material. This type of laser operating at 55 kHz is reported in [159]. This type of shutter is also suitable for mode-locking operation [160].

1.6. Phototropic Shutters

For their operation, phototropic (bleachable absorbing dye solution) shutters depend on the use of optical materials which absorb radiation at resonance. Depending on emission density, the transmission may either increase or decrease. In laser engineering, use is mainly made of materials whose transmission increases with increasing radiation intensity. These materials are employed to decouple amplifier stages and also to switch the Q of laser oscillators. The interaction between laser emission and a resonant-absorbing medium is examined in [161] which also includes an extensive bibliography. The discussion that follows will only be concerned with some aspects of non-coherent interaction between light and a resonant-absorbing medium essential to a proper understanding of the operation of phototropic shutters in lasers, and also the properties of the most commonly used resonant absorbers.

Resonant absorbers. The phototropic shutters employed at present are, with a few exceptions, resonant-absorbing materials added to optically transparent media. These shutters become transparent due to saturable absorption at the resonant wavelength. A great number of optical saturable absorbers are known, and their number will undoubtedly grow through the intensive search that is under way. The resonant absorption that can be employed to control ruby emission is displayed by many blue-green dyes, notably porphyrins, such as tetrabenzo-tetrazoporphyrins of diffe-

rent metals, known as phthalocyanines (Fig. 1.44). Their natural analogy is chlorophyl; polymethine dyes such as cryptocyanines, indanthrene, thiazine and some other dyes [162-164]. Of these materials, the most interesting are phthalocyanines which show a considerable light-fastness. Free phthalocyanine answers the formula $C_{32}H_{18}N_8$. The structural formulae of phthalocyanine and of its metal-organic compounds are shown in Fig. 1.45. In principle, it is possible to obtain compounds of phthalocyanine with any metal in the periodic table. At present, there have been obtained phthalocyanines of lithium, sodium, potassium, copper, silver, beryllium, calcium, zinc, cadmium, barium, mercury, aluminium, gallium, tin, lead, zirconium, hafnium, titanium, germanium, vanadium, antimony, chromium, molibdenum, manganese, iron, cobalt, nickel, platinum, palladium, osmium, praseodymium, erbium, uranyl, and some others. The molecular absorptions spectra of different phthalocyanine derivatives, their energy level diagrams, and energy level transition

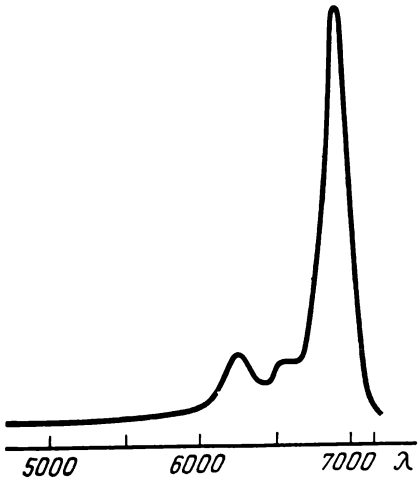

Fig. 1.44. Typical plot of absorption coefficient as a function of wavelength, λ, for phthalocyanines

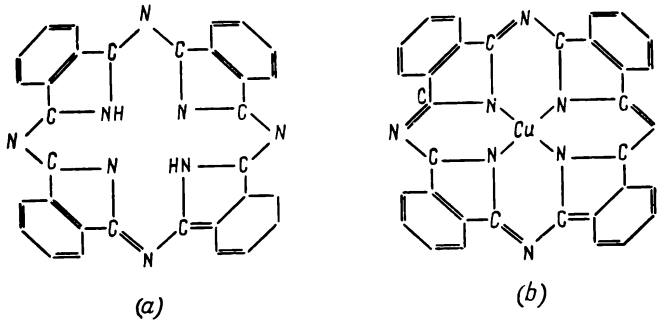

Fig. 1.45. Structural formulae of (*a*) phthalocyanine and (*b*) copper phthalocyanine

probabilities are to a great extent determined by the type of metal atoms. The neutral matrix into which the molecules of a phtalocyanine derivative are introduced also plays a marked part.

It is possible to prepare both solid and liquid solutions of phthalocyanines. So far, the attempts to employ solids with an addition of metallo-phthalocyanines have not yet yielded positive results. For example, a film fabricated from polyvinyl alcohol with an addition of copper phthalocyanine [165] has an insufficient light fastness. Of greater practical importance are liquid solutions of phthalocyanine derivatives. A specific feature of nearly all phthalocyanines is low solubility in many organic solvents. Phthalocyanine derivatives may be dissolved in various saturated hydrocarbons and their derivatives (such as heptane, octane, carbon tetrachloride, and some others), alcohols (ethanol, α-chlor-naphthalene), heterocyclic compounds (diethylene oxide, pyridine), and compounds of organic origin (turpentine). A typical energy level diagram for a molecule of metallo-phthalocyanine is shown in Fig. 1.46. With saturable absorption, singlet transitions of the form $S \rightarrow S^1$ play the most important part, the life time of reverse transitions, $S \leftarrow S^1$, being, as a rule, short (10^{-9} to 10^{-8} s). The fact that molecules undergo transitions of the form $S^1 \rightarrow T^1$, $S \rightarrow T$ and $T \rightarrow S$ may markedly affect the dependence of absorption coefficients upon radiation intensity. The solvent not only affects the structure of the S and T levels in the absorbing molecules, but also sets thresholds for the occurrence of self-focusing [166], stimulated Raman scattering, and stimulated Brillouin scattering. The Raman scattering thresholds for several solvents in comparison with those for CS_2 are given in [167]. The thresholds for stimulated Brillouin scattering, in terms of the threshold length of a cell in centimetres for a ruby laser, are listed in [168]. An analysis of publications on metallo-phthalocyanine solutions reveals several features in the absorption of light by these media. Among other things, an increase in the refractive index of a solvent tends to cause a red shift in the maximum of the absorption spectrum, λ_{max}. In lasers of a relatively low power output, use may be made of phthalocyanines of Groups III and IV of the periodic system, because these compounds form a multiplicity of solutions with a relatively high refractive index. In high-power lasers, it appears advantageous to employ phthalocyanines of the metals in Groups V through VII of the periodic system, because their solutions show high thresholds of self-focusing and stimulated scattering. There is a marked spread in relaxation time, τ, associated

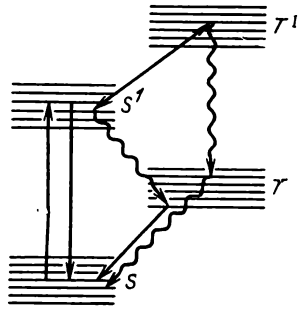

Fig. 1.46. Generalized energy level diagram of a phthalocyanine molecule

S and S^1 — ground and excited states; T and T^1 — triplet states

with the $S \rightarrow S^1$ transitions, between different solutions of metallophthalocyanines. For example, for solutions of magnesium phthalocyanine in diethylene oxide, toluene, pyridine, ethyl alcohol and acetone, the relaxation time respectively is 6.5×10^{-9}, 8.1×10^{-9}, 8.6×10^{-9}, and 3.0×10^{-9} s (see, for example, a summary table in [165]). This spread in τ between various media is explained by the fact that the life time of excited states is strongly dependent on the character of metal atoms and the type of solvent. In cases where the relaxation time for an $S^1 \rightarrow T$ transition is shorter than it is for the $S^1 \rightarrow S$ transitions, that is, when $\tau(S^1 \rightarrow T) < \tau(S^1 \rightarrow S)$, a greater proportion of molecules will be accumulated at triplet levels. As a rule, solutions with $\tau(S^1 \rightarrow T) < \tau(S^1 \rightarrow S)$ will not fluoresce and have a life time which is by two or three orders of magnitude greater than the life time of the excited state for fluorescing solutions for which $\tau(S^1 \rightarrow S) < \tau(S^1 \rightarrow T)$. For the emission of a ruby laser ($\lambda = 0{,}69$ μm), the absorption cross-section takes values anywhere between 10^{-16} and 10^{-17} cm^2. The spectral properties of metallo-phthalocyanines are examined in [162-164].

Within the emission region of neodymium-doped glasses ($\lambda = 1.06$ μm), resonant absorption is manifested by many polymethine dyes [162], for example, a range of thiapentacarbocyanines differing in anions (Nos. 2171, 2172, 2173, etc.), alkyls bonded to the nitrogen atoms (Nos. 2139, 2140, etc.), substituents in heterocyclic radicals (Nos. 3976, 3977, etc.). According to the type of solvent (methyl alcohol, pyridine, nitrobenzene, quinoline, alpha-nitrobenzene, etc.) the position of the absorption band maximum for different polymethine dyes may range from 0.98 to 1.09 μm, with some tendency to shift in the direction of longer wavelengths with an increase in the refractive index of the solvent. A major disadvantage of most polymethine dye solutions is that they are not sufficiently resistant to strong light which causes in them irreversible photochemical reaction. Besides, some dyes would decompose in long storage.

A polymethine dye in a combination with a liquid solvent may likewise be introduced into polymers. There is a mention in [169] of a polymethine-dye triacetate film prepared from a solution of cellulose triacetate in methylene-chloride with an addition of the dye dissolved in the same solvent. The film was 125 to 140 μm thick. The absorption band in this type of film is not so well defined as it is in a liquid solvent (Fig. 1.47). According to [169], polymethine-dye film may be stored for 8 to 10 months at 4° C without any appreciable changes in its characteristics. Depending on the density of light energy passing through the film, its triacetate base will be destroyed by from one to several light flashes.

It should be noted that organic dyes will not be fully bleached even by very strong radiation. Among other things, the residual losses may be due to the absorption of light by the dye molecules in excited states, that is, due to an $S^1 \rightarrow T^1$ transition. Another cause for residual losses lies in the bubbles that form, as laser emission is absorbed by irregularities, such as aggregations of dye molecules. According to [170], the "microexplosions" of these absorbing irregularities set off by a light pulse may produce bubbles a few tens of microns in diameter, which collapse in a matter of 10^{-3} to 10^{-1} s. These microbubbles form at a particularly high

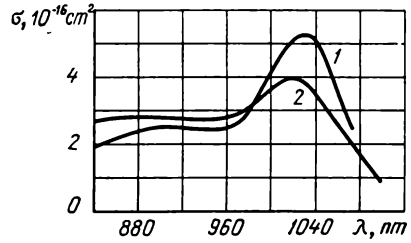

Fig. 1.47. Effective absorption cross-section, σ, as a function of wavelength, λ, for (*1*) a dye solution in nitrobenzene and (*2*) triacetate film

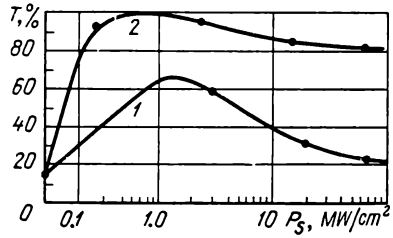

Fig. 1.48. Transmission, T, as a function of bleachable power per unit area, P_S, for solutions of vanadium phthalocyanine in toluene prepared by (*1*) mechanical stirring and (*2*) prolonged boiling

rate in solutions which contain sufficiently large aggregations of dye molecules (their presence is revealed by the violet opalescence of the liquids), the bubble formation being dependent on the manner in which the solution is prepared and may be enhanced if the solution is stirred or the pressure reduced. Figure 1.48 relates the transmission to the intensity of the bleaching radiation for two solutions of vanadium phthalocyanine in toluene, one of which was prepared by mechanical stirring at room temperature, and the other by boiling for a long time, which, as will be recalled, destroys molecule aggregations. A similar relationship exists between the power of light radiation and the transmission of polymethine dyes. The maximum bleaching of phthalocyanine solutions and polymethine dyes depends also on the initial optical density of the solution, which, for the most commonly used solutions, lies anywhere between 2.0 and 0.5. The maximum transmission attainable under the action of radiation ranges from 60 to 90%.

In addition to the organic dyes listed above, bleachable properties are displayed by, for example, KC-19 glasses [171] which may be used to control the radiation of ruby lasers and in which the principal dopant consists of semiconductor particles of CdSe in-

corporated in a glass matrix. Saturable absorption in these particles raises the transmission of the medium. From the viewpoint of controlling the emission of neodymium-doped glass lasers there is some interest in glasses with an addition of uranyl, UO_2^{**} [172] which can be bleached by light from flash tubes. However, these and similar materials have not yet found wide use as light-shutter materials.

Interaction of light emission with saturable optical absorbers. The manner in which laser radiation interacts with a saturable absorber depends on the duration of the light pulse, t_p, and the life time of the excited state, τ. For a better insight into physical processes taking place at different ratios of t_p and τ (assuming a two-level model), two cases are noteworthy, namely when the duration of the light pulse is considerably shorter than the relaxation time of the bleached state ($t_p \ll \tau$), and when the relaxation time of the bleached state is comparable with or is less than the duration of the light pulse ($t_p \geqslant \tau$). These cases can be investigated on the basis of the balance equations whose applicability is discussed in [161], and the mechanisms by which saturable absorbers (phototropic media) are bleached in [170-182]. In [173, 174, 176, 178, 179], it is shown that, neglecting relaxation to the main state, the bleached state of two-level and multi-level saturable absorbers varies in a wavelike manner. In the wake of a travelling wave of bleaching, the material is transparent to laser light. In two-level saturable absorbers [173, 176, 179], the populations of the energy levels equalize, while in a three-level absorber the energy levels may undergo a wavelike population inversion [174, 179]. The passage of a monochromatic light pulse through a layer containing two-level absorbers may be described by a system of equations for photon density, $\Phi(x, t)$, and the populations of the energy levels, $N_{1,2}(x, t)$ [178, 179]

$$\partial\Phi/\partial t + c\,\partial\Phi/\partial x = -\sigma c\,(N_1 - N_2)\,\Phi \tag{1.47}$$

$$(\partial/\partial t)(N_1 - N_2) = -2\sigma c\,(N_1 - N_2)\,\Phi + N_2/\tau \tag{1.48}$$

where σ is the photon absorption cross-section, c is the velocity of light through the medium, and τ is the life time of the excited state.

Equations (1.47) and (1.48) hold under the following initial and boundary conditions:

$$\Phi(x=0, t) = \Phi_0(t); \quad N_1(x, t=0) = N_0(t); \quad N_2(x, t=0) = 0 \tag{1.49}$$

If the life time of an excited state is many times the pulse duration, the last term in equation (1.48) may be dropped. Then for a rectangular light pulse and a uniform distribution of absorbing centres in a medium with a high initial optical density ($\sigma N L_m \gg 1$),

the solutions of equations (1.47) and (1.48) for Φ and $N = N_1 - N_2$ under the boundary conditions given in (1.49) will obviously be wavelike [176, 179]

$$\Phi(x, t) = \Phi_0 \{1 + \exp[\sigma(N_0 + 2\Phi_0)(x - vt)] - \exp[2\sigma\Phi_0(x - ct)]\}^{-1} \quad (1.50)$$

$$N(x, t) = N_0 \{1 + \exp[-\sigma(N_0 + 2\Phi_0)(x - vt)] - \exp[-\sigma N x]\}^{-1} \quad (1.51)$$

while the velocity of the travelling wave of saturable absorption is given by

$$v = 2\Phi c (N_0 + 2\Phi_0)^{-1} \quad (1.52)$$

It follows from the solutions given in (1.50) and (1.51) that the saturable absorption wave has a finite width and is shaped at a finite distance from the wave boundary. The wave width, with the absorption coefficient decreasing from its maximum value, $\alpha_0 = \sigma N_0$, to $1/210^{-p}\alpha_0$, is given by

$$\Delta = [\ln 10(10^p - 2)][\sigma(N_0 + 2\Phi_0)]^{-1} \quad (1.53)$$

where $p > 1$, $\tau_{bl} = (N_0 + 2\Phi_0)L/2\Phi_0 c$ is the time for which the wave bleaches the layer; $\tau'/\tau_{bl} = \ln 20/\sigma N_0 L_m$ where τ' is the time of wave formation, and L_m is the layer thickness.

It is important to note that the wave velocity is independent of σ. Yet a bleaching wave occurs at high values of photon cross-section, $\sigma \gg 1/NL_m$. This corresponds to high optical thicknesses, $D \gg 1$, where $D = \alpha_0 L_m$. It follows from (1.50) and (1.51) that the wave width corresponds to the optical density of the medium, $Df \gtrsim 4$. Thus, the wavelike bleaching can be obtained with optical thicknesses $D \gtrsim 2Df \gtrsim 8$. In diagrammatic form, the bleaching wave in a two-level phototropic medium is shown in Fig. 1.49. The profiles of the various wave parameters correspond to (1.50) and (1.51). At $t_p \gtrsim \tau$, the relaxation term in equation (1.48) cannot be neglected, and a solution for the equations with arbitrary values of parameters can only be obtained by numerical methods. These computations will be found in [175, 178, 180].

Consider the physical aspect of the relaxation case [178, 179]. Over the time $\Delta t \approx \tau/2$, the medium will be traversed by a bleaching wave distorted by relaxation very little. As a result, the slope of the pulse leading edge will increase, while the trailing edge will be deformed less because it will "see" the medium partly bleached by its leading part. Therefore, pulses for which $t_p = \tau$, become asymmetrical on emerging from the medium [161]. The parameters of the emerging pulses for which $t_p \gg \tau$ may be derived from an analytical solution of the system in the quasi-stationary approximation, that is, by satisfying the condition $d\Phi_0(t)/dt \ll \tau^{-1}\Phi_0(t)$ and neglecting the derivatives in (1.47) and

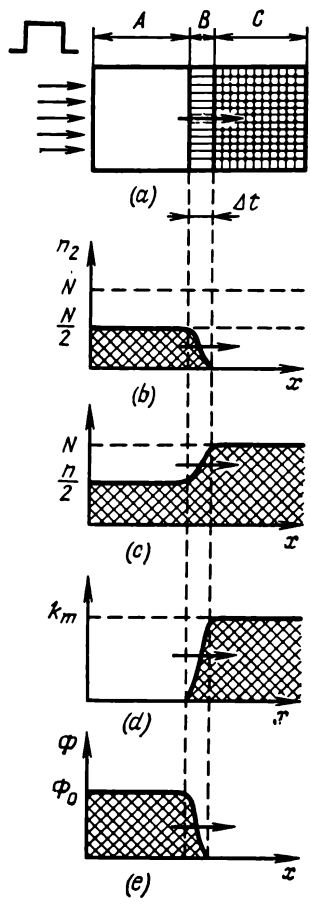

Fig. 1.49. Qualitative presentation of the bleaching effect in a medium with one kind of uniformly distributed absorbing centres, due to a rectangular pulse of resonant emission

(*a*) one-dimensional medium (*A*—bleached region; *B*—bleaching layer; *C*—unbleached region); (*b*) and (*c*) changes in the population inversion of levels *2* and *1* with the passage of a bleaching wave; (*d*) and (*e*) absorption coefficient and photon density of a medium as a function of position at a fixed instant of time

(1.48). Then, an implicit solution for the photon density in the medium will take the form [178]

$$\ln \frac{\Phi(x, t)}{\Phi_0(t)} = 2\sigma\Phi_0(t)\, c\tau \left(1 + \frac{\Phi(x, t)}{\Phi_0(t)}\right) - \sigma N_0 x \qquad (1.54)$$

It follows from (1.54) that a bleachable medium will transmit predominantly that part of the pulse for which the input energy flux density satisfies the condition $P_{in} \geqslant \alpha_0 L_m (h\nu/2\sigma\tau)$. Also, a decrease in the pulse height will be accompanied by a decrease in its duration because of clipping (strong absorption) of its leading and trailing edges.

Explicit solutions for equation (1.54) are given in [178]. According to [178], on passing through a solution of vanadium phthalocyanine at $D = 13$, the duration of the laser pulse was reduced to one-third of its original value. Figure 1.50 shows combined oscillograms of an input laser pulse at $\lambda = 1.06$ μm ($D = 0$) and of pulses passing through a solution of a polymethine dye in a variable-depth cell at $D = 9$. The energy of the input pulses was 0,3 J and their duration at half-height was 60 ns. It is seen that an increase in the optical density of the phototropic medium was accompanied by a decrease in the rise time and duration of the output pulses. A marked change in the output pulse occurred at $D \geqslant 5$. At $D = 9$, the pulse rise time (from 50% to 100% of its final value) reduced to one-fifth, and the pulse duration at half-height decreased to one-fourth in comparison with the input pulse. The clipping of the pulse leading edge was accompanied by a slight change in the form of the remaining portion of the pulse. At $D > 10$, the pulse duration was reduced still more due to the clipping of the trailing edge.

The experimental data cited above confirm that an optically dense medium is bleached in a wave-like manner. With this bleaching mechanism, the rise time of the output pulse decreases with increasing optical density, while the pulse waveform is affected most at $D > 4$. The average velocity of the bleaching wave can be determined from the above data, using the following approximate relationship: $v = L_m/\tau_p$, where τ_p is the duration of the clipped-off part of the pulse as determined at half-height of the original pulse, and L_m is the thickness of the medium. At $D = 9$, $L = 0.15$ cm, $\tau_p = 60$ ns. Thus, a bleaching wave is propagated through a solution of polymethine dye at a velocity of $v = 2.5 \times 10^6$ cm/s, or $0.8 \times 10^{-4}\ c$, where c is velocity of light in

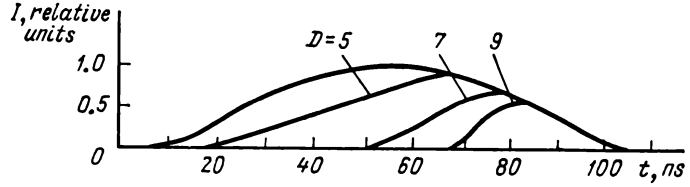

Fig. 1.50. Light pulses transmitted by a solution of polymethine dye of varying optical density, D

a vacuum. Taking this value of v and the experimental value of the absorption coefficient, $\alpha_0 = 60$ cm^{-1}, for low energy flux density (at $\lambda = 1.060$ μm), we find from the relation $t_r = (\alpha_0 v)^{-1}$ that the rise time of the output pulse is $t_r = 7$ ns. This figure checks well with the value of t_r obtained experimentally (6 to 10 ns at $D = 9$).

As already noted, there is already at present a great number of materials widely differing in relaxation time. Also the duration of pulses generated by laser oscillators varies over a wide range. Therefore, in tackling practical problems that involve the use of phototropic (bleachable) shutters, it is important in some cases to match the relaxation bleaching time to the light pulse duration so as to ensure an optimum cooperation between the light emission and the saturable absorber.

For example, in Q-switched lasers, the phototropic shutter is bleached by spontaneous emission to a level necessary to support the build-up of oscillations. Then the stimulated emission bleaches the shutter to a maximum value of transmission. With this arrangement, the lasing action is rapid. Obviously, in such cases preference should be given to a non-relaxation interaction between the emission and the saturable absorber, because relaxation losses would only upset the conditions of oscillation.

When phototropic shutters are employed to provide optical isolation between amplifier stages, the losses involved in maintaining the bleached state are not so great as in Q-switching. A shutter employed to isolate amplifier stages should be bleached only by the light pulse being amplified and not by spontaneous superfluorescence during optical pumping. Because of this, one is forced to employ phototropic media with a high optical density. Depending on the relative values of the duration of the pulse being amplified and the relaxation time of the excited states in a phototropic medium, the amplifier can either clip only the leading edge of the pulse (at $t_p \ll \tau$), or clip both the leading and trailing edges and limit the pulse height at the same time (at $t_p \gtrsim \tau$) [178]. The remaining portion of the pulse will pass through the medium without any losses of energy. The order of magnitude of the rise time, t_r, of such a pulse after its travel through the medium will be determined by the time over which the bleaching wave travels a distance equal to the wavefront width, that is $t_r \approx l_0/v_{bl}$. The value of l_0 is inversely proportional to the absorption coefficient at low energy flux density, that is, $l_0 \approx 1/\alpha_0$. Therefore, the pulse rise time is [178]

$$t_r = 2.5\,(h\nu/\sigma P_{in})$$

where P_{in} is the peak energy flux density of the input pulse in W/cm^2.

When phototropic shutters are employed to produce picosecond pulses by the mode self-locking method, additional factors come into play, which limit the relaxation time of the bleached state. The point is that in such cases the laser resonator oscillates in several axial modes and the intensity fluctuates with a characteristic time of the order of t_1/m, where t_1 is the quantum transit time in the cavity, and m is the number of modes existing in the cavity [151, 183]. Over the time t_1, the number of fluctuation spikes is m, and their height is random. If a phototropic shutter is to respond to the individual fluctuation spikes under such conditions, the relaxation time of the bleached state should be considerably shorter than t_1/m. Under the circumstances, a non-linear absorber will suppress small fluctuations in intensity more than strong fluctuations, so that the strongest fluctuation spike will be amplified and differentiated faster than the remaining ones and will in the long run bring about saturable absorption. Thus, in cases where picosecond pulses are to be produced, use must be made of materials with as short relaxation times of excited states as practicable.

Construction of phototropic shutters. Of practical interest among phototropic shutters are the liquid and film types. A liquid phototropic shutter is a glass or quartz cell filled with a solution of

a saturable optical absorber in an organic solvent. The cell may be fabricated from a heavy glass (or quartz) ring and two plane-parallel plates brought in perfect optical contact with the ring (Fig. 1.51). On its side, the ring has a filling hole. After filling, the hole is stopped with a ground glass or a PTFE stopper. Before they are brought into intimate optical contact, the cell parts are lapped flat to one fringe ($N = 1.0$), with a local error of not over 0.2 fringe ($\Delta N = 0.2$), and the entrance windows of the cell are made parallel to within 5 to 10 seconds of arc. Good cells can

Fig. 1.51. Solution cell

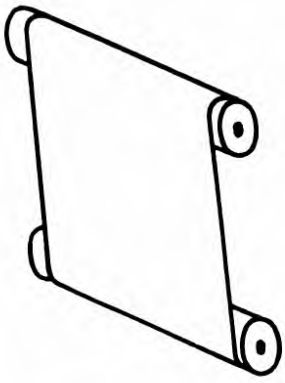

Fig. 1.52. Film shutter

be fabricated from K-8 glass. The solution depth is usually kept to a minimum (anywhere between 1 and 3 mm). An increase in the solution depth would increase losses due to stimulated Brillouin and Raman scattering. Besides, cells of low depth will shift the ray less when oriented at the Brewster angle to the incident light. To extend the service life of the solution, the diameter of the liquid-holding space should exceed the clear diameter, or suitable grooves should be made in the plane-parallel plates. As an alternative, cells may be of welded design. They are well adapted to generate nanosecond and picosecond pulses. They are also indispensable in all experiments where one has to adjust the concentration of the dissolved saturable optical absorber.

The construction of a film shutter is to a great extent determined by the instability of bleachable films to strong radiation (Fig. 1.52). This requires that the film be moved to an exposed portion for the next laser firing every or a few light pulses. As is seen in Fig. 1.52, this is done by a combination of two rolls, one paying out and the other taking up the film. This arrangement is quite sufficient because no special adjustment is necessary for

thin phototropic films. Because of the difficulties in the fabrication of phototropic films, the concentration of an optical saturable absorbing material cannot be matched precisely to the changing requirements of a specific experiment, and one has to be content with what is provided by the film types available. In some applications, for example as optical isolators between amplifier stages, this is quite sufficient (see page 88). A major advantage of film shutters is that they control the laser beam with a large cross-sectional area.

1.7. Electro-Optic Shutters

Electro-optic shutters utilize either the linear (Pockels) electro-optical effect in solids and liquids (Pockels shutters) [184] or the quadratic (Kerr) electro-optical effect (Kerr cells) [185].

An electro-optic shutter consists of an electro-optic or modulating crystal controlled by an electric field and placed between a polarizer and an analyzer (Fig. 1.53).

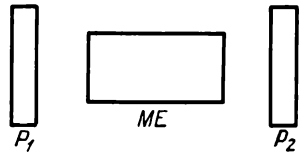

Fig. 1.53. Optical schematic of a half-wave shutter
P_1 — polarizer; ME — modulating (electro-optic) element; P_2 — analyzer

The performance of an electro-optic shutter is basically decided by the polarizer and the electro-optic crystal. The properties of electro-optic materials and the performance of electro-optic shutters are discussed in [186-191] which also contain a detailed bibliography. The discussion that follows will only be concerned with the behaviour of electro-optic shutters related to laser engineering.

Electro-optic elements based on the Pockels effect. At present, electro-optic elements are most commonly fabricated from crystals of class $\bar{4}2m$. With existing crystal-growing techniques, these crystals can be obtained with fairly good optical and mechanical properties. This is especially true of potassium dihydrogen phosphate (KDP), ammonium dihydrogen phosphate (ADP), rubidium dihydrogen phosphate (RDP), deuterium-doped potassium dihydrogen phosphate (DKDP). Other crystals in this class, namely DADP, ADA, KDA, RDA, and CDA, are not yet used on a practical scale, although some of their properties make them interesting for use in shutters.

With crystals of class $\bar{4}2\,m$ used in electro-optic elements, several arrangements are possible for the orientation of the electric field, the direction of light propagation and its polarization relative to the principal axes.

An analysis of optical indicatrix shows that when the field is directed along the optic axis, OZ, crystals in class $\bar{4}2\,m$ become biaxial, with their main axes, OX' and OY', making an angle of

45° with the OX and OY crystallographic axes, and the refractive indexes along the new axes become

$$n_{x'} \approx n_o + {}^1/_2 n_o^3 r_{63} E$$
$$n_{y'} \approx n_o - {}^1/_2 n_o^3 r_{63} E \qquad (1.55)$$

where n_o is the refractive index of the ordinary wave, and r_{63} is an electro-optic constant.

If light is directed along the OZ axis and its plane of polarization coincides with the OX direction, two orthogonally polarized components of equal amplitude will be propagated in the crystal

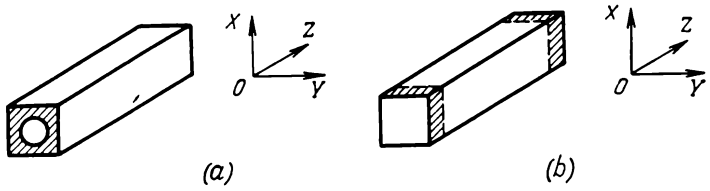

Fig. 1.54. Pockels modulator made from KDP crystal (the shaded areas are electrodes)

with different velocities. On travelling a distance l, these components will experience a phase shift, Γ, equal to

$$\Gamma = \frac{2\pi l}{\lambda}(n_{x'} - n_{y'}) = \frac{2\pi}{\lambda} n_o^3 r_{63} l E = \frac{2\pi}{\lambda} n_o^3 r_{63} V = \pi \frac{V}{V_{\lambda/2}} \qquad (1.56)$$

The quantity $V_{\lambda/2} = \lambda/2 n_o^3 r_{63}$ is the half-wave voltage.

With the above described orientation of the electric field, direction of light, and light polarization relative to the main axes, one has what is known as the longitudinal linear electro-optic effect. It is widely utilized in electro-optic elements fabricated from KDP crystals. With any other orientation in the direction and polarization of light relative to the main axes, the performance of a shutter will markedly be affected by the natural double refraction of the crystals.

Physically, a modulating element which utilizes the longitudinal electro-optic effect takes the form of a round or rectangular rod [189] with its length along the Z axis being 2 to 2.5 times its transverse dimension (Fig. 1.54). The electric field is established in the crystal by applying a suitable voltage to two electrodes with holes for the light beam (Fig. 1.54*a*), or to electrodes made to the side surface near the ends of the modulating crystal (Fig. 1.54*b*). Since the resultant electric field is not uniform, the piezo-electric voltage appearing across the crystal is likewise non-uniform, and the half-wave voltage does not remain constant in the radial di-

rection. However, these variations are unimportant for most applications of this type of shutter in lasers. The ends of the modulating crystal are made flat to a surface finish of Class 14, aligned parallel to within 5 to 10″.

Apart from the so-called primary or "true" electro-optic effect discussed above, the properties of the modulating crystal are greatly affected by the secondary or "false" electro-optic effect caused by the strains that are produced in the crystal by application of the electric field due to the reverse piezo-electric effect. These strains bring about additional changes in the refractive index. The effect of strains on the electro-optic properties of crystals under conditions of a static or slowly varying electric field are discussed in [186]. For KDP crystals with an electric field applied in the [001] direction, the expression for the total electro-optic constant has the form

$$r_{63} = r'_{63} + d_{36} p_{66} = r'_{63} + d_{36} c_{66} \pi_{66} \qquad (1.57)$$

where r_{63} is the electro-optic coefficient of a mechanically unconstrained crystal; r'_{63} is the electro-optic coefficient of a mechanically constrained crystal, corresponding to the true electro-optic effect; $d_{36}p_{66} = d_{36}c_{66}\pi_{66}$ is a quantity describing the elasto-optic effect specified by the piezo-electric modulus d_{36} and the elasto-optic coefficient p_{66} or the elastic stiffness constant c_{66} and the piezo-optic coefficient π_{66}. If the electric field changes in a shorter time than it takes the crystal to attain a state of equilibrium, elastic vibrations may be set up in the crystal [190]. Best of all, the effect of fast alternating fields on the behaviour of crystal has been investigated for KDP crystals.

The effect of the piezo-acoustical vibrations set up by a harmonic voltage on the overall electro-optic constant is investigated in [192]. The modulating elements of laser shutters are controlled by rectangular electrical pulses with fast rise times of the order of 10^{-9} to 10^{-8} s, and with durations from 0.1 μs to a few milliseconds. Because of this, what counts most is not the vibrations examined in [192], but the transients in the crystal that cause these vibrations to build up or damp out. The findings of an experimental study in the transmission of shutters incorporating axial modulating elements controlled by rectangular pulses are summed up in [193]. As is shown in Fig. 1.55, the pulse transmitted by the shutter has a level portion only at the beginning, which is followed by complex vibrations of high amplitude due to the superposition of several harmonic vibrations. As the height of rectangular electrical pulses approaches the half-wave voltage, distortions in the light pulse decrease in proportion to changes in the slope of the modulating characteristic of the shutter. The duration of the

undistorted portion of a light pulse is determined by the velocity of propagation of the shear strain wave from the periphery to the centre of the crystal. In [193], the velocity of a shear wave computed for a KDP crystal on the basis of the transmission-*versus*-time characteristic of the shutter is given to be 1.8×10^5 cm/s. Knowing the dimensions of a crystal in a plane normal to the Z-axis, the beam diameter and the beam position relative to the geometric axis of the crystal, it is possible to find the maximum duration of light pulses not distorted by the piezo-optic effects. The duration

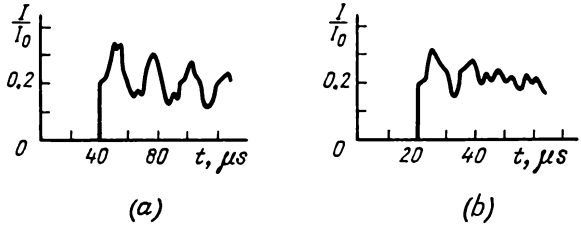

Fig. 1.55. Time plot of the transmission of a shutter activated by a rectangular electric pulse

(*a*) Pockels modulator made from KDP crystal measuring 24×24×50 mm; (*b*) Pockels modulator made from KDP crystal measuring 10×10×36 mm. The pulse height was 3.5 kV

of an undistorted portion of a light pulse is usually a few microseconds, after which the light pulse is distorted by the vibrations set up in the crystal. The amplitude and spectrum of these vibrations depend on crystal type, modulating-element geometry, method of mounting, and several other factors.

In addition the phase difference is also dependent on temperature. In a KDP modulating crystal utilizing the longitudinal electro-optic effect, the passage of the laser beam produces a radial temperature gradient. According to [194], this temperature gradient leads to an additional phase difference

$$\Gamma_T = \frac{2\pi n_o^3}{\lambda} \int_0^l a_{66}(x, y, z)\, dz \qquad (1.58)$$

where $a_{66} = p_{66}\varepsilon_6$, and ε_6 is the strain.

Thus, the phase difference brought about by the temperature gradient can be found, if one knows the strain field across the modulating crystal. In most practical cases, however, especially for single-shot pulses, the value of Γ_T is too low to affect operation of the laser.

At present, KDP, RDP, ADP, and DKDP crystals satisfy the requirements for shutter materials to a sufficient degree [191]. The leading characteristics of these crystals (transmission spectra,

electro-optic and piezo-optic coefficients, refractive indexes, distortion and temperature characteristics) have been investigated with sufficient detail in [188, 191]. The main criteria for application in lasers are low absorption (0.3-1) %/cm and low transmission in crossed polarizers.

In present-day technology, the principal materials for laser shutters are KDP and DKDP crystals. Although they have a fairly high half-wave voltage, they serve as a basis for most laser-beam devices in the wavelength region from 0.4 to 1.2 μm. Other crystals in this class either have no advantages over KDP and DKDP crystals, or they cannot be prepared to have satisfactory optical characteristics.

A disadvantage of KDP and DKDP crystals is their tendency to pick up moisture. Because of this, they need suitable protection in operation. In laboratory conditions and with proper care, however, KDP modulating crystals can be operated for a long time with their faces unprotected.

The situation is different as regards the use of other crystals as laser modulating elements. Cubic crystals in classes $\bar{4}3\,m$ and 23, such as CuCl, ZnSe, ZnTe, $Bi_1(GO_4)_3$, $N_4(CH_2)_6$, $Bi_{12}(GeO_{20})$, $N(C_2H_4NH_2HCl^-)_2$, $N(C_2H_4NH_2HBr^-)_2$ hold out little promise because of the difficulties in preparing large specimens with good optical properties.

Of considerable interest are crystals with high electro-optic coefficients, such as $BaTiO_3$, $Sr_xBa_{1-x}Nb_2O_6$, $K_{0.6}Zi_{0.4}NbO_3$, $KaTa_xNb_{1-x}O_3$, $KSr_2Nb_5O_{15}$ [187—189]. At room temperature, these crystals are ferroelectrics and display a much stronger electro-optic effect than KDP crystals. However, the prospects of using them as laser modulating elements have not yet been defined.

The use of crystals in class $3m$ [$LiNbO_3$, $LiTaO_3$] has been reported for example in [195, 196]. With these crystals, the best arrangement is such that the electric field is at right angles to the OZ axis and light is propagated along the optic axis [189]. In passing through the optical indicatrix, a plane normal to the OZ axis produces an ellipse with its major axes making an angle γ with the crystallographic axes, OX and OY, such that $\tan 2\gamma = E_x/E_y$. As the ratio E_x/E_y is changed, the ellipse rotates. The magnitude of the electro-optic effect characterized by the phase difference Γ depends only on $|E|$

$$\Gamma = (2\pi/\lambda)\, n_o^3 r_{22} E l \qquad (1.59)$$

where $E = \sqrt{E_x^2 + E_y^2}$. In this case, for each direction of the field it is necessary to specify a corresponding direction of light polarization. For example, at $E_y = 0$, light must be polarized along the OX or OY axis, while at $E_x = 0$ the direction of light polarization should make an angle of 45° with the OX and OY axes. A major disadvantage of $LiNbO_3$(LN) and $LiTaO_3$(LT) crystals is that a

high-density laser beam changes their refractive index. LN crystals are transparent in the region from 0.35 to 6 μm. However, the high-density laser beam in the visible region (say, ruby light) produces an undesirable tinge [195]. Therefore, LN crystals are more adapted for use in the infra-red. LN crystals are rather hard (Mohs' hardness 5) and take polish well. Since their half-wave voltage is lower than that of KDP crystals, they hold out special promise as regards their use in high-PRF lasers. There is a report [196] about the use of LN crystals as a Q-switch in a dysprosium-doped calcium-fluoride, high-PRF laser.

Mention should be also made of alpha-quartz crystals. Despite the low magnitude of their electro-optic effect, quartz crystals are attractive because of their high optical properties. In this case, use may be made of the transverse electro-optic effect, with light directed along the optic axis. However, because the optical activity greatly influences the electro-optic effect, modulation by means of quartz crystals involves the use of very high voltages, which is practically unfeasible. The effect of optical activity may be minimized by directing light through an angle of 5 to 7° away from the principal optic axis. Unfortunately, this misalignment introduces an irreducible phase difference.

Electro-optic elements based on the Kerr effect. The Kerr or quadratic electro-optic effect is most pronounced in crystals of the perovskite group, ABO_3, and liquids such as nitrobenzene, $C_6H_5NO_2$, and carbon disulphide, CS_2. The use of Kerr modulating elements in laser shutters is attractive because they are free from natural double refraction. When a light shutter is employed to provide feedback in laser cavities, Kerr modulating elements are preferable also because the phase difference is proportional to the square of the applied voltage [197, 198]. From this point of view, of special interest are crystals in the perovskite group which includes tantalate neobate (KTN) and barium titanate ($BaTiO_3$) which display an abnormally high Kerr effect. The phase difference for different orientations of the field, light and crystallographic axes may readily be derived from an analysis of the optical indicatrix which has the form

$$\sum_{ijkl}\left(\frac{1}{n_o^2}\delta_{ij}+r_{ijk}E_k+Q_{ijkl}P_kP_l\right)x_ix_j=1 \qquad (1.60)$$

where P_k represents the components of the shear polarization vector, $\delta_{ij}=0$ at $i\neq j$, $\delta_{ij}=1$ at $i=j$. For these crystals, the following coefficients of the Q_{mn} tensor are non-zero:

$$Q_{1111}=Q_{222}=Q_{333}=Q_{11}$$
$$Q_{1122}=Q_{2211}=Q_{1133}=Q_{3311}=Q_{12}$$
$$Q_{1212}=Q_{2323}=Q_{3131}={}^1/_2Q_{44}$$

Therefore, for light propagated in the XY plane and polarized at an angle of 45° to the OZ axis which coincides with the direction of the electric field, the phase difference Γ over the crystal length will be

$$\Gamma = (\pi/\lambda)(Q_{11} - Q_{12}) n_o^3 P^2 l \tag{1.61}$$

On applying an additional constant field, E_{bias}, which causes a fixed polarization, P_{bias}, of the medium in the direction of the Z-axis, then assuming that the modulating field is small in comparison with the field of the medium, that is, $\varepsilon E \ll P_{bias}$, we may write

$$\Gamma = \Gamma_{bias} + \Gamma_m = \frac{\pi n_o^3}{\lambda}(Q_{11} - Q_{12}) P_{bias}^2 + \frac{2\pi n_o^3}{\lambda}(Q_{11} - Q_{12}) \varepsilon P_{bias} El \tag{1.62}$$

The quantity $(Q_{11} - Q_{12}) P_{bias}$ is called the effective linear electro-optic coefficient. The fixed phase difference caused by the applied field is usually chosen such that the modulating characteristic has the highest slope: $\Gamma_{bias} = (2m + 1)\pi/2$, where m is an integer. The half-wave voltage for a crystal with a fixed polarization P_{bias} is

$$V_{\lambda/2} = \frac{\lambda}{2n_o^3 (Q_{11} - Q_{12}) P_{bias} \varepsilon_0 l_{xtl}} \tag{1.63}$$

where $\varepsilon_0 = (dP/dE)_0$ is the dielectric constant at the operating point, and l_{xtl} is the dimension of the crystal in the direction of the applied field. It is seen that $V_{\lambda/2}$ is inversely proportional to P_{bias}, that is, to the applied bias field, E_{bias}. This distinction of the quadratic electro-optic effect makes crystals in the perovskite group especially promising for applications where it is important to provide positive or negative feedback and not only to switch the Q of the cavity. Unfortunately, the use of KTN, $BaTiO_3$ and other similar crystals in laser engineering is limited because of the difficulties in growing high-quality specimens. The employment of crystals in the perovskite group as Q-switches will probably be limited by the fact that their performance depends on temperature because their Curie point lies near or within the operating temperature range.

Some liquids displaying the Kerr effect may likewise be employed as modulating elements in lasers. In the absence of an electric field, such liquids are isotropic. With an applied field, the same medium behaves like a crystal with its optic axis directed along the electric field. Under the circumstances, the velocity of propagation of light through the liquid depends on light polarization. The difference in phase between the light components pola-

rized parallel and perpendicular to the electric field over the length l is

$$\Gamma = (2\pi l/\lambda)(n_e - n_o) = 2\pi B_K l E^2 \tag{1.64}$$

where B_K is the Kerr constant.

Using the Havelock law, the difference in refractive index between the extraordinary and ordinary rays may be expressed [199] in terms of the difference in refractive index between the ordinary ray and the liquid in the absence of the field, n_{liquid}

$$-(n_e - n_o) = 2(n_o - n_{liquid}) \tag{1.65}$$

Among the liquids studied at present, the strongest Kerr effect is displayed by nitrobenzene, $C_6H_5NO_2$, the Kerr constant of which is by two orders of magnitude greater than that of other liquids; at $\lambda = 7000$ Å, it is 3.6×10^{-10} cm/V. The Kerr constant of nitrobenzene is sensitively dependent on its purity. The breakdown voltage for nitrobenzene is 5×10^4 to 10×10^4 V/cm. Nitrobenzene is transparent in the range from 0.45 to 1.1 μm. The Kerr constant of nitrobenzene is dependent on temperature

$$B_K = \frac{n_{liquid} - 1}{n_{liquid}} (\mu/kT)^2 (1/5\lambda) \tag{1.66}$$

where μ is the constant dipole moment, and k is Boltzmann's constant. In the temperature range from 20° to 40 °C, the value of B increases by 1.2% per degree Centigrade. The half-wave voltage of the Kerr cell is

$$V_{\lambda/2} = \sqrt{d_K^2 / 2B_K l} \tag{1.67}$$

where d_K is the separation between the electrodes of the Kerr cell.

Physically, a Kerr cell, a modulating element based on the quadratic electro-optic effect in a liquid, is a hermetically sealed container fabricated from metal or an insulating material, with glass or quartz windows into which electrodes from a noble metal or nickel are made (Fig. 1.56). Since the cell is filled with nitrobenzene, its joints must be sealed with materials which will stand up to chemical attack. In the Kerr cell shown in Fig. 1.56, the electrodes are spaced 8 mm apart, the electrode dimension along the light beam is 6 cm, and the half-wave voltage is about 25 kV.

Although Kerr cells are rather awkward in use and rather difficult to make, they are widely employed as Q-switches and feedback elements in laser oscillators because they can be made from readily available materials. The applicability of Kerr cells is somewhat limited by the fact that a high-intensity laser beam produces in the cell stimulated Raman scattering which causes changes in the spectral make-up. Yet, Kerr cells offer a very important advan-

tage over modulating crystals, namely, there is no distortion due to the piezo-optic effect with any waveform of control electrical pulses. For example, with a long rectangular electrical pulse, the light pulse transmitted by the Kerr cell will likewise be rectangular.

Polarizers. In addition to the various modulating elements examined above, any shutter has another important component, a polarizer. Not all of the known polarizers may be used in high-power

Fig. 1.56. Kerr cell

laser oscillators [200]. For example, the classical polarizer such as the Arens prism, the Wollaston prism, or the Nicol prism, cannot be used in high-power laser oscillators. The point is that their elements are cemented together by the Canada balsam, glycerine or castor oil which will not stand up to strong radiation. There is no cemented joint in the Glan-Foucault prism. In this prism, the two parts cut from Iceland spar are separated by a thin air film. However, because of the chosen direction of optic axes in the Iceland spar, the transmission of a Glan-Foucault prism does not exceed 52% of the original value (leaving out the absorption in Iceland spar). The most suitable polarizer for laser shutters is the Glan-Foucault prism modified by Archard and Taylor. In order to improve transmission, Archard and Taylor [201] arranged the optic axes of both prisms parallel with the entrance and top faces (Fig. 1.57). In this type of polarizer, light is incident on the air film at an angle which is greater than the angle of total internal reflection for the ordinary ray and less than the angle of total in-

ternal reflection for the extraordinary ray. In the wavelength range between 0.2 and 2 μm the refractive index of Iceland spar for the ordinary ray varies in the range $n_o = 1.903$ to 1.621, and for the extraordinary ray in the range $n_e = 1.576$ to 1.473. Therefore, the angle of total internal reflection for the ordinary ray should be chosen to match a refractive index anywhere between 1.903 and 1.621 (for example, at $n = 1.606$, the angle of total internal reflection is 38°30′). The losses of the polarized light on the entrance, intermediate and exit faces are about 12%. The absorption data for Iceland spar are listed in Table 1.12.

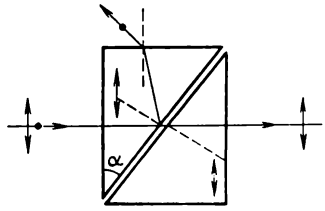

Fig. 1.57. Archard-Taylor polarizer

As is seen from Table 1.12, the best prisms for ruby and neodymium lasers would be those fabricated from Category 1 spar. Unfortunately, Category 1 does not guarantee sufficient stability towards strong radiation. The various impurities inevitably present in naturally occurring Iceland spar have an adverse effect on its stability. Damage caused by strong radiation appears as crazing and bubbles. At present, there are no other methods for selecting Iceland spar except by directly testing specimens for their stability towards high intensity light.

Table 1.12

Spar grade	Absorption, % cm			Wavelength measured, μm
	Category 1	Category 2	Category 3	
ИШ-У	50	55	60	0.22
ИШ-В	10	20	30	0.4
ИШ-М	1	3	10	0.7

In some cases [202], it is more convenient to use polarizers such as shown in Figs. 1.58 and 1.59. The polarizer shown in Fig. 1.58 has an advantage over the Archard-Taylor prism in that it consists of only one rhombic element. Besides, it shifts the axis of radiation, which is convenient in some configurations. Rhombic polarizing prisms have the same angle α as the Archard-Taylor polarizer. A rhombic prism will transmit 88.4% of one component and 0.05% of the other component of the output beam. A major disadvantage of the rhombic prism is that it has a lower strength than the Archard-Taylor prism. This is because light reflected from the faces forms zones where the rays intersect and the radiation den-

sity is twice the value of the input beam. The prism shown in Fig. 1.59 is employed in cases where both components of laser emission must be utilized. This beam-splitting polarizing prism is a combination of a rhombic polarizing prism and a trihedral prism, such as is used in the Archard-Taylor polarizer. Leaving out absorption, one arm of this prism transmits 88.2% of one radiation component, and the other arm 86.4% of the other component. Some investigators [203] have used polarizing elements in the form of Brewster-angled stacks or simple prisms.

Main characteristics of shutters and requirements for alignment. The most important characteristic of a shutter is its modulating

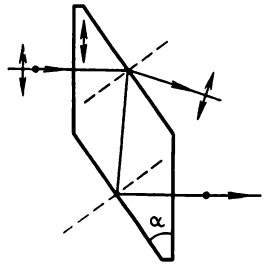

Fig. 1.58. Rhombic polarizer

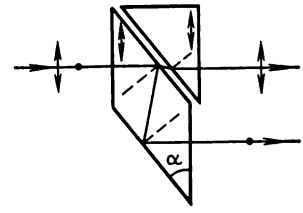

Fig. 1.59. Polarizing beam splitter

characteristic, that is, the relationship between light transmission and the magnitude of the applied electric field. The shutter shown in Fig. 1.53 (see, for example, [188]) has a modulating characteristic of the form

$$I/I_0 = \sin^2 \Gamma/2 \tag{1.68}$$

The phase difference for a Pockels modulating element fabricated from a KDP crystal is

$$\Gamma = \pi V/V_{\lambda/2} \tag{1.69}$$

The phase difference for a Kerr modulating element is

$$\Gamma = \pi V^2/V_{\lambda/2}^2 \tag{1.70}$$

The modulating characteristics of shutters depend above all on the type of electro-optic element used and the distribution of the electric field in that element. These factors determine the magnitude of the half-wave voltage, the dependence of this voltage on temperature and wavelength, the influence of the piezo-effects, radiation losses in the modulating elements, and the net transmission of crossed polarizers. In addition to these factors, the modulating characteristic is markedly affected by the alignment of, or rather

the amount of misalignment between, the shutter elements. Misalignment may be of any one of two types, namely relative to the optic axis of the shutter [204], and in a horizontal and a vertical plane. The former type of misalignment, which reduces to the transmission of light by two polarizers crossed at a certain angle and separated by a crystal plate with its axis directed arbitrarily relative to the direction of transmission of the polarizers is examined in [205]. Fig. 1.60 shows projections of the amplitude E_l of light vibrations on the optic axes of the crystal and the directions of transmission of the polarizers. In the crystal plate the electric intensity vector passing through the polarizer P_1 may be resolved into two components, E_x and E_y, according to the principal crystallographic axes. On passing through the crystal plate, the E_x and E_y waves come by a certain path length difference, Γ, so that the components passing through the polarizer P_2, namely E_{2x} and E_{2y}, are equal to the projections of E_x and E_y on the direction of transmission of the polarizer P_2. The transmission of the system will be

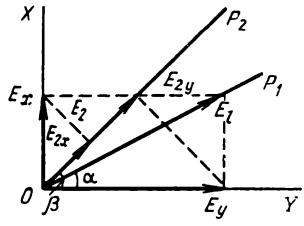

Fig. 1.60. Light component intensities on passing through a shutter

E_l — amplitude of light vibrations after passage through polarizer P_1 (see Fig. 1.53); E_x, E_y — components of E_l along the X and Y axes in the crystal; E_{2x}, E_{2y} — projections of E_x and E_y on the direction of transmission through P_2

$$I/I_0 = \cos^2(\beta - \alpha) - \sin 2\alpha \sin 2\beta \sin^2(\Gamma/2) \quad (1.71)$$

The first term of the equality depends solely on the angle between the polarizers and is independent of the path length difference, Γ. For shutters $\beta - \alpha = \pi/2 \pm \Delta\varphi$, where $\Delta\varphi$ is the tolerance on the misalignment of the polarizers about the optic axis. The transmission of the polarizers at $\Gamma = 0$ is

$$I/I_0 = \cos^2(\pi/2 \pm \Delta\varphi) = \sin^2 \Delta\varphi \quad (1.72)$$

Thus, the value of $\Delta\varphi$ is decided by the limit of transmission set for the "closed" shutter. For a transmission of 0.5%, this value is $\Delta\varphi = 4°$.

At $\beta - \alpha = \pi/2$, that is, when there is no transmission due to misalignment of the polarizers and the KDP modulating element utilizes the longitudinal electro-optic effect, the angle α is that between the direction of transmission of the polarizer and one of the major axes of the optical indicatrix in the $Z = 0$ plane, in which case $\alpha = (\pi/4) \pm \Delta\alpha$, where $\Delta\alpha$ is the tolerance on the angle of misalignment of the crystallographic axes in a KDP crystal relative to the axes of transmission of the polarizers. In such a case,

$$I/I_0 = \cos^2 2\Delta\alpha \sin^2(\Gamma/2) \quad (1.73)$$

At $\Gamma = \pi$, that is, when the shutter is open, the absorption in the shutter due to misalignment is

$$T_{absorp} = \sin^2 2\Delta\alpha \qquad (1.74)$$

At $\Delta\alpha = 3°$, $T_{absorp} = 0.5\%$. It is quite feasible to align a KDP crystal within the above limits, using an interference conoscopic pattern.

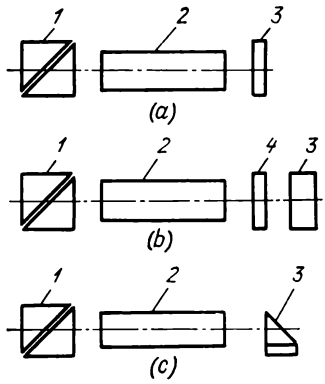

Fig. 1.61. Optical schematics of quarter-wavelength shutters-reflectors (*a*) opened by removal of a voltage and (*b*, *c*) opened by application of a voltage

1—Archard-Taylor prism; *2*—modulator; *3*—100%-reflecting mirror; *4*—phase-shifting TIR prisms equivalent to a quarter-wavelength plate and a 100%-reflecting mirror

The other form of misalignment is about the direction of the optic axis of a shutter. The misalignment of the Archard-Taylor polarizing prism in a horizontal and a vertical plane has no effect on the transmission or absorption of the shutter over a sufficiently wide range of TIR angles. In contrast, the misalignment of the modulating element about the direction of light has a considerable effect, because the transmission of the shutter depends not only on the angle between the direction of light and the optic axis of the electro-optic element, but also on the angle between the plane in which the misalignment is observed and the plane containing the optic axis and one of the crystallographic axes of the element. With a small angle θ between the Z-axis and the direction of light in KDP modulating crystals utilizing the longitudinal electro-optic effect, the following expression for the path length difference, Γ, can be derived from the equation of normals:

$$\Gamma = \frac{2\pi n_o^3 r_{63} E l}{\lambda} + \frac{\pi l}{\lambda} \frac{n_o^2 - n_e^2}{n_e^2} n_o \theta^2 = \pi \frac{V}{V_{\lambda/2}} + \Gamma_\theta \qquad (1.75)$$

if the direction of light departs from the *Z*-axis through an angle θ in the *XOZ* plane. If misalignment takes place in the *XOZ* or *YOZ* plane, the path length difference Γ_θ will be zero.

Optical systems and mechanical construction of shutters. The optical system of a shutter (see Fig. 1.53) may be modified or simplified. For example, when a shutter is to be employed as a Q-switch for a laser cavity in which the laser rod emits polarized light (for example, ruby oriented at 90°), the first polarizing prism is not mandatory. This modification of shutter has been used in the Soviet-made ОГМ-20 laser oscillator [206]. Another simplification

of the optical system is shown in Fig. 1.61 where it is combined with a 100% reflecting mirror to make up a quarter-wave shutter-reflector. In laser oscillators, the shutter usually controls the intensity of the light reflected from one of the mirrors. On being reflected from the mirror, the light beam traverses the modulating element twice. With a half-wave control voltage each time the light beam passes through the modulating element it undergoes a phase shift of a half-wavelength. If we drop the analyzer prism from a half-wave shutter, the control voltage may be halved, in which case the light beam will undergo a phase shift of a half-wavelength after two passes through the modulating element. This modification is called the quarter-wave shutter. The only polarizing prism in this type of shutter acts as both a polarizer and an analyzer. The quarter-wave shutter shown in Fig. 1.61*a* is closed when it is energized, and open when it is de-energized. For positive opening of a quarter-wave shutter, it is important to provide an additional fixed phase difference by means of, say, a quarter-wave plate (Fig. 1.61*b*). A disadvantage of this type of shutter is that it is sensitive to wavelength because of the presence of the quarter-wave plate. Instead of a quarter-wave plate and a 100%-reflecting mirror, use may be made of any other phase-shifting reflecting element. Such an element may be a roof prism of the type shown in Fig. 1.61*c* [203].

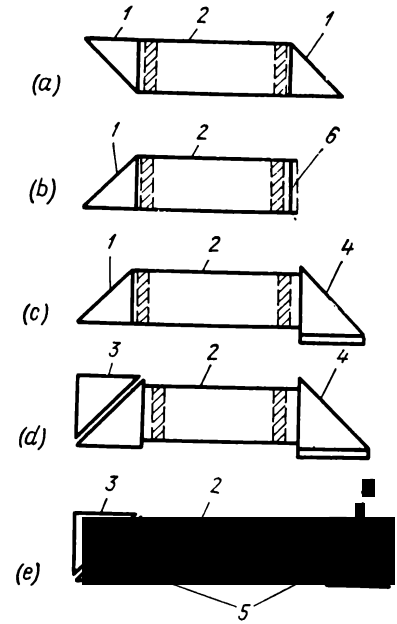

Fig. 1.62. Optical schematics of shutters with the elements cemented on reflecting and non-reflecting faces

1—prism with a Brewster-angled entrance face; *2*—KDP crystal with ring electrodes; *3*—Archard-Taylor prism; *4*—phase-shifting TIR prism; *5*—adapter rings; *6*—100%-reflecting coating

Physically, the above examined shutters may be built either as separate elements or as an integral assembly in which all the components are cemented together on their reflecting faces, or as an integral assembly in which the components are cemented together on non-reflecting surfaces (Fig. 1.62). The "distributed" type of design is inconvenient because mechanisms have to be provided to align each element in a horizontal and a vertical plane and with respect to the optic axis of the shutter. Besides, the ends of the

modulating elements must be protected, where use is made of hygroscopic crystals, such as KDP. For this purpose, the crystal may be enclosed in a hermetically sealed container with windows.

The most important disadvantage of this design is the Fresnel reflection from the ends. If the ends are aligned to be parallel with other elements of the laser cavity, the Fresnel reflection from the ends will markedly bring down the threshold energy for spurious oscillation. The total Fresnel reflection from the ends results in considerable loss if the ends are out of parallel by as little as about 1°.

Some of the drawbacks associated with the "distributed" design can be eliminated by cementing together the elements at their reflecting surfaces. In fact, a Brewster-angled element may be cemented even to the entrance face. With this arrangement, the elements need not be aligned separately, and the ends of the hygroscopic modulating elements are protected by cemented joints (Fig. 1.62*a*, *b*, *c*, and *d*). There is no Fresnel reflection from the ends in this arrangement, but a very serious problem is that of the strength of cemented joints, because the elements cemented together are fabricated from materials greatly differing in thermal and mechanical characteristics, while the cemented surfaces have stand up to high radiation densities for a long time. At present, no satisfactory methods appear to have been developed for cementing shutter elements, and so such designs have not yet come into wide use, although there have been encouraging reports in the literature. For example, mention is made in [203] of several types of shutters with elements cemented at their optical surfaces and even of a shutter cemented to a ruby rod. In all cases, the modulating element was a KDP crystal cut along the Z-axis. The investigators have called their method of cementing together the elements the optical semi-contact or quasi-contact. Prior to cementing, the surfaces should be thoroughly polished ($N = 0.1$ fringe, and $\Delta N = 0.05$ fringe). According to the investigators, the best type of cement is shellac or any other cement with suitable optical characteristics. After cementing, the shutter should be allowed to stay for at least a month. On the basis of tests, the investigators maintain that, provided the cementing process is applied correctly, the shutter may be employed in single-pulse operation at power densities of up to 60 to 70 MW/cm^2. The cases where the optical contact was disturbed, the cement burned through, or other injuries occurred are attributed by the investigators to departures from the prescribed procedures for the manufacture and assembly of the elements, and also to a non-uniform distribution of energy across the beam.

A shutter in which the elements are cemented together at non-optical surfaces is shown in Fig. 1.62*e*. This can be done with the

aid of glass or quartz plates with an opening for the light beam. This design is convenient in that all the elements are aligned and permanently fastened relative to one another. The ends of the modulating elements are protected by Archard-Taylor prisms cemented to plates with an opening for the light beam. In this type of shutter, however, a serious drawback is Fresnel reflection from the ends of the elements. Despite considerable Fresnel-reflection losses, this type of shutter may in some cases be employed in laser oscillators to advantage, mainly because the assembly is robust mechanically and stable towards laser radiation.

1.8. Controlled Electro-Optic Reflectors

Total internal reflection in anisotropic media. The electro-optic effect in conjunction with total internal reflection at the interface between an anisotropic and an isotropic medium provides a basis for electro-optic reflectors which may reflect light, depending on the applied electric field, in two directions differing by a small angle. Some types of electro-optic reflectors are referred to as single-crystal shutters, to stress the fact that optically such devices are single crystals performing the functions of all the elements of a conventional electro-optic shutter.

Total internal reflection at the interface between an anisotropic and an isotropic medium has not practically been utilized until quite recently. The advantages offered by total internal reflection have been revealed in development work on electro-optic reflectors [207, 208]. It has been found that they offer an efficient solution to many problems involved in the control of laser resonators.

As will be recalled, the directions of incidence, refraction and reflection of light at the interface between two media are interrelated as follows:

$$n_i \sin \theta_i = n_{refl} \sin \theta_{refl} = n_{refr} \sin \theta_{refr} \tag{1.76}$$

In the general case, the refractive indexes for incident, reflected and refracted waves may be derived from the equation of normals

$$\frac{N_1^2}{1/n^2 - 1/n_1^2} + \frac{N_2^2}{1/n^2 - 1/n_2^2} + \frac{N_3^2}{1/n^2 - 1/n_3^2} = 0 \tag{1.77}$$

where n is the refractive index of a wave vector N with its components N_1, N_2 and N_3 directed along the principal axis.

Without going into a further discussion of the general case, we shall take up the separation of radiation into two components under conditions of total internal reflection in uniaxial crystals, such as crystals of class $\bar{4}2\,m$, of importance to practical utilization.

For uniaxial crystals

$$n_1 = n_2 = n_o, \quad n_3 = n_e$$

In this case, one of the solutions to the equation of normals will be $n = n_o$. The other solution is

$$n^2 = \frac{n_o^2 n_e^2}{n_o^2 \sin^2 \beta + n_e^2 \cos^2 \beta} \tag{1.78}$$

where β is the angle between the OZ axis and the direction of the normal N.

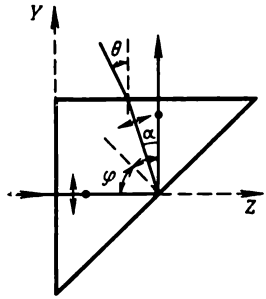

Fig. 1.63. Total internal reflection in a prism made from a uniaxial anisotropic crystal for a light beam parallel with the optic axis

φ—angle of incidence on the birefringent face; α—angle between the normals of the ordinary and extraordinary waves upon reflection

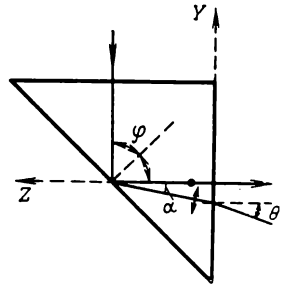

Fig. 1.64. Total internal reflection in a prism made from a uniaxial anisotropic crystal for a light beam at right angles to the optic axis

These solutions represent two emission components with different polarization. The refractive index of one component is independent of direction and is equal to n_o, while that of the other is direction-dependent and determined by equation (1.78). This dependence of the refractive index on direction may be utilized for separating unpolarized light into two orthogonally polarized components under conditions of total internal reflection at the interface between two media according to expression (1.76).

As a proof, consider the total internal reflection taking place at the hypotenuse face of a right-angle, equilateral prism cut from a crystal of class $\bar{4}2\,m$, so that one of the side faces is parallel with the optic axis, Z, and the other side face is parallel with one of the principal axes, X or Y. Consider two cases, with light passing through this prism parallel with the Z-axis (Fig. 1.63) and at right angles to the same axis (Fig. 1.64). In the former case, equation

(1.76) for two orthogonally polarized components may be rewritten as follows:

$$n_o \sin\varphi = n \sin\varphi, \quad n_o \sin\varphi = n \sin(\varphi - \alpha) \tag{1.79}$$

where α is the angle between the directions of reflection for the orthogonally polarized components.

Noting that in (1.78) the angle β is equal to $2\varphi + \alpha$, we obtain from equalities (1.78) and (1.79) for $\varphi = 45°$

$$\sin\alpha = \frac{n_o^2 - n_e^2}{\sqrt{(n_o^2 - n_e^2)^2 + 4n_e^4}} \tag{1.80}$$

For the extraordinary component of the beam emerging from the prism, the following equality holds

$$n \sin\alpha = \sin\theta \tag{1.81}$$

where θ is the angle between the wave normals of the ordinary and extraordinary waves. From (1.79) and (1.80), one obtains

$$\sin\theta = n_o \frac{n_o^2 - n_e^2}{n_o^2 + n_e^2} \tag{1.82}$$

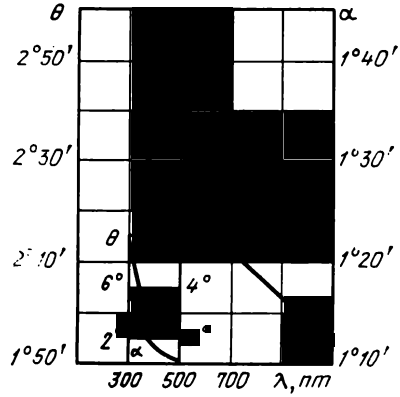

Fig. 1.65. Dispersion curves for α and θ in KDP crystal

As follows from (1.80) and (1.82), the angles α and θ depend on n_o and n_e which vary according to the spectral make-up of the radiation. The dispersion curves for α and θ in the case of KDP crystals [209] based on [210] and satisfactorily checking with experimental data are shown in Fig. 1.65.

Similarly, it is possible to compute α and θ for the case shown in Fig. 1.64, that is, when the beam enters the prism at right angles to the Z (optic) axis of the crystal. Using (1.77) and noting that $\varphi_i = \varphi = 45°$, and $\varphi_{refl} = 45° + \alpha$, we may write

$$\sin\alpha = \frac{n_o^2 - n_e^2}{\sqrt{(n_o^2 - n_e^2) + 4n_o^4}} \tag{1.83}$$

$$\sin\theta = n_e \frac{n_o^2 - n_e^2}{n_o^2 + n_e^2} \tag{1.84}$$

Electro-optic reflectors. An elementary electro-optic reflector using a modulating element and a right-angled prism combined in a single crystal is shown in Fig. 1.66*a*. The crystal of rectangular cross-section is cut along the Z-axis so that the entrance end

is at right angles to the Z-axis, and the exit end makes an angle of 45° with the Z-axis. The X and Y axes are parallel with the sides of the cross-section rectangle. One of the side faces is given a coat of 100%-reflecting material, or it may have a right-angled roof prism with its edge parallel to the Z-axis (Fig. 1.66*b*). The two electrodes made to the sides of the crystal near its ends enclose that part which is utilized as a modulating element (modulation region). This modulation region must satisfy the same requirements for quality, size and other characteristics as the modulating elements of shutters.

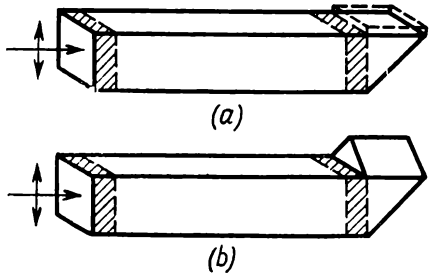

Fig. 1.66. Electro-optic reflector
(*a*) with reflecting coating on side face;
(*b*) with roof prism on side face

An electro-optic reflector operates on the following principle. Depending on the presence (or otherwise) of a half-wave voltage across the electrodes, the polarized light falling on the entrance face will be either reflected back or deflected through an angle. It should be noted that any departure of the phase difference from π due to variations in the electric field across the section as a result of the temperature gradient, stresses or strains, or due to

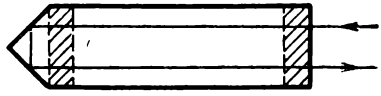

Fig. 1.67. Electro-optic reflector with a square entrance end

misalignment between the direction of light and the Z-axis, or due to the rotation of the reflecting plane about the Z-axis will give rise to two orthogonally polarized components; that is, not all of the incident radiation will be switched between the two directions.

Figure 1.67 shows an electro-optic reflector in which the wanted component of radiation, on being reflected twice from the faces of the roof prism, retraces in the same direction. This type of electro-optic reflector is intended for polarized light. Losses in this reflector are determined by losses in the material, improper relative orientation of the reflecting faces and crystallographic axes, and also by Fresnel reflection from the entrance end.

A similar electro-optic reflector free from Fresnel reflection from the entrance face is shown in Fig. 1.68*a*. The entrance face is oriented at the Brewster angle. Fig. 1.68*b* shows a controlled re-

flector with a Brewster-angled entrance face and a roof prism on the side as in the controlled reflector shown in Fig. 1.66.

A number of further advantages are offered by combining the prism shown in Fig. 1.64 and the above reflectors in a single crystal. One such combination using a prism whose Z-axis is at right angles to the incident beam, and the polarized-light reflector shown in Fig. 1.67 appears in Fig. 1.69. Unpolarized light enters by a side face and is separated into two components due to total internal reflection from the bevelled faces. One (extraordinary)

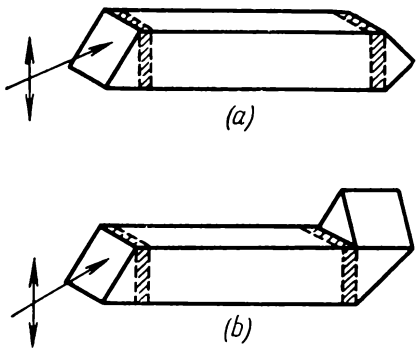

Fig. 1.68. Electro-optic reflectors with a Brewster-angled entrance face
(*a*) with an end as a roof prism; (*b*) with a roof prism on the side

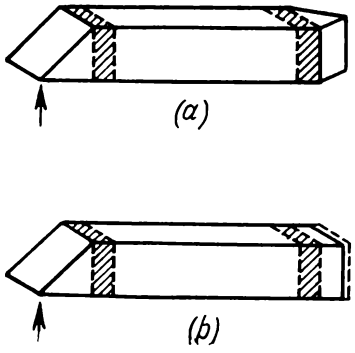

Fig. 1.69. Electro-optic reflectors for unpolarized light
(*a*) with an end as a roof prism; (*b*) with a reflecting coating on an end

component is deflected from the optical axis in the plane of incidence (and does not contribute to lasing action in the laser cavity). The other component directed along the Z-axis passes through the crystal region under control of an electric field, is reflected from the roof prism, and is finally either reflected back or deflected through an angle in a plane normal to the plane of incidence, depending on the presence (or otherwise) of an applied electric field. This type of reflector can handle unpolarized light and may be employed in neodymium-doped glass lasers. In such cases, the material should be DKDP crystals.

The electro-optic reflector shown in Fig. 1.69*b* is a single crystal which combines the prism shown in Fig. 1.64 and a field-controlled crystal region with a reflecting coating deposited on its square end. For its operation, this device requires a quarter-wave control voltage.

Temperature distortion of electro-optic reflectors. In all of the electro-optic reflectors examined above, the angle that the reflecting face makes with the Z-axis is temperature-dependent because of the anisotropy of the material [211]. This can be proved

as follows. In the general case, a change in the temperature of a crystal produces a strain which may be described by a strain tensor of the form $[\varepsilon_{ij}]$. If the temperature changes by a small amount and equally throughout the crystal, the strain is uniform, and all components are proportional to ΔT, that is

$$\varepsilon_{ij} = \alpha_{ij}\Delta T \tag{1.85}$$

where the α_{ij}'s are constants known as coefficients of thermal expansion and making up a symmetrical tensor. Reducing equation (1.85) to the principal axes simplifies the expression, and the tensor components take the form

Table 1.13

Material	α_{xx}	α_{zz}
ADP	39×10^{-6}	1.9×10^{-6}
KDP	21.6×10^{-6}	34.3×10^{-6}

$$\varepsilon_1 = \alpha_1\Delta T; \quad \varepsilon_2 = \alpha_2\Delta T; \quad \varepsilon_3 = \alpha_3\Delta T \tag{1.86}$$

where α_1, α_2, and α_3 are the main expansion coefficients.

Hence, a sphere in the crystal will be caused by changes in temperature to turn into an ellipsoid (a strain ellipsoid) with axes proportional to $(1 + \alpha_1\Delta T)$, $(1 + \alpha_2\Delta T)$, and $(1 + \alpha_3\Delta T)$. For reflectors fabricated from KDP crystals, $\alpha_1 = \alpha_2 = \alpha_{xx}$; $\alpha_3 = \alpha_{zz}$. The values of α_{xx} and α_{zz} for KDP and ADP are listed in Table 1.13.

Denote the angle between the side and hypotenuse faces of the prism shown in Fig. 1.63 as γ. Then, since $d\varphi = -d\gamma$ and

$$d\alpha = (\alpha_{xx} - \alpha_{zz}) \sin 2\gamma dT \tag{1.87}$$

for $\gamma = 45°$ the beam deflection, $\Delta\varphi$, under conditions of total internal reflection, as a function of changes in temperature, ΔT, may be written as

$$\Delta\varphi = {}^1/_2(\alpha_{xx} - \alpha_{zz})\Delta T \tag{1.88}$$

Emerging from the prism shown in Fig. 1.63, the ordinary component of laser light will be deflected due to temperature-induced misalignment through an angle $\Delta\theta_0$ equal to

$$\Delta\theta_0 = 2n_o\Delta\varphi \tag{1.89}$$

In controlled reflectors with a right-angled entrance face (see Figs. 1.66 and 1.67), the beam is reflected from two faces misaligned through an angle $\Delta\varphi$, so that, on emerging from the reflector we have

$$\Delta\theta_0 = 4n_o\Delta\varphi \tag{1.90}$$

In a controlled reflector with a Brewster-angled entrance face (see Fig. 1.68), the angle between the incoming and outgoing beams due to temperature-induced misalignment will be

$$\Delta\theta_0 = 4n_o \sqrt{\frac{1-(1/n_o^2)\sin^2\beta}{1-\sin^2\beta}}\,\Delta\varphi \qquad (1.91)$$

For the light component deflected by the reflector through φ upon application of the control voltage, the temperature-induced misalignment between the reflecting surfaces by an angle $\Delta\varphi$ will change the deflection angle by a proportional amount. Similarly for the light component deflected through the angle θ, the effect of temperature is such that the deflection angle is changed by $\Delta\theta$ given by

$$\sin\theta = n\frac{n_o^2-n_e^2}{n_o^2+n_e^2}\left[1-2(\alpha_{xx}-\alpha_{zz})\Delta T\right] \qquad (1.92)$$

The temperature dependence of $\Delta\theta_0$ is responsible for some specific features of electro-optic reflectors. Among other things, because of the symmetry of roof-prism reflectors about their optical axis, the temperature-induced misalignment between the reflecting surfaces by an angle $\Delta\varphi$ causes the on-axis beam to be reflected in two directions at an angle $2\Delta\theta_e$, where $\Delta\theta_e$ is given by (1.90). In a laser oscillator, this splitting-up of the reflected beam may cause its two halves symmetrical about the roof prism of the electro-optic reflector to overlap or separate completely. Besides, the temperature-induced misalignment between the reflecting faces strongly affects laser power output. From a practical point of view, a critical consideration in making prisms is the temperature at which $\Delta\varphi = 0$. During the fabrication of prisms, this requirement can be met in any one of two ways: the prism is fabricated either to have $\Delta\varphi = 0$ at the temperature maintained during fabrication, or to satisfy a predetermined tolerance, $\pm\Delta\varphi$ at that temperature, so that it will have $\Delta\varphi = 0$ at the operating temperature.

In electro-optic reflectors with a roof prism on the side (see Fig. 1.68*b*), the angle of the roof prism does not change with temperature, but the inclined faces go out of alignment. Instead of being split up, the reflected beam is then deflected to one side.

The reflection coefficient of electro-optic reflectors may vary from zero to unity, according to the applied voltage.

Single-crystal controlled reflectors offer a whole range of other advantages over shutters when used in laser oscillators.

1.9. Electrically Exploded Film Shutters

The physical basis of this type of shutter is the explosion of a metal film set off by an electric pulse. The shutter is a thin metal film to which electrodes are made and which evaporates instantaneously when a strong electric pulse is passed through it. Activation by electric current and the simplicity of design are important advantages of electrically exploded shutters over other types of shutters utilizing a thin metal film [212-214] burned through by the laser beam or by an auxiliary light source. The electric explosion of a metal film, although little investigated, is related to the well explored subject of exploding wires [215, 216].

As regards a theoretical model of exploding wires, opinions differ. Yet, there is a more or less clear understanding of how the various factors affect the explosion mechanism according to the surroundings and the rate of energy input to a specimen [215]. With the slow explosion of a wire in the atmosphere, where the energy required for the complete evaporation of the specimen is put in over an interval longer than is required for an instability to develop, there appear various magnetohydrodynamic instabilities which markedly affect the electric explosion. Originating on discontinuities of mechanical, thermo-elastic or capillary origin, the fast-developing magnetohydrodynamic instabilities may cause damage to the specimen being exploded before the energy sufficient for its complete evaporation has been put in. In [217] it is shown, for example, that the time required to attain the vaporization point is shortest where a neck develops in the wire and conditions are created for a vapour layer to form at right angles to the direction of current and for an arc to strike. As the vapour layers increase in number and length, the proportion of energy liberated in the condensed metal is progressively reduced, because the plasma of the arc has a resistance a few tens of times greater than that of the metal when it just starts vaporizing. Finally, an instant comes when the applied voltage is not sufficient to sustain the arcs, and these go out or, which is the same, the flow of current is broken. As a result, the material between the vapour layers has no time to vaporize. These events happen when energy input is extended over an interval of about 10 μs. If, on the other hand, the energy input time is shorter than the instability rise time, that is, when the specimen has no time to change in shape, the material will vaporize at practically the same rate from all of the surface. The threshold energy in this case is the sublimation energy which causes the metal to dissociate into free atoms. When the metal is strongly overheated (the energy input exceeds the sublimation energy by at least one order of magnitude), strong shock-waves may be set up on the surface of the specimen, that is, the metal at

the surface expands and turns into a neutral non-conducting vapour. The front of this surface vaporization (rarefaction) is propagated inside the metal at the velocity of sound. This process is accompanied by an increase in resistance owing to a decrease in the number of collective conduction electrons in the metal [218]. Thus, the break in the flow of current is actually due to the decrease in the number of collective conduction electrons throughout the metal and the resultant loss of metallic conduction. After that, the rise of current may be resumed as the metallic vapour is ionized. The front of the zone with the reduced number of collective conduction electrons follows the rarefaction front. On moving inside the exploding wire, the rarefaction wave picks up speed, because the remaining metal is progressively overheated as its conducting cross-section is decreased, and the rarefaction wave will "see" the layers of metal increasingly more over-heated. It is obvious that during a break in the flow of current the current pulse will decay in about the same time as the wave of the decreased number of collective conduction electrons travels from the surface to the centre, and that the current pulse decay time should decrease as the metal grows more and more overheated. The same instant that the flow of current is interrupted, a strong flash appears. The flash changes into a glow when the flow of current ceases completely, and reappears during the next current pulse produced by an arc discharge in the metal vapour near the vaporizing wire. The current decays and the glow rises in intensity steeply most simultaneously, the glow displaying a continuous spectrum. It is natural to assume that the strong flash of light is produced by the overheated metal. In [218], these processes are investigated for current pulses lasting from 2×10^{-2} to $15 \times \times 10^{-6}$ s, with the entire explosion occupying a time interval of not more than 4 μs.

It should be noted that at these rates of energy input, electromagnetic effects come to be felt. Among other things, at the rates of energy input limited by the rate of diffusion of the magnetic field, the direct and inverse skin and pinch effects are observed. Now the region within which energy is liberated is propagated from the surface into the bulk of the conductor at the rate of penetration of the magnetic field. Then a rarefaction wave is propagated inside the overheated conductor at the velocity of sound. With a further increase in the rate of energy input, the inverse skin effect gives rise to an additional electro-dynamic explosive force which may cause the conductor to vaporize in consecutive layers.

Because of strong thermionic emission, some conductors display no break in the flow of current when they are exploded in air. A break in the flow of current never occurs in wires electrically

exploded in a vacuum. This is because the surroundings display no restraining action, and favourable conditions are created for a break-down in the expanding vapours of metal [219].

All of the aspects of electric explosions discussed above have been investigated in wires It is not at all unlikely that electrically exploded films behave in an entirely different fashion, the more so that films strongly differ from wires in many respects (for example, the evaporation area of films is 10^2 to 10^3 times greater than that of wires fabricated from the same amount of conductor material). Yet, despite the many unclarified points as regards the kinetics and effects of electric explosion on the control of light transmission, the results cited in [212, 220] seem to support the idea of utilizing electrically exploded films in laser oscillators. Experiments have established that films 0.25 μm thick and 5 cm^2 in area when exploded by a current pulse from a 0.04 μF capacitor charged to 10 to 15 kV (with a stray inductance of not over 0.01 μH) were made transparent in a very short time (about 0.01 μs) and are therefore suitable as Q-switches for neodymium-doped glass lasers. The switch in the discharge circuit was a controlled air-spark-gap. The films used in the experiments were attached to a transparent substrate, such as glass or polyester film 10 μm thick. The transmission at a wavelength of 1.06 μm was under 1% prior to an explosion, 85% after the explosion for the polyester film, and about 91% for the glass substrate. As the energy input was decreased or increased, either the metal failed to vaporize completely or the substrate burned through.

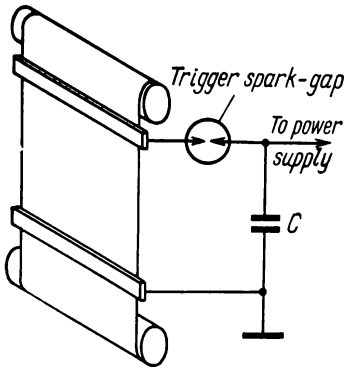

Fig. 1.70. Electrically exploded film shutter

Physically, a film shutter consists of two rolls driven by a suitable mechanism, which advance an aluminised polyester film to an unexposed portion for the next laser firing. Within the exposure zone, the aluminised film is clamped down at the edges by two flat electrodes connected to a discharge circuit. To minimise the resistance, stray inductance and capacitance of the discharge circuit, all circuit components are arranged as close to the exploded film as practicable (Fig. 1.70).

A distinction of exploded-film shutters is that they can only be driven to the "open" state. As it is opened by application of a firing signal, its transmission changes from zero to a certain fixed value. In order to close the shutter, the film has to be moved

to an unexposed position or changed altogether. It should be noted that the net transmission of an open film shutter is determined by the plasma discharge associated with the second current pulse (some energy is absorbed by the plasma, and the substrate may be burnt). This effect may however be minimized by closing the switch connected across the film immediately after the first current pulse.

The spread in opening time of a film shutter is decided by the spread in starting time of the discharge circuit. The time delay with which the film is made transparent relative to the trigger pulse (the time lag of the shutter) is related to the discharge time of the circuit and the time necessary for an explosion to develop in the film, factors which are in turn dependent on the circuit parameters, the size and properties of the film.

1.10. Optical Isolators

In single-pass travelling-wave laser oscillators and laser amplifiers, it is imperative to employ one-way optical isolators [221]. For its operation, an optical isolator depends on the Faraday rotation which consists in that the plane of polarization of light is rotated as it passes through some materials in the presence of a magnetic field. An optical isolator consists of two polarizers between which is placed an element displaying a non-reciprocal Faraday rotation. The non-reciprocal Faraday rotation is due to the fact that the direction of rotation depends on the direction of the magnetic field but is independent of the direction of wave propagation. In other words, the angles of rotation are added together as the wave travels in forward and reverse directions, and not cancelled out as is the case with the natural rotation of the plane of polarization in some materials. The principal planes of the polarizers make an angle of 45° with each other; therefore the wave passing through the first polarizer will no longer be attenuated in the second polarizer, if the non-reciprocal element has turned it likewise through 45°. For a wave travelling backwards, the Faraday rotation occurs in a direction such that the wave passed by the second polarizer will be blocked by the first polarizer. (In principle, an optical isolator may utilize other angles of rotation.)

For linearly polarized light, the Faraday rotation is described by an expression of the form

$$\theta_H = W_V H l \tag{1.93}$$

where θ_H is the Faraday rotation in degrees of arc, W_V is the Verdet constant for the medium traversed by the light, H is the magnetic field intensity in the direction of light propagation, and l is the light path length through the medium.

The optical schematics of several isolators are shown in Fig. 1.71*a* and *b*. With beams of a small clear diameter, it is convenient to employ multi-pass isolators as they require a shorter length for the medium and a lower intensity for the applied magnetic field (Fig. 1.71*b*). The polarizers used in an optical isolator may be Archard-Taylor prisms [222]. Unfortunately, such prisms

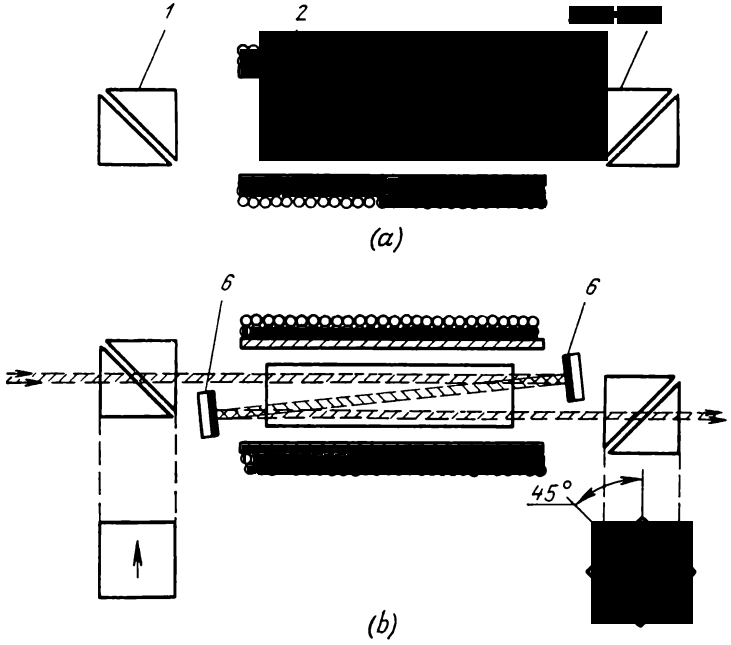

Fig. 1.71. Optical isolators

(*a*) single-pass; (*b*) three-pass; *1*, *5*—polarizers (Archard-Taylor prism); *2*—solenoid coil; *3*—non-magnetic former; *4*—glass rod of a high Verdet constant; *6*—100%-reflecting mirrors

are difficult and very expensive to make for large beam apertures ($\gtrsim 25$ mm). A high degree of polarization, low absorption, and high stability towards strong light may only be secured with a stack of plates the number of, and material for, which can be selected [223] on the basis of the following expression:

$$\Pi = \frac{1 - (2n/n^2 + 1)^{4m_p}}{1 + (2n/n^2 + 1)^{4m_p}} \qquad (1.94)$$

where Π is the extent of polarization by the stack, m_p is the number of Brewster-angled plates, and n is the refractive index. Figure 1.72 shows the arrangement of plates used in [224]. The plates are bevelled (an angle of about 1° is sufficient) to prevent the

propagation of a multiply reflected wave in the forward direction. This arrangement of the two halves of a stack (so that the normals to the surfaces are perpendicular) eliminates the transverse shift of the beam. For unpolarized light, the transmission of this stack is 0.4.

Physically, a non-reciprocal Faraday rotator is a rod of a transparent material with plane-parallel ends ground flat to at least a quarter-wavelength. A critical consideration in designing an optical isolator is the choice of a material. Since the Verdet constant decreases with increasing wavelength ($W_V = A/\lambda^2$, where A is a constant dependent on the material), it is especially difficult to select a proper material and a proper configuration for an isolator intended to operate in the infrared. By far the best choice is offered by some grades of glass which have low internal absorption,

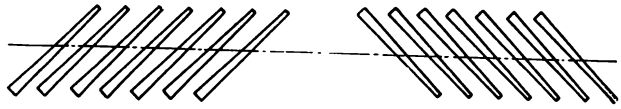

Fig. 1.72. Arrangement of plates in a stack

negligible stress-induced double refraction, and insignificant variations in refractive index. As regards the Faraday effect, preference may be given to lead glass [225], although in some cases other types of glass having a higher strength towards radiation may have to be employed.

The main requirements for the magnet used in a Faraday rotator may be summed up as follows: it should have high magnetic induction (2.5 to 10 kilogauss), a uniform magnetic field in both the direction of light propagation and the radial direction, an optimum size, weight and power drain, and should be properly cooled. As is shown in [226], if a Faraday rotator is to maintain transmission constant within 0.1%, the magnetic field should be uniform to within $\Delta H/H = \pm 4\%$. A highly uniform field and freedom from time instabilities in intensity so characteristic of electromagnets and caused by fluctuations in supply voltage are provided by a permanent magnet [226]. However, like an electromagnet energized from a d. c. source, a permanent magnet requires cooling to the temperature of liquid nitrogen. Proper cooling is important because the magnet gives up a large amount of heat (proportional to H^2) which gives rise to thermal stresses in the glass. Pulsed lasers may employ pulsed optical isolators. The operate time of these isolators must be longer than the duration of the transmitted light pulse, but at the same time, sufficiently short so as not to overheat the material [224]. This type of isolator may employ a pulse-energized air-cored solenoid.

It is usual to evaluate the efficiency of an optical isolator in terms of insertion losses and discrimination between the forward and reverse propagation of light, both expressed in decibels. Ordinarily, the discrimination is 26 to 30 dB (this value decreases with increasing beam aperture), and the insertion loss is 1.2 to 1.4 dB [222, 224, 226].

It is not at all easy to obtain a highly uniform magnetic field. Therefore, for plane-polarized light to be uniformly rotated across the optical rotator, it is important to choose an optimum proportion for the source of the magnetic field and the length of the rotator rod. This stems from general considerations. For a dielectric with a uniform distribution of the Verdet constant ($W_V = \text{constant}$, $\mu \simeq 1$, $\vec{B} = \vec{H}$) and for any light path length, we may write

$$\theta = W_V \int_{\vec{r}_1}^{\vec{r}_2} \vec{H}(\vec{r})\, d\vec{r} \tag{1.95}$$

where W_V is the Verdet constant, μ is the permeability, $\vec{H}$ and $\vec{B}$ are respectively the magnetic field and magnetic induction vectors, $\vec{r}_1$ and $\vec{r}_2$ are the points of entry and exit of light into and from the rotator rod. The integral in (1.95) can be evaluated for a rod of an infinite length. This is so because integrating the equation

$$\text{curl}\ \vec{H} = \vec{j}_{cond} + \vec{j}_{displ} \tag{1.96}$$

within the surface S bounded by a semi-circle resting on the light path at points $\vec{r}_1$ and $\vec{r}_2$, and noting the Stokes theorem, we get

$$\oint_L H_L dL = \int_S \vec{j}_{cond} d\vec{S} + \int_S \vec{j}_{displ} d\vec{S} \tag{1.97}$$

where L is the contour bounding the surface S, and H_L is the magnetic field component over the contour.

Since a magnetic field at infinity tends to zero, Eq. (1.97) may be rewritten as follows:

$$\int_{-\infty}^{\infty} H_L dL_l = i_{cond} + i_{displ} \tag{1.98}$$

where L_l is the light path, i_{cond} and i_{displ} are the total conduction and displacement currents determining the magnitude of H_L on the light path L_l.

It is seen from Eq. (1.98) that in the absence of displacement current ($i_{displ} = 0$), the limiting angle of rotation of plane-pola-

rized light is determined by the conduction current which gives rise to the magnetic field along the line of light propagation. In fact, the angle of rotation in such cases is the same for any light path whose magnetic field is decided by the same total conduction current.

As follows from Eq. (1.98), with special reference to a solenoid and a dielectric rod, the rotation of plane-polarized light will be uniform across the diameter, if the rotating element is longer than the solenoid so much that the magnetic-field component in the direction of light rays is close to zero. This quantity may somewhat vary according to the solenoid configuration. However, as the calculation [235] of practical designs shows, with an optical rod twice as long as the solenoid, the angle of rotation of plane-polarized light remains uniform across the diameter to within 1%. This agrees well with experimental results.

Chapter Two

Optical Systems of Pulsed Laser Oscillators

2.1. Systems Using Optico-Mechanical Shutters

According to [1, 2], if one leaves out spontaneous emission and transitions caused by optical pumping, lasing action in a three-level system may be described by a system of equations for the photon density, Φ in the laser cavity, and for the population inversion density, $N = N_2 - N_1$ as follows:

$$d\Phi/dt = (N\sigma l_a/t_1 - \gamma/t_1)\,\Phi \tag{2.1}$$

$$dN/dt = -2N\Phi\sigma l_a/t_1 \tag{2.2}$$

where σ is the resonance absorption cross-section, l_a is the length of the laser rod, and t_1 is the photon transit time through a laser cavity of length L. (Similar equations in which the factor "2" in equation (2.2) is replaced with the factor "1" describe laser emission in a four-level system.) At any instant, the losses γ in a laser oscillator with slow Q-switching comprise absorption and scattering losses in the cavity γ_{cav}, radiation losses by the semitransparent mirror γ_m and losses due to the Q-switch, $\gamma_Q(t)$. The losses in the cavity and on the mirror remain constant for the duration of lasing action. In contrast, the losses due to the Q-switch are time-dependent and markedly affect the laser action. The losses due to the Q-switch depend on the type of shutter and may, in each particular case, be described by an approximate function. For example, for Q-switching by a spinning prism the approximate time dependence of losses may be found experimentally. Since the angle of the prism as a function of time is

$$\theta_p(t) = 2\pi t/T_r \tag{2.3}$$

where T_r is the period of rotation of the prism, it is necessary to determine the dependence of losses on the angle of the prism. A plot relating the losses to the angle of the prism can be constructed on the basis of experimental data relating the threshold pump energy to the angle of the prism and the relative population inversion to pump energy. Then, utilizing the fact that the gain and loss in emission at the threshold of lasing action are equal, one can plot a curve relating the loss to the prism angle, and,

as a consequence, to time. In [2], the losses as a function of time are described by an approximate function of the form

$$\gamma = (t/t_{\min} - 1)^2 + \gamma_r + \gamma_m \qquad (2.4)$$

where time is counted from the point where the threshold curve intersects the inversion saturation level, and the quantity $t_{\min}$

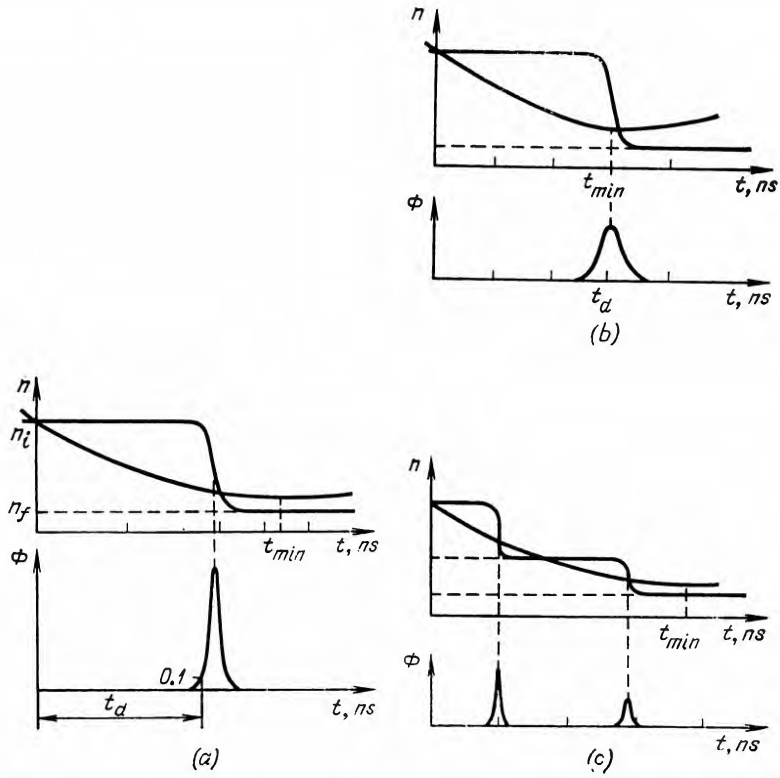

Fig. 2.1. Relative population inversion, n, and photon density, Φ, in a cavity Q-switched by a spinning prism, as functions of time (*a*); with different time to the onset of lasing action (with different cavity lengths) (*b*); with a short time to the onset of lasing action (*c*)

corresponds to the minimum threshold inversion. Using the dependence of the threshold population inversion on the angle of rotation, one can express $t_{\min}$ in terms of T_r.

Equations (2.1) and (2.2) have no analytical solution and can only be solved by numerical methods. In graphic form, the numerical solution [2] explaining the build-up and release of emission from a laser oscillator Q-switched by a spinning prism is presented in Fig. 2.1. The energy E liberated in the laser cavity is

decided by the difference between the initial inversion, n_i, and the final inversion, n_f, and is equal to

$$E = \frac{1}{2} h\nu (n_i - n_f) N_0 V_a \qquad (2.5)$$

where V_a is the volume of the ruby rod, N_0 is the concentration of chromium ions.

For a given value of n_i, the build-up of oscillation in the laser will be determined by the ratio $t_d/t_{\min}$ where t_d is the delay time and $t_{\min}$ is the time over which Q-switching causes the losses to decrease from the value corresponding to the initial threshold conditions to its minimum value. Referring to Fig. 2.1, at $t_d < t_{\min}$,

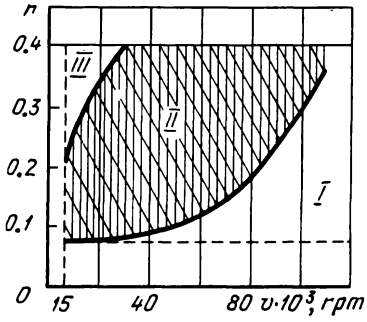

Fig. 2.2. Regions of laser operation at different speeds of the spinning prism and different relative population inversions

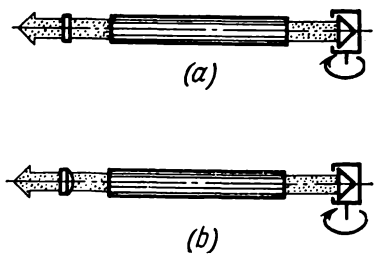

Fig. 2.3. Optical schematics of lasers using a spinning prism and an exit mirror
(*a*) flat; (*b*) spherical

the energy of the laser pulse falls below that at $t_d = t_{\min}$. It is also seen that at $t_d < t_{\min}$, several pulses may be produced.

Figure 2.2 shows the various regions of operation of a laser at different speeds of the spinning prism and different values of relative population inversion. In region *I*, the population inversion is insufficient for the system to oscillate. In region *II*, single pulses are produced. In region *III*, multiple pulses appear. The boundaries between the regions are rather arbitrary, because a decrease in population inversion (with the reflector spinning at constant speed) brings about a gradual decrease in the height of the respective pulses. Therefore, the boundary between regions *I* and *II* is a locus of points for which the height of the first pulse is 1% of the peak value, while the boundary between regions *II* and *III* is a locus of points for which the height of the second pulse is 1% of that of the first pulse.

Figure 2.3*a* illustrates an elementary laser Q-switched by a rotating roof prism. Even though the prism rotates at 60,000 rpm,

the switching time is very long, being of the order of 500 ns, and several pulses may well be produced. Also if only one light pulse is to be generated, the laser rod has to satisfy more stringent requirements for quality. The optical system shown in Fig. 2.3*b* cuts down the switching time by correcting the optical inhomogeneity of the laser rod [7]. For this purpose, the output mirror is replaced with a spherical one whose radius of curvature is determined on

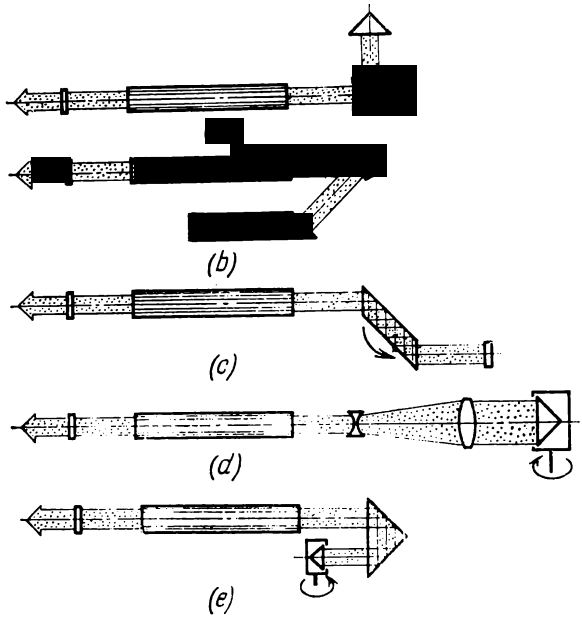

Fig. 2.4. Optical schematics of lasers using an elevated speed for a rotating reflector

the basis of an interferogram of the laser rod ends obtained, using a probe beam from a gas laser. This configuration may be used in conjunction with a laser material of low quality, such as ruby. Existing crystal-growing techniques produce ruby crystals with a considerable gradient of refractive index across the diameter. Therefore, all ruby crystals act as a negative lens whose focal distance can be estimated by the following equations

$$f = R/(n_r - 1) \tag{2.6}$$

$$R = d_a^2/4m_f\lambda \tag{2.7}$$

where n_r is the refractive index of ruby; R is the radius of the spherical wave at the exit from the ruby crystal, d_a is the diameter

of the ruby rod, m_f is the fringe count, and λ is the wavelength of the probe beam.

To correct the distortion of the wavefront due to the refractive index gradient, the end mirror is shaped to a sphere whose radius depends on the quality of the material and may range between 1 and 3 m.

In the optical systems shown in Fig. 2.4, the Q-switching time has been cut down owing to the inclusion of additional optical

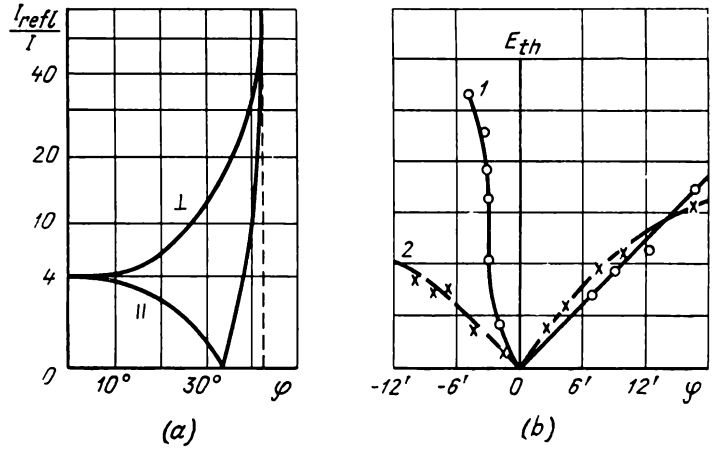

Fig. 2.5. Plots of (*a*) relative reflected light intensity in passing from a denser into a less dense medium and (*b*) the threshold energy of lasing action as functions of the prism angle

1—In a system incorporating a K-8 glass plate (10 reflections); *2*—In a system without additional plates

elements in the cavity without any increase in motor speed. For a laser oscillator with an additional prism (Fig. 2.4*a* and *e*), the effective angular speed, ω_{eff}, of the prism [8-9] is:

$$\omega_{eff} = m_{refl}\omega_m \tag{2.8}$$

where m_{refl} is the number of reflections from the rotating element (in our case, it is equal to 2, but may be greater), and ω_m is the angular speed of the motor. The pulse repetition frequency depends on the spin speed of the prism and the number of additional prisms closing the cavity (Fig. 2.4*a*). For the arrangements shown in Fig. 2.4*b*, the reflectivity rapidly increases with increasing the angle of incidence up to its critical value with multiple total internal reflections. This provides for an increased switching speed and a better angular mode selection [10-12]. Referring to Fig. 2.5*a*, the reflected light intensity suddenly changes as light passes from a denser medium into a less dense medium. According to [13], in

quantitative terms the reflected light intensity as a function of the reflector angle near the critical angle is given by

$$I = \left[\frac{\tan(\varphi - \psi)}{\tan(\varphi - \psi)}\right]^{2m_{refl}} \tag{2.9}$$

where I is the reflected light intensity, φ is the angle of incidence, ψ is the angle of refraction, and m_{refl} is the number of beam reflections in the specimen.

For a specimen prepared from glass with $n = 1.51$ and $m_{refl} = 10$, a departure by as little as 30″ in the angle of incidence from its

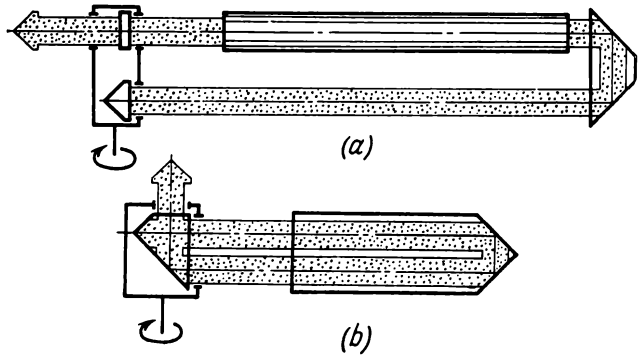

Fig. 2.6. Optical schematics of lasers with two rotating reflectors

critical value will cause the transmission of the specimen to change from 1 to 0.22. In relative terms, the dependence of the threshold energy on the prism angle is illustrated in Fig. 2.5*b*.

In the arrangement of Fig. 2.4*d*, the cavity incorporates a telescopic system [14]. The switching speed is increased in direct proportion to the magnification of the telescopic system.

In the optical system shown in Fig. 2.6, the motor shaft carries both reflectors of the cavity, that is the roof prism and the exit mirror. In addition to doubling the Q-switching speed, this arrangement ensures a greater depth of modulation [15, 16]. A distinction of the arrangement shown in Fig. 2.6*a* is that it can be employed as a master oscillator. With the shutter located on the beam output side, it may simultaneously be employed for amplifier isolation.

The operating principle of the oscillator, the optical system of which is shown in Fig. 2.6*b*, is self-explanatory [16]. The cavity has no additional elements, and both cavity reflectors are combined in a single prism. Owing to this arrangement, the cavity has a high Q when the cavity is switched into resonance and a low Q when it is switched out of resonance, the cavity elements

remain properly aligned, and the effective switching speed is $2\omega_m$. This arrangement is especially convenient in high-power-output, high-PRF lasers, while the shutter is such that it is possible to couple the beams out of several oscillators in a single common direction (Fig. 2.7).

In some cases, in order to obtain a single giant pulse, use is made of a spinning roof prism in conjunction with a controlled-transmission filter or a phototropic (bleachable-dye) shutter. This arrangement avoids the disadvantages inherent in each type of shutter separately. As regards the phototropic shutter, the low

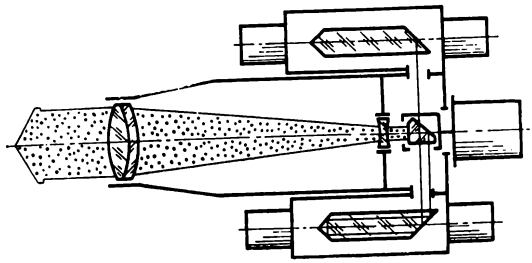

Fig. 2.7. Optical schematic of a pulsed laser with a single shutter common to all heads

initial transmission essential for building up a maximum population inversion requires an increased power to make it transparent. On its part, with high pump energies, the spinning prism allows several pulses to be emitted. With a spinning prism and a phototropic shutter integrated in a single system, the initial transmission of the shutter may considerably be raised and the spinning speed of the prism may be reduced [17, 18], with the result that the energy of the single giant pulse is increased.

2.2. Systems Using Phototropic Shutters

Phototropic (bleachable) shutters are employed to Q-switch the laser cavity in order to obtain nanosecond and picosecond pulses and unimodal operation (see Sec. 2.5).

Generation of nanosecond pulses. Pulses with a duration of several units to several tens of nanoseconds may be generated by a laser oscillator with a simple optical system. The optical cavity of such a laser consists of two plane-parallel mirrors, one semi-transparent and the other 100%-transmitting, between which a phototropic (bleachable) shutter and a laser rod are placed. In this two-component system, in addition to stimulated transitions in the laser material and the resonant absorption of radiation by the phototropic shutter, the kinetics of the lasing action is also

affected by changes in the population inversion caused by optical pumping and by the spontaneous transitions that occur in the laser material and the saturable absorbers.

In the unimodal approximation, the lasing action can be described by a system of equations for the photon density Φ and the difference in population between the energy levels in the laser material, $N = N_2 - N_1$, and in the saturable absorber, $M = M_2 - M_1$. Assuming a two-level model for both media, that is, $N_0 = N_1 + N_2$ and $M = M_1 + M_2$, we have

$$d\Phi/dt = (N\sigma_n l_n/t_1 - M\sigma_m l_m/t_1 - \gamma/t_1)\,\Phi + [a_n(N_0 + N)/\tau_n + a_m(M_0 + M)/\tau_m] \quad (2.10)$$

$$a_{n,m} = \frac{8\pi\nu^2}{c^3}\,\Delta\nu_{n,m}\nu/\eta_{n,m}$$

$$dN/dt = -2N\Phi\sigma_n l_n/t_1 - (N_0 + N)/\tau_n + \omega_a(N_0 - P) \quad (2.11)$$

$$dM/dt = -2M\Phi\sigma_m l_m/t_1 + (M_0 + M)/\tau_m \quad (2.12)$$

where σ_n and σ_m are the absorption cross-sections in the laser and saturable absorbing media, τ_n and τ_m are the times of the spontaneous decay of the upper level in both media, and t_1 is the photon transit time through the cavity. The coefficients a_n and a_m indicate the share of spontaneous emission in each system that enters the cavity mode in question; $a_{n,m}$ is the number of modes in the volume V within the line width $\Delta\nu_{n,m}$ divided by the quantum fluorescence efficiency $\eta_{n,m}$; and ω_a is the probability of the particles in the laser rod being excited by the pumping light. Simultaneous equations (2.10) to (2.12) cannot be solved analytically. A numerical solution of these equations for some practically important initial conditions will be found in [19]. The photon density and population inversion as functions of time for different initial photon densities obtained in [19] are given in Fig. 2.8. It is seen from equations (2.10) through (2.12) that the conditions for oscillation build-up have the form $\sigma_n l_n N - \sigma_m l_m M - \gamma \geqslant 0$ and may be satisfied either by decreasing the population M, if the initiating pulse has a sufficient magnitude, or by increasing the initial population inversion N along with an increase in the pump power.

With a suitably chosen pump power, the conditions for oscillation build-up may be satisfied at the initial photon density limited by spontaneous emission. Neglecting spontaneous transitions and pumping and also assuming that $L \approx l_n$ and $l_n \gg l_m$, equations (2.10) through (2.12) may serve as a basis for the expressions relating the photon density in a laser cavity to the population inversion and giving a useful estimate of the parameters of the

system in question:

$$\Phi = \Phi_i + (N_i/2\beta)\ln(N/N_i) - (N_i/2\alpha)[1 - (N/N_i)^{\alpha}] + \\ + (N_i/2)(1 - N/N_i) \quad (2.13)$$

$$M = (N_i/2\alpha)(N/N_i)^{\alpha} \quad (2.14)$$

where $\alpha = \sigma_m/\sigma_n$, $\beta = (\sigma_n c/V)(t_1/\gamma)N_i$, Φ_i and N_i are the initial photon density and population inversion.

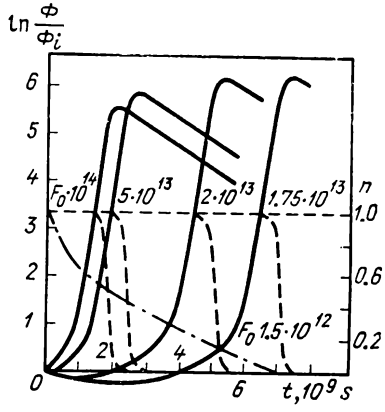

Fig. 2.8. Photon number and population inversion as functions of time with initiating pulses differing in the number of photons, F_0

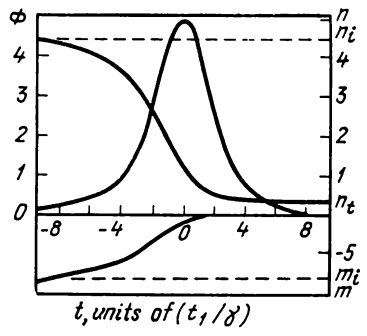

Fig. 2.9. Time dependence of the population inversion in the laser and absorbing materials and emission density in the cavity in units of t_1/γ

At $\alpha \gg 1$, the expression for the maximum density in a laser cavity has the form

$$\Phi_{max} = \Phi_i + N_i/2 - [1/\beta + (\ln\beta)/\beta]/2 \quad (2.15)$$

Changes with time in the photon density in the laser cavity and the population inversion in the laser and absorbing media for the case in question are illustrated in Fig. 2.9 [20].

In practice, the concentration of a saturable absorbing material and the pump level for the laser rod are matched so as to produce only one light pulse. The range over which the pump level can be adjusted so as to produce a single pulse is fairly narrow for any concentration of the saturable absorber. An increase in the pump level may lead to the generation of two, three or more light pulses, while a decrease may discontinue the lasing action. The same applies to temperature-induced changes in the gain of the laser material. Variations in the gain caused by the instability of optical pumping and the temperature of the laser material are also res-

ponsible for variations in the instant at which the laser pulse is generated relative to the firing of the flash tube. Another source of instabilities is the phototropic shutter because photo-chemical reactions may affect the characteristics of the bleachable material. It should also be noted that while the performance of the shutter remains the same at any point within the cross-section, the population inversion does not and depends on variations in the pumping of the laser rod and some other factors. As a result, the lasing action may be initiated and terminated at different times for different points within the cross-section and the spatial structure of the output pulse will change in time in a very elaborate manner.

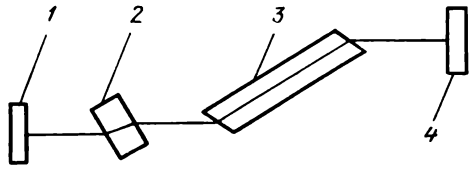

Fig. 2.10. Optical schematic of a laser oscillator for picosecond pulses
1—100%-reflecting mirror; *2*—bleachable shutter; *3*—laser rod; *4*—semitransparent mirror

On the other hand, the fact that the transmission of a phototropic shutter depends non-linearly on light intensity and that the population inversion in the laser rod is not uniform may be utilized for transverse mode selection (see Sec. 2.5) in cases where a unimodal laser beam is sought.

Generation of picosecond pulses. As already noted in Sec. 1.6, in order to generate picosecond pulses, the laser cavity must oscillate in a number of axial modes and the relaxation time of the high-transmission (bleached) state be such that the shutter may discriminate against the individual fluctuation spikes in the intensity of spontaneous noise [29-31].

The first condition is satisfied through the use of optical cavity elements without reflecting surfaces. A very convenient arrangement is to employ elements whose faces are oriented at the Brewster angle to the beam in the optical cavity, as shown in Fig. 2.10. Then the dielectric coating is applied to a plate having non-parallel surfaces.

The second condition is satisfied through the use of a shutter which has a short relaxation time for the high-transmission (bleached) state. In order to generate pulses with a duration of 10^{-11} to 10^{-13} s, the shutter must be capable of discriminating against the individual fluctuation noise spikes and of shortening the pulse during its generation. This can be achieved only if the relaxation time for the excited states of molecules is of the same

order of magnitude as the duration of the laser pulses. In some organic materials, the molecules in jumping from an excited to the ground state first undergo a non-radiative transition (with a relaxation time of about 10^{-11} s) to the metastable state, then a radiative transition (with a relaxation time of about 10^{-9} s) to the ground state. Accordingly, the bleached state of the medium relaxes first to a state with an intermediate value of absorption, then to the initial opaque state. It is not unlikely that a similar mechanism is at work in, for example, polymethine dyes with which pulses with a duration of about 10 ps can be generated.

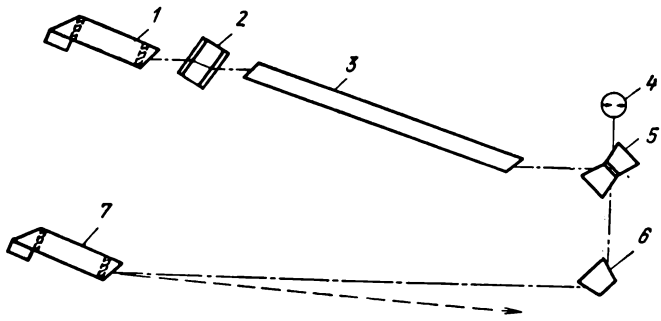

Fig. 2.11. Optical schematic of a laser generating single picosecond pulse
1, 7—electro-optic reflectors with roof prisms; *2*—bleachable shutter; *3*—laser rod; *4*—light-controlled spark-gap; *5*—90-degree rotating prism with Brewster-angled faces; *6*—beam splitter of two 90-degree rotating prisms with an adjustable air gap

The conditions for, and the character of, mode-locking depend on the optical arrangement and characteristics of a laser oscillator. Among other things, the position of the bleachable shutter relative to the cavity mirrors is an important factor. The separation between pulse peaks and their intensities (for the arrangement shown in Fig. 2.10) vary with the position of the shutter. The placement of a bleachable shutter at the point $X = L/m$ (where L is the cavity length, m is an integer, and X is the separation of the shutter from a 100%-reflecting mirror) raises the pulse repetition frequency, PRF $= mf_1$, where $f_1 = c/2L$ [31]. The placement of a bleachable shutter at $X/L = 0$ is most convenient from a practical point of view, because one can obtain a train of pulses with a maximum peak power and a maximum pulse period-to-duration ratio. In this case, for the number N_m of locked modes of the same amplitude, the pulse duration t_p is approximately given by

$$t_p \approx \frac{2.78 \times 2L}{\pi c N_m} \approx \frac{0.88}{c 2 \Delta\nu_{osc}} \approx 2t_1/N_m$$

where $2\Delta\nu_{osc}$ is the total width of the oscillation spectrum and $t_1 = L/c$.

In this case, the peak power increases N_m times in comparison with the average power of unlocked modes. A rough estimate of the potentialities of this method for a ruby laser oscillator

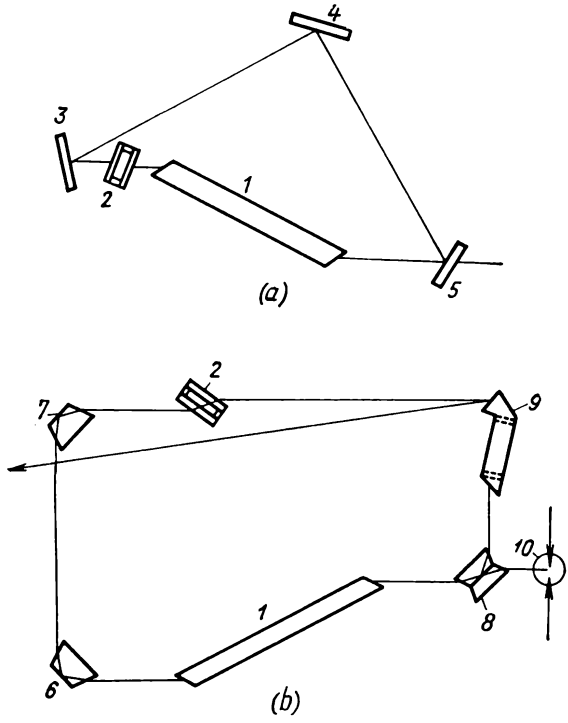

Fig. 2.12. Optical schematics of ring cavities

(*a*) for trains of picosecond pulses; (*b*) for single picosecond pulse; *1*—laser rod; *2*—bleachable shutter; *3*, *4*—100%-reflecting mirrors; *5*—semitransparent mirror; *6*, *7*—90-degree rotating prisms with Brewsterized entrance faces; *8*—beam splitter of two 90-degree rotating prisms with an adjustable air gap; *9*—transmitting electro-optic reflector with Brewsterized entrance faces; *10*—light-controlled spark-gap

($2\Delta\nu_{osc} \approx 10$ cm^{-1}) gives t_p of about 3×10^{-12} s, and for a neodymium-doped glass laser ($2\Delta\nu_{osc} \approx 250$ cm^{-1}), of about 10^{-13} s.

The beam emerging from the semitransparent mirror in such a laser is a train of picosecond pulses separated by an interval equal to twice the photon transit time through the laser cavity. If the intensity of this train of pulses is averaged over the entire time interval, the intensity distribution will correspond to a pulse with a duration of a few tens of nanoseconds produced by Q-switching. A single pulse is selected by passing the train through an electro-

optic shutter opened by a light-controlled spark-gap for the duration of one pulse. However, this method is unattractive because all the remaining pulses in the train are wasted. In a more efficient way, a single picosecond pulse can be obtained through the use of cavities from which the stored light energy can be coupled out at a predetermined time.

An optical system adapted to generate single picosecond pulses with the aid of electro-optic reflectors is shown in Fig. 2.11. In this arrangement, the entrance faces of all elements are oriented at the Brewster angle to the laser beam. The laser optical cavity consists of two electro-optic reflectors with a roof prism on the side, a phototropic (bleachable) shutter, a laser rod, and rotating prisms. Part of the laser emission is coupled out of the laser cavity through a small air gap between the prisms (which can be adjusted to control the transmission) and fed between the electrodes of a light-controlled spark-gap. The Q of the laser cavity is switched to a high value by manipulating one of the controlled reflectors. When the picosecond pulse inside the laser cavity grows sufficiently strong to break down the light-controlled spark-gap, the pulse generated by the spark-gap switches the second controlled reflector, and the laser pulse is coupled out.

Controlled electro-optic reflectors can be used in other optical arrangements for the generation of picosecond pulses, notably in ring systems, such as shown in Fig. 2.12. The optical system shown in Fig. 2.12*a* is employed in the laser oscillator described in [32]. In this laser, the output train of picosecond pulses is coupled out through a semitransparent mirror. A ring system employing electro-optic shutters and producing individual output picosecond pulse is shown in Fig. 2.12*b*. At first, the laser emission is built up in a closed circuit. When the energy within the laser cavity attains a maximum value, the electro-optic shutter is switched to enable the laser to discharge all of its energy in a single picosecond pulse.

2.3. Electro-Optic Control of the Laser Cavity

Electro-optic shutters and controlled electro-optic reflectors offer a promising approach to the control of laser oscillators. The dependence of the transmission (or reflectivity) of electro-optic devices on the applied control voltage may be utilized to generate nanosecond light pulses at high Q-switching speeds [33] by coupling out the stored energy [34], to generate picosecond pulses by means of mode-locking [35], to control the pulses by means of an external negative or positive feedback [36], etc.

Generation of nanosecond pulses with fast Q-switching. The operating principle of a Q-switched laser oscillator may be ex-

plained as follows. When the flash tube is fired, the laser is pumped in a non-resonant mode because its Q is switched to a low value (for simplicity, it may be assumed that one of the mirrors is removed from the cavity). Because of the non-resonant mode, no lasing action can take place, and there is only a build-up in the population inversion of the laser rod. When the population inversion reaches an optimum value, the Q of the laser cavity is suddenly switched to a high value (for simplicity, it may be assumed that the missing mirror is suddenly swung into the laser cavity), thereby switching the laser cavity into resonance and causing stimulated oscillations to be generated from spontaneous noise. For some time, called the delay time, t_d, the oscillation builds up linearly, then non-linearly until the gain of the laser material becomes saturated. As the excited states are depopulated the emission power decreases. During the time between the build-up and the decrease in the emission density in the cavity, some of the emission is coupled out through one of the cavity mirrors having a non-zero transmission. The output beam characteristics of an instantaneously Q-switched laser oscillator can be evaluated in terms of the theory developed in [37] from the balance of laser emission density and population inversion in the unimodal approximation. The expressions for output energy, pulse peak power, and the time delay of a single giant pulse for a three-level system under homogeneous broadening conditions have the form

$$E = (\gamma_a/2\gamma)(n_i - n_f) N_0 h\nu V \tag{2.16}$$

$$P = \gamma_a \varphi N_0 h\nu V/\gamma t_1 \tag{2.17}$$

$$t_d = \frac{t_1}{\alpha_0 l (n_i - n_p)} \ln\left(1 + \frac{n_i - n_p}{200\varphi_i}\right) \tag{2.18}$$

where n is the relative population inversion equal to $(N_2 - N_1)/N_0$; N_1 and N_2 are the atom number densities in the ground and excited states; $N_0 = N_1 + N_2$; t_1 is the photon transit time through the laser cavity; $n_p = \gamma/\alpha_0 l$; l is the length of the laser rod; α_0 is the absorption coefficient at the maximum of the emission line of the laser rod; γ are the total losses equal to the sum of the active losses, γ_a, and non-active losses, γ_n (γ_n includes absorption and scattering losses in the optical system; $\gamma_a = -\frac{1}{2}\ln R_1 R_2$; R_1 and R_2 are the coefficients of reflection of the end reflectors); n_i and n_f are the initial and final relative population inversions related by the expression

$$n_p \ln(n_f/n_i) = n_f - n_i \tag{2.19}$$

The quantity φ is given by

$$\varphi = \varphi_i + \frac{1}{2}[n_p \ln(n/n_i) - (n - n_i)] \tag{2.20}$$

where $\varphi = \Phi/N_0$, Φ is the photon density in the laser cavity and

$$\varphi_i \approx (n_i/n_i)\frac{1+n_i}{8\pi\tau_{life}} t_{cav}\Omega \qquad (2.21)$$

Here τ_{life} is the lifetime of the excited state, Ω is the solid angle of the laser beam, $t_{cav} = t_1/\gamma$ is the lifetime of a photon in the laser cavity. The power of a single giant pulse depends on time in a very involved manner which can only be calculated on a digital computer. A plot of photon density and population inversion as functions of time is shown in Fig. 2.13.

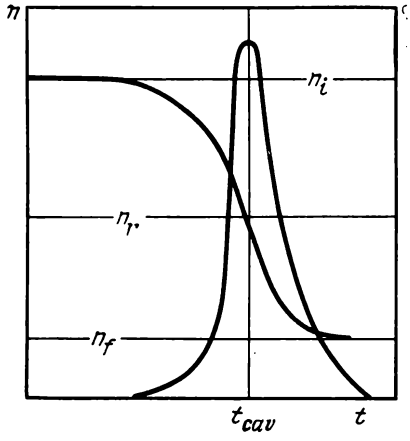

Fig. 2.13. Photon density and population inversion as functions of time for fast Q-switching

The fast Q-switching of laser oscillators can be performed by electro-optic shutters and reflectors. Shutters may be advantageous in laser oscillators using special (say, spherical) mirrors or special dielectric coatings. Where a roof prism is acceptable as the end reflector, preference may be given to electro-optic reflectors (Fig. 2.14*a* and *b*). The choice of a particular type of electro-optic reflector depends on several factors, such as the polarization of the fluorescence emitted by the laser rod, the temperature stability of the output characteristics, etc. To minimize Fresnel reflection from the rod ends, these should be oriented at the Brewster angle (Fig. 2.14*b*). Then a maximum inversion can be obtained during the pumping cycle and the losses at the ends of the optical elements may be reduced to a minimum during the lasing action. According to [38], with a ruby rod measuring 120 mm in length and 8 mm on the side and a type ИФП-1200 flash tube, a single-pulse laser may have an output energy of 2 or 3 J for a pump energy of 400 to 500 J. In operation at a frequency of a few hertz, the performance of controlled reflectors remains unimpaired after several thousand shots. According to [38], this optical system is suitable for pulsed, high-PRF laser oscillators operated on a long-term basis with a pulse energy of 0.3 to 0.5 J. The polarization of output pulses can be controlled, using the optical system shown in Fig. 2.15 [39]. In this arrangement, application of control pulses simultaneously to both electro-optic elements initiates the genera-

tion of pulses of unpolarized light. When, on the other hand, control pulses are applied to the electro-optic elements in turn, the output pulses will alternate in polarization. According to [40], the energy of polarized light pulses does not practically differ from that of unpolarized pulses, because the polarizers in a laser cavity

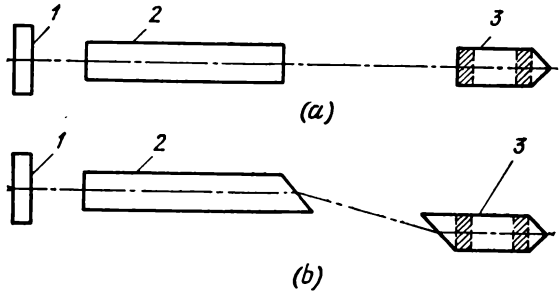

Fig. 2.14. Optical schematics of lasers using electro-optic reflectors
(*a*) with squared rod ends; (*b*) with Brewsterized rod ends; *1*—semitransparent mirror; *2*—laser rod; *3*—electro-optic reflector

employing a laser material which emits unpolarized light (such as neodymium-doped glass) control polarization without affecting the laser energy output (at least, this is true in the absence of induced anisotropy). The duration of the pulses generated by lasers with electro-optic Q-switches ranges from 10 to 30 ns (depending on

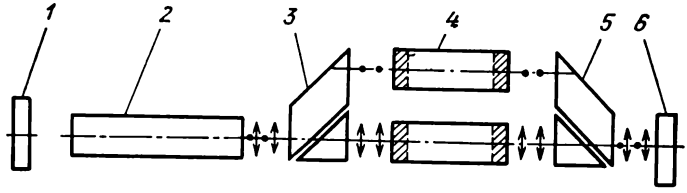

Fig. 2.15. Optical schematic of a controlled-polarization laser
1—semitransparent mirror; *2*—laser rod; *3, 5*—polarizing beam splitters; *4*—electro-optic Q-switch; *6*—100%-reflecting mirror

the pump energy, losses, and laser cavity length). Electro-optically Q-switched lasers compare favourably with other types in that they generate light pulses at precisely predicted instants and also in that they produce only one pulse with any pump level. This is because the Q-switch operates for a time sufficient for the build-up and discharge of only one pulse over a wide range of pump energy values.

Still another type of control is that in which the Q-factor of a laser is switched in steps. By properly selecting the values of the

successive steps of control voltage, it is possible to generate a continuous sequence of pulses. Of special interest is the Q-switching method in which the shutter is first opened just enough to allow the build-up to the threshold value, and is then opened fully upon the appearance of a weak light pulse. This type of Q-switching is to a certain extent similar to the generation of a single giant pulse by a laser employing a phototropic shutter, and may be used to obtain unimodal emission [41] (see Sec. 2.5).

With a few exceptions, slow Q-switching by means of electro-optic devices for obtaining several pulses has not found practical application. A theory examining laser oscillators which employ slow Q-switching is examined in [3, 6].

Generation of nanosecond pulses by coupling out stored energy (regenerative switching). A stored-energy (regeneratively-switched) laser operates on the principle that its Q is rapidly switched to a high value when the population inversion in the laser material is a maximum, and the cavity is "opened" when the radiation density is likewise a maximum [34]. In simpler terms, the process may be explained as follows. During the time interval between the flash-tube pulse and the attainment of an optimum population inversion (that is, in a matter of several hundred microseconds), the laser rod is, as it were, outside the cavity. When the population inversion is built up to an optimum value, the laser rod is placed in a cavity with 100%-reflecting mirrors which promote the build-up of lasing action, and the energy of excited atoms in the laser rod is converted to electromagnetic energy distributed inside the cavity. When the electromagnetic energy inside the cavity attains a maximum density, one of the mirrors is swung out, and the electromagnetic energy is coupled out of the cavity. The time required to couple out the stored energy or, which is the same, the duration of the light pulse, is equal to twice the cavity length divided by the velocity of light, that is $2L/c$. The rise and fall times of the pulse are solely determined by the time required to "swing out" the mirror.

By the theory set forth in [37], the expressions for the output energy E_p and power P_p for this case, neglecting gain and loss when the energy is coupled out, will have the form

$$E_p = N_0 V \varphi_p h\nu \tag{2.22}$$

$$P_p = E_p/2t_1 \tag{2.23}$$

The rise time of light pulses at any point across the beam is decided solely by the time required to "open" the cavity. Therefore, it is unimportant whether the lasing action is initiated earlier at one point than it is at any other point across the beam before the cavity is "open". The spread in the time at which the lasing

action begins at the various points across the beam may only affect the radiation density distribution across the beam by the time the resonator is "opened". This type of laser may employ shutters with various special-purpose polarizers and electro-optic reflectors. Figure 2.16*a* shows an arrangement for coupling out the energy stored in the cavity. As is seen, beam-splitting inside the optical cavity is accomplished by a polarizing beam-splitting prism, while the paths are selected by two delayed electric pulses equal to the half-wave voltage. This method of path-switching offers a number of advantages over switching the rise and fall

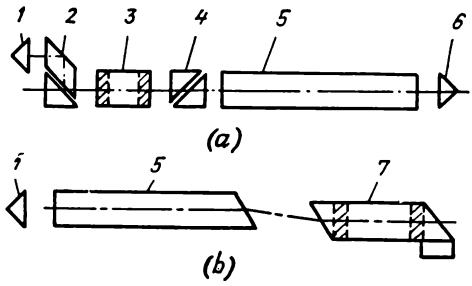

Fig. 2.16. Optical schematics of stored-energy (regenerative-switching) lasers (*a*) with an electro-optic shutter; (*b*) with an electro-optic reflector with a Brewsterized entrance face; *1*, *6*—roof prism; *2*—polarizing beam splitter; *3*—electro-optic Q-switch; *4*—Archard-Taylor prism; *5*—laser rod; *7*—electro-optic reflector

times of a single electric pulse, mainly because the time interval between the switched states of the shutter may be controlled more conveniently. Fig. 2.16*b* shows the optical system of a laser employing an electro-optic reflector with a Brewster-angled input window and a roof prism on the side. This arrangement is free from Fresnel reflection losses on the end faces of the optical components, and so pulses may be generated without any distortion in their trailing edges that might be caused by reflections. In the arrangement of Fig. 2.16*a*, multiple Fresnel reflections from the end faces of the optical elements produce a "tail" on the trailing edge of the light pulse.

Generation of picosecond pulses by mode-locking. In contrast to the generation of picosecond pulses described in Sec. 2.2 where the modes are made to self-lock through the interaction of fluctuation spikes in the spontaneous emission with a non-linear medium, picosecond pulses can be produced by locking the modes through periodic Q-switching during the build-up of the lasing action. According to [35, 42], pulses with a duration of 5×10^{-10} s were generated by locking 20 modes in a laser whose Q was periodically switched externally. The dynamics of this process is theoretically

discussed in [43] where it is shown that pulses are built up in two stages. During the first stage, the pulse duration is reduced due to an increase in the number of locked modes, while during the second stage the pulses are stretched as the modes are unlocked because of the dispersion of the medium inside the cavity. The pulse energy or the average radiation power changes in a manner similar to changes in the intensity of light from a Q-switched laser. Optimum conditions are obtained when a maximum average power and a minimum duration exist together. The frequency of external periodic Q-switching is selected to be equal to the frequency spacing between axial modes. (The frequency spacing between

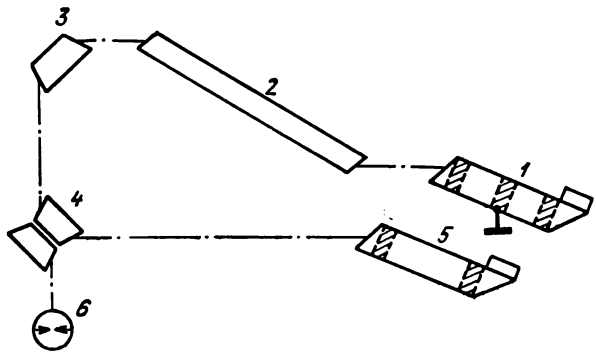

Fig. 2.17. Laser oscillator for picosecond pulses coupled out of the cavity
1, 5—electro-optic reflector; *2*—laser rod; *3*—Brewsterized rotating prism; *4*—two rotating prisms separated by an air gap, to couple part of emission out of the cavity; *6*—light-controlled spark-gap

axial modes is equal to the velocity of light divided by twice the length of the cavity resonator.) As a result, the pulse generated as the laser Q is switched to a high value and then periodically spoiled undergoes a change in waveform each time it passes through the cavity due to gain, losses, Q-switching, and dispersion. As with self-locking where the light is coupled out of the laser cavity through a semitransparent mirror, a train of picosecond pulses appears at the output. In mode-locked lasers producing picosecond pulses, use should preferably be made of optical systems incorporating Brewster-angled elements and controlled electro-optic reflectors. Since these systems have no elements capable of axial mode selection, a great number of axial modes can be locked. With two or more electro-optic controlled reflectors, one can switch the laser Q to a high value, spoil it periodically for mode-locking, and couple the output pulse out of the cavity. In order to accomplish the last-mentioned function, some of the laser emission should be coupled into a light-controlled spark-gap. When this

emission grows sufficiently in intensity, it causes the break-down in the spark-gap, and the latter generates an electric pulse which switches one of the reflectors so that a picosecond pulse can be coupled out of the laser cavity. The best electro-optic reflector suitable for this type of optical system is one with a roof prism on the side and with its ends oriented at the Brewster angle (Fig. 2.17). One controlled reflector is used to switch the laser Q to a high value and spoil it periodically, for which purpose appropriate voltages are applied to the electrodes around the modulating zone, while the middle electrode is returned to earth (a reflector with two independent Q-spoiling zones). The other controlled

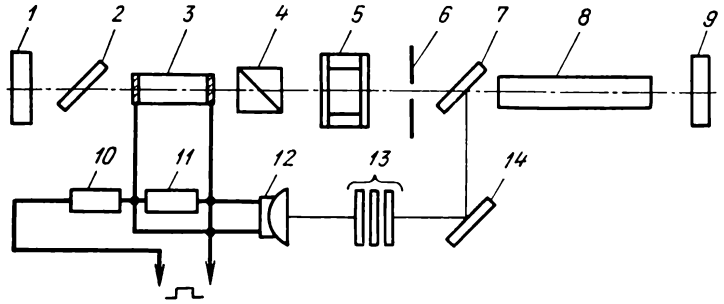

Fig. 2.18. Microsecond-pulse laser oscillator with external feedback
1, 9, 14—mirrors; *2*—quarter-wavelength plate; *3*—KDP crystal (z-cut); *4*—polarizer *5*—bleachable shutter; *6*—aperture; *7*—glass plate; *8*—laser rod; *10, 11*—resistors *12*—coaxial photo-cell; *13*—light filters

reflector is switched by a light-controlled spark-gap to couple picosecond pulses out of the cavity.

Pulse control by external feedback. In the laser cavity control methods discussed above, the electro-optic devices can only be in two states, one with a maximum and the other with a minimum transmission (or reflection), and the characteristics of the output light pulses are mainly determined by the laser cavity and laser rod.

In some cases, however, where it is important to control the waveform and duration of the output pulses, it is essential to vary the transmission (reflection) of the electro-optic device according to the intensity of the output beam. This objective is accomplished by means of external negative or positive feedback. In addition to an electro-optic device, a feedback circuit may contain a variety of optical elements (for example, beam splitters and filters), photodetectors (photo-electric cells or light-controlled spark-gaps) and also electronic devices supporting operation of the feedback circuit and providing a means for active control of light pulse characteristics (Fig. 2.18).

Theoretical and experimental results for lasers with external negative feedback are presented in [120-130]. Negative feedback is mainly employed to avoid spiking and to obtain flat-topped light pulses. For example, reference [130] presents the results of a study into operation of a Q-switched, negative-feedback, ruby laser having the following performance: output pulse duration, 700 ns; emission spectrum width, 3×10^{-2} cm^{-1}; pulse energy 50 mJ; droop of the pulse top, about 10%. The laser used a KDP quarter-wave Pockels shutter and a Kerr cell containing a solution of vanadium phthalocyanine in nitrobenzene in order to narrow the emission spectrum. The feedback path contained a coaxial photo-cell. Since the time lag of the lasing action is negligible owing to the high gain of the laser material and the short photon transit time, the time required for the signal to traverse the feedback circuit (the delay time) should not exceed a few nanoseconds, and the associated photo-detectors and electronic circuits should have a broad-band response.

Positive feedback may be employed for mode-locking in lasers generating picosecond pulses. No reports have so far been published on the use of this form of operation in external positive-feedback solid-state lasers, although some workers have reported mode-locking by means of positive feedback in gas lasers [45, 73]. Positive feedback may likewise be utilized to obtain unimodal emission. In greater detail, these problems are discussed in Sec. 2.5.

2.4. Optical Systems Using Electrically Exploded Film Shutters

An electrically exploded film shutter is capable of handling laser emission at any wavelength, provided it is not absorbed by the substrate material. The optical system of a laser using this type of shutter is shown in Fig. 2.19*a*. The film makes an angle of about 3 to 5° with the direction normal to the axis of the laser cavity. The film shutter is made transparent and the flash tube is fired in a synchronous manner, when the population inversion is a maximum. Since an electrically exploded film shutter remains fully transmitting after it has been exploded, the giant pulse may be followed by several spikes of spontaneous emission if the exciting flash persists long enough. The spikes of spontaneous radiation may be removed by a combination arrangement (Fig. 2.19*b*) in which a film shutter is supplemented by a phototropic (bleachable) shutter. The transmission of the phototropic shutter is such that no spontaneous emission will occur at less than full pump energy, while at full pump energy only one giant pulse will be generated after the film shutter is rendered transparent. A major advantage of this combination is that the shutter can be activated by an external firing pulse and that a single giant pulse is produced.

In [131], there is a description of a laser using two neodymium-doped glass rods with a phototropic (bleachable absorber) shutter placed between them and with a 100%-reflecting mirror separated by a film shutter. This laser proved capable of generating giant pulses with an energy of 130 J and a duration of 40 ns. Although the opening time of a film shutter is somewhat longer than that of an electro-optic shutter, it is considerably shorter than the time

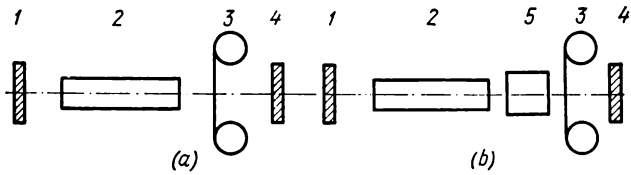

Fig. 2.19. Optical schematic of a laser oscillator
(*a*) with an electrically exploded film shutter; (*b*) with a bleachable and an electrically exploded film shutter; *1*, *4*—semitransparent and 100%-reflecting mirror; *2*—laser rod; *3*—electrically exploded film shutter; *5*—bleachable shutter

required for the lasing action to build up. In other words, a film shutter, like an electro-optic shutter, provides a means for rapidly switching the cavity Q to a high value (see Sec. 2.3).

2.5. Mode Selection Systems

The main criterion for the choice of a laser cavity and the mode-selecting elements described in Sec. 1.4 is the relative values of gain and loss for the selected and suppressed modes.

The gain of the laser material should exceed the loss suffered by the selected mode and be smaller than the loss for the suppressed modes. This relation can readily be secured in low-gain systems, that is, in continuously-pumped oscillators or pulse-pumped free-running oscillators operating near the threshold. In these oscillators, modes can be selected without any special selecting elements. For example, [24] describes continuously pumped YAG and ruby oscillators Q-switched by a spinning mirror in which the dominant transverse mode, TEM_{00}, was selected by the aperture of the laser rod, whose diameter was about 2 mm.

In high-gain pulse-pumped lasers, the output beam usually contains a great number of longitudinal and transverse modes. To avoid multi-modal operation, a large amount of discrimination against some modes is essential.

To select transverse modes in YAG and neodymium-doped calcium-tungstate lasers Q-switched by a spinning mirror, use was made of a stable plane-concave cavity with a slit and a knife edge

on which diffraction occurred in the plane of rotation of the mirror, at right angles to the plane of diffraction [24].

The efficiency with which a laser discriminates against the unwanted modes depends not only on its Q for these modes, but also on the manner in which the oscillation builds up from the spontaneous radiation of fluorescence. The importance of these two factors is discussed in [22]. As will be recalled, with fast Q-switching a laser pulse is produced in two steps [117], the first being a linear build-up during which the amplitude of the electromagnetic field in the modes rises exponentially, and the second being a non-linear build-up. The linear build-up is associated with a negligible change in the population inversion, and the time of linear build-up (the delay time to the threshold of oscillation) may be from a few

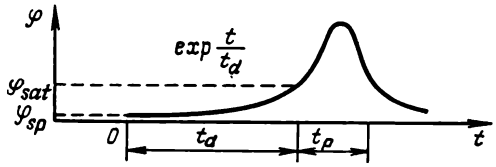

Fig. 2.20. Pulse from a Q-switched laser oscillator. (The scale along the ordinate axis is strongly compressed, $\varphi_{sat}/\varphi_{sp} = 10^{12}$ to 10^{15}.)

tens of nanoseconds to several microseconds, depending on the difference between the gain and loss in the cavity. During the non-linear build-up a light pulse is produced from the energy stored by the inverted energy levels, resulting in the gain saturation of the medium.

Mode selection in lasers with phototropic shutters. In lasers using phototropic (bleachable) shutters, the onset of lasing action occurs at the threshold value, just as the shutter is bleached. The output pulse of a laser using a phototropic shutter has the form shown in Fig. 2.20. The laser emission begins to build up from the spontaneous noise level, φ_{sp}, and the emission density in one of the modes keeps rising exponentially for a relatively long time called the delay time, t_d. When the emission density obtains a level sufficient to saturate the phototropic medium, $\varphi_{sat}(\varphi_{sat} \approx 10^{15}\varphi_{sp})$ the energy stored by the laser is given up as a light pulse for a relatively short time, t_p. The pulse time, t_p = 10 to 100 ns, is by about an order of magnitude shorter than the delay time. The delay time, t_d, depends on the initial inversion level in, and the relaxation time of, the excited states in the laser material and the bleachable absorber. Theoretical studies [22] and experimental investigations [23, 118] have shown that the delay time, t_d, for oscillators with a phototropic shutter is about 2 to 4 μs and the respective number of photon transits through the laser cavity, $m_{tr} = t_d/t_1$,

is about 10^3 (where t_1 is the time of one photon transit). According to [22], the power ratio of two modes by the instant when the shutter is bleached, t_{bl}, is

$$P_n(t_{bl})/P_m(t_{bl}) = (r_{1n}\gamma_n/r_{1m}\gamma_m)^{m_{bl}} \qquad (2.24)$$

where r_{1n}, γ_n and r_{1m}, γ_m are the reflection and loss coefficients for the nth and mth modes, respectively.

From the above ratio, it is an easy matter to calculate the difference in loss between two modes required to suppress one of them. For a laser cavity about 0.5 m long, the emission density ratio for two adjacent modes is about 10 for a difference in loss of only 0.1%. This difference in loss can readily be secured in practical cavities for both longitudinal and transverse modes. Practically any type of stable, aperture-controlled cavities using a homogeneous laser rod, a phototropic (bleachable) shutter may select the required modes or ensure a unimodal emission. In [22], use was made of a concentric and a convex-concave stable cavity (Fig. 2.21). The active element was a 90-degree ruby rod 75 mm long and 63 mm in diameter. The cavity length was 54 cm. The mirrors of the convex-concave cavity had a radius of 5 m. According to [22], although it cannot secure unimodal operation, an aperture is helpful in mode selection due to the fact that with a non-uniform distribution of the inverted population across the diameter of the laser rod, a saturable absorber may act as an aperture just as the shutter is bleached. This may also be facilitated by the symmetrical optical pumping from a helical flash tube. Indeed, it is mentioned in [24] that symmetrical optical pumping by helical flash tubes may somewhat improve mode selection. The laser beam reported in [23] showed diffraction divergence and had a peak pulse energy of 30 mJ. In [25] an optical system is described, built around a semiconcentric cavity incorporating a spherical mirror with a radius of $R = 30$ cm. A phototropic shutter was placed between the ruby and a spherical mirror. The flat mirror was a quartz plate 10 mm thick. An aperture with a diameter 0.8 to 1 mm was placed between the ruby and quartz plate. The ruby rod measured 120 mm in length and 7 mm in diameter. The spectrum width of the laser emission was 100 MHz, which corresponds to a pulse duration of 8 ns. The beam divergence was very close to the diffraction-limited one. In

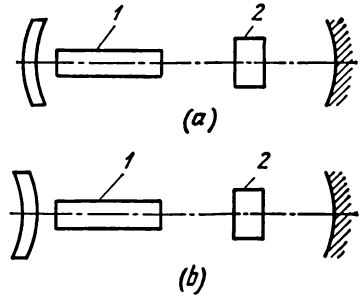

Fig. 2.21. Laser oscillator using (*a*) a concentric cavity and (*b*) convex-concave stable cavity
1—laser rod; *2*—bleachable shutter

[26] use was made of a plane-parallel cavity with a phototropic shutter (a passive Q-switch cell filled with cryptocyanine dissolved in methanol). The laser rod was fabricated from a ruby crystal of a very high optical quality, with parallel ends, 10 cm long. The cavity was fitted with an aperture 2 mm in diameter. The peak power output was 2 mW in the lowest-order transverse (TEM_{00}) modes which were purely Gaussian.

In order to improve the efficiency of mode selection, some workers have shifted the cavity into an unstable region. This was, for example, done in [27] so that the diameter of the mode-selecting aperture could be increased. The laser rods were fabricated from

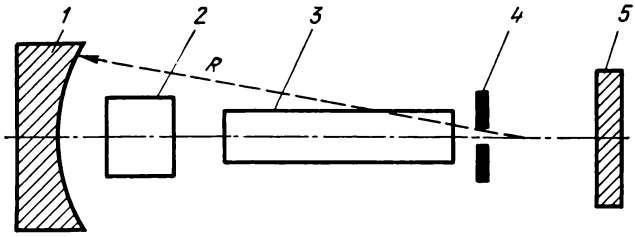

Fig. 2.22. Laser oscillator using a semiconcentric cavity shifted into an unstable region by increasing mirror separation
1 — 100%-reflecting mirror; *2* — bleachable shutter; *3* — laser rod; *4* — aperture; *5* — semitransparent mirror

ruby and neodymium-doped glass. The cavity was made up of a convex spherical mirror with a radius of $R_1 = 3$ m and a concave spherical mirror with a radius of $R_2 = 0.5$ m, separated by a distance somewhat greater than R_2. The unimodal emission was coupled out through the concave mirror. The diameter of the aperture could be adjusted between 0.25 and 0.4 cm. The unimodal emission had a peak pulse energy of 0.04 J. Similar results can be obtained with a semiconcentric cavity (Fig. 2.22) shifted into an unstable region by increasing the separation between the mirrors to $L = (1.1$ to $1.2)\ R$. Unfortunately, the effectiveness of shifting the cavity into an unstable region is markedly limited by inhomogeneities in the laser rod.

In some cases, it is important to generate high-energy pulses with a small angular spread. Special promise in this respect is held out by lasers employing an unstable cavity out of which the output radiation is "diffraction-coupled". With such cavities, the beam is much narrower than with a plane-parallel cavity. The optical schematic of a laser using a large neodymium-doped glass rod and an unstable cavity out of which emission is "diffraction-coupled" [28] is shown in Fig. 2.23. The output pulse had an energy of up to 30 J. A considerable proportion of the output laser beam

was concentrated in the core with a diffraction-limited divergence of 4″. The beam pattern markedly differed from that obtained from a laser using a similar laser rod but a plane-parallel cavity. The giant pulses were much shorter than those generated by lasers using a plane parallel cavity. This pulse compression may apparently be explained by the fact that the cavity configuration forced the light to spread across the laser rod.

Mode selection in electro-optic Q-switched lasers. A long time to the onset of laser emission may also be obtained in magneto-optic and electro-optic Q-switched lasers. A method for increasing the number of passes in a laser cavity with slow Q-switching by a pulsed optical Faraday isolator is described in [116]. With the properly selected magnitude and waveform of discharge current

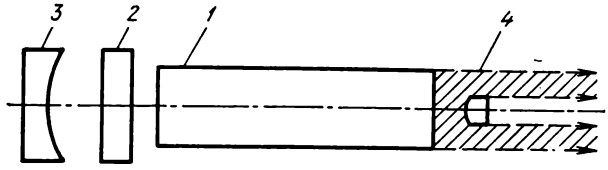

Fig. 2.23. Laser oscillator using a telescopic cavity
1—laser rod; *2*—bleachable shutter; *3*, *4*—100%-reflecting mirrors

through the solenoid, the number of passes through the cavity can considerably be increased in comparison with fast Q-switching. With 700 passes during the linear build-up of laser action, the emission spectrum of a laser using a ruby rod measuring 16 mm in length and 200 mm in cross-section and with a cavity 1 m long was about 4×10^{-2} cm^{-1}, and the angular beam spread corresponded to the lowest-order mode. Longitudinal modes were selected by a plane-parallel plate used as one of the reflectors, and the transverse modes, by an aperture. However, both the energy and power in this form of operation were approximately half as great as their maximum values obtained at a higher speed of Q-switching (approximately three times as high). Thus, mode selection in a laser using an optical isolator is accompanied by considerable losses of energy in the output emission. A much better choice as regards mode selection is offered by electro-optic Q-switched lasers where Q-switching may well be slow. Besides, unimodal operation in an electro-optic Q-switched laser can be obtained by applying a step voltage pulse to the electro-optic shutter at the instant when the population inversion in the laser rod is a maximum. Qualitative time waveforms of the voltage pulse applied to an electro-optic shutter and the resultant laser pulse are shown in Fig. 2.24.

As is seen, the Q is switched in two steps. The lasing action is initiated near the threshold, when the voltage pulse first applied

to the shutter has a peak value. Towards the end of the long linear build-up of oscillation, the mode having the highest Q in comparison with adjacent modes goes into the region of nonlinear build-up first. Thus, a weak unimodal pulse is generated during the first step of Q-switching. When this pulse attains its maximum value, a second voltage pulse is applied to the shutter, setting it to a maximum transmission. As a result, the lasing action keeps building up with a minimum of losses in the cavity, and a unimodal giant pulse is thus generated.

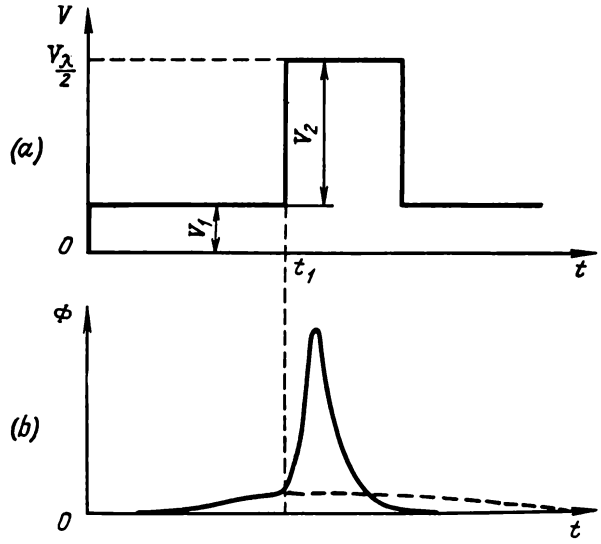

Fig. 2.24. (*a*) Voltage pulse shape and (*b*) light pulse shape from an electro-optically stepped Q-switched laser oscillator

Since the first step of Q-switching produces a pulse at varying times, the light spark-gap that applies the second voltage pulse is caused to break down by the pulse appearing at the end of the first step. The optical schematic of such a laser is shown in Fig. 2.25.

The efficiency of a stepped Q-switched laser as regards mode selection can conveniently be evaluated in terms of the difference in build-up time between two adjacent modes. Obviously, if the difference in build-up time is equal or exceeds the half duration of a pulse, all of the energy stored by the excited states will be used up to sustain only one of the modes during the second step of Q-switching. According to [37], the difference in build-up time between adjacent modes may be described as

$$\Delta t = t_d \Delta\gamma / (\alpha_0 \ln_i - \gamma) \qquad (2.25)$$

where Δt is equal to half the pulse duration, $\Delta\gamma$ is the difference in loss between two adjacent modes, and γ is the loss for the mode being suppressed.

Mode selection in electro-optic Q-switched lasers may be accompanied by piezo-optic vibrations [119] which might appear in the electro-optic crystal (after application of an electric pulse) in the same time interval as the light emission. These piezo-optic vibrations might disturb the build-up of lasing action examined above and impair the mode selecting properties of the system. This is the reason why with stepped Q-switching special measures should be taken to avoid interference due to the piezo-optic effect. Among

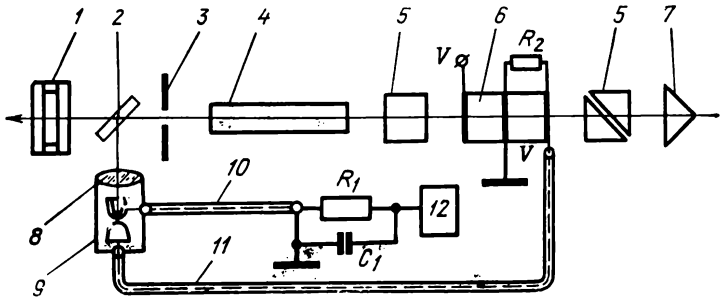

Fig. 2.25. Schematic of an electro-optically stepped Q-switched laser oscillator
1—resonant reflector; *2*—emission coupling-out plate; *3*—aperture; *4*—laser rod; *5*—polarizing prism; *6*—electro-optic crystal; *7*—roof prism; *8*—lens focusing laser emission into a spark-gap; *9*—spark-gap; *10*—charge cable; *11*—discharge cable; *12*—power supply

other things, this can be done by keeping to a minimum the rise time of the first control voltage pulse. Other methods for eliminating the piezo-optic interference associated with stepped Q-switching call for appropriate changes in the geometry and mounting of the electro-optic element in the shutter.

A further development in stepped Q-switching is slow Q-switching and the use of external positive feedback from the cavity to the Q-switch [44]. This method of cavity control eliminates piezo-optic interference. In [44], longitudinal modes were selected by a resonant reflector, while transverse modes were selected by a "piezo-optic" aperture. This was done by exciting piezo-electrically one of the harmonics of the mechanical resonant frequency in the electro-optic element so that the transmission of the shutter was purely Gaussian.

The optical cavity of the laser oscillator shown in Fig. 2.26 consists of a 98%-reflecting mirror and a resonant reflector composed of two quartz plates *6* (14 mm thick and spaced 7 mm apart). The cavity length is 80 cm. The laser rod *5* is a ruby or neodymium-doped glass with an active length of 80 mm and a diameter of

8 mm. The laser rod is optically pumped by a ИФП-800 flash tube enclosed in a quartz reflector. The cavity Q is switched by a quarter-wave shutter composed of a *Z*-cut DKDP crystal *2* (measuring 10 × 10 × 40 mm) and an Archard-Taylor polarizer *3*. The crystal ends are fitted with silver-paste strip electrodes for connection to the shutter control circuit. By means of a plane-parallel

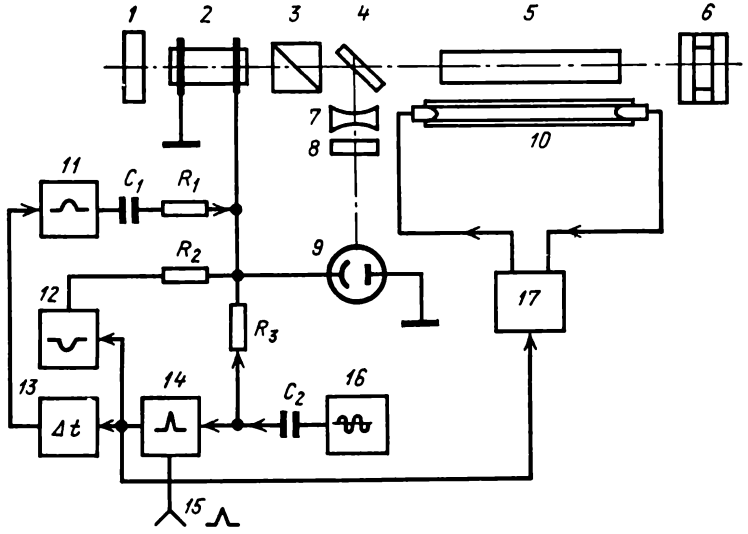

Fig. 2.26. Single-frequency laser oscillator using positive feedback and a "piezoelectric" aperture

glass plate *4* some of the emission is directed onto a coaxial photocell *9* (type ФЭК-09) whose cathode is returned to an electrode on the crystal *2*. The amount of positive feedback can be adjusted by rotating plate *4*, a negative lens *7*, and also neutral and colour light filters *8*. The crystal *2* is energized from a Г3-7А signal generator *16* via capacitor C_2 and resistor R_3. The same voltage is used to synchronize the control voltages applied to the shutter and the control unit *17* which fires the flash tubes *10*. For this purpose, the sinusoidal voltage is transformed by a converter *14* into a train of short pulses out of which a single pulse is gated by applying a trigger signal to input *15*. The pulses from the pulse converter *14* may be used to synchronize operation of the laser with other systems. Arrival of a trigger pulse causes the flash tube *10* to fire. At the same time, an inverter *12* feeds a negative voltage, V_{off} (a Gaussian pulse of 1 ms duration), via resistor R_2 to the cathode of the photo-cell *9* and the electrode of the crystal *2*, thereby causing the electro-optic shutter to close to prevent spon-

taneous emission from the laser (Fig. 2.27*a*). At the instant when the population inversion in the laser rod is a maximum, a delay circuit *13* and a pulse inverter *11* energize the shutter via capacitor C_1 and resistor R_1 with a positive pulse, V_{on}, which causes the electro-optic shutter to open a little. The duration of the pulse generated by the inverter *11* corresponds to the period of the sinusoidal voltage, V_{ex}, furnished by the signal generator *16* (see Fig. 2.27*b*).

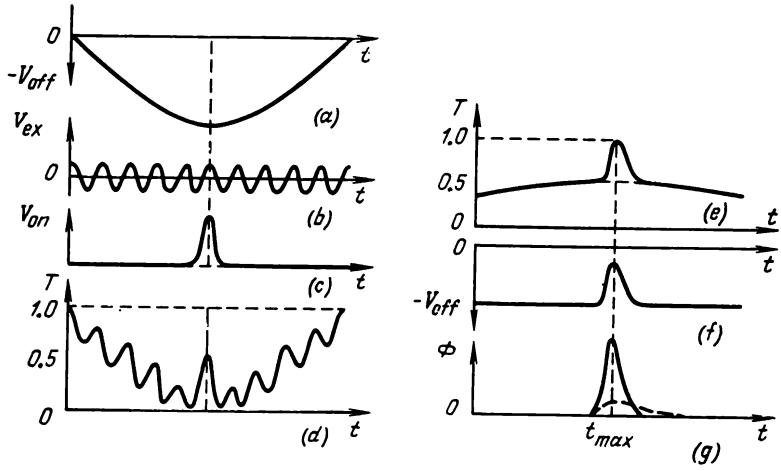

Fig. 2.27. Waveforms of control voltages across an electro-optic shutter, shutter transmission, and laser output pulse

(*a*) cut-off voltage, V_{off}; (*b*) voltage setting up piezo-optical vibrations in the electro-optic element, V_{ex}; (*c*) voltage applied in synchronism with the trigger voltage for slow Q-switching, V_{on}; (*d*) shutter transmission; (*e*) shutter transmission near t_{max} on an exaggerated scale; (*f*) change of voltage due to feedback; (*g*) laser pulse shape (— with feedback; – – – – without feedback)

The transmission of the shutter due to the combined action of V_{off}, V_{on}, V_{ex}, and the feedback voltage is shown in Fig. 2.27*d*, while Fig. 2.27*e* shows the transmission of the shutter on an enlarged scale near the point t_{max}. The sudden increase in the transmission near t_{max} is due to the voltage pulse in the positive feedback circuit (see Fig. 2.27*f*), which appears when a light pulse is generated in the laser cavity. The light pulse generated by the laser is shown in Fig. 2.27*g*.

According to [44], the above described laser has proved capable of generating unimodal pulses with energies of 0.1 to 0.15 J using a neodymium-doped glass rod and 0.15 to 0.2 J using a ruby rod, with a pulse duration of about 30 ns and a repetition frequency of 0.5 Hz.

2.6. Laser Amplifiers

Basic theory. The amplification of light pulses has been examined by several workers [46-49, 3, 132], using balance equations (differential equations of energy and ion conservation).

This approach provides a satisfactory approximation for an analysis of many practical problems. The applicability of this approach is examined in [132].

The amplification of an electromagnetic wave other than plane, say cylindrical or spherical, may also be described, using balance equations which, in the general case, have the form

$$(1/c)(\partial|\Phi_s|/\partial t) + \operatorname{div}\Phi_s = \sigma N|\Phi_s| - \rho|\Phi_s| \qquad (2.26a)$$

$$\partial N/\partial t = -\alpha\sigma N|\Phi_s| \qquad (2.26b)$$

where $\Phi_s = c\Phi$ is the flux of photons through unit section, $\mathbf{c}$ is the velocity-of-light vector, Φ is the spatial photon density distribution of the light being amplified, N is the spatial population inversion distribution, α is the coefficient determined by the level structure of the inverted population (in the case of identical statistical weights, $\alpha = 2$ for a two-level model and $\alpha = 1$ for a three-level model), ρ is the lumped (non-saturable) loss coefficient, and σ is the light absorption cross-section.

Assuming that the population inversion and the photon density are independent of the y, z coordinates in the case of a plane wave, or the z, φ coordinates in the case of a cylindrical wave, and the θ, φ coordinates in the case of a spherical wave, setting $x = r$ for uniformity, and introducing the function $\Psi = r^a\Phi$ (where $a = 0, 1, 2$ for the plane, cylindrical and spherical wave, respectively), the equations (2.26) for the three cases may be re-cast as follows:

$$(1/c)(\partial\Psi/\partial t) + \partial\Psi/\partial r = \sigma N\Psi - \rho\Psi \qquad (2.27a)$$

$$\partial N/\partial t = -\alpha\sigma r^{-a}N \qquad (2.27b)$$

The boundary and initial conditions corresponding to equations (2.27) are

$$N(t=0, r) = N_0, \quad \Phi_s(t=0, r_0) = \Phi_{s0} \qquad (2.28)$$

Integrating equations (2.27) with respect to t and setting $f = \int_0^t \Phi_s dt$ gives the following expression for the population inversion on the Cartesian, spherical and cylindrical coordinates

$$N = N_0 r^{-a} e^{-\alpha\sigma f} \qquad (2.29)$$

Using Eq. (2.29), it is an easy matter to see that

$$\Psi\sigma N = (N_0/\alpha)\, r^a\, (\partial/\partial t)\, e^{-\alpha\sigma f r^{-a}} \tag{2.30}$$

Transforming equations (2.27) with the use of equality (2.30) gives an equation of the form

$$(1/c)\,(\partial f/\partial t) + \partial f/\partial r = (N_0/\alpha)\, r^a \left(1 - e^{-\alpha\sigma f r^{-a}}\right) - \rho f \tag{2.31}$$

Denoting $\xi = cf$ and the right-hand side of Eq. (2.31) as $V(f, r)$, reduces Eq. (2.31) to a non-linear equation in partial derivatives of the form

$$\partial f/\partial \xi + \partial f/\partial r = V\,(f,\, r) \tag{2.32}$$

which can be solved by the characteristic method, using the equations

$$dr = d\xi \tag{2.33a}$$

$$dr = df/V\,(f,\, r) \tag{2.33b}$$

For convenience, f may be written as $f_s = \int_0^t \Phi_s dt$ (giving the number of photons in the light being amplified, that have passed through unit section at point r by the time t). Then, in the general case

$$f = r^a f_s$$

In the general case, this equation has no solution. However, one can obtain approximate solutions in two cases, namely at a very small value of f_s and a very large value of f_s. Then in the former case, that is with linear amplification in the inverted population, or on satisfying the condition

$$\alpha\sigma f_s \ll 1 \tag{2.34}$$

the solution can be written as

$$f_s = f_{s0}\,(r_0/r)^a e^{(\sigma N - \rho)\,(r - r_0)} \tag{2.35}$$

where f_{s0} is the number of photons passing through unit section at point r_0 over the time interval from 0 to t.

It should be noted that on satisfying the condition $r_0 \leqslant \leqslant r e^{-(\sigma N - \rho) r/a}$ in the cylindrical and spherical cases ($a = 1,2$) the radiant flux density will decrease in comparison with its initial value at $r = r_0$.

With the other simplification, that is

$$e^{-\alpha\sigma f r^{-a}} \ll 1 \tag{2.36}$$

Eq. (2.33) reduces to an ordinary linear differential equation whose solutions on Cartesian, cylindrical and spherical coordinates have respectively the form

$$f_s = f_{s0}e^{-\rho r} + (N_0/\alpha\rho)\,e^{-\rho r}(1 - e^{\rho r}) \tag{2.37a}$$

$$f_s = f_{s0}(e^{-\rho r}/r) + (N_0/\alpha)(e^{-\rho r}/r) \times \times [(r_0/\rho - 1/\rho^2) - e^{\rho r}(r/\rho - 1/\rho^2)] \tag{2.37b}$$

$$f_s = f_{s0}(r_0/r)^2 e^{-\rho r} + (N_0/\alpha)(e^{-\rho r}/r^2)[(r_0^2/\rho - 2r_0/\rho^2 + 2/\rho^3) - - e^{r\rho}(r^2/\rho - 2r/\rho^2 + 2/\rho^3)] \tag{2.37c}$$

It should be noted that even at sufficiently high values of r, the conditions (2.34) and (2.36) may be satisfied at different times during the amplification of the pulse, say, Eq. (2.34) at the beginning and Eq. (2.36) at a later time. For example, with a rectangular pulse having steep sides, the photon density will grow with no bound near the wavefront, while a condition of saturation will exist in the remaining part of the pulse being amplified.

In the general case, Eq. (2.33) must be integrated numerically [50].

A distinction of the cylindrical and spherical cases is a minimum in the curve relating f_s to the distance r in the inverted population, with both the position of the minimum and the slope of the curve being strongly dependent on the initial conditions given by (2.37). With a further increase in r, the curves for the spherical and cylindrical cases approach that for the plane case.

Population inversion for light amplification. For the amplification of laser light, the laser material must be maintained at a high population inversion and a high gain. In practice, this entails a number of difficulties because the excited laser material is unstable.

One of the parasitic effects reducing the population inversion in a pumped laser material is amplified spontaneous emission (superfluorescence). It occurs in any laser material with a population inversion. However, its detrimental effect, namely the tendency to reduce population inversion and to generate strong noise, is only felt at high gain (10^3-10^4). At these values of gain, there is a sudden increase in intensity, a decrease in beam divergence, and a change in the waveform of the fluorescence pulse in both ruby [53] and neodymium-doped glass [54]. There were obtained superfluorescence pulses [53] independent of the pump time and having energies of about 100 J and a duration of about 100 μs.

In high-gain laser materials, ordinary superfluorescence pulses may be accompanied by giant pulses of superfluorescence [55], when photons are amplified during one pulse to a point where

most of the active particles are made to lase. According to [55], the condition for giant pulses of superfluorescence to be produced may be written as

$$k(t_0/t_{ex})(N_2/N_i)(\Omega_{eff}/2\pi) > 1 \qquad (2.3^3)$$

where t_{ex} is the lifetime of particles in an excited level, t_0 is the photon transit time through the laser material, N_i and N_2 are the initial population inversion and the population of the upper operating level, respectively, and Ω_{eff} is the effective solid angle of fluorescence determined by the laser rod geometry.

Near threshold defined by (2.38), the duration of the radiated pulse will be several t_0, while above the threshold the duration of a superfluorescence pulse will tend to t_0. In [55], such pulses with a duration of about 10 ns and an energy of about 4 J were obtained after the gain of the laser material had been increased from 10^4 to 10^8 by turning on the electro-optic shutter placed between an end of the laser rod and a reflecting mirror. In these experiments, the time during which a photon passed through the laser rod was about 16 ns. The pulse appeared 25 to 30 ns after the shutter had been turned on. Thus, a giant pulse of superfluorescence appeared after two or three passes through the laser material. Giant pulses of superfluorescence with an energy of up to 70 J and a duration of about 70 ns were also observed in [56].

With a sufficiently high gain, superfluorescence may be accompanied by parasitic oscillations caused by feedback due to the radiation scattered in the laser material. A source of feedback may be also the rough side surface of the rod [57]. This effect may be minimized through the use of immersion or cladding with a high absorption at the wavelengths of laser emission (1.06 μm for a neodymium-doped glass laser). To minimize the effect of superfluorescence and parasitic oscillation, the laser material intended for high-gain work should be distributed among a number of optically isolated cascaded stages.

The simplest way to optically isolate amplifier stages is to space them a great distance apart, thereby minimizing the solid angle within which parasitic emission can occur. Unfortunately, this method is inefficient and unnecessarily increases the physical size of the laser system. A more efficient way to isolate amplifier stages optically is to employ various shutters (bleachable, electro-optic, and electrically-exploded films). When bleachable shutters are used for this purpose, they form together with the laser rod a two-component amplifying and absorbing medium manifesting a well-pronounced threshold behaviour towards the intensity of incoming light pulses. Electro-optic shutters in this function are convenient because they can only be opened during the passage of pulses. However, electro-optic shutters have to meet more stringent requi-

rements as regards their residual transmission in the "closed" state than when they are used in laser oscillators. Electrically exploded films show no residual transmission in the "closed" state, but, since they cannot be closed again after they have been made transparent, they may well pass superfluorescence pulses and parasitic oscillation in the wake of the amplified pulses. All of the shutters listed above, show two-way transmission in the open state. With amplified pulses of high energy the reflected wave may cause damage to the input stages of the amplifier system. Besides, at high gain, a "giant" pulse of superfluorescence may appear at the instant just as the shutter is opened. In order to obtain a one-way transmission in an amplifier system, use is made of optical isolators based on the Faraday effect.

Thus, a high-gain medium can be obtained by securing a high level of population inversion in each of the optically isolated amplifier stages in which superfluorescence and parasitic oscillation due to scattering in the medium has no marked effect on the population inversion level.

The laser rods employed in amplifier stages may markedly differ in geometry and size from those used in laser oscillators. This is especially true of output amplifier stages having a large cross-section and length. Because of this, they might promote several parasitic processes which accompany optical pumping and may reduce the population inversion. For example, the population inversion might be reduced by so-called whispering modes locked inside the rod [58]. Whispering modes may be prevented by roughing the surfaces [59], by making annular or axial flats on the side surfaces [60], by providing slits in a combination with a rough surface [59], or by using immersion or cladding [59]. The population inversion may also be reduced by the amplification of the pump light in the spectral region coincident with the fluorescence spectrum of the laser material. To prevent this, resort is made to cladding that absorbs the pump emission at the wavelength coincident with the fluorescence spectrum of the laser rod. For example, for neodymium-doped glass rods cladding may be made from samarium-doped glass [59] or a solution of samarium-nitrate in glycerine [59].

Still another factor limiting the increase in population inversion by optical pumping is the parasitic emission due to Fresnel reflections from the ends of the laser rod. In principle, this detrimental effect might be avoided by applying anti-reflection coatings to the rod ends. Unfortunately, anti-reflection coatings have a relatively low damage threshold. Therefore, parasitic emission is prevented by tilting one or both ends of the laser rod through a small angle (usually, 1.5 to 3°). To avoid inconveniences in adjustment because of the resultant optical wedge, these tilted ends may be made pa-

rallel. A disadvantage of this method is the loss of the amplified emission because of Fresnel reflection from the tilted ends. In amplifying polarized light, use may be made of laser rods with Brewster-angled ends. This device may be effective only if optical pumping does not bring about thermal distortions in the laser rod. That might lead to double refraction. In turn, double refraction would distort the polarization structure of the emission, and this, after the succeeding reflections from the Brewster-angled ends, would cause additional losses and upset the initial intensity distribution of the amplified emission in a plane normal to the direction of light.

Single-pass travelling-wave laser amplifier. This consists of optically isolated amplifier stages through which the light beam to be amplified passes in one direction only [61]. In travelling-wave laser amplifiers, the utilization of the inverted-population medium

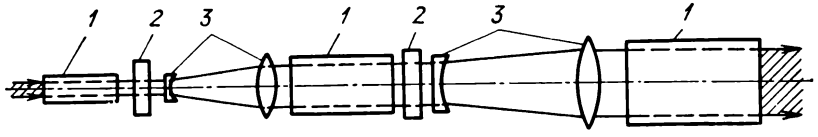

Fig. 2.28. Travelling-wave amplifier
1—laser rod; *2*—shutter; *3*—beam-expanding telescope

within the linear amplification region is negligibly small, and the output energy is limited by gain saturation or by the damage of the laser material. Because of this, the early stages should preferably have a small cross-section so that the pump energy will not be wasted in building up a population inversion in large volumes of the laser material. In the non-linear amplification region, as the emission energy density approaches its maximum safe value (for the laser material used), the beam should be broadened because the maximum safe energy may then be raised (in proportion to the broadening of the laser rod). This may be repeated until the limits are reached, imposed by the difficulties in optically pumping laser rods of a large cross-section (Fig. 2.28). Experimental and theoretical studies into the amplification of light pulses by travelling-wave laser amplifiers have been carried out in [62-70]. Among other things, in [62-64, 66, 69] it was found that when a strong light pulse was propagated through a non-linear medium the pulse maximum appeared to travel at superlight velocity, and a method is proposed to raise the power of the laser beam by reducing the pulse duration through control of the leading edge by shutters. In [64-66], a description is given of high-gain amplifiers consisting of several shutter-separated stages matched in cross-sections either through the natural beam divergence or by means of telescopes.

The rod ends were either given an anti-reflection coating or tilted at the Brewster angle. These amplifier systems were capable of producing pulses with a duration of several nanoseconds and with an energy of up to 500 J and also pulses with a duration of several picoseconds and an energy of a few tens of joules.

Greater energies can be obtained either by connecting several amplifiers in parallel [71] or by using amplifier stages of a large cross-section. With such laser rods, however, there are difficulties in obtaining a uniform pumping of the laser rod. Round laser rods

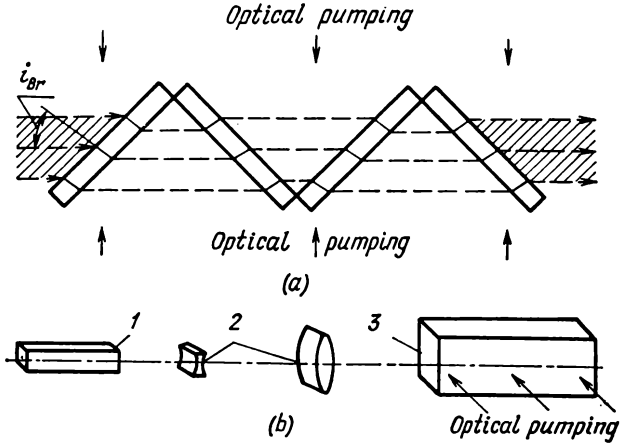

Fig. 2.29. Output amplifier stages using flat rods

(*a*) flat (square or round) laser plates arranged in a zig-zag fashion; (*b*) matching of amplifier stages using rectangular laser rods; *1*—preamplifier rod; *2*—beam-expanding cylindrical telescope; *3*—face-pumped rod used in the output amplifier stage

of large cross-section may readily be fabricated from glasses with a reduced concentration of neodymium. Another approach [72] is to employ discs arranged at an angle to the beam being amplified. If the discs are immersed in a liquid, they may be arranged at any angle. In air, in order to reduce losses due to reflections from the ends, the disc should preferably be Brewster-angled relative to the amplified beam. The discs may be arranged either in parallel or in a zig-zag fashion. These discs may be face-pumped as shown in Fig. 2.29*a*. Among the disadvantages of this method are the complex design and large size of amplifier stages. In [72] an amplifier is described, with an active stage whose output pulses may have an energy of up to 80 J.

As already noted, the amplified beam may in some cases be broadened by cylindrical telescopes. In such cases, the rod should be rectangular in cross-section so that it can be face-pumped for uniform distribution of the pump energy (Fig. 2.29*b*). The gain of

the laser material and the magnification of the telescopes in this type of stages should be chosen such that the energy per unit area of the output rod end will not exceed the damage threshold of the material. Amplifier stages with rectangular rods and cylindrical telescopes for beam-diameter matching between stages may be combined with other types of amplifiers discussed below as well as they are used at the output of a single-pass travelling-wave amplifier.

Multi-pass laser amplifier. In a multi-pass laser amplifier, the beam is reflected consecutively from plane-parallel or curved mirrors so that it traverses the rod many time. Multi-pass amplifiers are efficient in both the linear and non-linear regions of laser-beam amplification. For the linear amplification of weak pulses, use may be made of multi-pass amplifiers with plane-parallel mirrors. The point is that with linear amplification the transmitted pulse leaves initial population inversion practically unaffected, and the same inverted population may naturally be used repeatedly [74, 75]. In practical laser amplifiers, on passing through the laser rod, the beam is reflected in the reverse direction as shown in Fig. 2.30. The beam will be able to traverse the rod a sufficiently large number of times, if measures are taken to limit superfluorescence. For this purpose, shutters must be placed between the reflectors and the rod (Fig. 2.30*b*). The need for a shutter markedly complicates the design of multi-pass amplifiers. For low values of gain, use may be made of amplifiers without optical isolation and a small number of passes (two or three passes).

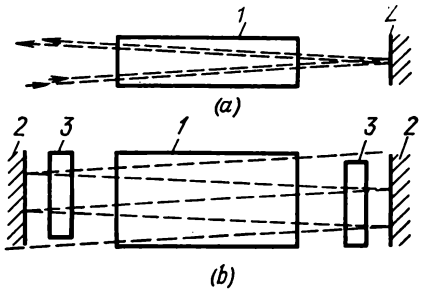

Fig. 2.30. Multi-pass laser oscillator (*a*) two-pass amplifier; (*b*) multi-pass amplifier with pulse-switched Q; *1*—laser rod; *2*—100%-reflecting mirror; *3*—shutters

Multi-pass amplifiers with plane-parallel mirrors are advantageous where the beam to be amplified has a small light diameter, for example, a single-mode beam. A major disadvantage of these amplifiers is the incomplete utilization of the inverted population because the beam takes different paths through the rod in the forward and reverse directions. Besides, in amplifiers with a large number of passes one has to reckon with the need to control light transmission at several points at a time (each time the beam is reflected from a mirror). Therefore, where a high value of gain is sought, switched-gain amplifiers discussed below should preferably be used instead of multi-pass amplifier with plane parallel mirrors.

For the non-linear amplification of light pulses with an energy density close to the gain saturation of the laser rod or the damage threshold of the material, use may be made of multi-pass amplifiers with curved mirrors, capable of beam-broadening. As with single-pass travelling-wave amplifiers, a major problem in high-gain multi-pass amplifiers is the optical pumping of the laser rod. The laser rods in multi-pass amplifiers with spherical mirrors may take the form of a cylinder with a low dopant concentration or a plate arranged at an angle to the amplified beam. In some cases, it may be advantageous to use multi-pass amplifiers with cylindrical mirrors. In these amplifiers, the laser rod should be rectangular in cross-section so that it can be side-pumped. A very important feature of multi-pass amplifiers with cylindrical mirrors is the beam spreading after the repeated passes between the mirrors (in which case, all rays experience tautochronism). Figure 2.31*a* shows a three-pass amplifier employing convex-concave mirrors. If the mirrors are arranged to be confocal, the three-pass amplifier will be a telescopic one. A telescopic three-pass amplifier reduces the angular spread of the output beam and, at the same time, broadens it in proportion to the magnification of the telescopic system. Another type of multi-pass amplifier is one with convex-convex mirrors. Convex-convex mirrors make it possible to spread the amplified parallel light beam into a divergent one. In a three-pass amplifier with convex-convex mirrors, the collimated beam becomes divergent after the first reflection, and the angle of divergence is again changed after the second reflection (Fig. 2.31*b*). Depending on the radii of the convex mirrors, the beam divergence may either decrease or increase after the subsequent reflections (Fig. 2.31*c*). In such an amplifier, the energy density of the amplified beam changes according to the gain of the laser rod and the magnification of the convex-convex mirror system. In both cases, the divergent beam emerging from the laser rod may again be collimated by a cylindrical lens (not shown in Fig. 2.31*b* and *c*) which together with the convex mirror makes up

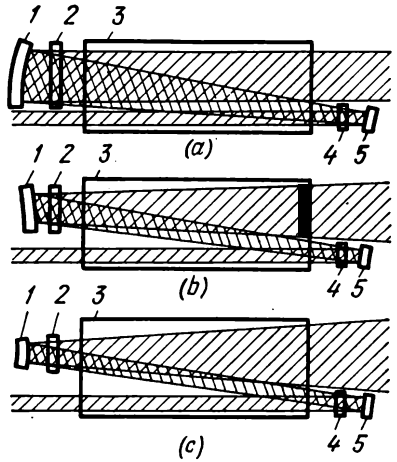

Fig. 2.31. Three-pass amplifier using curvilinear cylindrical mirrors
(*a*) with telescopic arrangement of convex-concave mirrors; (*b*) with convex-convex mirrors; (*c*) with plane-convex mirrors; *1*, *5*—mirrors; *2*, *4*—shutters; *3*—laser rod

a mirror-lens telescopic system. This type of amplifier does not require large reflecting areas as is the case with telescopic ones. Besides, amplifiers with convex-convex mirrors have a higher self-focusing threshold for the laser rod because of the angular spread in the amplified beam. In order to obtain a maximum attainable population inversion, the reflecting mirrors in all multi-pass amplifiers with curved mirrors must be optically isolated from the laser rod. This purpose can conveniently be solved by phototropic (bleachable) or electrically exploded film shutters (because the amplified beam has a large light diameter).

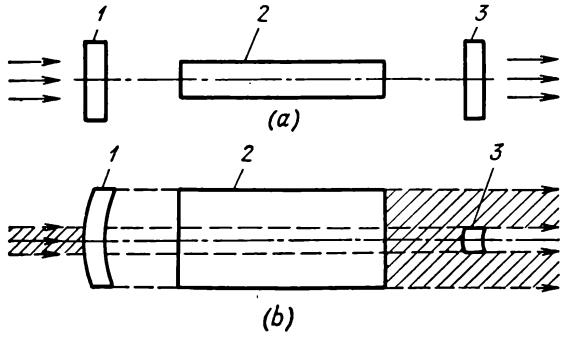

Fig. 2.32. Regenerative laser amplifiers
(*a*) regenerative amplifier using a plane-parallel cavity; *1*, *3*—semitransparent mirror; *2*—laser rod; (*b*) regenerative amplifier using a telescopic cavity; *1*—semitransparent concave mirror; *2*—laser rod; *3*—100%-reflecting convex mirror

Regenerative laser amplifier. As its name implies, a regenerative laser amplifier utilizes positive feedback [76, 77]. The optical system of a regenerative laser amplifier [76] consists of two semi-transparent mirrors with transmissions r_1 and r_2 between which is placed the laser rod. The beam to be amplified is admitted through the mirror r_1, is multiply regenerated in the laser rod due to reflections from the mirrors r_1 and r_2, and emerges through the semi-transparent exit mirror (Fig. 2.32*a*). Regenerative amplification can be realized in other types of cavities, both stable and unstable.

Figure 2.32*b* shows the optical system of a regenerative amplifier employing a telescopic optical cavity [78] in which amplification is accompanied by an increase in the cross-section of the amplified beam so that a large volume of the inverted population contributes to amplification.

Regenerative amplifiers have much in common with laser oscillators and differ fundamentally from single- and multi-pass amplifiers in that they have an optical cavity. Incidentally, the provision of an optical cavity makes them selective towards the spectral

make-up of the amplified beam. There may be also other differences. For example, in a regenerative amplifier with a telescopic optical cavity, the amplified beam may receive a different amount of amplification and have to travel different distances at different points of the cross-section. Irrespective of the type of cavity used, light amplification is possible only if the population inversion is kept below the point of lasing action. A regenerative amplifier can amplify both CW emission and pulses of any duration up to that comparable with the time during which the beam travels twice the distance between the mirrors. At shorter durations, runner-up pulses may appear due to reflections from the mirrors.

In regenerative amplifiers using feedback controlled by a shutter placed between one of the mirrors and the laser rod and turned on at the instant when amplification begins, it is possible to amplify light at population inversions exceeding the threshold of lasing action, but it is possible only for a time interval much shorter than is necessary for spontaneous emission to build up. The use of such regenerative amplifiers is examined in [79, 80]. In [80], a regenerative amplifier boosted a single-frequency emission with a line width of 0.005 cm^{-1}. The spacing between the longitudinal modes in the master oscillator and the regenerative amplifier was 0.008 cm^{-1} at a non-stability of 0.025 cm^{-1}. The input signal was amplified from 10^{-2} W/cm^2 to 10^8 W/cm^2, but the beam divergence increased from 2×10^{-4} to 1.5×10^{-3} rad.

Regenerative laser amplifiers appear to be advantageous in cases involving weak CW emissions or long pulses, where they can provide a large amount of amplification.

Switched-gain laser amplifiers. Also known as multi-pass resonator amplifiers, they are efficient in amplifying weak light pulses with a duration shorter than twice the photon transit time [81]. Such an amplifier is in effect a laser oscillator in which the mirrors are capable of changing transmission and reflectivity in steps from 0 to 1 [37] before and after the onset of oscillation. When the pulse to be amplified is coupled into the amplifier, the entrance mirror is "open", and the exit mirror is "closed". Once the pulse to be amplified is inside the amplifier cavity, the entrance mirror is "closed", and the cavity with 100%-reflecting mirrors begins to amplify the light, starting from the level determined by the energy of the input pulse. When the light intensity has been raised to the desired value, the exit mirror is "opened", and the beam is coupled out of the cavity. According to [37], the energy balance in the cavity at any instant for a two-level system (with the pulses being amplified having a duration which is greater than the time taken by one complete round-trip in the cavity) may be written as

$$E = E_0 + \frac{h\nu}{2} V [(N_t - N) + N_0 n_p \ln (N/N_t)] \qquad (2.39)$$

where E_0 and E are the energies of the pulse before and after amplification, respectively, N_i and N are the population inversion densities at the beginning and end of amplification, N_0 is the active centre density, V is the volume of the laser rod, n_p is the peak inverted population equal to $\gamma/\alpha_0 l_a$, where γ is the loss in the cavity, l_a is the laser rod length, α_0 is the absorption coefficient of the laser rod at the centre of the fluorescence line.

Some of the energy stored by the laser rod is lost because of scattering and absorption in the cavity elements. This part of the total energy, E_{loss}, is given by

$$E_{loss} = N_0 V h\nu \frac{n_p}{2} \ln (N/N_t) \qquad (2.40)$$

If the amplified light pulse is coupled out of the cavity when the energy is a maximum, the pulse duration will be $2L/c$, and its energy $E = {}^1/_2 (n_i - n_p) V N_0 h\nu$. If the duration of the pulses being amplified is shorter than the complete round-trip time, the amplification process may be analyzed, using equation (2.34), the continuity conditions for the number of photons per pulse after reflections from the mirrors. So that equation (2.30) can be conveniently transformed in analyzing changes in the pulse shape caused by amplification, expression (2.31) giving the total number of photons should be replaced with the expression

$$f(x) = \int_0^t e\Phi(x, t)\, dt$$

giving the number of photons passing through the cross-section at point x by the time t. Then the quasi-linear differential equation in partial derivatives will reduce to a system of equations which can be solved by a numerical method to obtain the pulse shape at the various stages of amplification.

The energy of the pulses amplified by a switched-gain amplifier should not exceed the damage threshold of the laser material. This requirement should be remembered in deciding upon the size of the laser rod and the cavity parameters. In a practical realization of a switched-gain laser amplifier, use may be made of a variety of electro-optic devices switched by light-controlled spark-gaps. Especially attractive in this respect are electro-optic reflectors around which a wide variety of optical systems can be arranged for switched-gain laser amplifiers.

Figure 2.33 shows the optical system of a switched-gain amplifier consisting of two electro-optic reflectors (with a Brewster entrance window and roof prism on the side) between which are placed a laser rod and rotatable prisms with Brewster-angled entrance faces. At the entrance to the amplifier, some of the light

beam to be amplified is diverted onto a light spark-gap which generates an electrical signal to switch the electro-optic reflectors after the input pulse is admitted inside the cavity.

A second light spark-gap is located at the exit from a semi-transparent device made up of two prisms one of which rotates the beam inside the cavity through an angle of 90°. The light spark-gap is set to break down when the emission density inside the cavity becomes a maximum. The electrical signal generated by the

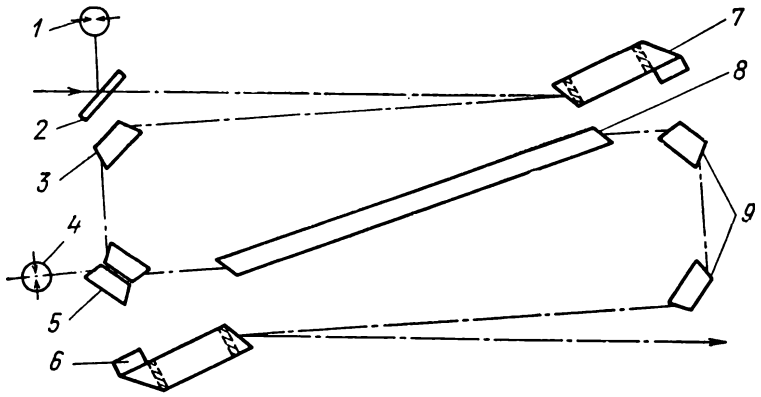

Fig. 2.33. Switched-gain laser amplifier

1, 4—light-controlled spark-gaps; *2*—beam-splitter; *3, 9*—90-degree rotating prisms with entrance faces Brewster-oriented relative to output emission; *5*—two 90-degree rotating prisms with an air gap giving partial transmission owing to disturbed total internal reflection; *6, 7*—electro-optic reflectors with a roof prism on the side; *8*—laser rod

light spark-gap switches the second electro-optic reflector so that the amplified beam can be coupled out of the cavity.

Such an amplifier can boost without any distortion light pulses with durations from a few picoseconds to twice the photon transit time.

2.7. Optical Systems for Second-Harmonic Generation

The conversion of laser emission into that at twice the original frequency is based on the non-linear interaction of the emission with crystals. The non-linear reaction of a dielectric medium to the effect of the laser emission consists in that the wave of polarization induced by the electric field of light and propagated in the dielectric is markedly distorted if the electric field is strong enough. In fact, this distortion may grow cumulatively as the wave of polarization is propagated through the medium. This may be interpreted as a progressive enrichment of the polarization spectrum in harmonic components. A theory of this process has been examined in a number of monographs and reviews [82, 83].

At present, several types of crystals are known to be suitable to generate harmonics. Above all, these are crystals belonging to class $\bar{4}2m$ (KDP, ADP, DKDP, etc.), perovskite ferroelectrics ($LiNbO_3$, $LiTaO_3$, etc.), crystals having the structure of tungstate bronzes ($Ba_2NaNb_5O_{15}$, etc.), hexagonal-pyramide crystals ($LiIO_3$, etc.), and also a number of crystals belonging to other classes and possessing piezo-electric properties. At the present state of the art, however, most of the above listed crystals cannot yet be grown as large specimens having good optical and mechanical characteristics. Most suitable for practical utilization in high-power harmonic generators are KDP crystals, although they are not among the best as regards conversion efficiency.

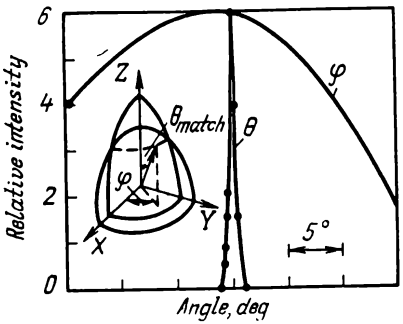

Fig. 2.34. Intensity of the ruby-light second harmonic as a function of KDP crystal orientation

A non-linear element for second-harmonic generation (SHG) is a crystal cut along the phase-matching direction, that is, one along which the input frequency is effectively converted into its second harmonic over the entire path of propagation of light through the crystal. The phase-matching direction is related to the direction of polarization of the interacting waves at the fundamental frequency and the direction of polarization of the second harmonic. The phase-match condition for interactions of the $00 \rightarrow e$ form (in which the ordinary wave at the fundamental frequency is converted into an extraordinary wave at the harmonic frequency) is the equality in refractive index between the wave at the fundamental frequency and the wave at the second-harmonic frequency, that is, $n_o(\omega) = n_e(2\omega)$ [85]. The phase-matching angle, θ_{match} (Fig. 2.34) may be found by the following equation:

$$\cos^2 \theta_{match} = \frac{1 - n_e^2(\omega)/n_o^2(2\omega)}{1 - n_e^2(\omega)/n_o^2(\omega)} \qquad (2.41)$$

where $n_o(\omega)$, $n_o(2\omega)$ and $n_e(\omega)$, $n_e(2\omega)$ are the refractive indexes for the ordinary and extraordinary rays of the laser beam of the fundamental and second-harmonic frequencies, respectively.

In a KDP crystal, for ruby emission $\theta_{match} = 50°49'$, and for neodymium emission $\theta_{match} = 41°31'$ [86]. From the plot of second-harmonic emission output power as a function of the angles θ_{match} and φ shown in Fig. 2.34 it is seen that the maximum power output at the second harmonic occurs at $\varphi = 45°$. The $00 \rightarrow e$ interaction

is an efficient method for the generation of the second harmonic of plane-polarized light, with the plane of polarization of the second harmonic being at right angles to the plane of polarization of the fundamental.

Another type of interaction between the laser emission and the medium is the $0e \rightarrow e$ interaction [88, 89], for which the phase-match condition may be written as follows

$$\frac{n_o(\omega) - n_e(\omega)}{2} \geqslant n_e(2\omega) - n_e(\omega) \tag{2.42}$$

In this case, the angle θ_{match} may be found by the equation given in [88]

$$\cos^2 \theta_{match} = \frac{2\left[2n_e(2\omega) - n_o(\omega) - n_e(\omega)\right]}{n_e(\omega)\left[1 - n_e^2(\omega)/n_o^2(\omega)\right] - 2n_e^2(\omega)\left[1 - n_e^2(\omega)/n_o^2(2\omega)\right]} \tag{2.43}$$

For KDP crystals, the output emission is a maximum at $\varphi = 0$. It should be noted that the condition described by equation (2.43) is not satisfied at short wavelengths, notably for ruby emission. For neodymium emission, θ_{match} is approximately equal to 59° [88]. A distinction of the $0e \rightarrow e$ interaction is the conversion of unpolarized emission into the second harmonic. If the primary emission is plane-polarized, its plane of polarization should appropriately be oriented relative to the crystallographic axes of the KDP crystal, and the second harmonic will be generated due to the interaction of the ordinary and extraordinary rays of the emission. In this case, the plane of polarization of the second harmonic makes an angle of 45° with the plane of polarization of the fundamental.

The SHG efficiency of KDP crystals in the case of the $00 \rightarrow e$ and $0e \rightarrow e$ interactions is investigated in [90-92]. The dependence of SHG efficiency on the power of the primary radiation is shown in Fig. 2.35. As is seen, this relationship is linear only at low efficiency of the order of 10 to 15%; with increasing P_0 the efficiency changes in proportion, tending to a definite limiting value.

The power density of laser light may be increased by focusing the beam in a non-linear crystal. However, focusing by spherical lenses increases the angular beam spread, thereby causing the direction of propagation to depart from the phase-matching direction, and with increasing power, this limits the efficiency to 20% [87].

The SHG efficiency of KDP crystals may be enhanced by means of optical systems some of which are discussed below.

Use of cylindrical optics in second-harmonic generation. Referring to Fig. 2.34, SHG efficiency is strongly dependent on the direction in which the beam is propagated in the plane containing the phase-matching angle and is insensitive to beam divergence

in a plane perpendicular to it. Focusing the laser beam by a cylindrical lens raises emission density in the crystal without practically any increase in the beam divergence in the phase-matching plane [93]. Besides, a cylindrical focusing lens provides a means for controlling the angular beam spread in the plane containing the phase-matching angle without any accompanying change in the emission density in the crystal. This is convenient from a methodological point of view in investigating the effects of beam divergence and laser light density on SHG efficiency. In order to obtain an optimum SHG efficiency, it is important to select a correct focal distance for the lens. This is done on satisfying the condition $\alpha_{ext} = \theta_1 - \theta_{match}$ where α_{ext} is the angle of deflection of the extreme ray in the unfocused beam from the phase-matching direction, θ_1 is the angle between the optic axis of the crystal and the extreme focused ray of the beam given by

$$\cos\theta_1 = \cos\theta\,(2\cos\beta - 1) \qquad (2.44)$$

and the angle β defines the beam convergence in the focusing plane and is such that $\tan 2\beta = d/f$, where d is the beam diameter and f is the focal distance of the lens.

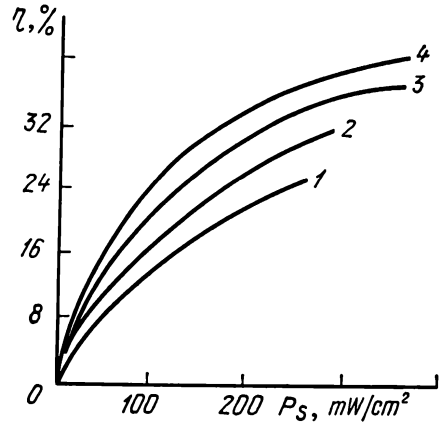

Fig. 2.35. SHG efficiency as a function of the fundamental emission averaged over the crystal length for different lengths, l (*1*) 15 mm; (*2*) 25 mm; (*3*) 40 mm; (*4*) 50 mm

The focal distance of a lens for the $00 \rightarrow e$ and $0e \rightarrow e$ interactions is different. For a beam diameter of 10 mm and a beam divergence of $2\alpha_{ext} = 2'$, the focal distance is $f = 150$ mm in the case of the $0e \rightarrow e$ interaction, and $f = 600$ mm in the case of the $00 \rightarrow e$ interaction. Thus, with all other conditions being equal, the focal distance of a lens for the $0e \rightarrow e$ interaction may be one-fourth of that for the lens used in the $00 \rightarrow e$ interaction, without decreasing the length of coherent interaction of waves in the crystals. This latter condition is satisfied only with an optimum orientation between the cylindrical lens and the non-linear crystal, that is when the focusing plane is at right angles to the plane containing the phase-matching angle in the crystal. The orientation can best be checked by taking a combined far-field photograph of the second harmonic excited in the non-linear crystal by a strongly divergent laser beam and of the beam focused by the cylindrical lens.

A typical far-field photograph for SHG in a crystal 40 mm long and a cylindrical lens with a focal distance of $f = 380$ mm appears in Fig. 2.36. The numerals *1* and *2* mark the intensity distribution of the harmonic for two different positions of the cylindrical lens

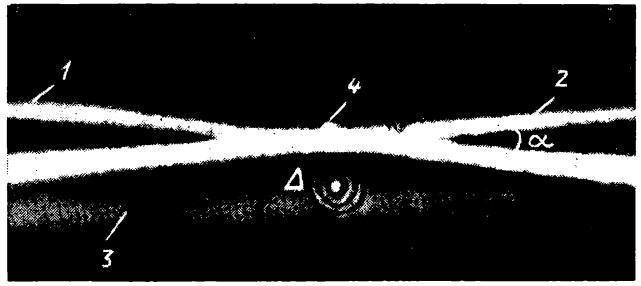

Fig. 2.36. Far-field photograph of the second harmonic produced in a non-linear crystal by (*1*, *2*) focused, (*3*) diverging, and (*4*) defocused laser beam

placed in front of the crystal, while the numeral *3* marks the central maximum in the harmonic intensity distribution when a diverging spherical lens is placed in front of the crystal. The distance Δ corresponds to the angle through which the crystal should be turn-

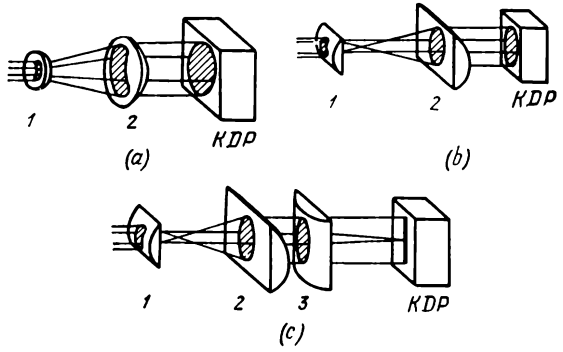

Fig. 2.37. Laser-beam shaping optical systems
(*a*) telescopic axially symmetrical system; (*b*) telescopic system of cylindrical lenses; (*c*) focused telescopic system using cylindrical lenses

ed, and the angle α represents the angle through which the cylindrical lens should be turned in order to obtain an optimum orientation.

Theoretical and experimental studies of the optical systems shown in Fig. 2.37 are summed up in [93]. It has been found that

telescopic systems having either the same magnification in all directions across the beam (Fig. 2.37*a*) or different magnifications in two mutually perpendicular planes (a system of cylindrical lenses, Fig. 2.37*b*) cannot secure a marked increase in SHG efficiency for the simple reason that the decrease in beam divergence due to the telescopic system is accompanied by a marked decrease in laser light density (Fig. 2.38).

The optical system shown in Fig. 2.37*c* avoids the above limitations and secures an optimum relationship between laser light density and beam divergence in the principal plane of the crystal. This is a combination of a telescopic system made up of two cylindrical lenses oriented so that the beam is broadened in the principal plane of the crystal, and a third cylindrical lens which focuses the beam in a plane perpendicular to the principal plane. Practically, this beam-shaping system may be made of two lenses, one negative cylindrical and the other positive spherical. The computations made for SHG [93] by a KDP crystal 5 cm long, using the output beam from a neodymium-doped glass laser with a power density of 20 MW/cm^2 and beam divergence of 2′, have shown that with the above telescopic system the SHG efficiency may be as high as 70% (Fig. 2.38), while without a focusing system the SHG efficiency is only as low as 6%. When the fundamental input is taken from a unimodal laser oscillator with diffraction-limited beam divergence, a sufficiently high SHG efficiency can be obtained only if the beam is focused by a cylindrical lens.

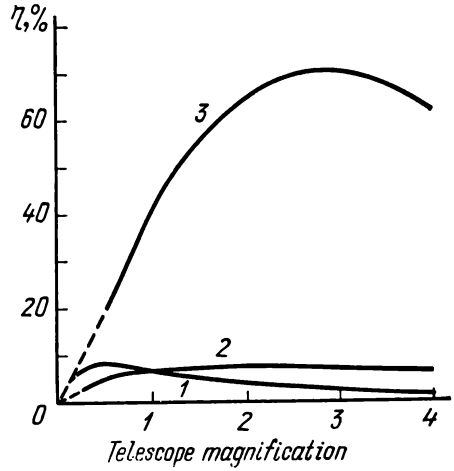

Fig. 2.38. SHG efficiency as a function of system magnification in a crystal 50 mm long

1—axially symmetrical telescopic system; *2*—telescopic system of cylindrical lenses; *3*—focused telescopic system using cylindrical lenses

Second-harmonic generation in the laser cavity. This is another efficient method for enhancing SHG efficiency. A non-linear crystal is placed inside a laser cavity made up of 100%-reflecting mirrors for the primary laser light; one of the mirrors is totally transparent to the second harmonic. With this arrangement, practically all of the second-harmonic light can be coupled out of the cavity.

Second-harmonic power output as a function of laser oscillator parameters (internal loss coefficient, pumping speed, fluorescence lifetime, total number of active particles, stimulated emission coefficient or absorption per photon or atom) can be determined by solving the velocity equations for free-running lasing action [94, 95].

In addition to second-harmonic generation, a non-linear element inside the laser cavity changes the shape of the laser pulse [96, 97], because the non-linear relationship between the cavity losses and the power of the primary laser light results in internal negative feedback.

Consider a Q-switched laser oscillator with a non-linear element placed inside its optical cavity. Within the region where SHG efficiency and power are related linearly and assuming low losses due to harmonic generation, the differential equations of conservation for the relative photon density φ and for the relative population inversion n may be written as follows [97]:

$$d\varphi/dt = \left(\frac{n}{n_p'} - 1 - \frac{a\varphi}{\gamma_{in}}\right)\varphi \tag{2.45}$$

$$dn/dt = -2\frac{n}{n_p'}\varphi \tag{2.46}$$

Here, φ and n are the photon density and the inverted population, respectively, referred to the active particle density N_0; $n_p' = \gamma_{tn}/\alpha_0 l$ is the relative population inversion at the instant when the photon density in the cavity is a maximum without second-harmonic generation. The time is in units of $T = t_1/\gamma_{in}$ (t_1 is the photon transit time) and counted from the instant when the Q is switched to a high value. Initially, $n = n_i$, and the photon density φ_i determined by spontaneous emission is so small that $\varphi_i \approx 0$.

In the laser rod, a uniform population inversion is assumed, very close to the plane wavefront propagated along the cavity axis, and the cavity is assumed to be oscillating in one longitudinal mode whose frequency corresponds to the maximum of the fluorescence line of the laser rod (with uniform line broadening). Equations (2.45) and (2.46) have an analytical solution from which some of the most important parameters of the second harmonic generation inside the cavity can be determined. Thus, by cancelling out the time, one obtains a linear differential equation of the first order whose solution is

$$\varphi(n) = Cn^k - \frac{n_p'}{2k} - \frac{n}{2(1-k)} \tag{2.47}$$

where C is a constant expressed in terms of the initial population inversion of the material and the quantity n_p'; and $k = a/2\alpha_0 l$. Using the expression for φ as a function of n and the condition $d\varphi/dt = 0$ describing the instant when the photon density in the cavity is a maximum, one can determine the peak photon density φ_p and the peak power P_0 of the primary laser light as follows

$$P_0 = N_0 h\nu c S l \varphi_p / L \tag{2.48}$$

$$\varphi_p = n_i (u - v)/2k \tag{2.49}$$

where S is the cross-sectional area of the laser rod, L is the cavity length, c is the velocity of light, $u = (k - kv + v)^{1/(1-k)}$, and

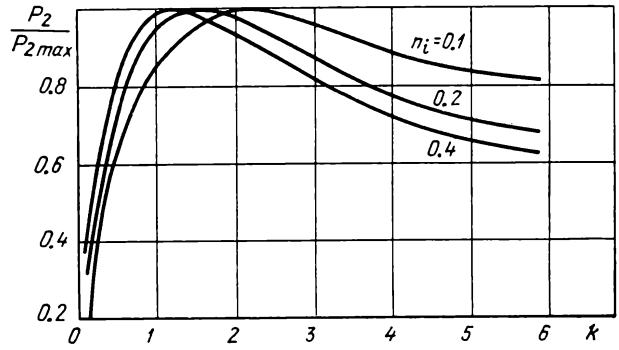

Fig. 2.39. Plot of $P_2/P_{2\max}$ as a function of the parameter k for different values of n_i
(1) $P_{2\max}$=2.5 MW; (2) 25.5 MW; (3) 150 MW

$v = n_p'/n_i$. The peak power, P_2, of the second-harmonic laser light is equal to $\gamma_{p\,\mathrm{SHG}}$ (the maximum power loss associated with second-harmonic generation). The dependence of $P_2/P_{2\max}$ on k for several values of the initial population inversion n_i, at the following parameters: $N_0 h\nu = 4.65$ J/cm^3, $S = 0.5$ cm^2, $l = 8$ cm, $L = 75$ cm, and $\gamma_{in} = 0.15$, is illustrated in Fig. 2.39.

The fact that the maxima, $P_{2\max}(k)$, shift in the direction of decreasing values of k with an increase in the population inversion suggests the existence of an optimum value for the proportionality factor, a, which connects the second harmonic power and the square of the fundamental power for extra-cavity SHG.

The energy density of the second-harmonic laser light is

$$E_2 = \frac{\gamma_{in}}{2}\left[(n_i - n_f) + n_p' \ln \frac{n_f}{n_i}\right] N_0 h\nu V \tag{2.50}$$

where n_f is the final population inversion which can be found from the relationship

$$(n_f/n_i)^k \left[v/2k + \frac{1}{2(1-k)}\right] + (v/2k) = (n_f/n_i)\frac{1}{2(1-k)} \quad (2.51)$$

$$\text{at } k \neq 1$$

With the parameters defined as above, the laser pulse shape found by the numerical integration of equations (2.45) and (2.46) is shown in Fig. 2.40.

In order to determine the energy parameters of SHG inside the laser cavity by the above described method, it is important to know the proportionality factor, a, connecting the second harmonic power and the squared power at the fundamental frequency. For SHG efficiency not exceeding about 1%, use may be made of Kleinmann's relation (equation (123) in [84]). For high values of SHG efficiency, the findings of [93] may be used. Since, however, there is usually a difference of a few per cent between the SHG efficiency found by computation and by experiment [91], one may use the value of a or k determined from the experimentally measured extracavity SHG efficiency for a fixed value of laser beam power output.

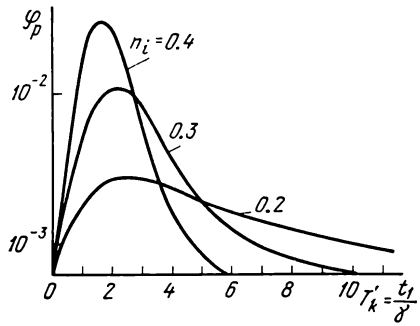

Fig. 2.40. Pulse waveform at the fundamental frequency in a cavity containing a non-linear element (computer solution)

Experimentally, the above-described type of optical cavity using mirrors with multilayer dielectric coatings can hardly be built, because we have no workable process for depositing coatings that would have total reflection at one wavelength and absolute transmission at any other. For example, in [98], the cavity, containing an YAG crystal and a $LiIO_3$ non-linear element 10 mm long and having a phase-matching angle of 30°, was made up of a roof prism and a dielectric mirror with a reflectivity of $R = 99.8\%$ at $\lambda = 1.06$ μm and $R = 15\%$ at $\lambda = 0.53$ μm.

The second-harmonic emission can be fully coupled out of the cavity by means of a polarizing prism which separates in space the orthogonally polarized light components. The fundamental-frequency emission and the second-harmonic emission are orthogonally polarized in the case of the $00 \rightarrow e$ interaction.

A system made up of a non-linear crystal, a polarizing prism, and a mirror is in effect a non-linear reflector. In sketch form,

this type of reflector is shown in Fig. 2.41. On passing through a polarizing beam splitter (see [202] in Chapter 1), the fundamental-frequency component falls on a non-linear crystal cut in the phase-matching direction for the $00 \rightarrow e$ interaction. On being reflected from the roof prism and on passing through the non-linear crystal for a second time, the fundamental frequency and the second-harmonic frequency polarized in two mutually perpendicular planes again enter the beam splitter prism which transmits the fundamental frequency and couples the second harmonic out of the cavity.

A non-linear reflector may be used in any type of laser cavity and with any type of Q-switching. In [99], the above-described non-linear end reflector was used in an electro-optically Q-switched

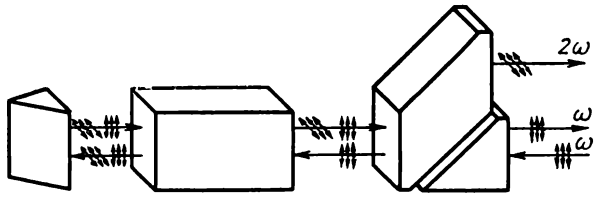

Fig. 2.41. Optical schematic of a non-linear reflector

ruby laser oscillator. The second-harmonic power output obtained by means of a KDP crystal 20 mm long was 20 MW, while the fundamental-frequency power output in a cavity without a non-linear crystal and with optimum mirrors was 25 MW. Thus, it is possible to secure a high efficiency for SHG inside the laser cavity and to control the shape of the laser beam without any special focusing systems.

2.8. Alignment of Optical Systems

In designing a laser system it is important to determine the necessary and sufficient limit of accuracy for the relative alignment of its optical elements. Departures from proper alignment between the optical elements affect the energy, angular spread and spectral make-up of the laser beam to a different degree. The parameters of the laser beam are mostly affected by misalignment of the cavity mirrors. For a cavity made up of plane-parallel mirrors, a maximum Q can only be obtained when the mirrors are precisely parallel. Then the on-axis beam will make a maximum number of passes. In a cavity with non-parallel mirrors, the light beam can make only a limited number of passes.

For example, in [100-102] it is shown that the tilt of the mirrors through an angle of a few seconds may cause the lasing action

to cease altogether. This is, however, true of laser materials having an extremely high spatial homogeneity, for example, gas lasers with flat mirrors. The effect of misalignment between the cavity mirrors on the threshold energy of solid-state lasers according to the quality of laser material, cavity type, and the reflectivity of the exit mirror is investigated, for example, in [103-105]. Qualitatively, the threshold-energy parameters of lasers using different types of laser materials depend on misalignment of their optical elements in about the same manner. Quantitatively, however, this dependence is different and is determined above all by the homogeneity of the laser material. In this respect, of special interest are ruby and neodymium-doped glass, firstly because they are widely used and, secondly, because they differ in alignment procedures and requirements.

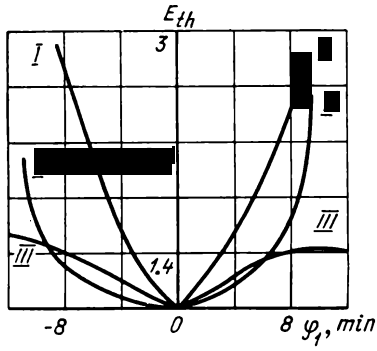

Fig. 2.42. Pump energy threshold as a function of the cavity mirror tilt for different rubies

The threshold energy as a function of mirror tilt for rubies differing in quality is shown in the plot of Fig. 2.42. Curve *I* is typical of rubies of a relatively high optical quality; with them, the threshold energy shows a well defined rise even at a small angle of mirror tilt (about 1′). Curve *II* is typical of rubies for which the refractive index gradient is two or three times greater. These crystals show a considerable misalignment region within which the threshold remains practically unchanged. Curve *III* is characteristic of rubies of a low optical quality. These crystals are insensitive to mirror misalignment over a wide range of angles.

Because of the high optical homogeneity, the threshold energy of neodymium-doped-glass lasers is more sensitively dependent on the accuracy of alignment, especially that of polished-side laser rods (Fig. 2.43). In addition to an increase in the threshold energy, an increase in the mirror tilt brings about a reduction in the slope of the threshold-energy curves (Fig. 2.44) and in the efficiency of the laser.

In the misalignment angle range 0—1′, the threshold energy of a neodymium-doped-glass laser changes by a factor of 3, while that of a ruby laser under the same conditions changes by as little as a few per cent. An optically inhomogeneous rod in a plane-parallel cavity gives rise to "deformation" of the latter [106]. In a special case, the cavity is transformed from a plane-parallel into a spherical one which is less sensitive to mirror misalignment.

In addition to optical inhomogeneity, one is also to consider the distortion caused by the non-uniform pump energy distribution in the laser rod during the pump cycle. The focusing effect of the side surface, coupled with poor heat abstraction, leads to a non-uniform heating and deformation of the laser rod. Its core is heated more, and the ends become spherical [107].

In a plane-parallel cavity, the change in the orientation of the longitudinal axis of the laser rod through up to 30′ has a negligible effect on the threshold energy, the emission mode structure, and the direction of the beam.

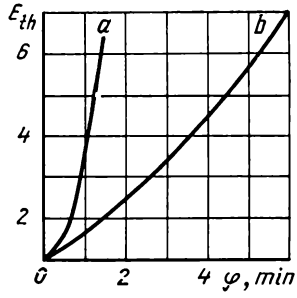

Fig. 2.43. Pump energy threshold as a function of the cavity mirror tilt for neodymium-doped glass
(*a*) polished-sided rod; (*b*) rough-sided rod

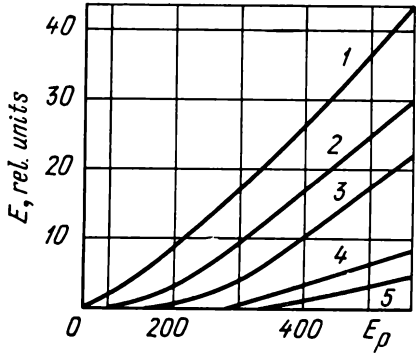

Fig. 2.44. Threshold for lasing action as a function of pump energy for different tilts of cavity mirrors. The cavity mirrors are tilted as follows
1—5″; *2*—15″; *3*—30″; *4*—1′; *5*—15′

In a misaligned cavity, the beam direction is changed. Referring to Fig. 2.45, when the end mirrors are brought out of alignment, the beam is no longer at right angles to the mirrors but deviates in the direction of the tilted mirrors through an angle θ_d, while the near-zone emission maxima undergo a displacement, Δ, towards the distant ends of the mirrors. The beam displacement should be taken into account in deciding on the clear diameter and mount for the mirror. Besides, it should be remembered that mirror misalignment brings about an increase in the angular beam spread [104, 108] in the direction of misalignment. The divergence angle at right angles remains unchanged.

With a large amount of misalignment, the laser beam breaks up into separate discrete directions as shown in the photograph of Fig. 2.46. This is true of both ruby and glass lasers. The smaller the slope of the threshold curves, the smaller the change in the beam direction.

As already noted, the mirror tilt causes a change in the mode make-up of the laser emission. As the angle between the mirrors is increased to a few minutes, the number of modes is markedly

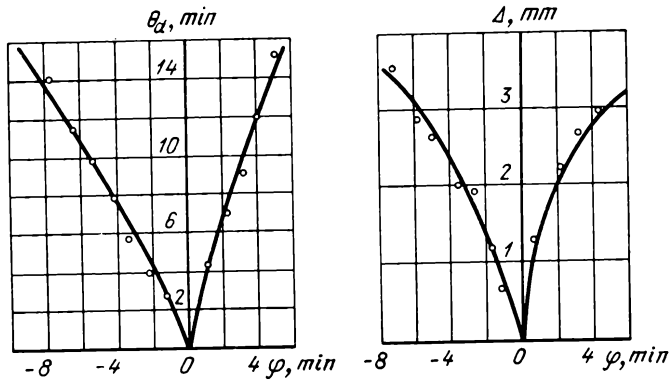

Fig. 2.45. Direction and shift of laser beam according to the tilt of the cavity mirrors

decreased, the spikes grow in amplitude, while the intervals between them are extended and become stabilized. Instead of an opaque mirror, the plane-parallel cavity may utilize a roof prism.

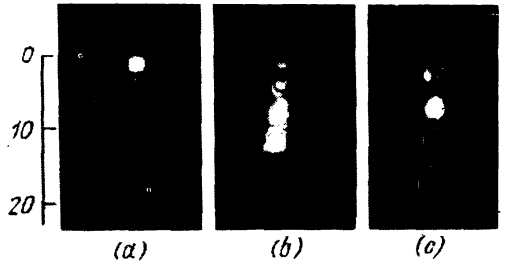

Fig. 2.46. Break-up of laser beam at different tilts of mirrors
(*a*) 0″; (*b*) 60″; (*c*) 90″

However, the use of a prism instead of a mirror entails a number of specific problems. Among other things, the alignment between the prism edge and the crystallographic axis of the laser rod must be more precise. This is because a ruby crystal with its *c*-axis aligned at right angles to the optical axis of the cavity will emit a nearly 100% plane polarized light at low levels of pumping. At higher pumping levels, the polarization decreases [109].

Let the plane of vibration for the vector $\bar{E}$ of the wave incident on the prism make an angle α with the prism edge. Double reflection from the side faces of the prism produces a phase difference δ between the p- and s-components, and the plane-polarized wave becomes elliptically polarized. Introducing the concept of the equivalent reflection, r_{eq}, of the prism and deeming that the amplitude of the plane polarized wave before reflection was E_1, and that the amplitude of the component having the same polarization after reflection is E_2, then according to [110] we get

$$r_{eq} = (E_2/E_1)^2 \tag{2.52}$$

According to α and the phase shift δ, the resultant amplitude will be

$$E_2 = E_1 \sqrt{\cos^4 \alpha + \sin^4 \alpha + 2 \cos^2 \alpha \sin^2 \alpha \cos \delta} \tag{2.53}$$

or

$$r_{eq} = \cos^4 \alpha + \sin^4 \alpha + 2 \cos^2 \alpha \sin^2 \alpha \cos \delta \tag{2.54}$$

A plot of r_{eq} as a function of the angle α for glass and sapphire prisms is shown in Fig. 2.47. The prism has a minimum reflectivity when the plane of vibration of the vector $\bar{E}$ for the incident wave makes an angle of 45° with the prism edge. This is also true of a prism made from an isotropic material. Account should be taken of the additional phase shift between the two components which form as the wave traverses the crystal in a direction normal to its axis.

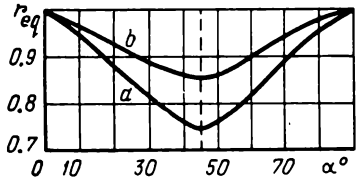

Fig. 2.47. Equivalent reflection of a prism for plane-polarized light as a function of the angle between the prism edge and the plane of vibration of the vector $\bar{E}$
(*a*) for sapphire; (*b*) for glass

Thus, at low pump energies a rectangular prism from any anisotropic material approaches very closely a mirror in its effect, if its edge makes an angle of 0 or 90° with the crystallographic axis of the ruby. With good alignment, the reduction in energy may be as low as less than 2%. A sapphire prism will be equivalent to a mirror if its crystallographic axis is at right angles to its edge. This also holds for the ruby in which one end has the shape of a roof prism. The loss of energy is a maximum in cases where the prism edge makes an angle of 45° with the crystallographic axis of the laser rod.

If, for one reason or another, the crystallographic axis of the laser rod and the edge of the roof prism cannot be aligned precisely, the prism should preferably be made from a material having a low refractive index, such as glass or fused quartz. No advantage can be gained from a roof prism made directly on the crystal.

Laser adjustment methods. The optical elements of lasers can be aligned and their alignment can be tested under service conditions by several methods.

Autocollimation method [111]. The elements of a cavity made up of mirrors and a laser rod can be aligned by a "three-cross" method which consists in that, using an autocollimator, an image of the autocollimating cross from the distant (opaque) mirror is consecutively aligned with an image of the cross from the front end of the laser rod and the exit mirror. The accuracy of alignment by this method is decided by the magnification of the autocollimator. If two distant points are visible from the centre of the autocollimator objective pupil at an angle α_{lim} and if this angle is limit-

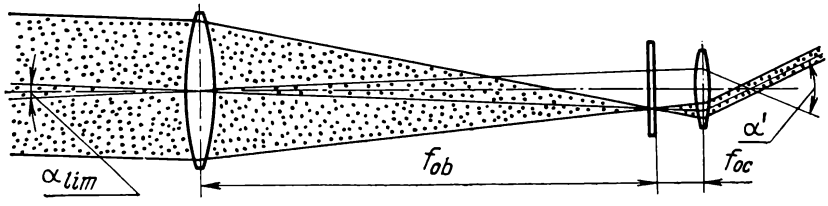

Fig. 2.48. Rays in an autocollimator

ing for a given optical system, it can be found by using the relationship illustrated by the sketch of Fig. 2.48. The apparent magnification of the system is $M = \alpha'/\alpha_{lim}$. The resolving power of the eye is $\alpha' = 60''$. Hence, the resolving power of the system is $\alpha_{lim} = 60''/M$. Since for an autocollimator $M = f_{ob}/f_{oc}$, where f_{ob} is the focal distance of the objective and f_{oc} is the focal distance of the ocular, then,

$$\alpha_{llm} = (60''/f_{ob})\, f_{oc} \qquad (2.55)$$

Thus, an autocollimator using a 200-mm objective and a 20-mm ocular will align the cavity mirrors parallel to within 6″. Despite the high accuracy with which the three surfaces may be aligned, this method does not secure a maximum Q of the cavity. Among other things, this method of alignment cannot detect the wedge-like shape of the laser rod or the deflection of the beam within the rod because of the refractive index gradient, and these defects cannot therefore be compensated for in alignment. As a result, the beam traversing the rod will depart from the original direction and strike the mirror at an angle. The magnitude of this angle depends above all on the quality of the rod material, and for some crystals, such as ruby, it may run into several minutes.

A higher accuracy in cavity mirror alignment can be secured if the rays producing an image of the autocollimating mark are

allowed to be reflected from an opaque mirror and pass through the laser rod before the mark image is matched with the cross-hairs from the front mirror and the front end of the rod. In practice this method is successfully used to align glass lasers. In a ruby laser, an image of the cross from the mirror is heavily blurred due to the inhomogeneity of the ruby crystal, and it cannot be readily matched with the collimator reticle. With a rod diameter of less than 12 to 15 mm, the matter is still more complicated because of the limited field of vision and the insufficient amount of light transmitted by the long and thin ruby crystal. Referring to the plot of Fig. 2.49, markedly different threshold energies are required for the same ruby crystal, depending on whether it has been aligned by the "three-cross" method or the "transmitted-light" method.

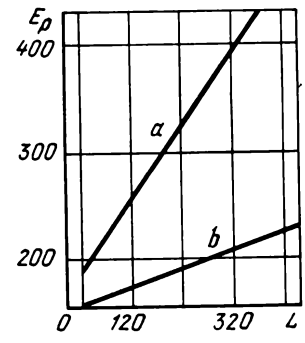

Fig. 2.49. Pump energy threshold as a function of mirror separation for different methods of alignment
(*a*) "three-cross" method; (*b*) "transmitted-light" method

The *optical-lever method* [112] is self-explanatory from reference to Fig. 2.50. A low-divergence beam from a gas laser *1* used as the probe, passes through an aperture in mirror *2*, enters the optical cavity, is reflected from its mirrors *4* and *5*, is again reflected from the

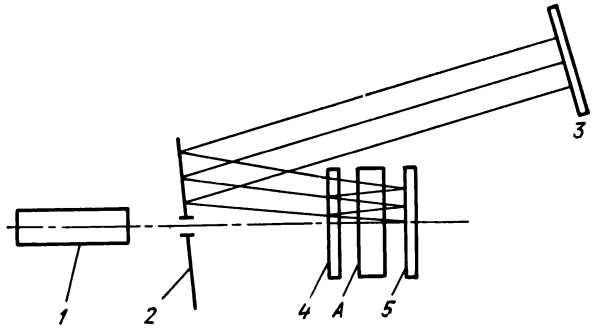

Fig. 2.50. Cavity alignment by the optical-lever method (*A* — laser rod)

mirror *2*, and strikes a screen *3* on which it produces a number of luminous spots in the case of improper alignment and only one luminous spot coincident with the aperture in the mirror *2* in the case of correct alignment. The accuracy of mirror alignment is determined by the separation between the mirrors.

The *interference method* of alignment (Fig. 2.51) avoids the limitations of the autocollimation method, secures a high accuracy, and can readily be monitored [113]. This method consists in that

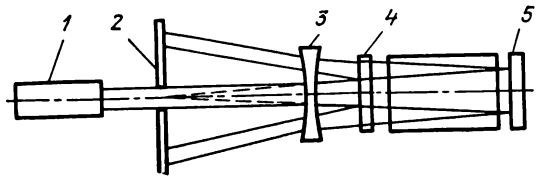

Fig. 2.51. Cavity alignment by the interference method

the probe beam from a gas laser *1* is allowed to pass through an aperture in a screen *2* and a low-power negative lens *3* and to illuminate the cavity mirrors *4* and *5*. The position for, and the power of, the lens are chosen such that the mirrors are fully filled with light. The screen displays two spots which, when superimposed, produce an interference pattern consisting of a number of interference fringes which will be concentric about the light source only if the reflecting surfaces are parallel with one another.

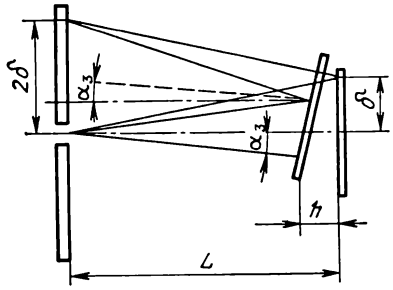

Fig. 2.52. Ray paths in the interference method of cavity alignment

The amount of non-parallelism can be determined from the displacement of the centre of the fringes from the light source (Fig. 2.52). The angle of tilt for the mirrors can be found from the equation

$$\alpha_m = \frac{h\delta}{2(L-h)L} \tag{2.56}$$

If $L \gg h$, then

$$\alpha_m = h\delta/L^2 \tag{2.57}$$

By the interferometer method, mirrors can be aligned parallel to within 5″.

If the optical cavity of a laser oscillator is made up of spherical mirrors, they can be aligned with the laser rod removed (Fig. 2.53) as follows [114]. Screens *1* and *2* with pin-holes in their centres are placed as close as practicable in front of the mirrors. The probe light beam from a gas laser *5* is allowed to strike the exit mirror *3* and the distant mirror *4* through the pinholes. The mirror *4* is adjusted for tilt until the reflected laser beam passes through the pinholes in the screens *2* and *1*. The mirror *3* is adjusted similarly.

When the probe beam, on being consecutively reflected from the mirrors *4* and *3*, passes through the pinhole in the screen *2*, the adjustment of the mirror *3* may be discontinued, because the cavity

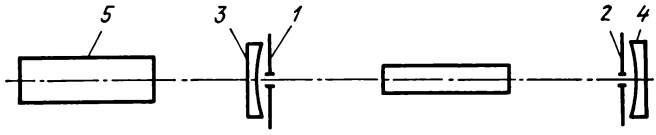

Fig. 2.53. Alignment of a laser using spherical mirrors

has already been aligned as required. After that, the laser rod is placed between the mirrors and adjusted for position until the reflections from the rod ends are lined up with the pinholes in the screens.

For proper alignment of optical elements, use is made of special alignment mechanisms. They should be sufficiently sensitive in order to align the optical elements of lasers to the accuracy ensured by the above described methods.

In sketch form, a mirror alignment mechanism is shown in Fig. 2.54 [115]. A mirror *1* set up in a mount *2* is made fast to a movable base *3*. A bell-crank *4* pivoted on screws *5* and *6* is linked to the base by a leaf spring *7*. Another bell-crank *8* is likewise linked to the base by leaf springs. The position of the base and, as a consequence, of the mirror is determined by three points *I*, *II*, and *III* which are at an angle of 90° to one another. At point *I* there is a ball fitting into tapering holes in the flange *12* and the base. The spherical end of the screw *5* enters a prismatic groove in the flange and bears against the flat surface of the flange. The base is positively locked by two cylindrical springs *10* and *11*. This mechanism provides for a two-step (coarse and fine) alignment of the mirrors in two planes. The mirrors are tilted in two mutually perpendicular directions about the *ox* and *oy* axes. Coarse alignment of the mirrors is secured with the screws *5*, and fine alignment, with the screws *6*.

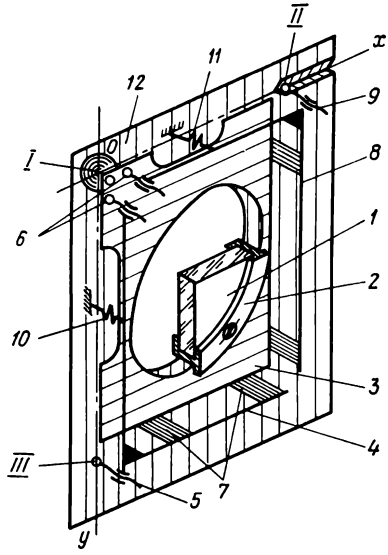

Fig. 2.54. Mechanism for tilting cavity mirrors about two mutually perpendicular axes

The angle of tilt of a mirror is given by

$$\alpha_m = l_3 t_s / l_2 l_1 \tag{2.58}$$

where t_s is the pitch of the fine alignment screw, l_1 is the distance from the axis of the screw *5* to the centre of the ball, l_2 is the distance from the axis of the screw *6* to the pivot of the bell-crank *4*, and l_3 is the distance from the axis of the screw *5* to the pivot of the bell-crank *4*.

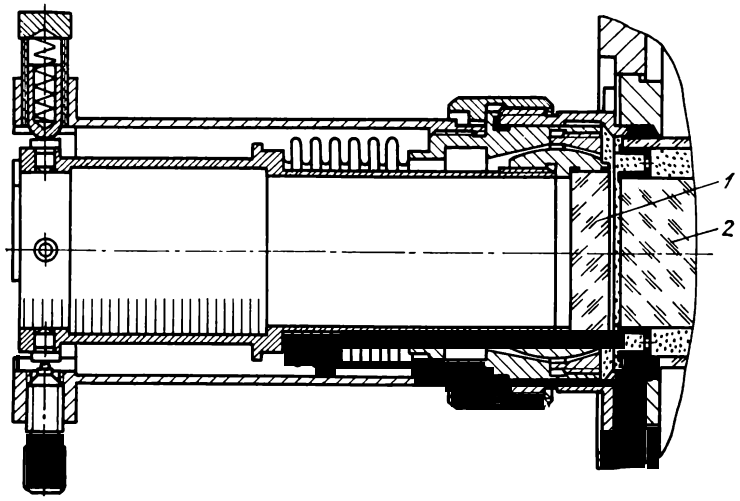

Fig. 2.55. Mirror-tilt mechanism
1—mirror; *2*—laser rod

With this arrangement, a still higher sensitivity can be secured without any increase in the size of the mechanism. For this purpose, the axis of the coarse adjustment screws should be lined up with the pivots of the bell-cranks. Then, $l_3 = 0$ and the angle of tilt of the mirror will be given by

$$\alpha_m = \frac{l_4 (1 - \cos \arctan t_s/l_2)}{l_1} \tag{2.59}$$

where l_4 is the distance between the flange and the pivot of the bell-crank.

The mirror tilt mechanism shown in Fig. 2.55 is hermetically sealed, and the rod ends need not be sealed additionally. The immersion liquid between the laser end *2* and the mirror *1* protects the end against damage by the intense light and minimizes reflections at the interface.

Chapter Three

Electrical Components of Laser Oscillators

3.1. Optical Pumping Tubes

The key element of a laser pump which converts electric energy into light is a lamp or tube. It may be continuous or flashing. A pump lamp or tube is usually filled with xenon or crypton. Emission from pump tubes is extremely complex in its spectral make-up depending on the composition of the emitter, operating conditions, the material of the transparent envelope, etc. Only a tiny fraction of the energy emitted by a pump tube, determined by the absorption spectrum of the laser material, goes to excite active centres. Therefore in the case of a flash tube the principal energy characteristic is the limiting flash energy determined by the duration of the flash, the volume and radius of the luminous body [1]. In fact, the limiting flash energy designed for a definite discharge circuit determines the energy rating of a flash tube. For a continuous pump tube, the principal characteristic is the limiting power of glow.

The operating conditions for pump tubes are determined by the firing voltage, V_f, the spontaneous breakdown voltage, V_s, and the extinction voltage, V_{ex}. The firing voltage is defined as the minimum supply voltage at which the pump tube will reliably be caused to fire by a high-frequency initiating pulse. The spontaneous breakdown voltage is defined as the supply voltage which causes the pump tube to discharge spontaneously (in the absence of an initiating pulse). The extinction voltage depends on the discharge power. At low discharge power, the extinction voltage becomes comparable with the firing voltage, while at high discharge power, the extinction voltage is markedly smaller than the firing voltage [2]. Flash tubes are arranged to operate on a voltage between the firing voltage and the spontaneous breakdown voltage. Continuous pump lamps are arranged to operate on a voltage between the extinction voltage and the firing voltage.

Continuous pump tubes. These tubes are used to pump low-threshold laser rods, such as yttrium aluminium garnet. A YAG laser can be pumped by an iodine-cycle tungsten incandescent lamp. These lamps come in sizes from 600 W to 4 kW. The emission spectrum of ordinary tungsten lamps in the visible and near-infrared regions is very close to the black-body radiation spectrum

(Fig. 3.1). The small additions of iodine introduced to establish the iodine cycle have nearly no effect on the emission spectrum [3].

Because of the difference between the emission spectrum of a tungsten lamp and the absorption spectrum of a YAG crystal, the overall efficiency of the laser system with this type of pumping is low. With a pump lamp operating, for example, at 3200° K and with a laser rod a few millimetres in diameter, the power absorbed

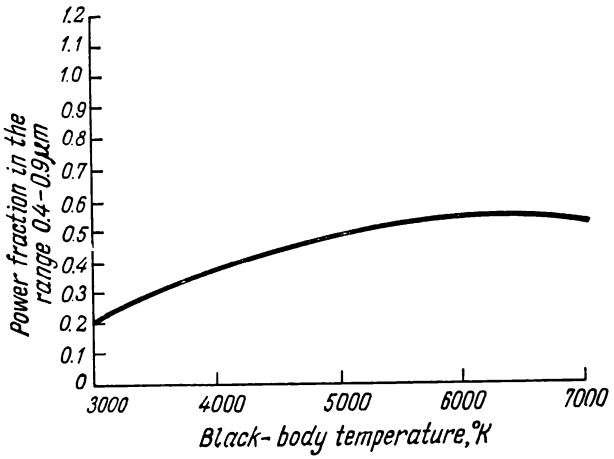

Fig. 3.1. Black-body emission spectrum

by the crystal will not exceed a few per cent of the total power in the emission spectrum. An advantage of incandescent lamps is the high stability of emission. However, extreme care is required in handling incandescent lamps, because seals may be inadvertently disturbed, cracks appear, or the quartz envelope be overheated.

More promising as regards the pumping of YAG lasers are arc tubes operating at low current densities. A distinction of arc tubes is the fact that their emission spectrum contains strong lines [4] which may markedly contribute to the optical pumping of the laser rod. The presence of strong lines in the emission spectrum of arc tubes is due to the high transmittance of the ionised plasma. According to [5] with a current density of about 100 A/cm^2, which is typical of continuous pumping, the xenon plasma column 1 cm in diameter is practically transparent at a wavelength of 8000 Å. With a current density of 2000 A/cm^2, the transmittance is halved.

The line spectrum corresponds to discrete transitions between the bound energy states of gas atoms and ions. The continuous spectrum is mainly produced by the recombination emission of

gas ions when they capture electrons into a bound state. The spectrum make-up depends on the concentration and temperature of electrons and ions. Referring to Fig. 3.2, the emission spectrum of high-pressure xenon and crypton arc tubes shows bright lines in the infrared region, close to the absorption bands of the YAG crystal. Direct-current crypton tubes are a better choice for pumping YAG lasers than xenon tubes, because the absorption lines of

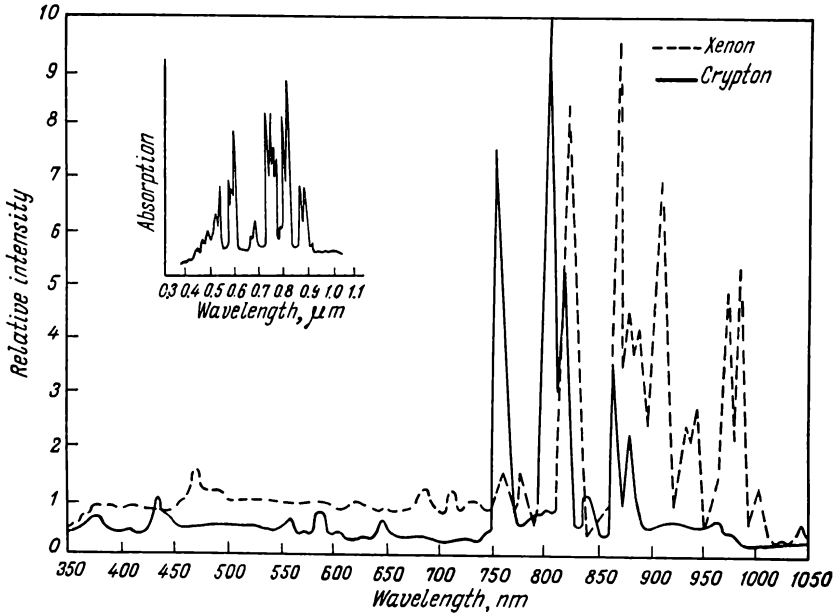

Fig. 3.2. Emission spectra of xenon and crypton high-pressure tubes (at the top of the figure is the absorption spectrum of neodymium-doped YAG crystal)

the former are closer to the absorption bands of the crystal. For example, crypton shows a bright line at a wavelength of 8100 Å corresponding to one of the main absorption lines of neodymium in a YAG crystal [6, 7, 8]. As an example, Fig. 3.3 shows the characteristics of a neodymium-doped YAG laser, with crypton, xenon and argon tubes used for pumping.

There are also mercury arc tubes with additions of other metals [9], for example, mercury-potassium arc tubes. Because a high temperature is required to sustain the arc discharge and also because of the corrosive action of the alkali metals, the envelopes of these tubes are made from single sapphire crystals. Among the disadvantages of mercury-potassium tubes are high cost, the need for temperature control, limited power output, and the need for a.c. supply which might modulate the laser beam.

As a rule, the efficiency of arc tubes increases with increasing discharge current density the limit for which is only set by the thermal load on the tube. The optimum pressure (for a cold tube) is about 4 atmospheres. For crypton tubes, the highest efficiency is obtained with a tube length-to-diameter ratio 10 : 1 to 15 : 1. With

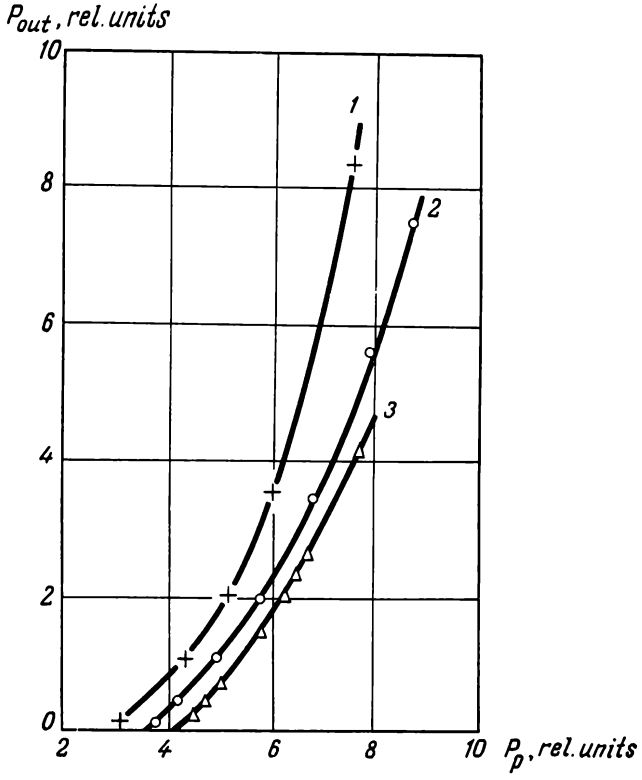

Fig. 3.3. Laser output power as a function of pump power in YAG laser oscillator using (*1*) crypton, (2) xenon and (*3*) argon continuous lamps

a greater relative diameter, the level of plasma excitation is brought down, while smaller relative diameters lead to greater losses in the walls because the ratio of the power emitted to the power lost in the walls depends on the ratio of the total plasma volume to the surface area of the walls. The maximum power input to a continuous arc lamp is determined by the surface area of the heat-dissipating quartz envelope. The tube envelope is subject to tensile and thermal stresses. The latter are caused by the temperature gradient between the internal and external surfaces of the envelope,

The tensile stresses are due to the high gas pressure inside the tube. It is the total safe stress that sets the limit to the power density dissipated by the surface of the tube envelope.

The characteristics of some of the crypton tubes are summarized in Table 3.1.

Table 3.1

Tube type	Emission power, W	Operating voltage, V	Firing voltage, V	Electrode separation, inside diameter, mm	Cooling
DKpTB-3000	3000	90-110	600-800	50×4	liquid
DKpTB-5000	5000	90-110	>600	80×5	liquid

A block diagram of a power supply for these tubes is shown in Fig. 3.4. The keep-alive arc is maintained by a d.c. supply furnishing a voltage exceeding the firing potential. The tube is caused to

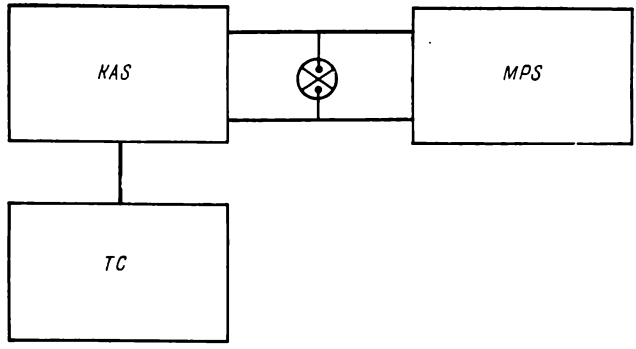

Fig. 3.4. Block diagram of a power supply for a continuous lamp
KAS—keep-alive supply; *TC*—trigger circuit; *MPS*—maintaining power supply

fire by a trigger circuit which generates a high-voltage, high-frequency initiating pulse. The peak voltage and frequency of the initiating pulse must be such that the resultant ionised plasma has a conductivity sufficient for the development of the main discharge. The trigger circuit is basically similar to those used to fire flash tubes and will be described in greater detail later. The d.c. supply is a rectifier with no special requirements for stability, in which the current can be adjusted or removed from the arc tube altogether with a ballast resistor. After an arc discharge in the tube is

initiated, a second supply is turned on, furnishing a voltage equal to the operating potential of the tube. After that, the arc initiating supply may be disconnected. The sustaining power supply is a rectifier with a voltage and power meeting the requirements of continuous pump tubes. Naturally, the stability of the sustaining rectifier should be compatible with the requirements for the stability of the laser beam.

Flash tubes used in laser pumps, including the physical basis of the power discharge, design of the various elements of flash tubes, fabrication techniques, and characteristics, are covered in detail in [10]. Commonly used sources for pumping solid-state lasers are xenon flash tubes in which xenon is at a pressure of 300 to 600 mm Hg. Typical flash tube geometries include helical, coaxial, U-shaped tubular, and straight tubular. Helical and coaxial flash tubes are employed in cases where the laser rod should be illuminated symmetrically. Most commonly, use is made of a wide-bore flash tube because of the ease of maintaining good performance and combining it with different cavity geometries. As an example, the characteristics of some of the wide-bore flash tubes manufactured in the Soviet Union are listed in Table 3.2.

Table 3.2

Tube type	Flash energy, J	Operating voltage, V	PRF, 1/s	Min. flash duration, μs	Max. firing voltage, V	Min. spontan. breakdown voltage, V	Electrode separation, inside dia., mm	Cooling
ИСПТ-6 000	600	1 450	10	800	600	3 000	120×7	Water, 3 m/s
ИФП-1 200-2	800	2 000	1/8	500	700	2 500	120×7	Natural
ИФП-2 000	2 000	1 500	1	750	600	2 000	130×11	Air
ИФП-8 000	8 000	2 600	1/30	1 500	1 800	3 500	250×16	Natural
ИФП-20 000	20,000	4 650	1/30	1 500	2 000	6 000	580×16	Natural
ИФП-40 000	40,000	5 000	1/30	1 800	3 000	7 500	1 000×16	Natural

According to [11], the analytic relationship for the resistivity ρ (ohms·cm) and current density j (A/cm^2) of a flash tube has the form

$$\rho = 1.15 j^{-0.5} \tag{3.1}$$

whence the resistance of a flash tube is [12]

$$R_t = 1.3\,(l/d)\,i^{-0.5} \tag{3.2}$$

where l and d are the length of the discharge gap and the bore diameter of the tube, respectively, and i is the instantaneous discharge current.

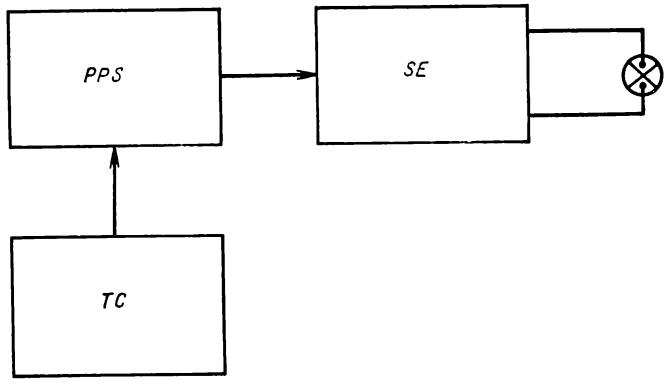

Fig. 3.5. Block diagram of a power supply for flash tube
PPS—pulse power supply; *SE*—storage element; *TC*—trigger circuit

Equation (3.2) alternatively describes the dynamic resistance of most stock-produced wide-bore flash tubes with a length four times their diameter, operating over a wide range of current values. For

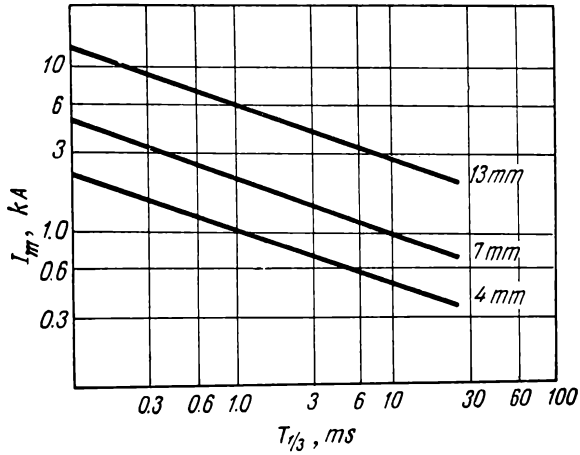

Fig. 3.6. Peak current as a function of pulse duration at one-third of pulse height for straight flash tubes varying in inside diameter, connected in a single-section energy storage source

xenon tubes filled to a pressure of 300 mm Hg, equations (3.1) and (3.2) hold for the range from 100 to 10,000 A/cm^2, provided the maximum rate of current change, di/dt, does not exceed 15 A/μs.

Since flash tubes need strong electric pulses of short duration to drive them, they are usually employed in conjunction with an energy storage circuit such as shown in Fig. 3.5. As a rule, an energy storage circuit consists of one or several *LC* pi-sections connected in series. The energy storage circuit is charged by a pulsed supply source. For a single-section energy-storage circuit, the maximum safe instantaneous load on the tube envelope with an

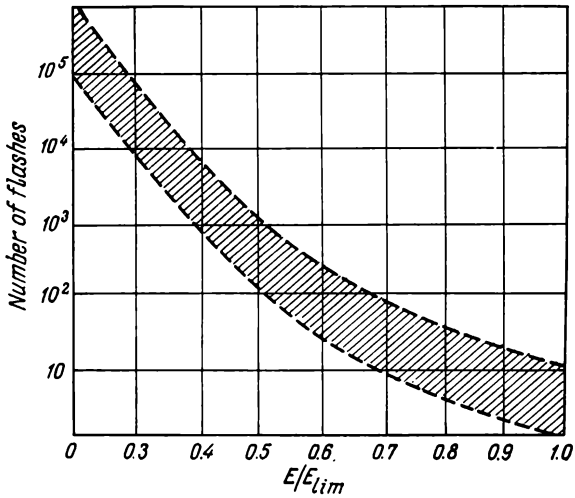

Fig. 3.7. Number of flashes as a function of flash energy ratio, E/E_{lim}

inside diameter of d is related to the peak value of current, I_m, by the following equality [13]:

$$W_m = 0.414 I^{7/4} d^2 \tag{3.3}$$

The dependence of peak current on pulse duration at one-third of the pulse height obtained experimentally for straight flash tubes differing in inside diameter and driven by a single-section energy-storage circuit is shown in Fig. 3.6 [13]. The plot of Fig. 3.7 borrowed from [14] shows the number of shots from a flash tube as a function of the ratio of the flash energy, E, to the limiting flash energy, E_{lim}.

3.2. Energy Storage Circuits

Although in some special applications flash tubes may be driven by shock-excited oscillators, MHD-oscillators and similar devices, in conventional low-power lasers it has proved more advantageous to use energy-storage circuits built around banks of capacitors

because of simplicity, ease of construction and reliability. As already noted, an energy storage circuit may consist of either a single *LC* pi-section (Fig. 3.8*a*) or several *LC* pi-sections (Fig. 3.8*b*). The principal energy-storage element is a capacitor or capacitors. The coils are provided to control the input of capacitor-stored energy into the flash tube. Naturally, since a large amount of energy should be stored, high-value capacitors designed for operating voltage running into thousands of volts are used in

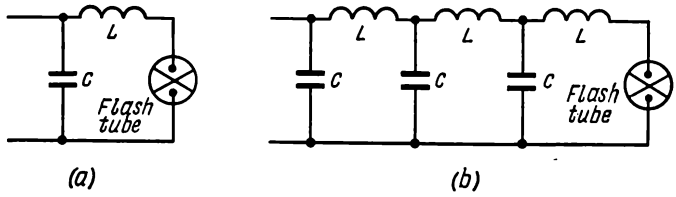

Fig. 3.8. Energy storage arrangements
(*a*) single-section *LC*-circuit; (*b*) multi-section discharge circuit

these circuits. Of the capacitors available commercially, these requirements are best satisfied by some types of paper-oil and paper-film capacitors, such as Soviet-made ИМ3-100, ИМ15-150, and ИМ3-250 types (the letters ИМ stand for "pulse oil", and the numerals specify the operating voltages and the capacitance. For example "3-100" stands for 3 kV and 100 μF). These capacitors are large in size and will operate at low rates of firing pulses, not more than 10 pulses per minute. As a rule, they are employed in stationary high-energy laser systems. The characteristics of some of paper-film capacitors are listed in Table 3.3.

Table 3.3

Capacitor type	Voltage rating, V	Nominal capacitance, μF	Frequency, Hz	Loss tangent at 50 Hz, max
К42И-1	2000	50	10	0.01
К50И-8	400	500	0.1	0.012
К50И-8	500	300	10	0.012
К75-17	1000	50	max 100	0.008
К75-18	1000	100	3	0.08
К75-20	4000	100	$^1/_{30}$	0.008

According to [15] and [16], losses in capacitors at the instant of an electric discharge through a flash tube may amount to 20% of the energy stored.

When several energy-storage circuits are connected in parallel to a single pulse power supply, they must be isolated, for example by resistors as shown in Fig. 3.9. Otherwise, energy may be partitioned at random when the flash tubes fire because of the spread in resistance among them, or all energy-storage circuits may discharge into one flash tube, should it break down of its own accord. The resistance or reactance should be greater than the internal resistance of the flash tube by several orders of magnitude.

The energy stored may be expended differently, depending on the values of L and C. At low values of L, an aperiodic discharge

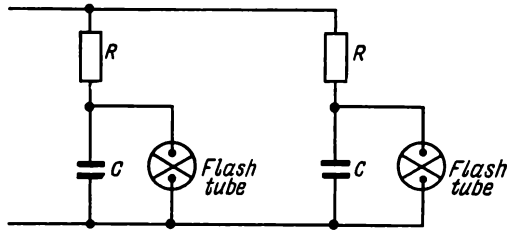

Fig. 3.9. Two energy-storage circuits connected in parallel to one pulse supply

may take place, causing the flash tube to fail because of the high rate of current rise. At high values of L, an oscillatory discharge may happen, such that light energy will be emitted in portions, corresponding to positive and negative half-cycles. In [13, 17], it is shown that as regards optical pumping by flash tubes, the optimum operating conditions are obtained when the flash tube resistance is within the range given by

$$\sqrt{L/C} \leqslant R_t \leqslant 2\sqrt{L/C} \tag{3.4}$$

corresponding to discharges with the following time characteristics:

$$i(t) = 2.11 I_p e^{-0.5t/\tau} \sin\left(\sqrt{3}/2\right)(t/\tau) \tag{3.5}$$

$$i(t) = 2.71 I_p (t/\tau)\, e^{-t/\tau} \tag{3.6}$$

where I_p is the peak current occurring at the instant $\tau = \sqrt{LC}$ in equation (3.6).

At the same time, according to equation (3.2), the flash tube resistance should satisfy the condition

$$R_t \leqslant 1.3\,(l/d)\, i_{\max}^{-0.5} \tag{3.7}$$

where $i_{\max}$ is the maximum safe instantaneous discharge current. These two equations, namely (3.4) and (3.7), should be used as a guide in selecting the capacitance and inductance for an energy-storage circuit consisting of a single LC pi-section.

The energy dissipated by a flash tube is given by

$$E = \int_0^\infty i(t)^2 R_0(i)\,dt \simeq \int_0^\infty i(t)^{3/2}\,dt \tag{3.8}$$

where $R_0 = 1.3\ l/d$. Since the resistance of a flash tube is a function of an independent variable, the energy dissipation can be determined by solving a nonlinear differential equation, and an exact solution for this equation can only be obtained on a computer. In some cases, however, E may be computed approximately. For example, [13] gives an approximate expression for E in the case of a critically damped circuit, that is, for $R_t = 2\sqrt{L/C}$, on the assumption that the flash tube resistance remains unchanged and the connecting leads have a negligible resistance.

According to [13], the expression for E has the form

$$E \simeq (0.58 R_0 I_p^{3/2} + I_p^2 R_w) T \tag{3.9}$$

where $R_0 = 1.3\ l/d$, $T = 3.2\,\tau$, and R_w is the resistance of the connecting wires. The energy computed by equation (3.9) agrees well with the energy stored by a capacitor, $0.5\ CV^2$. It should be remembered, however, that expression (3.9) may only serve as an approximate guide as regards the limits of safe operation and that equation (3.9) gives reduced values of energy in comparison with actual limiting values.

The assumption of a constant resistance for a flash tube is still more valid with multi-section energy-storage circuits, and the discharge current may be described by a relationship of the form

$$I_c \simeq (R_0/54)^{2/3} (C/L)^{1/3} V^{4/3} \tag{3.10}$$

where I_c is the flash tube current in the central constant-amplitude part of a rectangular pulse, C is the capacitance of the capacitor in one section in μF, L is the inductance of the coil in one section in μH, and V is the voltage to which the pulse-shaping circuit is charged. The pulse duration at one-third the pulse height is

$$T = 2.7 N (LC)^{0.5} \tag{3.11}$$

where N is the number of sections in the energy-storage circuit.

3.3. Pulsed Power Supply

The functions of a typical pulse power supply used in the energy-storage circuits of pulsed lasers are to charge the capacitors linearly to a voltage required for operation of the flash tube before the laser emits a light pulse, and to discontinue charging for a time interval (up to 15 ms) over which the flash tube recovers.

Besides these basic functions, a pulse power supply should discharge the storage capacitors during the recovery period, generate a synchronizing pulse for the H. V. pulse generator which controls the electro-optic shutter, and finally, send out (or receive) a synchronizing pulse to or from other devices.

In block-diagram form, a pulse power supply consisting of a current source, a rectifier, a control circuit, and a flash tube trigger circuit is shown in Fig. 3.10. The actual circuit configuration may vary, depending on the objectives sought. In cases where

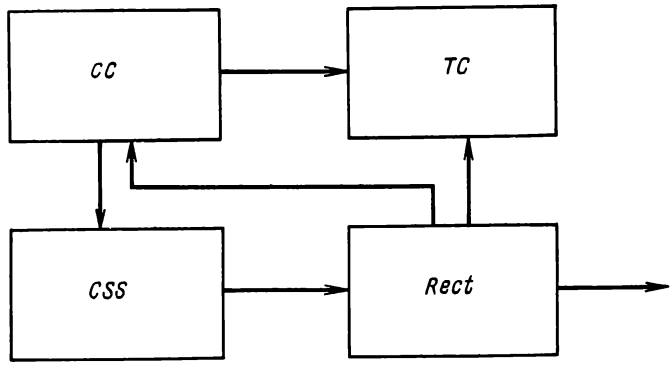

Fig. 3.10. Block-diagram of a pulse power supply
CSS—current source and switch assembly; *Rect*—rectifier; *CC*—control circuit; *TC*—trigger circuit

single-shot pulses are required for optical pumping, the pulse power supply may actually consist of a rectifier plugged into a mains outlet and a trigger circuit. In order to limit current inrushes when the circuit just begins to charge, there may be a ballast resistor or a ballast coil at the output of the rectifier. The ballast resistor may be any one of high-voltage types, such as the Soviet-made ПЭВ. The use of ballast chokes is examined in [18, 19].

The H. V. circuits may be switched by vacuum relays, such as Soviet-made types ВВ-5 and ВВ-20.

In cases where single-shot pumping pulses are needed, all functions of the control circuit may be performed manually. In order to obtain periodic pumping pulses from a rectifier incorporating a ballast resistor or choke, switching may be done by controlled thyristors placed either in the primary circuit of a step-up transformer or in the output circuit of the rectifier.

With a relatively small voltage across the storage capacitors, the supply circuit reduces to a well-known voltage-doubler circuit [20].

In laser oscillators operating at high PRF (up to 100 Hz) and low pump energy levels, the energy storage circuit reduces to a

combination of a d. c. supply and a resonant circuit incorporating a buffer capacitor and pump capacitors [21-23].

A wide range of capabilities is offered by the pulse power supply circuit shown in Fig. 3.10. Some of the modifications of the functional elements that make up the pulse power supply are discussed below.

Rectifier-type current source. Mains voltage may conveniently be converted to direct voltage by inductive-capacitive converters which take the form of symmetrical T-networks [24]. The circuit of a single-phase inductive-capacitive converter is shown in Fig. 3.10.

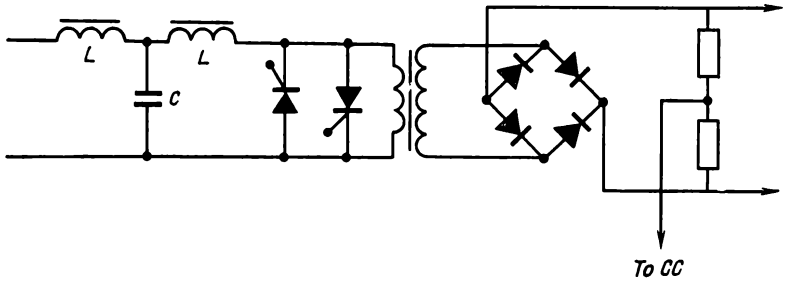

Fig. 3.11. Rectifier-type supply to energize storage circuits for high-power flash tubes

The circuit parameters are selected from the condition of resonance

$$\omega^2 LC = 1 \qquad (3.12)$$

where $L_1 = L_2 = L$ is the coil inductance in H, C is the capacitance in F, and ω is the angular frequency in s^{-1}.

The output current of an inductive-capacitive converter is almost independent of load impedance and is directly proportional to supply voltage. Under conditions of a short-circuit, the input current should theoretically be zero. At no-load, the input current and the output voltage should theoretically rise to infinity. This behaviour of the circuit is explained by the fact that under conditions of a short circuit a T-network reduces to a series combination of L_1 and the L_2C resonant circuit, while at no-load the network reduces to a series resonant circuit.

Since operation at no-load is dangerous to an inductive-capacitive converter, appropriate measures should be provided, for example, a relay at the input controlled by output voltage to turn off the circuit when the output voltage of the converter exceeds a safe value.

The circuit of a rectifier type of supply is shown in Fig. 3.11. The rectifier is a bridge circuit energized with voltage from the step-up

winding of a transformer. The primary of the step-up transformer is connected across the output of an inductive-capacitive converter. As the energy storage circuit is charged, the voltage across the primary winding of the step-up transformer rises from zero to the operating voltage of the energy storage circuit, while the current remains unchanged. A similar condition exists at the rectifier output where the current remains nearly unchanged in magnitude as long as the storage capacitors are charged. The output of the rectifier is shunted by a switching element which serves to connect the rectifier to the rest of the system or to disconnect it by introducing a short-circuit. This switching element may be made up of symmetrical thyristors.

The control circuit of a pulse power supply performs all the functions essential to ensure operation of the associated laser oscillator, synchronization with other devices, safety to personnel, etc.

The primary function of the control circuit is to set the pulse repetition frequency for the laser oscillator. Depending on the laser application, the control circuit may be designed for a single frequency or it may be tunable over a wide frequency range. The control circuit should turn on the rectifier for the duration of a charge cycle, start the firing circuit, and cause the switching device to turn off the rectifier for the duration of the recovery time of the flash tube.

During the charging cycle, the control circuit should see to it that the voltage across the capacitors rises to precisely its assigned value. At the instant when the flash tube fires, it should generate a pulse to turn on the electro-optic shutter; when the pulse power supply is turned off, the control circuit should allow the storage capacitors to discharge.

The control circuit may be set up in a variety of configurations. As a rule, it is made up of a master oscillator, flip-flops, delay lines, and comparators.

3.4. Flash Tube Trigger Circuit

Although the trigger circuit is part of the pulse power supply (in the case of pulsed lasers) or the keep-alive source (in the case of continuous lasers) both functionally and physically, it deserves a separate examination because of its applicability to different types of laser.

The discharge of storage capacitors through the associated flash tube is initiated by H. V. pulses following at a frequency of 0.1 to 0.2 MHz and with an amplitude sufficient to ionize the gas inside the flash tube. The circuits generating pulses that initiate a gas discharge in flash tubes are called firing or trigger circuits

[2]. The firing circuits for gas-discharge flash tubes may be either external (also called parallel) or internal (also called series). In an external (or parallel) firing circuit (Fig. 3.12*a*) one end of the secondary winding of an H. V. pulse transformer is connected to a discharge circuit, while the opposite end is taken directly either to the flash tube envelope or to the laser (pump) housing isolated from chassis earth.

With an internal (or series) firing circuit (Fig. 3.12*b*), the transformer secondary is connected to the output circuit of the pulse

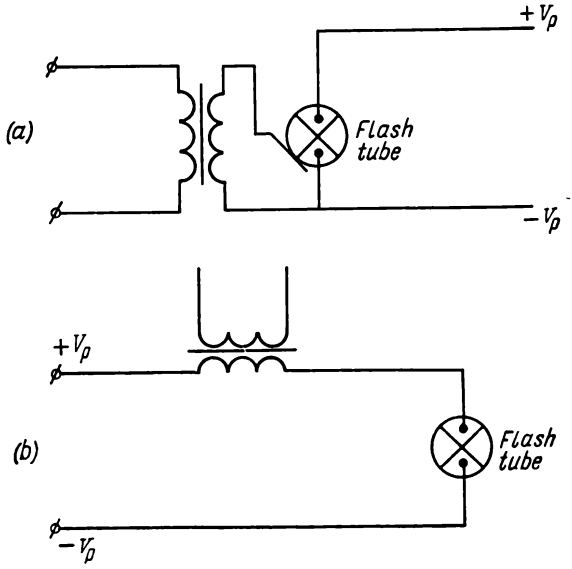

Fig. 3.12. (*a*) External and (*b*) internal firing of flash tubes

power supply connected either to the energy-storage circuit or directly to the discharge circuit, in series with a flash tube (or a bank of flash tubes).

Among the distinctions of the external (parallel) firing circuit are the small size of the pulse transformer and the possibility of firing a large number of flash tubes in one or several pump units in synchronism. With an external firing circuit, the pump housing must be reliably insulated from chassis earth.

The internal (series) firing circuit offers a number of advantages over the external (parallel) firing circuit. Among other things:

(1) As the storage capacitors discharge through the flash tube, the plasma fills the inter-electrode space to a fuller extent and more uniformly, which improves the electrical efficiency of the

pump system and allows the laser rod to be pumped more uniformly over its entire length [24].

(2) The flash tube envelope is free from crazing, so that the flash tube service life is extended considerably.

(3) The laser may be simplified in design and reduced in size because the pump unit need not be insulated from the base and outer housing of the oscillator.

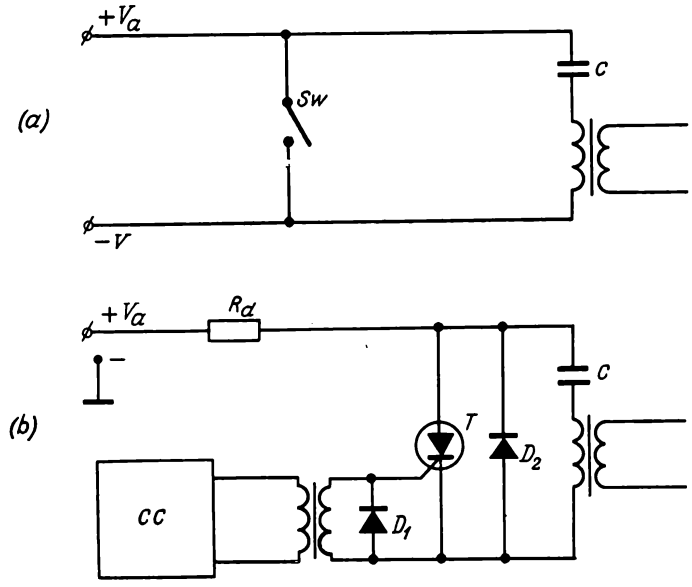

Fig. 3.13. Flash-tube firing circuit controlled by (*a*) a switch and (*b*) a thyristor

(4) The temperature-stabilization system may use simpler elements.

(5) Since the metal housing of the pump unit is earthed, radio interference is kept to a minimum.

It is important to note that the secondary winding of the transformer in the internal firing circuit should be wound with a heavy-gauge wire having a resistance smaller than that of the flash tube.

With both external and internal firing, the first pulse peak should be from 15 to 20 kV in amplitude and 5 to 8 μs in duration, depending on the discharge gap of the flash tube.

The firing circuit operates on a well-known principle, namely a storage capacitor, C, is charged by a d. c. supply to a predetermined level, $+V_p$; then, at a predetermined instant, it is allowed to discharge through a controlled switch Sw into the primary of

a pulse transformer (Fig. 3.13*a*). The energy stored by the capacitor C is chosen to be anywhere between 0.7 and 5 J, according to flash tube type and number.

The switch may be an electromechanical device (such as a relay), a thyratron, a controlled spark-gap, or thyristors. These types of switch differ in circuit configuration, anode voltage V_a, and the capacitance of the storage capacitor C.

The most efficient type of switch for the laser firing circuits is that using thyristors (Fig. 3.13*b*). With a relatively low anode

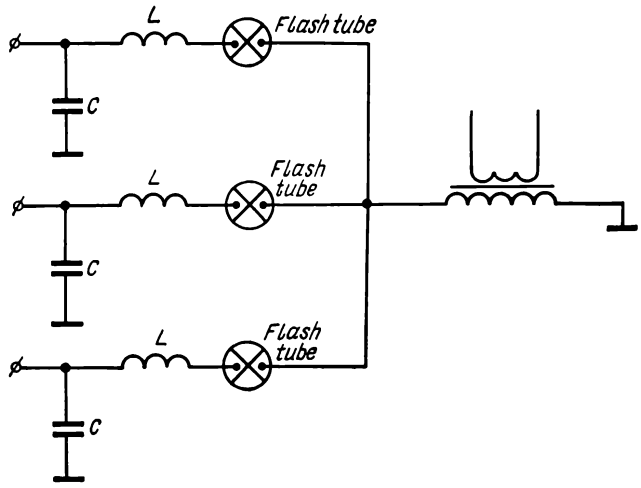

Fig. 3.14. Firing circuit for flash tubes connected in parallel

voltage (500 to 1000 V), a thyristor-controlled firing circuit can furnish strong firing pulses because a thyristor is capable of passing strong current pulses (800 to 2000 A) at high rates of current rise (τ_{rise} = 2 to 3 μs). Thyristor-controlled circuits can be started by pulses of a relatively low voltage (2 to 8 V), and they are insensitive to interference because a sufficiently high current (from 0.3 to 0.8 A) is required to turn on a thyristor (Fig. 3.13) [25].

With high-power thyristor-controlled circuits several flash tubes connected in parallel can be fired internally from a single firing transformer (Fig. 3.14). Each flash tube is connected in series with a small-value coil which prevents shunting the several flash tubes connected in parallel because of the spread in internal resistance of the flash tubes at the instant of firing. Practically, the supply leads may well do the job of a small-value coil.

3.5. High-Voltage Pulse Generator

In laser systems, H. V. pulse generators are employed to control electro-optic shutters. In a Q-switched laser, the rise time of these pulses should not exceed the time to the onset of lasing

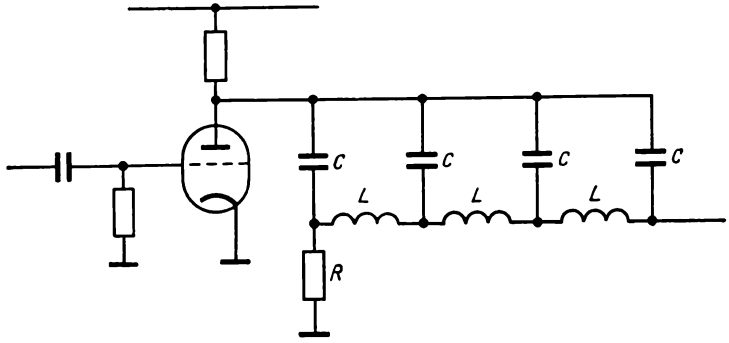

Fig. 3.15. Circuit of a high-voltage short-pulse generator using a thyratron and a discharge line

action (about 20 to 30 ns). The total pulse duration may be from 100 to 200 ns. Pulses of a greater duration are not required or may be even undesirable, because should the shutter remain open

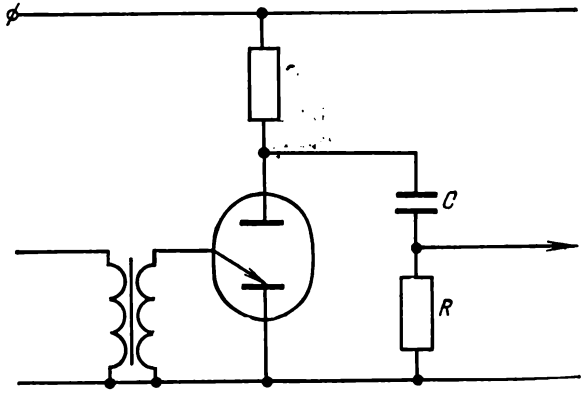

Fig. 3.16. Circuit of a high-voltage short-pulse generator using a vacuum spark gap

and the exciting flash persist long enough after the giant pulse, the laser will yield spikes of spontaneous emission. These spikes appear because the population inversion in the laser rod usually attains a maximum before the exciting flash ceases. The pulse vol-

tage should be equal to the control voltage of the shutter and may vary over a vide range, according to the type and design of shutter which may be a capacitive load of a few units or even tens of picofarads. Accordingly, H. V. pulses may be generated by different methods. Yet, all types of H. V. pulse generators depend for their operation on the discharge of either a capacitor or a pulse-shaping line through a switching element having a sufficient speed of response. The switching element may be a thyratron, a spark gap, or a vacuum discharge tube, each requiring a distinct control circuit.

A schemaic diagram of an H. V. negative-pulse generator using a ТГИ1-130/10 thyratron is shown in Fig. 3.15. When an enabling pulse is applied to the thyratron grid, the pulse-shaping line discharges through the thyratron and resistors, and a rectangular pulse of negative polarity appears at its open-circuited end. This generator may furnish pulses with a rise time of not over 20 ns, and with an amplitude of up to 10 kV at a frequency of up to 1000 Hz.

Figure 3.16 shows a schematic diagram of an H. V. pulse generator using a type ВИР-14 vacuum discharge tube, generating positive pulses with a fast rise time (below 20 ns) and with an exponential decay. The pulses (3 or 4 kV) necessary to break down the ВИР-14 tube are generated by a suitable control circuit. This type of generator may furnish pulses with an amplitude of up to 20 kV.

Chapter Four

Laser Instabilities and Distortions

4.1. Thermal Processes in Optical Elements

Sources of heat dissipation. Operation of any laser is accompanied by the interaction of laser light with its optical components (laser rod, electro-optic reflectors, shutters, mirrors, and the like). As a result, some of the absorbed radiation is converted to heat, and temperature gradients of the form $T = T(\bar{r}, t)$ arise in the optical components.

The dissipation of heat may be visualized by assuming the existence of sources of unit density, $q(\bar{r}, t)$, distributed throughout the volume of the optical element. Depending on the type of laser component, the density is decided either by the action of only laser emission, in which case it is $q^e(\bar{r}, t)$ or the action of the pump, in which case it is $q^p(\bar{r}, t)$ or both, that is, $q(\bar{r}, t) = q^p(\bar{r}, t) + q^e(\bar{r}, t)$. For example, for electro-optic shutters $q^p(\bar{r}, t)$ is always 0. For laser rods, on the other hand, both $q^p(\bar{r}, t)$ and $q^e(\bar{r}, t)$ are nonzero. Ordinarily, however, it may be assumed that $q^e \ll q^p$. The form of the function $q^e(\bar{r})$ for monochromatic laser light is determined by its spatial distribution (see Sections 1.4 and 2.5). For example, when a laser is oscillating in the lowest angular mode, the function $q^e(\bar{r})$ in a plane normal to the direction of beam propagation is Gaussian very nearly. If laser light has a complex spectral make-up, the form of the function $q^e(\bar{r})$ may be found only if, in addition to the spatial distribution of laser emission, one also knows its spectral make-up and the dependence of the absorption coefficient of the laser material on wavelength and temperature, which are either specified in advance, or may be determined for any laser optical system. The time function of heat dissipation in a laser element, $q^e(t)$, depends on the shape of the output pulses and on changes in the absorption coefficient with temperature. In the case of nanosecond, picosecond and other nonrecurrent or recurrent pulses, the pulse shape and pulse repetition period are either specified in advance, or may be found experimentally. However, the shape of a heat dissipation pulse in an optical element may markedly differ from that of the light pulse because of changes in the absorption coefficient with the rise in the ambient temperature during the light pulse. The total energy dissipated as heat in the laser rod due to the action of a light pulse

may be found experimentally. In some cases, the function averaged over the pulse duration, found by an approximation method, using experimental and computed data will have the form

$$\widetilde{q^p}(\bar{r}) = \frac{1}{t^p} \int_0^{t_p} q^p(\bar{r}, t)\, dt$$

As already noted, heat is dissipated by the laser rod because it interacts not only with laser emission, but also with pump energy. Owing to optical pumping, $q^p(\bar{r}, t)$, heat is dissipated because of the so-called non-active losses (scattering and absorption) in the laser material, and also because of non-radiative transitions between the energy states in excited active ions. In both cases, the spatial distribution of heat dissipation can be found from many, sometimes difficult-to-define factors. Among other things, one must know the distribution of energy fluxes concentrated on the laser rod by the pump (see Sec. 1.1) which can only be done approximately, if at all. Furthermore, as regards the non-active losses, one must know the spectral distribution of energy concentrated on the laser rod and the spectral dependence of its absorption coefficient. For the radiation absorbed by active ions, one must take into account also the kinetics of transitions between energy states [1]. Thus, the form of the function $q^p(\bar{r})$ is extremely difficult to obtain by computation. The accuracy of the results will not always justify the effort expended.

The function $q^p(t)$ is above all determined by the time dependence of pump light intensity, and also by the temperature dependence of the absorption coefficient of the laser material and the energy transitions of active ions. For example, with pulsed pumping, the time dependence of light pulse intensity is decided by the parameters of the discharge circuit (see Sections 3.4 and 4.5) and may be determined experimentally with a sufficient accuracy. However, changes in the temperature of the laser rod during a light pulse may bring about marked changes in the physical characteristics of the material essential to its interaction with laser emission. Therefore it is practically impossible to determine the true time dependence of heat dissipation for short pumping pulses. Experimentally, say, by means of a calorimeter, one can only determine the total heat energy that the laser rod absorbs during optical pumping. In effect, for short pumping pulses experimental methods only give the heat averaged over the volume of the laser rod and over the duration of the light pulse

$$\overline{q^p} = \frac{1}{t_p V} \int_0^{t_p} dt \int_V q^p(\bar{r}, t)\, d\bar{r}$$

With continuous pumping or with pumping using light pulses of long duration, finding the value of $\overline{q^p}$ averaged over volume and time is complicated by the heat exchange between the laser rod and the surroundings.

Thus, instead of the actual distribution of heat sources, $q^p(\bar{r}, t)$, experiments and computation can practically give only either its average value, $\overline{q^p}$, or, in the best of cases, the distribution $\overline{q^p}(\bar{r})$ valid for the pump pulse duration, t_p. Designating as t_{cool} the time between the light pulses acting upon an optical element, then for periodic pumping, the time of a complete cycle will be $t_{cycle} = t_p + t_{cool}$. In general form, heat dissipation in laser rods may be represented by rectangular pulses of height $\overline{q^p}$ and of duration t_p, having a duty ratio of $\Lambda = (t_p + t_{cool})/t_p$. In other optical elements of a laser, heat dissipation may be represented as rectangular pulses having a spatial distribution of the form $\overline{q^p}(r)$ and a pulse duty $\Lambda \to \infty$ for single heat dissipation pulses, and $\Lambda \to 1$ for continuous heat dissipation.

It should be noted that in one and the same laser oscillator or amplifier operating at t_{cycle}, both the duration of heat dissipation pulses, t_p, and the pulse duty Λ for the laser rod may greatly differ from those for other elements. For example, with continuous heat dissipation in the laser rod, heat dissipation in other elements may be in the form of nanosecond pulses following at a frequency of a few kilohertz.

Heat exchange on the surface of optical elements. An optical element is cooled because its surface comes in contact with a gaseous, liquid, or solid medium. For a non-stationary heat exchange between an optical element and a liquid, gas or solid, the boundary conditions may be written as follows [2]:

$$T(t)|_\Sigma = T_m(t)|_\Sigma$$
$$\lambda_m (\partial T_m/\partial n)|_\Sigma = \lambda (\partial T/\partial n)|_\Sigma \qquad (4.1)$$

where λ_m and λ = heat conductivity of the cooling medium and optical element, respectively
$(\partial T/\partial n)|_\Sigma$ = derivative of the normal to the surface of the optical element
$T_m(t)$ = temperature of the cooling medium
$T(t)|_\Sigma$ = temperature on the surface of the optical element

With a liquid or gaseous cooling medium, when the temperature is changing at a low rate, that is, when $\partial T/\partial t$ is small, the boundary conditions may be written [2] as follows:

$$(\partial T/\partial n)|_\Sigma + (\alpha/\lambda)[T(t) - T_m] = 0 \qquad (4.2)$$

where α is the coefficient of heat exchange in W/m^2 deg. The boundary conditions are written on the assumption that the value of α is independent of time and temperature. This assumption agrees rather well with the actual conditions under which optical elements are cooled. Although different surfaces of an optical element may have different values of α, the main contribution to the total heat exchange of the element comes from one surface having the greater area and a maximum value of α. The effect of other surfaces on heat processes in an optical element may in most cases be neglected. For example, this is true of the end faces of optical elements transmitting laser light, surfaces for mechanical attachment, etc. Therefore, in the subsequent discussion, the quantity α will apply to the surface which determines the heat exchange of an optical element.

In cases where $\alpha \to \infty$, that is, heat exchange proceeds at a very high rate, equation (4.2) will take the form

$$T|_{\Sigma} = T_m = \text{constant} \tag{4.3}$$

that is, the temperature on the surface of the optical element is assumed to be specified in advance.

In cases where $\alpha \to 0$, we have

$$(\partial T/\partial n)|_{\Sigma} = 0 \tag{4.4}$$

that is, the heat flux on the surface is zero. The actual values of α for, say, water range between 2×10^3 and 7×10^3 W/m^2 deg and depend on the rate of heat flux.

In some cases it may be desirable to control heat dissipation in an optical element, say, in order to change the existing temperature gradient. This can be done by causing the value of α or T_m to change in the desired manner. As the value of α or T_m at the surface of an optical element is changed, a new temperature gradient will be set up in it some time later. By the principle of linear superposition which applies to the linear differential equation of thermal conductivity, the resultant temperature gradient in the optical element will then be equal to the sum of the two gradients obtained by causing the values of α and T_m to change, and also the gradients due to internal sources of heat dissipation. In other words, the resultant temperature gradient may be arranged to have the desired distribution at a certain instant.

Analysis of temperature fields in optical elements. The temperature field in an optical element is uniquely specified by the spatial-time distribution, $q(\bar{r}, t)$, physical properties of the optical element, and the conditions under which its surface is cooled.

In the general case, the differential equation of thermal conductivity has the form

$$\frac{\partial}{\partial t}[c\gamma T(\bar{r}, t)] = \operatorname{div}[\lambda \operatorname{grad} T(\bar{r}, t)] + q(\bar{r}, t) \tag{4.5}$$

where c and γ are the heat capacity and density of the optical element. For isotropic media in which λ is independent of the spatial coordinates of the element in question, equation (4.5) may be rewritten as follows

$$\frac{\partial T(\bar{r}, t)}{\partial t} = a\nabla T(\bar{r}, t) + \frac{q^p(\bar{r}, t)}{c\gamma} \tag{4.6}$$

where $a = \lambda/c\gamma =$ coefficient of thermal conductivity, $[a] = \text{m}^2/\text{s}$, $\nabla =$ del (or nabla)

Noting the boundary conditions defined by (4.1) through (4.4), the solution of the linear differential equation of thermal conductivity uniquely describes the temperature gradient $T(\bar{r}, t)$ of an optical element at any time. The manner in which $q^p(\bar{r})$ depends on time determines the effect of heat sources at high and low values of duty ratios for pump or emission pulses. In practical solid-state pulsed laser oscillators, the value of t_{cool} may vary over a wide range (from 2×10^{-2} to 5×10^2 s), while t_p remains practically unchanged (10^{-3} to 10^{-2} s).

(a) *Pulsed heat dissipation* ($\Lambda \to \infty$). At high values of Λ, the cooling period t_{cool} is so long that the optical element has time to cool completely. Because optical pumping occupies a short time interval, the concurrent heat exchange may be neglected. Therefore, at $\alpha = 0$, the boundary condition takes the form

$$(\partial T/\partial n)|_\Sigma = 0 \tag{4.7}$$

The validity of this approximation, which actually implies that the adopted pumping model is adiabatic, has been proved experimentally [3].

The solution of equations (4.6) and (4.7) for the boundary conditions $T(\bar{r}, 0) = 0$ is well known [2]. For example, for a plate whose width and length are much greater than its thickness, the solution has the form

$$\theta\left(\frac{x}{h}, Fo\right) = \frac{T\left(\frac{x}{h}, Fo\right)}{T_m} =$$

$$= \int_0^{Fo} dFo \int_0^1 Po\left(\frac{x}{h}, Fo\right) d(x/h) + 2\sum_{n=1}^{\infty} \cos \mu_n (x/h) \times$$

$$\times \exp(-\mu_n^2 Fo) \int_0^{Fo} \exp(\mu_n^2 Fo)\, dFo \int_0^1 Po\left(\frac{x}{h}, Fo\right) \cos \mu_n (x/h)\, d(x/h) \tag{4.8}$$

where $Po = \dfrac{q\left(\frac{x}{h}, Fo\right) h^2}{\lambda T_m} =$ Pomerantsev's criterion

$Fo = at/h^2$ = Fourier's criterion
T_m = temperature of the surroundings
$\mu_n = n\pi$ = roots of the characteristic equation

$$\theta = \frac{T\left(\frac{x}{h}, Fo\right)}{T_m} = \text{dimensionless temperature}$$

$$\int_0^1 Po\left(\frac{x}{h}, Fo\right) \cos \mu_n (x/h)\, d(x/h) = \text{Fourier cosine integral}$$

representation of the function $Po(x/h, Fo)$

It is readily seen from equation (4.8) that with the pump energy uniformly distributed over the cross-section of the plate, q = constant, and varying in a rectangular fashion with time, the solution will be as follows:

$$\theta(Fo) = Po_s Fo; \quad Po_s = qh^2/\lambda T_m$$

For small values of time, that is, when $\mu_n^2 Fo \ll 1$, the solution is inconvenient, because at $Fo < 0.1$, the series in (4.8) is poorly convergent [2], that is ,a great number of terms is required to obtain θ. In such a case, a direct solution of (4.6) and (4.7) will give

$$\theta(x/h, Fo) = Po(x/h)\, Fo \tag{4.9}$$

Obviously, if $q(x/h)$ is a time-dependent function, equation (4.9) will take the form

$$\theta\left(\frac{x}{h}, Fo\right) = \int_0^{Fo} Po\left(\frac{x}{h}, Fo\right) dFo \tag{4.10}$$

It is physically obvious from equation (4.10) that the temperature gradient during the pump cycle replicates the distribution of heat sources (since the pump cycle occupies a negligible time interval, the thermal energy of heat sources cannot undergo a marked redistribution). It is only seldom that the condition $\mu_n^2 Fo \ll 1$ will not be satisfied during the pump cycle, and then only at very small values of h, very large values of a (at very low temperatures), and a long pump time, t_p. If the condition is not satisfied, calculations should be made by equation (4.8).

The cooling period which follows the pump cycle is characterized by a temperature gradient which can be obtained from the solution of equation (4.6) where $q(\bar{r}, t) = 0$, with the boundary conditions defined by (4.2) and the initial conditions being such that $T^{cool}(x, 0) = T^{heat}(x, t_p)$, where the superscripts "cool" and "heat"

apply to the cooling and heating periods. Accordingly, the solution of this problem has the form

$$T_m - T(x, t) = \sum_{n=1}^{\infty} B_n \cos \mu_n (x/h) \exp\left(-\mu_n^2 Fo\right)\left(T_{pF}/h\right) \quad (4.11)$$

where

$$B_n = \frac{2\mu_n}{\mu_n + \sin \mu_n \cos \mu_n}$$

μ_n = roots of the characteristic equation $\cot \mu = \mu/Bi$

$T_{pF} = \int_0^h T_p\left(\frac{x}{h},\ t_p\right) \cos \mu_n (x/h)\, d\,(x/h)$ = final Fourier cosine integral representation of the function $T_p\left(\frac{x}{h},\ t_p\right)$.

If the initial temperature distribution is uniform, independent of x and is equal to $T_0 - T_m$, then from equation (4.11) we have

$$\frac{T(x, t) - T_m}{T_0 - T_m} = \sum_{n=1}^{\infty} A_n \cos \mu_n (x/h) \exp\left(-\mu_n^2 Fo\right) \quad (4.12)$$

where $A_n = \frac{2 \sin \mu_n}{\mu_n + \sin \mu_n \cos \mu_n}$ = initial temperature amplitudes

A_n, μ_n = tabulated values, given in [2]

The numerical computation of (4.12) and the nomograms corresponding to various cooling conditions ($0.001 \leqslant Bi \leqslant 1000$), various media, and dimensions of the element being cooled ($0.0001 \leqslant Fo \leqslant 1000$) are given in [2]. With the values of Fo and Bi specified in advance, one can readily and precisely find $\theta(x, t) = \frac{T(x, t) - T_m}{T_0 - T_m}$. Two limiting cases of cooling may be examined, namely: $Bi \to \infty$ and $Bi \to 0$. With $Bi \to \infty$, $\mu_n = (2n - 1)\frac{\pi}{2}$, and the surface comes up to the temperature of the surroundings at once, and equation (4.12) takes the form

$$\theta(x, t) = \sum_{n=1}^{\infty} (-1)^{n+1} \frac{4}{(2n-1)\pi} \cos \frac{(2n-1)\pi x}{2h} \exp\left[-\frac{(2n-1)^2 \pi^2 Fo}{4}\right] \quad (4.13)$$

Then the cooling rate, $\partial\theta/\partial t$, will be

$$(\partial\theta/\partial t)\,|_{Bi \to \infty} = (a/h^2) \sum_{n=1}^{\infty} \mu_n^2 A_n \cos \mu_n (x/h) \exp\left(-\mu_n^2 Fo\right) \quad (4.14)$$

Thus, the cooling rate increases with decreasing h^2 and with increasing a, that is, it is determined by the thermal lag a and size of the element being cooled. For comparison, let us write

$\partial\theta/\partial t$ for $Bi \to 0$ (actually, $Bi < 0.1$). Then $\mu_n \to (n-1)\pi$, $A_n \to 0$, $A_1 = 1$. In this case, equation (4.12) will take the form

$$\theta(x, t) = \cos\left(\sqrt{Bi}\,\frac{x}{h}\right)\exp(-BiFo) \qquad (4.15)$$

and

$$\partial\theta/\partial t = (\alpha/c\gamma h)\cos\left(\sqrt{Bi}\,\frac{x}{h}\right)\exp(-BiFo),$$

that is, the cooling rate is proportional to α and inversely proportional to h.

Thus, in the absence of the nomogram given in [2] for a flat laser rod the temperature field during the cooling stage at $Bi \geqslant 100$ should be computed by equation (4.13), at $Bi \leqslant 0.1$ by equation (4.15) and at $0.1 \leqslant Bi \leqslant 100$, by equation (4.11).

(b) *Continuous heat dissipation* ($\Lambda \to 1$). By reducing t_{cool}, that is, by letting Λ tend to unity, we obtain conditions under which heat dissipation tends to be continuous. According to [4, 5], this condition is characterized by the quantity t^*_{cool}. If $t_{cool} \leqslant t^*_{cool}$, then heat dissipation may be assumed to be continuous, and the temperature field may be calculated, using the relationship given below. According to [4, 5], the cooling conditions may be any. Since t_{cool} enters into a dimensionless criterion: $Fo = at_{cool}/h^2$, then from [4, 5], $Fo^* = 5 \times 10^{-2}$, and the condition for a transition to continuous heat dissipation takes the form $Fo \leqslant 5 \times 10^{-2}$. For example, in the case of a flat glass laser rod for which $h = 4 \times \times 10^{-3}$ m, $a = 0.4 \times 10^{-6}$ m^2/s, and $t^*_{cool} = 0.2$ s. Thus, at a frequency of $f \geqslant 5$ Hz, heat dissipation may be regarded as continuous. Now the expression for the temperature field will be obtained by solving (4.6), taking the boundary conditions as defined by (4.2) and the initial conditions being $T(x, 0) = T_0$. As already noted, the temperature jump $T_m - T_0$ required for computation is supplied by the heat source, and so the expression for the temperature field has the following form

$$\frac{T(x, t) - T_0}{T_m - T_0} = 1 + \frac{1}{2}Po(1 - x^2/h^2 + 2/Bi) - \\ - \sum_{n=1}^{\infty}(1 + Po/\mu_n^2)A_n \cos\mu_n (x/h)\exp(-\mu_n^2 Fo) \qquad (4.16)$$

At $Fo \to \infty$, that is in the stationary case which is most interesting from a practical point of view, equation (4.16) may be written as follows

$$T(x) = T_m + (q/2\lambda)(h^2 - x^2 + 2h^2/Bi) \qquad (4.17)$$

A high rate of heat exchange ($Bi \to \infty$) simplifies expression (4.17) for the temperature field

$$T(x) = T_m + (q/2\lambda)(h^2 - x^2) \tag{4.18}$$

According to [1] where the effect of heat sources on the temperature field is estimated for a parabolic distribution of the form $q(x)/q(0) = 1 + C_1 x^2$, where C_1 is constant, the maximum error in $T(x)$ computed by equations (4.16) and (4.17) does not exceed 25%, which is quite satisfactory for design purposes.

(c) *Periodic heat dissipation.* When the value of t_{cool} is such that the computed value of Fo is greater than 5×10^{-2}, but is smaller than a certain value of $Fo(Bi)$, that is, when $5 \times 10^{-2} < Fo < Fo(Bi)$, heat dissipation is periodic. In this case, the temperature field is markedly affected by the cooling periods between firings. The lower bound $Fo(Bi)$ may be found for some specific cooling conditions from the nomograms in [4, 5]. For example, at $Bi = 0.1$, $Fo = 10$. At $Fo \geqslant 10$, heat dissipation is similar to that discussed for high values of Λ.

Mathematically, the problem reduces to solving the equations of thermal conductivity, separately for the jth pump cycle and the jth cooling cycle.

For the pump cycle:

$$\begin{aligned} \partial T_j^p / \partial t &= a(\partial^2 T_j^p / \partial x^2) + q^p / c\gamma \\ T_j^p(x, 0) &= T_{j-1}^{cool}(x, t_{cool}) \end{aligned} \tag{4.19}$$

For the cooling cycle:

$$\begin{aligned} \partial T_j^{cool} / \partial t &= a(\partial^2 T_j^{cool} / \partial x^2) \\ T_j^{cool}(x, 0) &= T_j^p(x, t_p) \end{aligned} \tag{4.20}$$

where t_p is the duration of the pump cycle.

The boundary conditions for expressions (4.19) and (4.20) have the form of (4.2).

Since the solution obtained in [6, 7] is of no practical interest as such, we shall immediately give an expression for the temperature field with heat dissipation uniformly distributed throughout the bulk in a quasi-stationary state which is characterized by a faithful replication of the temperature field from pulse to pulse at the respective instants of time [1]

$$T_{st}^p = T_m + (t_p q/c\gamma) \sum_{n=1}^{\infty} A_n \cos \mu_n (x/h) [1 - \exp(-\mu_n^2 Fo_{cool})]^{-1} \tag{4.21}$$

$$T_{st}^{cool} = T_m + (t_p q/c\gamma) \times$$

$$\times \sum_{n=1}^{\infty} A_n \cos \mu_n (x/h) \{\exp(1 - \mu_n^2 Fo) / [1 - \exp(-\mu_n^2 Fo_{cool})]\} \tag{4.22}$$

where A_n = as defined in (4.12)
$Fo_p = at_p/h^2$
$Fo_{cool} = at_{cool}/h^2$

From a brief analysis of the design relationships for the temperature field in the case where $5 \times 10^{-2} < Fo < Fo(Bi)$ it may be concluded that the quasi-stationary state as defined by equations (4.21) and (4.22) is attained during the time interval found from the condition

$$j(t_{cool} + t_p) = ph^2/a \tag{4.23}$$

where j = number of cycles
p = coefficient dependent on Bi

Besides, it may be shown that the temperature differential across the laser rod in the quasi-stationary state at $\mu_n^2 Fo \ll 1$ is independent of the rate of heat exchange. This obvious conclusion stems from the fact that at $\mu_n^2 (Fo_{cool} + Fo_p) \ll 1$ the situation approaches very closely the case of continuous heat dissipation discussed above, that is, $\Lambda \to 1$ and $Fo_{cool} \to 5 \times 10^{-2}$, and, as follows from (4.17), $T(x) - T(0) = q/2\lambda$, that is, independent of the cooling conditions.

In conclusion, it should be noted that for optical components of a shape other than a thin plate or a long cylinder, the computation of the temperature field is rather cumbersome, and one is forced to use approximate methods for solving the problem of heat conduction.

Among them are the numerical integration of the equation of thermal conductivity [8] and variational calculus [9] the application of which to the problems of heat conduction in laser oscillators has been examined in [10, 11].

From the above analysis of the causes of heat dissipation and their distribution, it may be concluded that the distribution $q(\bar{r}, t)$ for a laser rod cannot practically be computed; one can only find $\bar{q}$ averaged over volume and time. For the remaining optical components, it is sometimes possible to compute $q(\bar{r})$ averaged only over time.

Because of this, the above relationships for the computation of temperature fields in laser rods only give an approximate value of $T(\bar{r}, t)$ which differs from the actual value the more, the greater the initial non-uniformity of the temperature field used to determine the average value, $\bar{q}$. However, the above relationships are quite applicable to practical cases where one seeks to determine, at least approximately, the limiting operating temperature for optical elements.

Anisotropic optical elements. Computation of the temperature field, $T = T(x_1, x_2, x_3, t)$, for anisotropic optical elements involves

the solution of an equation describing thermal conductivity in anisotropic solids.

$$\partial T/\partial t = a_{ij}(\partial^2 T/\partial x_i \partial x_j) + q(x_1, x_2, x_3, t)/c\gamma \qquad (4.24)$$
$$(i, j = 1, 2, 3)$$

for the boundary conditions defined by (4.2)

$$N_i a_{ij}(\partial T/\partial x_j)|_\Sigma = -\alpha(T|_\Sigma - T_m) \qquad (4.25)$$

where $a_{ij} = \lambda_{ij}/c\gamma$ = second-rank thermal-conductivity tensor
N_i = vector of an external normal to a point on the surface
$x_1, x_2, x_3 = X, Y$, and Z, respectively.

For the indexes repeated twice, summation is carried out from 1 to 3. As a rule, anisotropic materials are used in the manufacture of electro-optic reflectors, shutters and some other laser elements. Their geometries are such that it is practically impossible to select a characteristic dimension, and the temperature field, $T = T(x_1, x_2, x_3, t)$, turns out to be dependent on all the three coordinates, x_1, x_2, x_3. In some special cases, it is a relatively easy matter to solve equations (4.24) and (4.25). For example, for a parallelepiped whose edges are chosen to be parallel with the principal axes of the ellipsoid of thermal conductivity

$$a_{ij}x_i x_j = 1 \qquad (4.26)$$

If the coordinate axes x_1, x_2, and x_3 are oriented along the edges of the parallelepiped, the solution can be obtained by separating the variables. For a symmetrical temperature field, the solution has the form [12]

$$T(x_1, x_2, x_3, t) = \sum_{c_1, c_2, c_3=1}^{\infty} A_{c_1, c_2, c_3} \times$$
$$\times \cos x_1 n_1 \cos x_2 n_2 \cos x_3 n_3 \exp\{-a_{ij} n_i n_j t\} \qquad (4.27)$$

where $n_i = \mu_{c_i}/R_i$, R_i is the length of the respective edge, and A_{c_1, c_2, c_3} are the initial thermal amplitudes derived from the relations for the isotropic problem on hand. This universality of A_{c_1, c_2, c_3} is due to the fact that at $t = 0$ the anisotropic properties have no effect on the function $T(x_1, x_2, x_3, 0)$. To recall:

$$A_{c_i} = \frac{2\sin\mu_{c_i}}{\mu_{c_i} + \sin\mu_{c_i}\cos\mu_{c_i}} = (-1)^{(c_i)+1}\frac{2Bi\sqrt{Bi^2 + \mu_{c_i}^2}}{\mu_{c_i}\left(Bi^2 + Bi + \mu_{c_i}^2\right)}$$

where μ_{c_i} is derived from the characteristic equation

$$\cot\mu_{c_i} = \mu_{c_i}/Bi_i$$

As is noted in [12], in some cases a solution for the anisotropic problem can be derived from the respective isotropic problem by replacing $a_o\delta_{ij}$ with a_{ij} where δ_{ij} is the Kronecker delta. This important conclusion stems from the correspondence principle according to which a solution for (4.27) changes into a solution for an isotropic problem by replacement

$$a_{ij} \rightarrow a_o\delta_{ij}$$

By simple manipulations, the ellipsoid of thermal conductivity described by (4.26) can be reduced to the major axes [13]. Then the equation of thermal conductivity (4.24) takes the form

$$\partial T/\partial t = a_1\partial^2 T/\partial x_1^2 + a_2\partial^2 T/\partial x_2^2 + a_3\partial^2 T/\partial x_3^2 + \frac{q(x_1, x_2, x_3, t)}{c\gamma} \qquad (4.28)$$

Then transforming for

$$x_i' = x_i/\sqrt{a_i} \qquad (4.29)$$

equation (4.28) can be reduced to the form

$$\partial T/\partial t = A(a_1, a_2, a_3)\Delta T + q(x_1', x_2', x_3', t)/c\gamma \qquad (4.30)$$

Physically, the first step in the transformation of coordinate axes is simply the rotation of the axes, and the transformation for (4.29) represents deformation without rotation (compressive or tensile).

Thus, a solution for equation (4.24) may be obtained from the solution of the reduced equation (4.30) describing an isotropic medium. In conclusion, it should be noted that the simplicity of this solution of equation (4.24) for an anisotropic medium depends to a great extent on boundary conditions, because the translation of equation (4.24) into a new system of coordinates, x_1', x_2', x_3', should be accompanied by the translation of the boundary conditions, equation (4.25), as well, which may entail considerable difficulties [14] in solving equations (4.24) and (4.25).

4.2. Optical Distortions in Laser Components

As already noted (see Sec. 2.1), laser rods may show a residual gradient of refractive index and birefringence due to imperfections in the manufacturing techniques. Similar distortions originating in production methods may, to a varying degree, be present in the materials used for other laser components, for example, electro-optic crystals, phototropic media, optic glasses and the like. Such micro- and macrodistortions are distributed in the material at random (see Sections 1.2 and 1.3), and their effect on the laser emission generated or amplified is difficult to evaluate. The only way to minimize these optical distortions is to improve manufacturing methods.

Apart from the residual optical distortions inherent in a particular material, there are distortions caused by intense light. For example, optical pumping or the emission being amplified may give rise to a gradient of refractive index because of a nonuniform distribution of the population inversion. Besides, practically all laser components may be heated by optical pumping or the laser beam being amplified. The temperature gradient set up by energy dissipated as heat is also accompanied by a refractive index

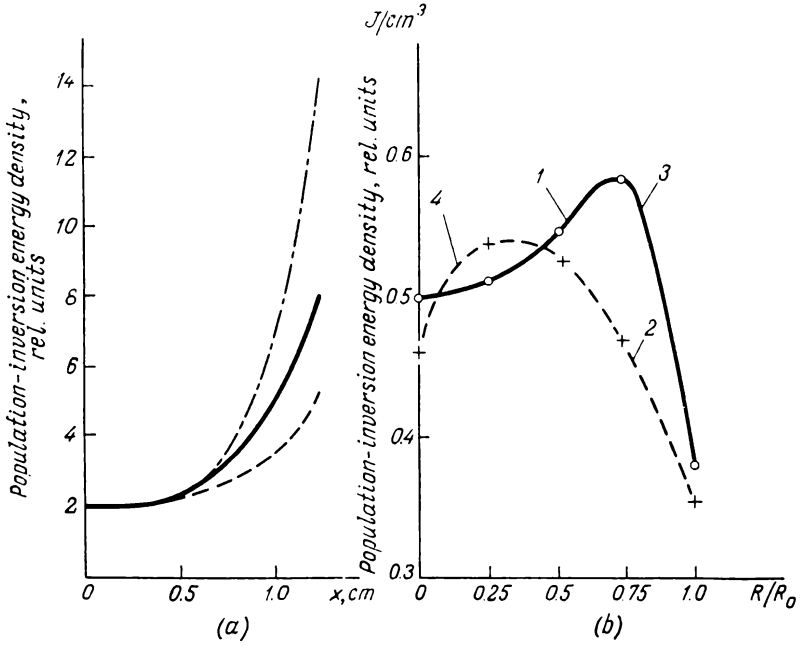

Fig. 4.1. Distribution of energy stored by the inverted population in (*a*) a neodymium-doped glass disc 2.5 cm thick arranged at an angle of 45° with the pump light and (*b*) a rod 4.5 cm in diameter

(*a*)– – – –1% neodymium; ———2% neodymium; —.—.—3% neodymium; (*b*)———in a plane passing through the centre of the laser rod and the centres of two tubes of a four-cavity pump unit, symmetrical about the laser rod; – – – –in a plane turned through 45° relative to the previous one

gradient and birefringence. There may also be other distortions. For example, in electro-optic materials a change in temperature brings about a change in the electro-optic and piezo-optic constants.

Dependence of refractive index on population inversion. The nonuniform distribution of population inversion in laser materials is examined in [15, 16]. The distribution of the absorbed pump energy for laser rods fabricated from ruby and neodymium glass

is discussed in [1]. Fig. 4.1*a* shows the distribution density of the energy stored by the inverted population in the disc of a zig-zag amplifier (see Sec. 2.6), adjusted for the absorption spectrum of neodymium glass and the emission spectrum of the flash tube [17]; Fig. 4.1*b* presents the same relationship found experimentally for a cylindrical neodymium glass laser rod in a four-tube pump cavity. In [18] it is shown that with nonuniform population inversion across the amplified laser beam having a Gaussian pump energy density, the phase front of the laser light is distorted. These points have been corroborated experimentally in [19]. At the same time, a change in the population inversion entails a change in the refractive index. For a four-level model, this effect has been examined in [20]. Assuming, as is done in [20], that the change in the refractive index due to optical pumping is caused by active ions, say, neodymium ions in the excited state, the necessary computations may be done using the Lorentz-Lorenz equation.

As a proof, let n_i be the refractive index associated with the concentration of ions in the ground state, N_1. Also let N_1 be such that

$$N_1 = N - N_3(r, t)$$

where N = concentration of ions in the glass
N_3 = concentration of Nd ions in metastable level 3

Then the dependence of the refractive index on polarizability for neodymium ions in the ground state may be written as follows

$$(n_1^2 - 1)/(n_1^2 + 2) = N(4\pi/3)\alpha_1 \tag{4.31}$$

where α_1 is the average polarizability of neodymium ions in the ground state given by

$$\alpha_1 = (e^2/4\pi^2 m)\sum_p f_{p,1}/(\nu_{p,1}^2 - \nu^2)$$

Here, e and m are the charge and mass of an electron, $\nu_{p,1}$ is the frequency of the transition from the ground state to the p-state, and $f_{p,1}$ is the oscillator force for the transition from the ground state to the p-state. The sum is taken over all excited states. Besides it is assumed that the absorption of neodymium ions in the ground state of frequency ν may be neglected. If active ions are excited to state 3, the refractive index related to ions becomes a complex number for the transition frequency $\nu = (E_3 - E_2)/h$, where E_2 and E_3 are the energies associated with the excited states 2 and 3, and h is Planck's constant. Designating the refractive index and the absorption coefficient as n_i and k_i, we may write for this case that

$$\frac{(n_i - ik_i)^2 - 1}{(n_i - ik_i)^2 + 2} = (4\pi/3)[N_1\alpha_1 + N_3\alpha_{3a}] \tag{4.32}$$

where $\alpha_{3\alpha}$ is the polarizability of ions in state 3 given by

$$\alpha_{3\alpha} = (e^2/4\pi^2 m) \sum_q \frac{f_{q,3}}{[(\nu_{q,3}^2 - \nu^2) + i\gamma\nu]} \tag{4.33}$$

where γ is the half line-width for the transition from state 3 to state 2, and the sum in expression (4.33) is taken over all states, except state 3.

Change of refractive index may be written as follows

$$\Delta n(r, t) = n_i - n_1 \tag{4.34}$$

Solving equations (4.31) and (4.32) for n_1, k_i and n_i and noting that n_i and n_1 are comparable with unity, while k_i is small in comparison because of the low concentration of neodymium ions or because of a low oscillator force (or both), we may write the following

$$\Delta n(r, t) \approx 2\pi(\alpha_3 - \alpha_1) N_3(r, t) - \frac{1}{6}[e^2 f_{2,3} N_3(r, t)/(2\pi m\gamma\nu)]$$

$$k_i(r, t) \approx e^2 f_{2,3} N_3(r, t)/(2\pi m\gamma\nu) \tag{4.35}$$

where the absence of a second subscript at α_3 corresponds to the assumption that the transition frequency ν is not a resonant one with any state q

For a case where ν is not a resonant frequency

$$\Delta n(r, t) = 2\pi(\alpha_3 - \alpha_1) N_3(r, t); \quad k_i = 0$$

The polarizabilities α_1 and α_3 may be determined for a specific scheme of transitions between the energy levels of active ions. For example, for neodymium glass at $\nu = 4.78 \times 10^{14}$ s^{-1}, and for the specific transition scheme between energy levels, we may write

$$\Delta n(r, t) \approx \frac{(e^2/2\pi m) f_{4,1}\nu_{3,1}(2\nu_{4,1} - \nu_{3,1}) N_3(r, t)}{(\nu_{4,1}^2 - 2\nu_{4,1}\cdot\nu_{3,1} + \nu_{3,1}^2 - \nu^2)(\nu_{4,1}^2 - \nu^2)} \tag{4.36}$$

Assuming that for neodymium $\nu_{3,1} = 3.4 \times 10^{14}$ s^{-1}, $\nu_{4,1} = 2.1 \times \times 10^{15}$ s^{-1}, and $f_{4,1} = 1$, then $\Delta n \approx 5 \times 10^{-24} N_3$. For an excited-ion concentration of about 10^{19} cm^{-3}, the change of refractive index is about 5×10^{-5}.

For the case where $h\nu$ is equal to the difference in energy between states 2 and 3, the last term in equation (4.35) is non-zero. However, for neodymium glass at $\nu = 3 \times 10^{14}$ s^{-1}, $\gamma = 6.7 \times \times 10^{12}$ s^{-1}, $f_{2,3} = 10^{-6}$ and $N_3 \approx 10^{19}$ cm^{-3}, it is negligible in comparison with the first term related to the change of refractive index at the same frequency, equal to 4.5×10^{-5}. It appears that the refractive index may change by the same order of magnitude when strong light pulses are amplified at a gain very close to saturation. Because of this, the trailing edge of a light pulse will "see" a population markedly altered by its leading edge. As a light pulse advances through the inverted population, the angular spread of

the amplified laser beam increases in going away from the front of the light pulse. This may happen with bleachable (phototropic) media.

Dependence of refractive index on temperature gradient. We shall discuss the dependence of the refractive index on the temperature gradient in two cases most representative of laser engineering, namely in an infinite cylinder and in a thin plate (see Fig. 4.2). In the cylinder, the temperature gradient is only a function of the radius, and the amplified light is propagated along the z-axis. In the thin plate with a thickness $x = 2h$, the temperature gradient is only a function of x, and the amplified beam is propagated in the z-direction. Other directions of the temperature gradient and the amplified light will not be considered. From the

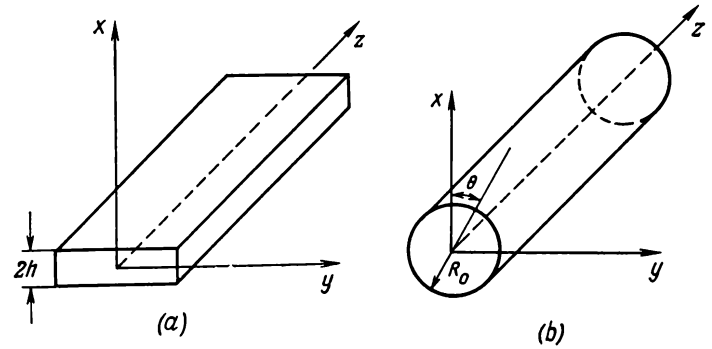

Fig. 4.2. Laser rods as (*a*) a thin plate and (*b*) a long cylinder

symmetry of the problem it may be assumed that the temperature gradient is a continuous symmetrical function, that is

$$\partial T/\partial x\,|_{x=0} = \partial T/\partial r\,|_{r=0} = 0 \tag{4.37}$$

Taking up separately the change of refractive index, Δn, due to temperature, that is $\Delta n\,|_{\sigma_{ij}=0}$, and due to thermoelastic stresses, that is, $\Delta n\,|_{T=0}$, we may write

$$\Delta n(x, t) = \partial n/\partial T\,|_{\sigma_{ij}=0} T(x, t) + \partial n/\partial \sigma_{ij}\,|_{T=0}\sigma_{ij} \tag{4.38}$$

where σ_{ij} are the components of the thermoelastic stress tensor. According to [21], the components of the thermoelastic stress tensor in the case of a symmetrical temperature gradient may be written as follows:

— for the plate

$$\begin{aligned} &\sigma_{xx} = \sigma_{yz} = \sigma_{zx} = \sigma_{xy} = 0 \\ &\sigma_{yy} = \sigma_{zz} = \gamma\,[\bar{T} - \bar{T}(x, t)] \\ &\varepsilon_{zz} = \alpha\bar{T} \end{aligned} \tag{4.39}$$

— for the cylinder

$$\begin{aligned}\sigma_{rr} &= \gamma[\bar{T} - \bar{T}(r, t)]\\ \sigma_{00} &= \gamma[\bar{T} + \bar{T}(r, t) - T(r, t)]\\ \sigma_{zz} &= \gamma[2\bar{T} - \bar{T}(r, t)]\end{aligned} \tag{4.40}$$

where $\bar{T} = \frac{1}{2h}\int_{-h}^{h} T(x, t)\,dx =$ average temperature

$$\bar{T}(r, t) = \frac{1}{r^2}\int_0^r T(r, t)\,r dr; \quad \gamma = \alpha E/(1 - \nu) \tag{4.41}$$

In [22] it is shown that the changes in optical properties caused by stresses may be described by an expression of the form

$$\Delta B_i = \pi_{ij}\sigma_j \quad (i, j = 1, 2, \ldots, 6) \tag{4.42}$$

where π_{ij} = component of the tensor giving the piezo-optic effect

$\Delta B_i = -2\Delta n_i / n_0^3$ = change in the components of the relative dielectric impermeability tensor

Substituting in equation (4.42) a column matrix made up of the components of the thermoelastic stress tensor and using the matrix of piezo-optic coefficients [22] which for an isotropic material has the form

$$\left\{\begin{array}{cccccc} \pi_{11} & \pi_{12} & \pi_{12} & 0 & 0 & 0\\ \pi_{12} & \pi_{11} & \pi_{12} & 0 & 0 & 0\\ \pi_{12} & \pi_{12} & \pi_{11} & 0 & 0 & 0\\ 0 & 0 & 0 & (\pi_{11} - \pi_{12}) & 0 & 0\\ 0 & 0 & 0 & 0 & (\pi_{11} - \pi_{12}) & 0\\ 0 & 0 & 0 & 0 & 0 & (\pi_{11} - \pi_{12}) \end{array}\right\} \tag{4.43}$$

gives an expression for variations of the refractive index. It turns out that for the plate

$$\begin{aligned}\Delta n_x(x, t) &= [T(x, t) - \bar{T}]\varphi_1\\ \Delta n_y(x, t) &= [T(x, t) - \bar{T}]\varphi_2\\ \Delta n_z(x, t) &= [T(x, t) - \bar{T}]\varphi_3\end{aligned} \tag{4.44}$$

and for the cylinder:

$$\begin{aligned}\Delta n_r(r, t) &= T(r, t)\psi_1 + \bar{T}(r, t)\psi_2 - \bar{T}\psi_3\\ \Delta n_0(r, t) &= T(r, t)\psi_4 - \bar{T}(r, t)\psi_2 - \bar{T}\psi_3\\ \Delta n_z(r, t) &= \{2\bar{T} - T(r, t)\}\psi_4\end{aligned} \tag{4.45}$$

where

$$\varphi_1 = \psi_1 = \gamma n_0^3 \pi_{12}; \quad \psi_2 = \gamma n_0^3 \frac{\pi_{11} - \pi_{12}}{2}$$

$$\varphi_2 = -\psi_4 = -\gamma n_0^3 \frac{\pi_{12} + \pi_{11}}{2} \qquad (4.46)$$

$$\psi_3 = \gamma n_0^3 \frac{3\pi_{12} + \pi_{11}}{2}$$

Similar expressions for Δn_i can be derived from the velocity components of light propagated through a stressed isotropic medium as is done in [23, 24] for a flat and a cylindrical laser rod. Computation of ΔB_i by equation (4.42) shows that as the optical indicatrix changes, the terms $\Delta B_4 = \Delta B_5 = \Delta B_6 = 0$; that is, the optical indicatrix changes along the x, y, and z axes (in the case of a flat laser rod) and along the r, θ, and z axes (in the case of

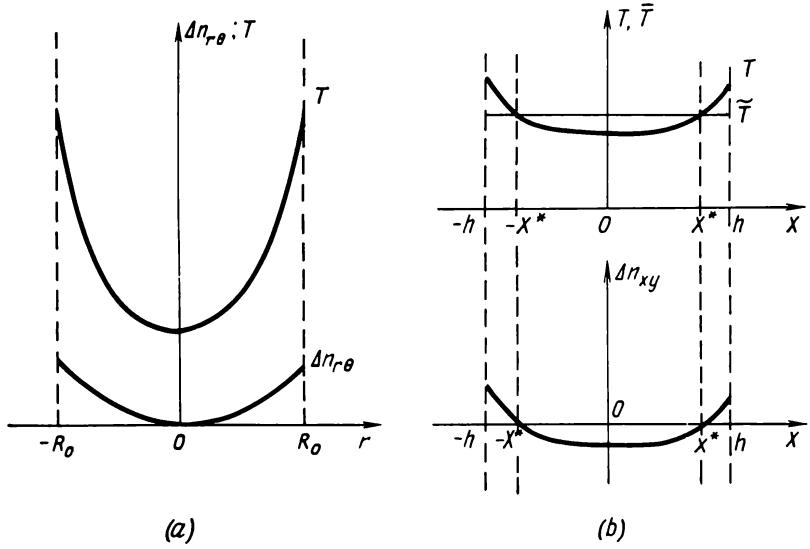

Fig. 4.3. Distribution of birefringence, Δn, and temperature T across (a) a cylindrical laser rod and (b) a flat laser rod ($\bar{T}$ is the average temperature)

a cylindrical laser rod). It should be added that an isotropic medium becomes anisotropic, similar to a uniaxial crystal in the case of the flat laser rod ($\Delta B_2 = \Delta B_3$) and a biaxial crystal in the case of the cylindrical laser rod. Expressions (4.44) and (4.45) can be used to compute the magnitude of induced birefringence for an electromagnetic wave propagated along the z-axis. According to [22], birefringence for a plate is given by

$$\Delta n_{xy}(x) = n_x(x) - n_y(x) = [\varphi_1 - \varphi_2][T(x) - \bar{T}] \qquad (4.47)$$

while for a cylindrical laser rod the expression is

$$\Delta n_{r\theta}(r) = \psi_2 [2\bar{T}(r) - T(r)] \tag{4.48}$$

Since

$$\lim_{r\to 0} \bar{T}(r) = \lim_{r\to 0} \frac{1}{r^2} \int_0^r T(r)\, r dr = \frac{1}{2} T(0)$$

then for a cylindrical laser rod

$$\Delta n_{r\theta}(0) = 0$$

The dependence of birefringence on the characteristic dimension obtained on the basis of (4.47) and (4.48) for a cylinder and a plate is shown in Figs. 4.3*a* and *b*.

As follows from the above expressions, the distribution of birefringence across the laser rod is described by a symmetrical function of the form $\Delta n_{xy}(x) = \Delta n_{xy}(-x)$, and birefringence is zero at $(\cdot)r = 0$ for the cylinder, and at points $x_{1,2} = \pm x^*$ (where $T(x^*) = \bar{T}$) for the plate. Furthermore, birefringence has the same sign throughout the cylinder and changes sign twice at $(\cdot)x_{1,2} = \pm x^*$ in the plate. Besides, with any symmetrical temperature profile the following equality is always satisfied in the plate:

$$\overline{\Delta n}_{xy} = \frac{1}{2h} \int_{-h}^{h} \Delta n_{xy}(x)\, dx = 0 \tag{4.49}$$

From the expressions describing the refractive index distributions, Eq. (4.44), one may conclude that there is no birefringence along the x-axis, that is, $\Delta n_{zy}(x) = 0$, while birefringence along the y-axis is equal to that along the z-axis

$$\Delta n_{xy}(x) = \Delta n_{xz}(x)$$

4.3. Propagation of Laser Light in a Medium with a Nonuniform Distribution of Refractive Index

Wavefront distortion. The propagation of laser light in a direction such that at right angles to it the refractive index is distributed nonuniformly is accompanied by wavefront distortion [25-29]. An equation describing the ray path for a case where $n = f(x)$, and laser light is propagated in the Z-direction (which is at right angles to the X-direction as is shown in Fig. 4.2) may be derived from the minimum of a variational integral of the form

$$P = \int_0^Z n(X) \sqrt{1 + (X')^2}\, dZ \tag{4.50}$$

where $X' = dX/dZ$.

Since the functional of a variational problem, such as described by equation (4.50), is

$$F(x, x') = n(x)\sqrt{1 + (x')^2}$$

then the solution for the Euler equation

$$\partial F/\partial x = (d/dZ)(\partial F/\partial x')$$

according to [30] will be as follows:

$$Z + C_2 = \mp \int_{x_1}^{x_2} \frac{dx}{\sqrt{\frac{n^2(x)}{C_1} - 1}} \tag{4.51}$$

where C_1, C_2 = constants of integration which may be defined from initial conditions

x_1, x_2 = coordinates of the points at which the ray enters and leaves the optical element

Equation (4.51) describes the path of the ray propagated along the Z-axis for a given refractive index distribution, $n(x)$. In some cases, it may be desirable to describe the wave surface of laser light passing through a medium with a refractive index distribution $n(x)$. An appropriate equation can be derived from the solution to the equation of the wave eikonal [31]

$$(\text{grad } P)^2 = n^2(x) \tag{4.52}$$

which, when written in full, is a nonlinear differential equation in partial derivatives

$$(\partial P/\partial x)^2 + (\partial P/\partial z)^2 = n^2(x) \tag{4.53}$$

The complete integral for equation (4.53) has the form

$$P(x, z) = \pm \int_0^x \sqrt{n^2(x) - a^2}\, dx + az + b \tag{4.54}$$

where a and b are two arbitrary parameters which define the family of integral surfaces. Assuming that the sought integral surface passes through the straight line such that $x = 0$ and $P = n(0)z$, we get

$$P(x, z) = \pm \int_0^x \sqrt{n^2(x) - n^2(0)}\, dx + n(0)z \tag{4.55}$$

Since the equation of a wave surface has the form $P = C =$ constant, then from equation (4.55), we have

$$z = \frac{C}{n(0)} \pm \int_0^x \sqrt{\frac{n^2(x)}{n^2(0)} - 1}\, dx \tag{4.56}$$

The normal to a plane curve (such as described by equation (4.56)) at the point (z^*, x^*) is given by an equation of the form

$$z - z^* = \mp \frac{x - x^*}{\sqrt{\frac{n^2(x^*)}{n^2(0)} - 1}} \tag{4.57}$$

which gives a measure of the divergence angle for the plane wave passing through a laser element.

The angle made by the normal, equation (4.57), with the Z-axis is

$$\psi = dx/dz = \mp \sqrt{\frac{n^2(x^*)}{n^2(0)} - 1} \tag{4.58}$$

Hence, the divergence angle is

$$\varphi = 2\psi = \mp 2 \sqrt{\frac{n^2(x^*)}{n^2(0)} - 1} \tag{4.59}$$

Determine the distribution $n(x)$ which causes the transmitted plane wavefront to change into a spherical one. It is clear that if

$$z = \pm \sqrt{a^2 - x^2} \quad (x \leqslant a) \tag{4.60}$$

where $a =$ constant, then the plane curve described by equation (4.60) is a circle, and the wave surface is spherical (with a cylindrical laser rod) or cylindrical (with a flat laser rod).

Using (4.56) and (4.60), we have

$$\pm \sqrt{a^2 - x^2} = \frac{C}{n(0)} \pm \int_0^x \sqrt{\frac{n^2(x)}{n^2(0)} - 1}\, dx \tag{4.61}$$

Differentiating (4.61) with respect to x, we get

$$x^2/(a^2 - x^2) = [n^2(x)/n^2(0)] - 1$$

Then

$$n(x) = n(0) \sqrt{a^2/(a^2 - x^2)}$$

which, at small values of x, is equivalent to the following expression

$$n(x) \cong n(0)\,[1 + x^2/2a^2] \tag{4.62}$$

In other words, if variations in the refractive index throughout a medium are described by equation (4.62), the medium acts like a lens. A similar refractive index distribution, equation (4.62), is obtained in [32].

The refractive index distribution in an optical element may be different for the orthogonally polarized components of the laser light passing through the medium. Therefore, if the distribution is

described by equation (4.62), two spherical waves will be formed at the exit from the optical element, that is, the optical element will act as a combination of two lenses differing in focal length. This has been investigated in [28].

Change of optical path length and birefringence. Because of the nonuniform temperature distribution in a laser rod, the optical path length for the rays travelling different trajectories will be different. It is shown in [23] that the change of optical path length along the Z-axis (see Fig. 4.2) may be described as follows

$$\Delta P = L\left[\Delta n + (n-1)\varepsilon_{zz}\right] \tag{4.63}$$

where L = laser rod length in the Z-direction
ε_{zz} = strain tensor component

From the relations given in [33] for the velocities of light polarized in the r, θ, an z directions and propagated in a stressed isotropic medium, one can readily compute the magnitudes of the stress-induced changes of optical path length Δn_r, Δn_θ, and Δn_z. Then, for a cylindrical rod, expression (4.63) will take the form [23]

$$\Delta P_r(r) = L\{[\beta + \gamma(2B_\perp)]T(r) + \gamma(B_\parallel - B_\perp)\bar{T}(r) + [2\alpha(n-1) - \gamma(3B_\perp + B_\parallel)]\bar{T}\} \tag{4.64}$$

$$\Delta P_\theta(r) = L\{[\beta + \gamma(B_\parallel + B_\perp)]T(r) + \gamma(B_\perp - B_\parallel)T(r) + [2\alpha(n-1) - \gamma(3B_\perp + B_\parallel)]\bar{T}\}$$

where

$$B_\parallel = \frac{n}{E}\left[\frac{q}{v} - 2\nu\frac{p}{v}\right]$$

$$B_\perp = \frac{n}{E}\left[(1-\nu)\frac{p}{v} - \nu\frac{q}{v}\right]; \qquad \beta = \frac{dn}{dT}\bigg|_{\sigma_{ij}=0}$$

E = Young modulus
ν = Poisson coefficient
$\frac{p}{v}$, $\frac{q}{v}$ = photoelastic constants describing change of the refractive index due to deformation parallel or perpendicular to the plane of polarization of the transmitted light

Obviously, for a thin plate (see Fig. 4.2), a similar expression can be written [24]

$$\Delta P_x(x) = L\{[\beta + \gamma(2B_\perp)]T(x) + [\alpha(n-1) - \gamma(2B_\perp)]\bar{T}\}$$

$$\Delta P_y(x) = L\{[\beta + \gamma(B_\perp + B_\parallel)]T(x) + [\alpha(n-1) - \gamma(B_\parallel + B_\perp)]\bar{T}\} \tag{4.65}$$

The case examined in [23] applies to an isotropic medium in which the distortion in the optical indicatrix

$$B_{ij}x_ix_j = 1, \quad \text{where } B_{ij} = 1/(n_{ij})^2 \quad (i, j = 1, 2, 3)$$

reduces to simple tension or compression, so that one need not be concerned with the rotation of the optical indicatrix about the original axes, that is, with the appearance of the terms ΔB_4, ΔB_5, and ΔB_6, which is likely to happen in anisotropic media and with a complex form of the stress tensor. A more complete description of changes in the optical properties, that is, a complete description of stress-induced distortion in the optical indicatrix is only possible, using matrix equation (4.42) which connects changes in the components of the relative dielectric impermeability tensor with changes in the stress tensor components.

Using (4.44) and (4.45) derived on the basis of (4.42), for a cylinder we have

$$\begin{aligned} \Delta P_r(r) &= L\{[\beta + \psi_1]T(r) + \psi_2\bar{T}(r) + [2\alpha(n-1) - \psi_3]\bar{T}\} \\ \Delta P_\theta(r) &= L\{[\beta + \psi_4]T(r) - \psi_2\bar{T}(r) + [2\alpha(n-1) - \psi_3]\bar{T}\} \end{aligned} \tag{4.66}$$

and for a plate

$$\begin{aligned} \Delta P_x(x) &= L\{[\beta + \varphi_1]T(x) + [\alpha(n-1) - \varphi_1]\bar{T}\} \\ \Delta P_y(x) &= L\{[\beta + \varphi_2]T(x) + [\alpha(n-1) - \varphi_2]\bar{T}\} \end{aligned} \tag{4.67}$$

With a uniform temperature field, equations (4.64), (4.66) and (4.65), (4.67) change into

$$\Delta P_x = \Delta P_y = \Delta P_r = \Delta P_\theta = LT[\alpha(n-1) + \beta] \tag{4.68}$$

Because of the pump-induced birefringence there is a difference in optical path length for two of the orthogonally polarized components, x and y or r and θ, of the transmitted light. Using equations (4.67), for a plate we have

$$\Delta P_x(x) - \Delta P_y(x) = L[\varphi_1 - \varphi_2][T(x) - \bar{T}] \tag{4.69}$$

A similar relationship exists for a cylindrical laser rod.

If one takes into account also the bending of orthogonally polarized rays which enter an optical element at different points, x_1, and x_2, and leave the same optical element at the same point x, then the optical path length difference for these rays will be

$$P_x(x) - P_y(x) = L\{n_x(0) - n_y(0)\} \pm \int_0^x \{\sqrt{n_x^2(x) - n_x^2(0)} - \sqrt{n_y^2(x) - n_y^2(0)}\}\, dx$$

Or, transforming with (4.47)

$$P_x(x) - P_y(x) = L\{\varphi_1 - \varphi_2\}\{T(0) - \bar{T}\} \pm \int_0^x \{\sqrt{n_x^2(x) - n_x^2(0)} - \sqrt{n_y^2(x) - n_y^2(0)}\}\, dx \quad (4.70)$$

Hence, the bending of rays makes a further variable contribution to the difference in optical path length between the orthogonally polarized rays.

Propagation of Gaussian beams through a medium with nonuniform refraction and gain. In the above cases, distortions in light pulses passing through an optically nonuniform medium have been treated on the basis of the ray approximation, neglecting the wave properties of laser light. In the general case, laser light is not a plane wave, because its intensity is distributed nonuniformly across the beam. As is noted in Sec. 1.4, any distribution of laser light intensity may be described by a system of orthogonal functions, called propagation modes, which are solutions of the wave equation (see [98] to Chapter 1). The dominant Gaussian mode may be described as

$$u(r, z) = (w_0/w)\exp\{-j(kz - \Phi) - r^2(1/w^2 + jk/2R)\}$$

where $\Phi = \arctan(2\lambda/\pi w_0^2)$ (the phase shift)

$$w^2(z) = w_0^2[1 - (\lambda/\pi w_0)^2]; \qquad R(z) = z\,[1 + (\pi w_0/\lambda z)^2]$$

$w(z)$ being the beam radius, $R(z)$ the radius of curvature of the wavefront, $k = 2\pi/\lambda$ the propagation constant, and w_0 the beam radius in a plane where the phase front is plane.

The intensity distribution across beams of higher orders is given by the product of the Gauss and Hermite functions on the Cartesian coordinates or by the product of the Gauss function and the Laguerre polynomials on the cylindrical coordinates. In any case, the parameters $w(z)$ and $R(z)$ are the same for all types of wave beams, while the intensity distribution across the beam and the magnitude of the phase shift are variable depending on the order index. This implies that the curvature of the phase front and the manner in which it changes are the same for all propagation modes.

A mathematical analysis of laser beam distortions described by these functions is extremely involved. Therefore, some investigators have limited themselves to the dominant mode of laser light propagated in a medium with the optical distortions discussed above. The propagation of a Gaussian beam through a lens-like medium is examined in [18] where the theoretical analysis taking into account the wave properties of laser light is based on a scalar wave equation which is satisfied by any field component or potential of

coherent light, namely

$$\Delta V + \tilde{K}^2 V = 0$$

where $\tilde{K} = K(r, z) + j\alpha(\bar{r}, z)$, with $K(r, z)$ defining the profile of refractive index change, and $\alpha(r, z)$ defining the profile of laser light gain or loss.

In terms of the refractive index, n, the function $K(r, z)$ is expressed as

$$K = 2\pi n/\lambda$$

The function $\alpha(r, z)$ is related to the initial and final powers, P_1 and P_2, by the following expression

$$P_2 = P_1 e^{-2\alpha z}$$

For laser light propagated in the z-direction, the solution of the wave equation may be written as follows

$$V = \psi(x, y, z) \exp(-j\Phi)$$

where $\Phi'(z) = \tilde{K}(z)$. For $\tilde{K}_0 = \text{constant}$, $\Phi = \tilde{K}_0 z$.

Another case examined in [18] is the behaviour of Gaussian beams in a medium where the refractive index and gain are quadratic functions, with special reference to gas lasers where the two parameters decrease from centre to periphery. In such a case, $\tilde{K}$ may be written as

$$\tilde{K}^2 = \tilde{K}_0^2 - \tilde{K}_0 \tilde{K}_2 r^2$$

Assuming that ψ is slowly varying in the z-direction and is a quadratic function of radial distance, the wave equation reduces to an equation of the form

$$\partial^2\psi/\partial x^2 + \partial^2\psi/\partial y^2 + (\tilde{K}^2 + \tilde{K}_0^2)\psi - 2j\tilde{K}\partial\psi/\partial z = 0$$

where

$$\tilde{K}_0 = K_0 + j\alpha_0 \qquad \tilde{K} = K_2 + j\alpha_2$$

K_0 is the propagation constant (wave number) in the centre of the inhomogeneity region, α_0 is the respective coefficient of negative or positive absorption, K_2 and α_2 are the constants of the quadratic relation.

In order to determine the parameters of the Gaussian beam, the function ψ is written as follows

$$\psi = \exp\left[-j\left(P + \tfrac{1}{2} Qr^2\right)\right]$$

where P and Q are complex parameters dependent on z.

Substituting this expression in the equation for ψ gives

$$Q^2 r^2 + 2jQ + \tilde{K}_0(2P^1 + Q^1 r^2) + j\tilde{K}_0^1 + \tilde{K}_0 \tilde{K}_2 r^2 = 0$$

Hence,

$$P^1 = -j(Q/\tilde{K}_0 + \tilde{K}_0^1/2\tilde{K}_0)$$

$$Q^2 = \tilde{K}_0 Q^1 + \tilde{K}_0 \tilde{K}_2 = 0$$

The last equation is a Riccati equation. Solving this equation gives the values of P and Q, then the values of $w(z)$ and $R(z)$ for a laser beam passing through a medium in which the refractive index and gain (absorption) are quadratic functions. Among other things, it is shown in [18] that in a gainless (lossless) lens-like medium conditions may exist such that a Gaussian beam will be propagated without any change in the beam radius. Similar results were obtained earlier in [34]. Gaussian beams may be channelled similarly in a medium with a uniform distribution of refractive index but with a gain which is a quadratic function of r. Analysis of the laser beam propagation carried out in [18] for the conditions just defined has yielded the following expressions for the radius of curvature R_m and the radius of a Gaussian beam w_m in terms of the constant α_2

$$R_m = 2\sqrt{\pi/\alpha_2\lambda}, \quad w_m^2 = 2\sqrt{\lambda/\pi\alpha_2}$$

The amplitude of such a beam increases as given by

$$\exp(\alpha - 1/R_m)z$$

Besides, it follows from the above analysis that in an amplifying medium whose R and w differ from R_m and w_m, the beam diameter and the radius of curvature of the phase front will pulsate as the beam propagates through the medium, approaching certain equilibrium values.

In [35, 36] the cases are investigated where the centre of the refractive index inhomogeneity is displaced relative to the centre of gain inhomogeneity, for different quadratic relations in the x- and y-directions and with the refractive index varying with the distance in the z-direction.

The refractive index and gain profiles of solid-state laser oscillators may markedly differ from those for gas lasers. Among other things, their lens-like behaviour may be opposite to that of gas lasers, and the profiles may show a very involved dependence on distance in a direction at right angles to the axis of beam propagation (see Sec. 4.2). This factor may cause a considerable increase in the angular beam spread.

Since the gain of solid-state lasers is much greater than that of gas lasers, the gain profile may affect the angular beam spread of the laser beam still more.

4.4. Measurement of Thermal Distortions in Laser Elements

Measurement of focal length for a lens-like medium. In some cases, analysis of laser operation does not call for an accurate knowledge of distortions in the wavefront of light transmitted through the laser material; instead, an approximate estimate of the radius of curvature of the wavefront will quite suffice. Precisely this is the case in the stability analysis of a cavity resonator incorporating a small-size laser rod, for example, in pulsed and continuous YAG lasers. In such cases, beam distortions are estimated

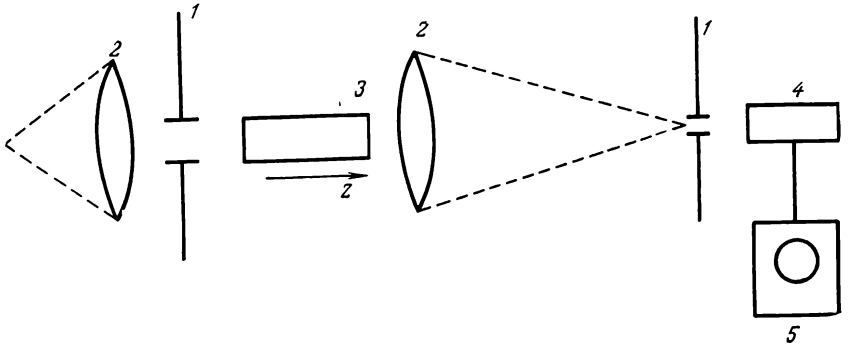

Fig. 4.4. Set-up for measuring the focal length of a thermal lens in a laser rod
1—aperture; *2*—lens of a known focal length; *3*—laser rod; *4*—photomultiplier tube; *5*—oscilloscope

on the basis of the focusing action of the medium. For this purpose a probe beam from, say, a gas laser is allowed to pass through the object under investigation, and the focal length is measured at the instant when lensing occurs.

With processes slowly varying with time, the focal length may be determined either by recording the cross-section of the laser beam on a photographic plate, or by the autocollimation method. In the latter case, one determines the defocusing of the tube, Δ, caused by the presence of a lens-like medium between the mirror and objective of the autocollimator. Then the focal length is found from the relationship [37]

$$f = F_o^2/\Delta$$

where Fo is the focal length of the autocollimator objective. However, these methods are inapplicable to fast processes. In such cases, the focal length may be determined by the method described in [38] (Fig. 4.4). The focus may be located from the dependence of the intensity of light passing through a stop on its position relative to the object under investigation (along the Z-axis). The

focal length is measured before pumping and at the instant of interest. Knowing the focal length of the lens in the system, the focal length of the resultant thermal lens can be found from the displacement of the intensity maximum.

Figures 4.5 and 4.6 show typical plots of focal length as a function of pump power for neodymium-doped glass [39] and YAG crystal [26, 28]. If the radius and centre of curvature of the plane curve, equation (4.56), obtained by passing the *xz* or *rz* plane through the wave surface are varying, the effective focal length can only be determined with low accuracy. However, this accuracy is comparable to that with which one can determine the stability region of the cavity or the temperature difference between the centre and edge of the laser rod, which likewise

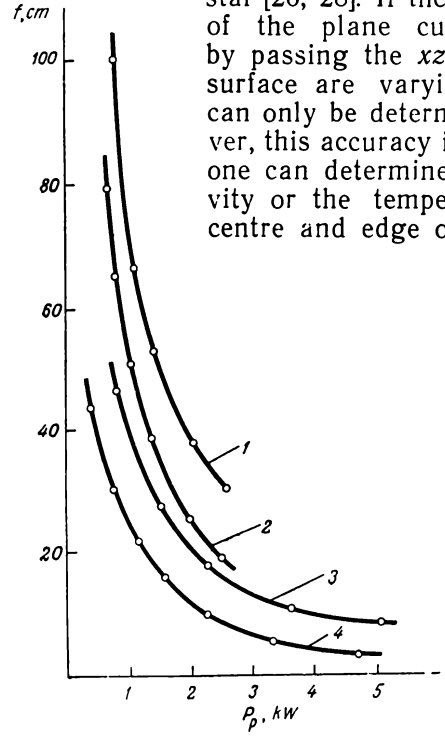

Fig. 4.5. Focal length as a function of pump power for neodymium-doped glass
1, *2*—orthogonally polarized light components focused by a cylindrical laser rod; *3*, *4*—orthogonally polarized light components focused by a flat laser rod

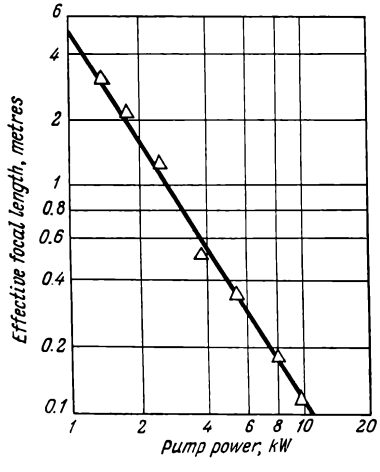

Fig. 4.6. Effective focal length as a function of pump power for neodymium-doped YAG crystal

call for certain assumptions. Thus, assuming a uniform heat dissipation in a laser rod of radius R_0 (or the half-thickness of the laser rod, h_0) and a high rate of heat abstraction from the side surface, the temperature distribution will be of the form

$$T(r) = T_c + T_1\left(1 - \frac{r^2}{R_0^2}\right)$$

The temperature difference between the centre and edge of a cylindrical laser rod is $T_1 = qR_0^2/4\lambda$ (for a flat laser rod, $T_1 = qh_0^2/2\lambda$), where λ is the thermal conductivity and q is the bulk heat dissipation density. With this temperature distribution, the change of refractive index will be given by

$$n = n_0(1 - 2r^2/b^2)$$

In [32] it is shown that a laser rod of length L_a with the above refractive index gradient is equivalent to a thick lens with a focal length given by

$$f = b/2n_0 \sin(2L_a/b)$$

and with the distance from the principal plane to the end being $(b/2n_0)\tan(L_a/b)$. For the thermal lens in question, the parameter b is

$$b_\xi = \sqrt{4n_0\lambda/a_\xi q}$$

where the symbol ξ designates a particular component of polarized light. For example, in a round laser rod $\xi = r$ for the radial component, and $\xi = \theta$ for the tangential component. According to [39], the parameter a_ξ may be found from the difference in optical path length between the centre and edge of the laser rod referred to its length and the temperature difference. A plane-mirror cavity with a thermally induced lens is equivalent to a spherical-mirror cavity and is characterized by the following parameters [32]:

$$\rho_{1,2} = 1 - \frac{d_{1,2}}{f}$$

where $d_{1,2}$ is the distance from the principal planes of the lens to the respective mirrors. When the lens is symmetrical about the mirrors, $\rho_1 = \rho_2 = \rho$, such that $\rho_\xi = \cos(2L_a/b_\xi) - L_{am}2n_0 \times \times \sin(2L_a/b_\xi)/b_\xi$, where L_{am} is the distance from the end of the laser rod to the mirror.

According to the cavity stability criterion (see Sec. 1.4), the value of the parameter b_ξ at the point where the cavity changes to an unstable condition is derived from the equation

$$1 + \cos(2L/b_\xi) = 2(L_{am}n_0/b_\xi)\sin(2L_a/b_\xi)$$

The difference in temperature between the edges and core of a laser rod and the cavity stability boundaries for various operating conditions can be determined from the experimental dependence of f on pump energy. The validity of the assumption that in small-size laser rods the temperature is a parabolic function of radius has been confirmed by direct interferometric measurements carried out in [40].

Interferometric measurements of $\Delta P(x)$ and $T(x)$. In cases where one needs a precise knowledge of wavefront distortions or temperature distribution in an optical element, resort is widely made to the interferometric method which utilizes the relationship

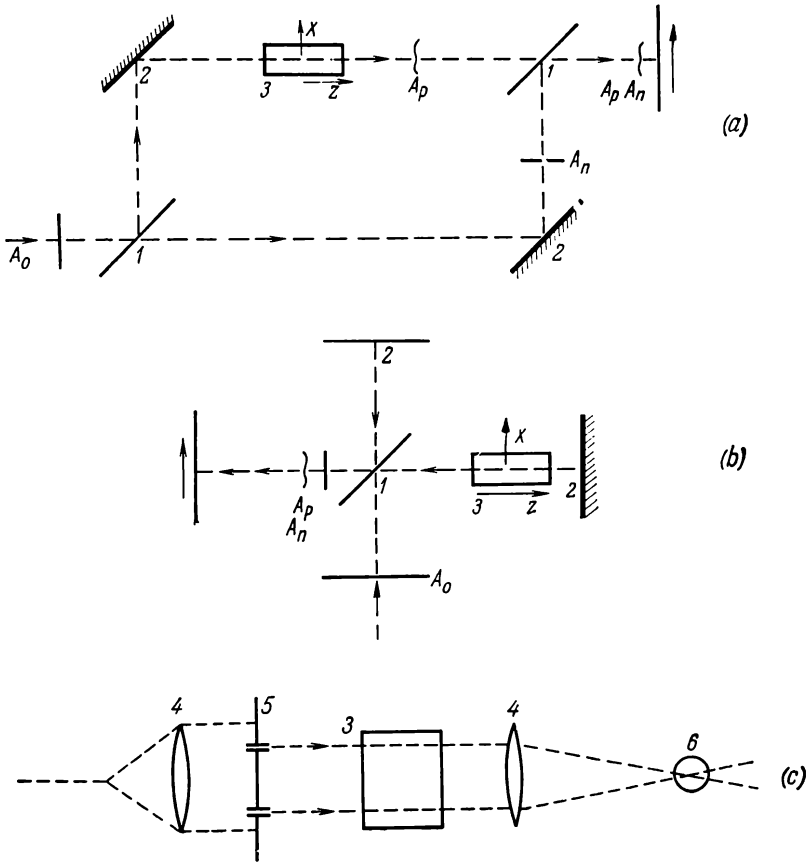

Fig. 4.7. Optical schematics of interferometers
(*a*) Mach-Zehnder; (*b*) Michelson; (*c*) Rayleigh; *1*—semitransparent mirror; *2*—100%-reflecting mirror; *3*—specimen; *4*—positive lens; *5*—screen with two slits; *6*—cylindrical lens

existing between the optical path length and temperature, Eqs. (4.66) and (4.67). With this method, the element under investigation is placed in one arm of an interferometer operating as a beam splitter. Most commonly, use is made of the Mach-Zehnder interferometer and the Michelson interferometer shown in Fig. 4.7*a* and *b* in sketch form. The interferometric procedure consists in obtaining a fringe pattern produced by interference between an

undisturbed wave and the wave that has passed through the active element and whose front is distorted. The recording facility may be a photographic camera or, in the case of fast processes, a high speed framing camera [41] or photomultiplier tubes. The change of optical path length, $\Delta P(x)$, is connected to the change in the number of interference fringes (both light and dark), Δm, by the relation $\Delta P = \Delta m\lambda/2$. As a rule, the accuracy of the interferometric method does not exceed one-quarter to one-half of a fringe.

The interferometric method may be used to determine the optical parallelism of the two ends of a laser rod and also the homogeneity of the glass itself. For this purpose, use is made of the Michelson interferometer in which one of the mirrors is replaced by the end of the laser rod under test. The Rayleigh interferometer [31] is less sensitive to vibrations than the Mach-Zehnder or Michelson interferometer, because both beams pass through the same element and the path length difference is noted between two points in its section (see Fig. 4.7*c*). In [42] the Rayleigh interferometer was used to measure the thermo-optic properties of neodymium-doped glasses.

The distribution $\Delta P_x(x) - \Delta P_x(0)$ derived from the fringe pattern may be utilized to determine the temperature profile. For example, on the basis of equation (4.67), the following relationship may be written for a flat laser rod:

$$\Delta P_x(x) - \Delta P_x(0) = L[\beta + \varphi_1][T(x) - T(0)] \tag{4.71}$$

using which one can get an idea about the temperature gradient across the laser rod. Utilizing the optical path length change for the radially and tangentially polarized light, the following relationship can be derived for a cylindrical laser rod:

$$T(r) - T(0) = \frac{f_{r\theta}(r) - f_{r\theta}(0)}{L[2\beta + \psi_1 + \psi_4]} \tag{4.72}$$

where $f_{r\theta}(r) = \Delta P_r(r) + \Delta P_\theta(r)$. The constants ψ_1 and ψ_4 in the above relationship are such that $\psi_1 + \psi_4 = \gamma n_0^3(\pi_{11} - \pi_{12})/2$ and may be determined from the known physical constants of optical materials.

The experiments carried out in [43] show that ray-bending may either decrease (positive lens action) or increase (negative lens action) the area of the fringe pattern of an optical element in comparison with its actual area. Taking into account ray-bending, the coordinates (ξ) of the fringe pattern may be correlated to the coordinates (x) of the actual section of a laser rod, that is, $\xi = f(x)$. If the length of an optical element along the beam is short and the refractive index changes but little across the section, the ray path

inside the optical element may be visualized as a straight line passing through the point of entry of the ray into the element, x_1, at an angle $\pm\sqrt{\frac{n^2(x_1)}{n^2(0)}-1}$ with the Z-axis. The meaning of this assumption is that the ray bends near the entrance and exit ends of the element (Fig. 4.8), while the further bending of the ray

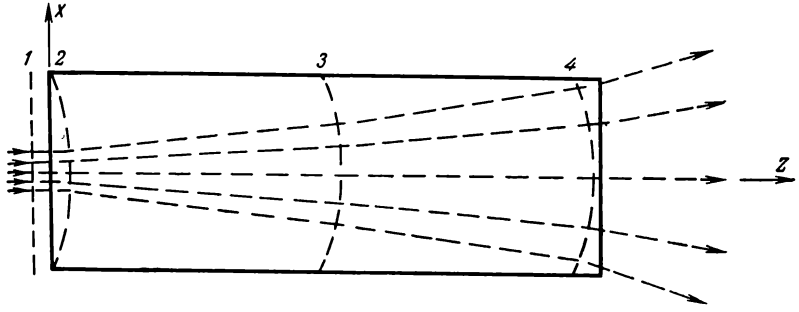

Fig. 4.8. Distortion of a plane wavefront passing through a laser rod with a symmetrical refractive index gradient, $n(x)$
1 — plane wavefront of the incident light; *2, 3, 4* — wavefront distortion along the *Z*-axis

directly on the surface of the exit end may be neglected. Then, we have

$$\xi = x_1 + L\sqrt{\frac{n^2(x_1)}{n^2(0)}-1} + Z^*\sqrt{\frac{n^2(x_2)}{n^2(0)}-1} \qquad (4.73)$$

where x_1 = coordinate of the point of entry of the ray into the optical element
L = length of the optical element in the direction of ray propagation
Z^* = distance from the exit end to the plane of the fringe pattern

$$x_2 = x_1 + L\sqrt{\frac{n^2(x_1)}{n^2(0)}-1}$$

Using geometric constructions, it is an easy matter to obtain an inequality which can be satisfied so that the accuracy of measurement will be better than $\lambda/2$. This inequality has the form

$$(L/2)\left[\frac{n^2(x_1)}{n^2(0)}-1\right] \leqslant \lambda/2 \qquad (4.74)$$

The meaning of this condition is that the length of the bent ray path inside the element exceeds the length L of the element by less than $\lambda/2$. According to [41], the typical value of $\Delta n(x_1) = n(x_1) - n(0)$ is about 10^{-5}. Using this value and also inequality (4.74), one can estimate the length L at which the ray bending

inside the element may be neglected, that is, that the ray may be assumed to be propagated in a straight line parallel to the Z-axis

$$L \frac{n(x_1) - n(0)}{n^2(0)} 2n(0) \leqslant \lambda$$

Hence, at $\lambda = 6.3 \times 10^{-7}$ m and $\Delta n(x_1) \cong 10^{-5}$, we have

$$L \leqslant 10^{-1} \text{m}$$

When the above condition is satisfied, equation (4.73) takes the form

$$\xi = x_1 + Z^* \sqrt{\frac{n^2(x_1)}{n^2(0)} - 1} \qquad (4.75)$$

Obviously, if Z^* is likewise smaller than 10^{-1} m at $\Delta n(x_1) \approx 10^{-5}$, then it may be assumed, within the accuracy limits of the experiment, that $\xi = x$. Thus, in order to simplify the interpretation of

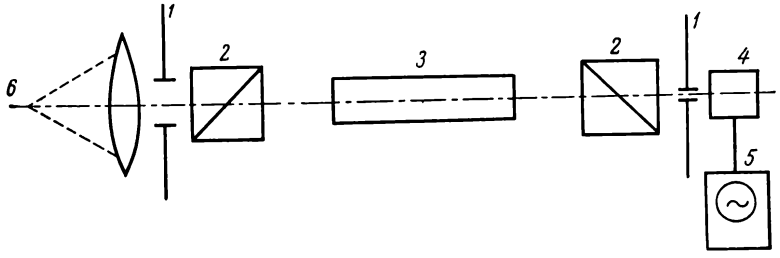

Fig. 4.9. Set-up for measuring induced birefringence in a laser rod
1—aperture; *2*—Glann prism; *3*—laser rod; *4*—photomultiplier tube; *5*—oscilloscope; *6*—monochromatic light source

a fringe pattern, its plane must be placed as close as possible to the exit end of the optical element ($\leqslant 10^{-1}$ m), whose length at $\Delta n(x_{\max}) \approx 10^{-5}$ should not exceed 10^{-1} m.

Unfortunately, investigation of the temperature field in anisotropic laser rods, using fringe patterns and equations (4.71) and (4.72), is greatly handicapped by the extreme complexity of fringe patterns. This drawback is nonexistent in holographic interferometry [44]. In this method the first step is to obtain a hologram of a passive (not pumped) laser rod. Then the rod is pumped, and the new wavefront is passed through the hologram left in the same place, and it interferes with the wavefront that has been recorded. The resultant interference fringe pattern reveals only thermal distortions in laser rods [45].

Once the temperature field distribution, $T(x, t)$ is determined, it is an easy matter to find the distribution of refractive indexes for the orthogonally polarized light components, the extent of in-

duced birefringence (equations (4.47) and (4.48)), and the distortion of the wavefront (equation (4.56)).

Investigation of birefringence and temperature gradients by the polarization method. In cases where one is interested in birefringence and the related processes rather than in wavefront distortions, interferometry may be dispensed with. A simpler way to determine birefringence is to employ the polarization method in conjunction with one of the optical set-ups listed in [46] and shown in Fig. 4.9. In addition the polarization method produces a conoscopic pattern of the object under investigation. In the test set-up of Fig. 4.9, the object is placed between crossed polarizers *1* and *2*. It is seen from equations (4.42), (4.44), and (4.45) that $\Delta B_4 = \Delta B_5 = \Delta B_6 = 0$, that is, the axes of the deformed indicatrix of an isotropic medium in a flat laser rod are oriented along the *xyz* axes (see Fig. 4.2). Thus, the ellipsoid is deformed without being rotated relative to the original coordinate system. Then, if the angle between the planes of polarization of polarizers *1* and *2* is equal to $\pi/2$, and the angle between the plane of polarization of polarizer *1* and the *x*-axis of the laser rod is $\pi/4$, the transmission of the polarizer-laser rod-polarizer system as determined from the ratio of the transmitted light intensity, I, to the incident light intensity, I_0, is connected to the magnitude of induced birefringence by the following expression [46]:

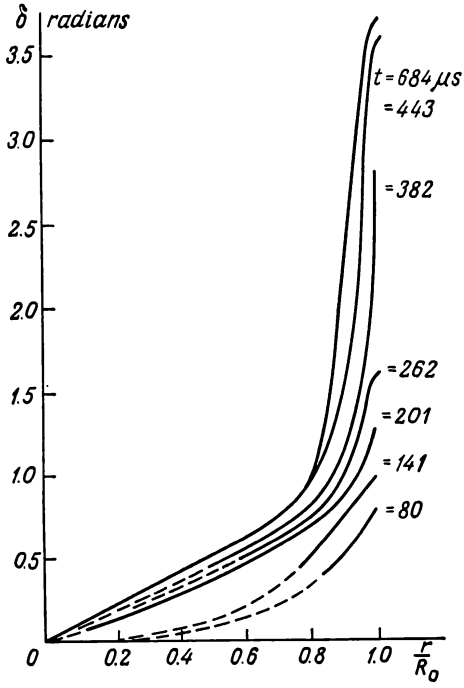

Fig. 4.10. Phase difference between orthogonally polarized light components, δ, as a function of radius at different instants of time, t, since the firing of the flash tube t

$$I(x, t)/I_0 = \sin^2 \frac{\pi L \Delta n_{xy}(x, t)}{\lambda} \qquad (4.76)$$

For a cylindrical laser rod, the above expression will have the same form if the angle between the plane of polarization of polarizer *1* and the axis of the deformed ellipsoid is $\pi/4$.

The expression for birefringence derived above does not take into account the additional path length difference between the orthogonally polarized light components caused by ray bending. Therefore, relationship (4.76) will become the more precise, the better condition (4.74) is satisfied.

The investigation of birefringence by the above method has been reported in a number of publications. Some of the workers [47, 48]

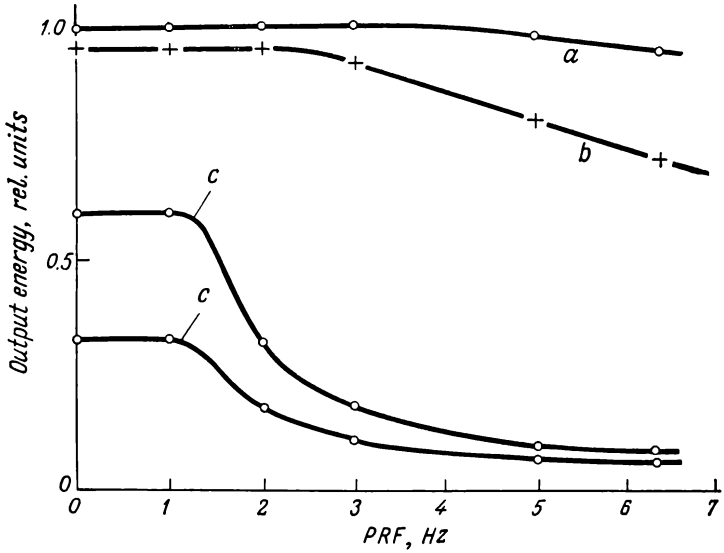

Fig. 4.11. Output energy as a function of PRF for neodymium-doped-glass lasers

(*a*) with a cavity using no polarizing elements; (*b*) with a three-mirror cavity using a Rochon prism throwing the orthogonal components onto two reflecting mirrors; (*c*) with a three-mirror cavity using a Rochon prism blocking the polarized components in turn

have employed this set-up to obtain qualitative photographs of a cross-section through a cylindrical laser rod, while others [41] have measured the phase difference between the radial and tangential polarization components of light passing through the laser rod. The manner in which the phase difference between the orthogonally polarized light components varies with time in a single-shot neodymium-glass laser [41] is shown in Fig. 4.10. Besides, it has been shown more than once (for example in [26]), that an increase in the induced stresses in a laser rod entails marked changes in the conoscopic pattern. Such investigations are especially important in an analysis of the field pattern and the dependence of output energy on pump energy in laser oscillators whose cavities contain polarizing elements. As an illustration, Fig. 4.11 relates output

energy to pulse repetition frequency for a neodymium-glass laser oscillator whose cavity contains a polarizing element [49].

Furthermore, birefringence patterns of stressed laser rods and other laser components give a clue to their temperature gradients. For example, as follows from equations (4.47) and (4.48), for a plate we have

$$T(x) - T(0) = \frac{\Delta n_{xy}(x) - \Delta n_{xy}(0)}{\varphi_1 - \varphi_2} \tag{4.77}$$

For a cylindrical laser rod, this relationship is more elaborate

$$\frac{\Delta n_{r\theta}(r)}{\psi_2} = \frac{2}{r^2}\int_0^r T(r)\, r dr - T(r) \tag{4.78}$$

or

$$r^2 T(r) - 2\int_0^r T(r)\, r dr = -\frac{\Delta n_{r\theta}(r)}{\psi_2} r^2 \tag{4.79}$$

Differentiating the above equation gives

$$dT(r) = -\frac{1}{\psi_2}\left\{2\frac{\Delta n_{r\theta}(r)}{r} dr + d(\Delta n_{r\theta}(r))\right\} \tag{4.80}$$

Hence,

$$T(r) - T(0) = -\frac{1}{\psi_2}\left\{2\int_0^r \frac{\Delta n_{r\theta}(r)}{r} dr + \Delta n_{r\theta}(r)\right\} \tag{4.81}$$

where φ_1, φ_2, and ψ_2 are the constants which can be obtained from the known physical constants of optical materials.

Naturally, the above relations are only applicable to a weakly focussing medium for which ray bending may be neglected.

4.5. Correction of Laser Light Distortions

Methods for reducing optical nonuniformity in laser components. Since birefringence and wavefront distortions are above all caused by the nonuniform absorption of pump energy or the light being amplified by laser elements, the most natural way to improve the characteristics of laser light is to make the population inversion and heat dissipation in the laser rod more uniform. The distribution of the absorbed pump energy in various laser rods (Sec. 1.1) has been investigated by many workers (see for example [25 to 28, 41]) who have brought out the principal factors affecting the resultant thermal gradient. Among other things, the absorbed energy distribution has been found to be dependent on the operating conditions of the laser rod. In cases where the objective of

pumping is to produce a maximum population inversion (for example, in the generation of nano- and picosecond pulses), the population inversion and the temperature distribution in the laser rod are more uniform due to an increase in the transmission of the laser material.

The factors that affect the absorbed energy distribution most of all are the geometry and size of the laser rod and its absorption coefficients for the pump light. For example, it is much easier to secure a uniform absorbed energy distribution by adjusting the concentration of active centres in a side-pumped flat laser rod than in a cylindrical laser rod.

The distribution of population inversion and temperature in laser rods is also affected by the finish of the laser rod sides, the refractive index at the interface, and some other factors.

It appears that in some cases thermal distortions may well be reduced, for example, by cooling or heating adjusted so that the resultant temperature gradient in the laser rod will be equal in magnitude but opposite in sign to that produced by pumping. For this purpose, in [50], the laser rod was first subjected to several idle pump cycles (with no emission of laser light) in order to establish an advance temperature gradient, then an operating pump cycle followed (that is, the laser rod was pumped until it emitted a laser pulse). The result was an appreciable improvement in the characteristics of the output beam. It should be stressed, however, that little headway has as yet been made in the use of methods for laser emission control on the basis of suitably chosen thermal conditions before or during lasing action, and their future prospects may only be a guess at best.

Correction of laser beam distortions through improvements in the characteristics of optical materials. Although these methods are limited by the state of the art, encouraging results have been obtained in some cases. For example, the absorption coefficients of such materials as KDP and DKDP, have materially been reduced over the past years through improvements in their manufacture. This method of reducing optical distortions by bringing down the interaction of intense emission with the medium, is highly efficient, and with those concerned with the development of new processes for the manufacture of optical materials it ranks topmost.

Other methods for minimizing optical distortions are based on the choice of constants that determine the effect of temperature on the optical properties of a medium. For example, [51] describes a glass composition having an extremely high transmission at a wavelength of 1.06 μm with a very small coefficient of temperature expansion equal to 40×10^{-7} to 60×10^{-7} mm/deg. It is not at all unlikely that in the near future materials will appear, having still lower coefficients of temperature expansion.

Instead of reducing to zero the thermo-optic constants, it appears more effective to minimize the coefficients determining the dependence of the path length difference on the temperature field (see Sec. 4.2). For example, according to [23, 24], the path length difference between the points $x = 0$ and $x = x'$ for a cylinder and a plate, on the basis of equations (4.64) and (4.65), can be written as follows:

$$\Delta_r(r) = nL\left\{\beta/n - [\alpha/(1-\nu)]\left[\frac{\overline{T}(r)}{T(r)}(1+\nu)(p/v - q/v) - 2\times\right.\right.$$

$$\left.\left.\times(1-\nu)(p/v) + 2\nu q/v\right]\right\} T(r)$$

$$\Delta_x(x) = L[\beta + \gamma(2B_\perp)]\, T(x)$$

$$\Delta_y(x) = L[\beta + \gamma(B_\perp + B_\parallel)]\, T(x)$$

It is seen that for a cylinder the condition $\Delta_r(r) = 0$ depends on the form of the distribution $T(r)$, and this handicaps the choice of parameters for the host glass that would make the cavity resonator free from thermal distortions. In contrast, the condition $\Delta_x(x) = \Delta_y(x) = 0$ for a plate is independent of $T(x)$ and may be satisfied through a proper choice of β [deg C]$^{-1}$ for the most typical values of other parameters of laser glasses, namely $B_\perp = 3.5 \times 10^{-7}$ cm^2/kg, $B_\parallel = 0.42 \times 10^{-7}$ cm^2/kg, $E = 6.98 \times 10^5$ kg/cm^2 and $\nu = 0.225$.

According to [24], the condition for minimum thermal distortions is satisfied by flat laser rods fabricated from neodymium glass with $\alpha = 10^{-5}$ [deg C]$^{-1}$, $\beta = -6.2 \times 10^{-6}$ for the X-polarized light component and $\beta = -3.5 \times 10^{-6}$ for the Y-polarized light component.

At present, there are neodymium glasses with thermo-optic constants in which thermal optical distortions are reduced to a minimum. An investigation of cylindrical rods fabricated from neodymium glasses varying in composition is presented in [52], also giving the focal lengths of thermal lenses and covering the thermal distortions of optical cavities fabricated from different grades of glass, both stock-produced and experimental. Among other things, it is shown that by varying the glass composition one can both control the focal length of a thermal lens over a wide range, and change its sign. Similar results have been obtained for the path length difference. While their efficiency in converting optical pumping energy into laser light is about the same as of the glasses discussed in Sec. 1.3, these new "self-compensating" glasses reduce the divergence angle by a factor of 2.5 to 3. In [53] a description is given of rectangular laser rods fabricated from neodymium glasses varying in composition, notably glasses with

a thermo-optic constant minimizing the thermal distortions of polarized light.

In [54], it is proposed to control glass composition in order to obtain a uniform path difference gradient for the radial or tangential component of laser light. Relevant data are cited for glasses of different compositions and it is shown that either $\Delta_r(r) = 0$ or

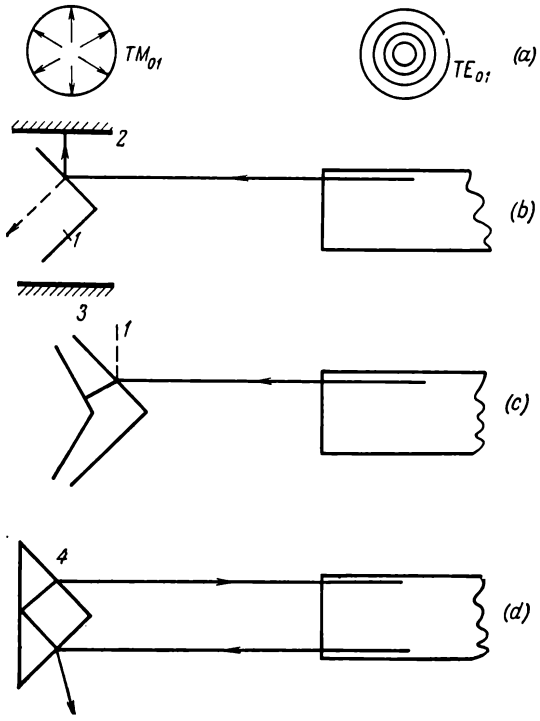

Fig. 4.12. Separation of radially and tangentially polarized components of laser light by means of

(*a*) a cone with the Brewster angle at the vertex (*1*) and a coaxial mirror (*2*) discriminating against the tangential light; (*b*) a cone with the Brewster angle at the vertex (*1*) and a conical mirror (*3*) discriminating against the radial light; (*c*) a conical TIR prism (*4*) discriminating against the radial light

$\Delta_\theta(r) = 0$ may be obtained. That is, it may be arranged for any light component to pass through the laser rod having a radial temperature gradient without any wavefront distortions while the other will suffer wavefront distortions similar to those occurring during the passage through a lens.

Methods for separating the radial and tangential components of laser light (Fig. 4.12) are proposed in [55]. For example, the radially polarized light may be discriminated against through the

use of a transparent cone with the Brewster angle at the vertex, arranged coaxially with a cylindrical mirror (Fig. 4.12*b*). The tangential component of laser light may be discriminated against likewise by means of a transparent cone, but in a combination with a conical mirror which will reflect light incident at an angle of 90° (Fig. 4.12*c*). Instead of two cones, use may be made of a conical prism (Fig. 4.12*d*).

As already noted, changes in the parameters of the host glass cannot secure thermal distortion compensation for the two orthogonally polarized components of light simultaneously. Therefore, it seems natural to examine the conditions under which the optical path length for a given component will be held constant and independent of the radius, taking the sum of the components rather

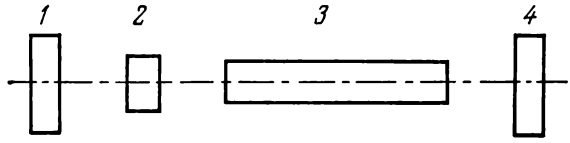

Fig. 4.13. Optical schematic of a laser compensated for the distortions of the wavefront formed by the sum of orthogonally polarized light components
1—100%-reflecting mirror; *2*—λ/8 Faraday rotator; *3*—laser rod; *4*—semitransparent mirror

than each component separately [56]. From the expression for the optical path length in a cylindrical optical element (Sec. 4.2) we get

$$[\Delta P_r(r) - \Delta P_r(0)] + [\Delta P_\theta(r) - \Delta P_\theta(0)] = \Delta_r(r) + \Delta_\theta(r) =$$
$$= 2nLT(r)\left\{\beta - \frac{\gamma}{E}\left[-\frac{3-5\nu}{2}\frac{p}{v} - \frac{1-3\nu}{2}\frac{q}{v}\right]\right\}$$

As is seen, the right-hand side of the above expression can be equated to zero, that is, the compensation condition for the sum of polarized components can be satisfied through a proper choice of values of α and β [56].

The sum of the optical path lengths for mutually orthogonal components can be obtained by means of a Faraday rotator which rotates the planes of polarization through $\pi/2$ and $\pi/4$ and channels the transformed light either to the entrance of the same laser rod (Fig. 4.13) or to the entrance of another laser rod held under the same conditions as the first (Fig. 4.14) [56].

The first method for summing optical path lengths is employed in laser oscillators. In this case, a Faraday rotator is placed between the laser rod and a totally reflecting mirror. Owing to this arrangement, the beam is forced to traverse the Faraday rotator twice, and the plane of polarization of the beam is turned through

$\pi/2$. The second method for summing optical path lengths is employed in laser amplifiers (see Fig. 4.14). In this case, use is made of a quarter-wave Faraday rotator. By this arrangement, the optical path length in the first laser rod, $\Delta_r(r)$ (or $\Delta_\theta(r)$) is added together with the optical path length, $\Delta_\theta(r)$ of the second laser rod where the temperature gradient is similar to that of the first rod.

A method for reducing thermally induced birefringence in synthetic cubic-symmetrical laser crystals, notably neodymium-doped

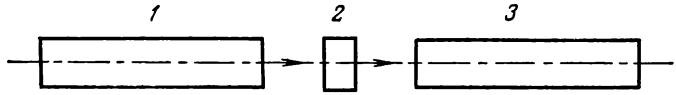

Fig. 4.14. Optical schematic of a laser amplifier compensated for the distortion of the wavefront formed by the sum of orthogonally polarized light components
1—first laser rod; *2*—$\lambda/4$ Faraday rotator or *Z*-cut quartz plate; *3*—second laser rod held under the same conditions as the first

YAG crystals, is discussed in [57]. More specifically, it is proposed that a crystal should be grown in the [001] or equivalent direction, but so that one of its crystallographic axes will be parallel to the direction of laser light (Fig. 4.15). Then, by rotating the crystal about the axis parallel to the direction of laser light, it may be oriented relative to a polarizing device so that birefringence will

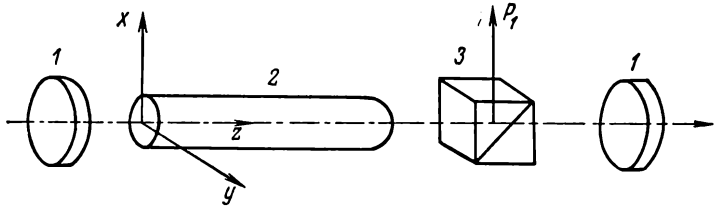

Fig. 4.15. Orientation of a polarizing element in a laser using a YAG crystal grown in the [001] direction
1—laser cavity mirror; *2*—laser rod; *3*—polarizer

be kept to a minimum. From the polar diagrams of birefringence in Fig. 4.17 it is seen that birefringence may be minimized only when a crystal has been grown along one of its axes. In such a case, the magnitude of birefringence is much smaller than it is in a crystal grown in the usual [111] direction or in the [110] direction. A plot relating laser power output to pumping power for crystals grown in the [001] and [111] directions is shown in Fig. 4.16. It is also seen that the orientation of the laser rod relative to the direction of the polarizer is likewise essential.

A method for reducing induced birefringence and thermal distortions in YAG laser rods of rectangular cross-section (see Fig. 4.2*a*)

is proposed in [58]. From an analysis of the stress indicatrix for a plate variously oriented relative to the crystallographic axes of a YAG crystal, it is seen that when heating is nonuniform in the x-direction birefringence will be a minimum for the light beam propagated in the z-direction if the z, x and y axes are oriented in the [111], [10$\bar{1}$], and [$\bar{1}$2$\bar{1}$] directions, respectively. Then the induced birefringence will be by a factor of 2.5 lower than, say, when the z, x, and y axes are oriented in the [001], [010], and [0$\bar{1}$0] directions. Thermally induced distortions in the x-component of

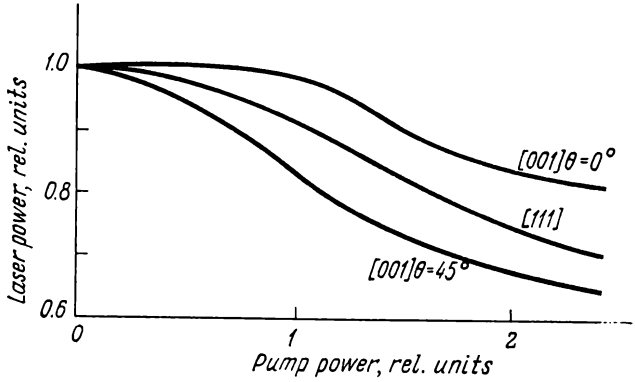

Fig. 4.16. Laser power as a function of pump power for a laser using a YAG crystal grown in the [001] and [111] directions. 0 is the angle between the crystallographic axis of the laser rod and the direction of the plane of polarization of the polarizer

polarized light are also markedly reduced. Furthermore, since with a symmetrical temperature distribution in the plate, the plane passing through the indicatrix at right angles to the direction of light propagation produces an ellipse with its major axes directed along the x and y axes, birefringence will cause no distortion in the linearly polarized light (along the x or y axis).

Correction of wavefront distortions. In some cases wavefront distortions may be compensated through the use of corrective optical elements [59]. This can be done, for example, in cases where the characteristics of the laser components remain unchanged in the course of oscillation or amplification. More specifically, this is possible with short (nano- or picosecond) light pulses or steady-state repetitive or continuous emission. Unfortunately, this method is sensitive to operating conditions, notably the magnitude of pump energy, to which should be added the complexity of selecting and making appropriate corrective elements. In cases where the wavefront of the distorted beam has a constant radius of curvature, the requisite compensation may be secured with either a positive

or a negative lens. To reduce the number of reflecting surfaces, a corrective sphere may be attached to the end of a cavity element, say, the laser rod or a mirror [60].

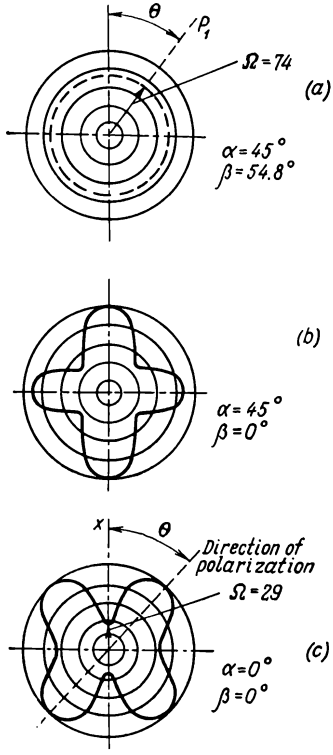

Fig. 4.17. Polar diagrams of birefringence as a function of the orientation of a polarizer relative to a YAG rod cut in different directions (*a*) — [001]; (*b*) — [111]; (*c*) — [110]. Ω — birefringence in relative units; θ — angle between the crystallographic axis and the direction of polarization; α, β — angles between the axis of the laser rod and the crystallographic axes

The method proposed in [61] utilizes a corrective element fabricated from a material such that the temperature derivatives of the refractive indexes in the compensating element and the laser rod be opposite in sign (Fig. 4.18). The essence of this method will be clear from the following simplified consideration which defines the general requirement for the corrective element, although it ignores the bending of light rays. Suppose that the dependence of the refractive index on temperature has the form

$$n = n_0 + \beta (T - T_0)$$

where n_0 = refractive index at temperature T_0

β = temperature coefficient of the refractive index

If, for example, the temperature field in a laser rod is a parabolic function of the radius, that is $T(r) = \varkappa - \delta r^2$, where $\varkappa$ and δ are determined by heat dissipation inside and by cooling on the surface of the laser rod, then the change of refractive index with radius will be given by

$$\Delta n (r) = \beta (\varkappa - \delta r^2 - T_0) \quad (4.82)$$

Depending on the sign of β, the derivative of this function will be either positive or negative, and the medium will act on laser light like a concave or a convex lens, respectively. Since the cavity length is limited by plane-parallel mirrors, the optical path length, P, is independent of radius. Since

$$P = P_m + P_a (n_a - 1) + P_{corr} (n_{corr} - 1)$$

where n_a, n_{corr}, P_a, and P_{corr} are the refractive indexes and lengths of the laser rod and corrective element, it is an easy matter to

show that the condition for $\Delta P = 0$ will be

$$P_a \Delta n_a (r) = - P_{corr} \Delta n_{corr} (r)$$

or, noting equation (4.82),

$$P_{corr} = - (\beta_a / \beta_{corr}) P_a$$

Experimental values of β for some materials are given in Table 4.1. For a Nd : YAG laser, the corrective material may be polystyrene. It should be noted that similar compensators may be employed in both laser oscillators and laser amplifiers. This method,

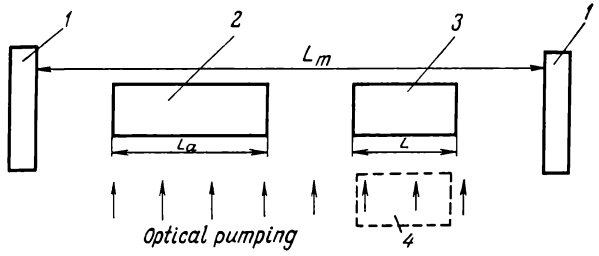

Fig. 4.18. Laser oscillator temperature-compensated for optical distortions in the laser rod

1—mirror; *2*—laser rod; *3*—corrective element; *4*—auxiliary light source to control temperature gradient in the corrective element

however, needs further development, and it is too early to make any final conclusions about its capabilities.

An efficient method of correcting laser beam distortions in the laser rod is proposed in [62]. By this method, light in the laser rod is caused to traverse a zig-zag path so that it passes through symmetrically arranged sections with a temperature gradient equal in magnitude but opposite in sign (Fig. 4.19). A promising approach is offered by a modification of this method in which laser light is caused to traverse a zig-zag path made up of face-pumped laser discs oriented at the Brewster angle to the laser beam [63 to 65]. If pumping is uniform across the diameter of the disc, the laser beam will be propagated at a small angle to the thermal gradient and, on passing through sections with temperature gradients of opposite sign, will undergo distor-

Table 4.1

Material	$\beta \times 10^5$, °C
Sapphire (7065 Å)	+12.6
Nd : YAG (1.06 μm)	+4.8
Polystyrene (0.76 μm)	−200
NaCl (60° C, 1.1 μm)	−3.64
NaF (0.546—3.5 μm)	−16

tions that mutually cancel out. As already noted in Sec. 2.6, zig-zag optical paths are employed in laser amplifiers intended to amplify light beams of a large cross-section.

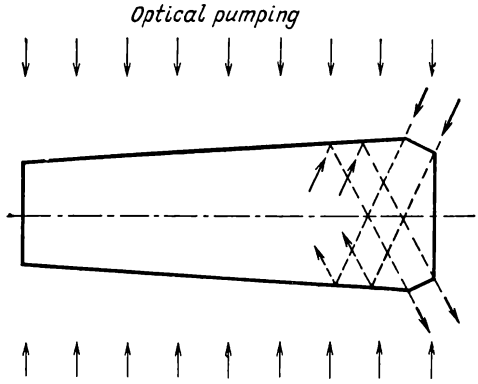

Fig. 4.19. Face-pumped flat laser rod in which laser light is propagated in a zig-zag path

The method of correcting thermal distortions in a tubular laser rod discussed in [66] involves the use of an optical compensator in the shape of a ring metallized on the internal and external surfaces. The metal deposits are heated by an r. f. oscillator so that

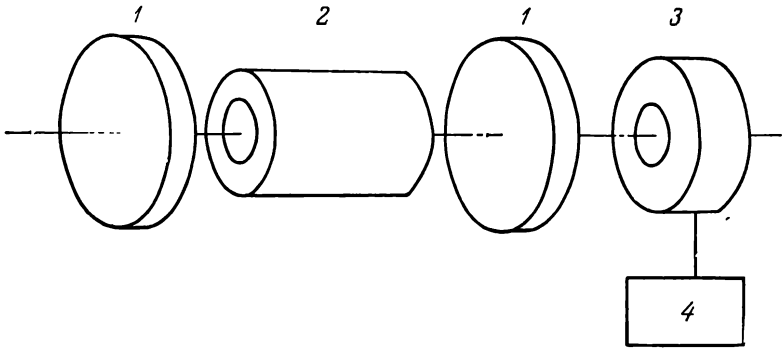

Fig. 4.20. Thermal lensing compensation in a laser using a tubular laser rod
1—reflecting mirror; *2*—laser rod; *3*—thermal-lensing compensator; *4*—r.f. oscillator

the optical distortions in the material will correct the wavefront distortions of laser light due to the thermal gradient in the laser rod (Fig. 4.20).

In a series chain of amplifiers, the overall correction of optical distortions caused by the nonuniform distribution of population inversion and temperature can be obtained by adjusting the concentration of active centres in the various stages.

Correction of laser light distortions caused by birefringence. In laser oscillators in which the optical cavity contains a polarizing element, which may be the case when Q-switching is done by an electro-optic shutter, the harmful aftereffects of induced birefringence can effectively be minimized through the use of optical systems capable of controlling simultaneously the two orthogonal components of polarized light. With these two-component systems, the characteristics of laser light are made independent of induced birefringence over a fairly wide range of pulse repetition frequency. Incidentally, this purpose may be served by the two-component systems described in Sec. 2.3.

A still greater promise is held out by two-component systems incorporating electro-optic reflectors. Fig. 4.21 shows a simple la-

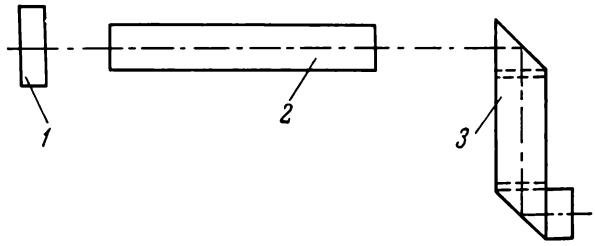

Fig. 4.21. Optical arrangement of a laser for control of light of arbitrary polarization

1—stack; *2*—laser rod; *3*—electro-optic reflector with reflecting faces oriented relative to the crystallographic axes so as to ensure simultaneous modulation of the two orthogonally polarized light components

ser optical system incorporating a transmitting electro-optic reflector which offers a means for simultaneously controlling two orthogonally polarized light components. With an electric field applied between the control electrodes, the two light components are not parallel with the cavity axis and fail to reach the 100%-reflecting mirror. When the electric field is removed, the two orthogonally polarized components are parallel with the cavity axis and reach the reflecting mirror, thereby maintaining the conditions for lasing action.

According to [67], birefringence can be corrected by including in the laser optical system a compensating element which has characteristics similar to those of the laser rod and in which birefringence can be induced so that it will be opposite in its action to the birefringence in the laser rod. This method has not yet been used in practice because of the difficulties associated with the development of a suitable compensating element. Therefore one can only guess about the advantages of the method, although it may prove more convenient for laser rods of a large cross-section than, say, two-component systems.

4.6. Temperature Stability of Laser Oscillators

In addition to optical distortions and the accompanying wavefront distortions and birefringence, the temperature gradient (Sec. 4.2) in laser materials may be accompanied by other temperature-induced processes which materially affect the various characteristics of laser light.

Effect of temperature on properties of laser materials. In the general case, a change in the temperature of the laser rod brings

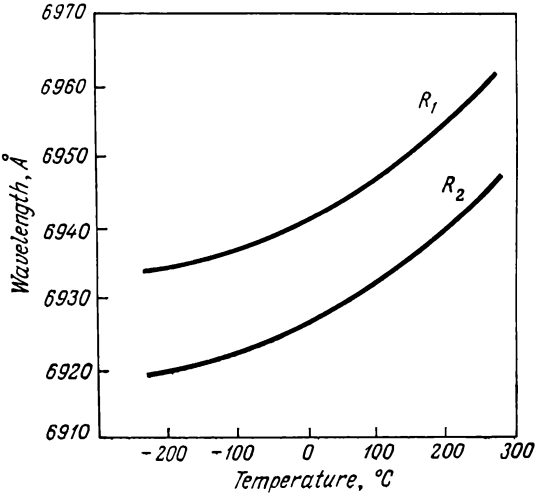

Fig. 4. 22. Wavelength of the fluorescence line, R_1 and R_2, of ruby as a function of temperature

about changes in its spectral characteristics, namely emission wavelength λ, emission spectrum width $\Delta\nu$, spontaneous transitions between the excited and ground states A_{ij}, quantum fluorescence efficiency η, and the population of energy levels. As a result, changes in temperature bring about changes in the gain of the laser material which for the maximum of the fluorescence line (assuming a three-level system and the Lorenz line) may be written as follows [68]:

$$\alpha_0 = \sigma_0 (N_2 g_2/g_1 - N_1) \tag{4.83}$$

$$\sigma_0(T) = \frac{\lambda_0^2(T)\, A_{21}(T)\, g_1}{4\pi^2 \eta^2(T)\, \Delta\nu(T)\, g_2} \tag{4.84}$$

where g_1 and g_2 are the statistical weights of the levels contributing to an induced transition.

For ruby light, the dependence of its wavelength on temperature in the range from —80° C to 20° C has the following form [68]:

$$\lambda(T) = 6943.25 + 0.068\,(T - 20) \qquad (4.85)$$

Plots relating the lifetime of an excited state and $\Delta\nu$ to temperature [68, 69] appear in Figs. 4.23 and 4.24. From the plot of the lifetime of an excited state as a function of temperature it is seen that the quantum fluorescence efficiency of ruby for a transition of the form $^2E \rightarrow {}^4A_2$ is likewise a function of temperature. For

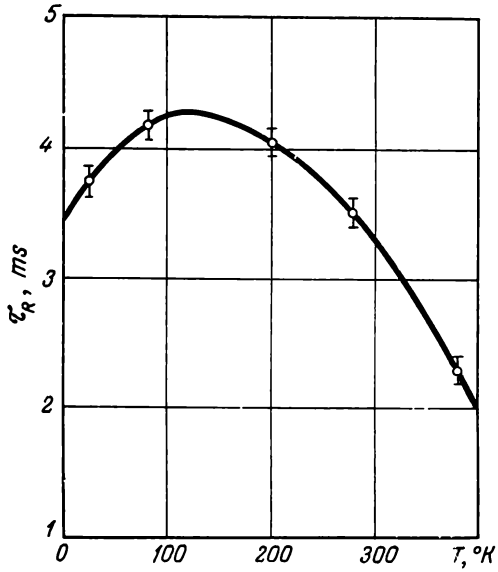

Fig. 4.23. Lifetime of a metastable state in ruby as a function of temperature

example, at room temperature $\eta = 65\%$ [70]. Using the above relation, it is an easy matter to compute the absorption cross-section for different temperatures (for example, at room temperature $\sigma_0 = 2.5 \times 10^{-20}$ cm^2). An increase in temperature entails an increase in the fluorescence line width (see Fig. 4.22), because of which gain decreases with increasing temperature.

The spectral characteristics of neodymium-doped glass and YAG are likewise dependent on temperature strongly. The absorption spectrum of neodymium in glass materially changes with changes in temperature [71] (Fig. 4.25). As temperature decreases, one notes not only a decrease in the band half-width, but also the disappearance of some bands (for example, the band with a maximum at 612 μm). In contrast, an increase in temperature builds up the intensity of these bands. While a transition from 77° K to 300° K

causes the absorption at the maxima of bands to be halved (apparently, mainly due to the band broadening), the further rise in temperature to 700° K brings about a decrease of as little as 10 to 12%. Decreasing temperature from 77° to 4.2° K produces no marked changes in the absorption spectrum, while the band narrowing appears to be negligible.

As is seen from Fig. 4.26, the lifetime of an excited state (for

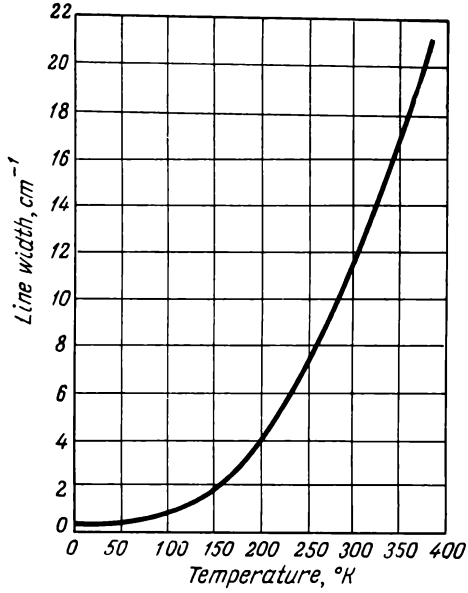

Fig. 4.24. Temperature dependence of the width of the R_1 line in ruby

a transition of the form ${}^4F_{3/2} \rightarrow {}^4I_{11/2}$) for Nd^{3+} ions in glass and YAG crystals in the range $300° K \leqslant T \leqslant 500° K$ depends on temperature but slightly [71, 72]. The effect of temperature on the relative fluorescence efficiency at a wavelength of 1.06 μm in the case of broadband excitation is negligible. For example, the rise in temperature from 300° K to 500° K brings down the efficiency by 10% for YAG : Nd crystals and by 15% for neodymium-doped glass [72]. The respective plots appear in Fig. 4.27. These data may be used to compute the dependence of the absorption (or amplification) cross-section on temperature for neodymium-doped glass and YAG crystals. However, the computed values may differ greatly from those found experimentally because of the complexity of the actual energy level structure of ions. Experimentally the dependence of the absorption coefficient at $\lambda = 1.06$ μm on temperature was investigated in [73] (the measurement technique is

also described in [74]). The investigators worked on the assumption that the absorption coefficient at a wavelength of 1.06 μm is directly proportional to the equilibrium population, N_2, of the $^4I_{11/2}$ level, while the absorption cross-section is independent of temperature (the population of the ground level in equation (4.83) is designated N_1). A plot of the absorption coefficient as a function of temperature appears in Fig. 4.28.

Phototropic (bleachable) media employed as shutters depend for their action on the fact that they are saturable absorbers. There-

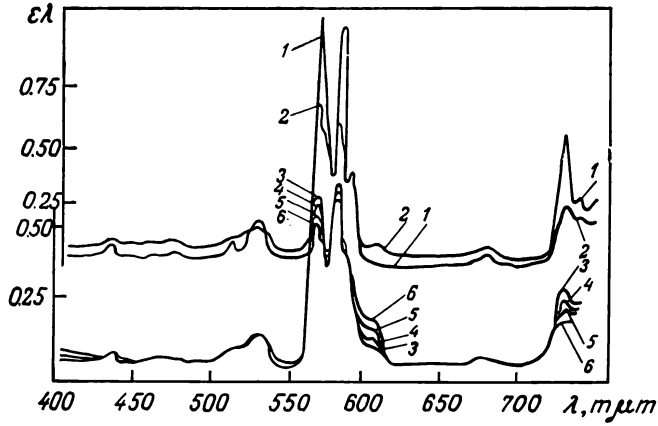

Fig. 4.25. Temperature dependence of the absorption spectrum of neodymium (°K)
1—77; *2*—300; *3*—400; *4*—500; *5*—600; *6*—700

fore, changes in temperature affect their properties for the same physical reasons as in amplifying laser materials. However, the laser wavelength changes by a markedly smaller amount than the half-width of the absorption line of phototropic media, while the temperature dependence of other physical factors usually have no appreciable effect on the absorption coefficient for laser light, provided the temperature varies by as little as a few tens of degrees.

In electro-optic shutters, a change in temperature brings about a change in the half-wave voltage (see Sec. 1.7) because of changes in the refractive index and electro-optic constants. As an example, Figs. 4.29 and 4.30 show plots of n_o, n_e and r_{63} as functions of temperature for KDP crystals [46]. Apart from the half-wave voltage, temperature changes may also affect the direction of reflected light in electro-optic reflectors (see Sec. 1.8). These changes in the half-wave voltage and the direction of reflected light cause an increase in the harmful losses in the laser cavity.

In nonlinear elements used for second harmonic generation (see Sec. 2.7), the phase-matching angle is likewise dependent on temperature because of the temperature dependence of refractive indexes.

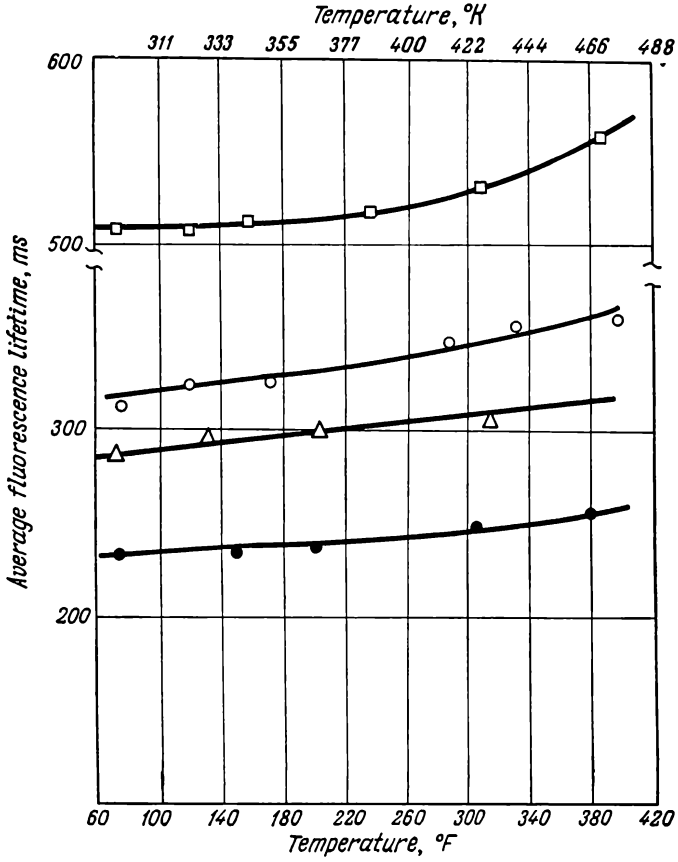

Fig. 4.26. Temperature dependence of the average lifetime of fluorescence (at $\lambda = 1.05$ μm) for YAG : Nd (•) and neodymium-doped glasses: 0835, ND-11, ED-2 (□, ○, △)

In any case, the magnitude of temperature instability may be found by specifying limits of changes for the characteristics of laser light.

Thermal stability of laser oscillators. We have seen that variations in temperature entail proportionate variations in the intensity spectral make-up, mode structure, and pulse shape of laser light. Therefore, if laser light is to have fixed or reproducible characte-

ristics, it is important to stabilize the temperature of laser components. This can be done either by causing the temperature field to be completely restored by the beginning of each firing cycle in pulsed operation, or by securing a fixed temperature field in continuous operation.

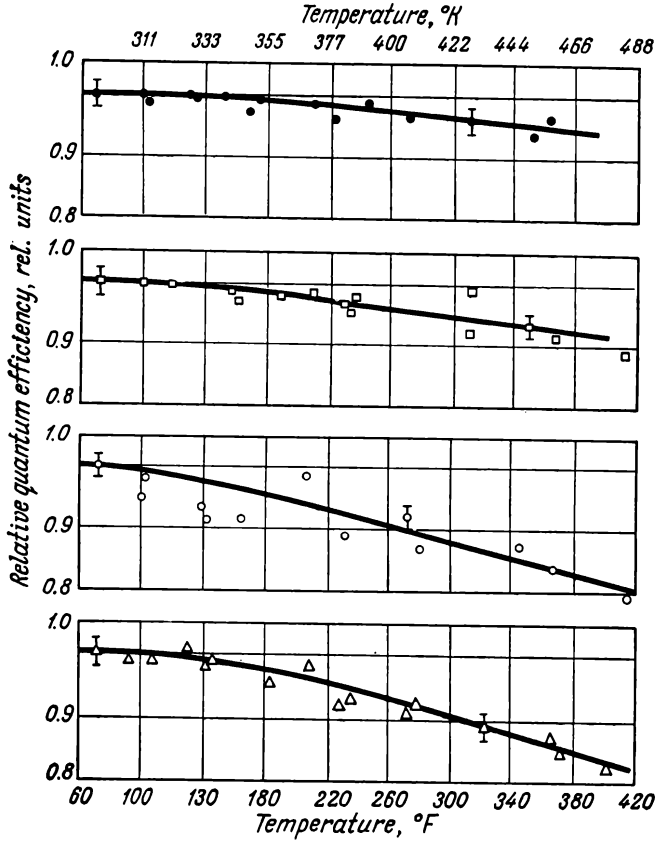

Fig. 4.27. Temperature dependence of the quantum efficiency of fluorescence (at $\lambda = 1.06$ μm) for YAG : Nd (•) and neodymium glasses: 0835, ND-11, ED-2 (□, △, ○)

Depending on the manner in which heat is dissipated, the temperature stabilization of laser operation may seek different objectives and, as a consequence, different methods may be employed to achieve them. In cases where heat is dissipated in pulses with a high period-to-duration ratio, the thermal stabilization of a laser consists in that the temperature of the optical element heated by laser light is restored in the shortest possible time. This interval,

however, need not be shorter than the time to the onset of laser emission (Sec. 3.2). The duration of the cooling period according to the cooling conditions and the properties of the element being cooled and the cooling method can be estimated from equations (4.12) and (4.13).

With heat dissipated periodically, the same temperature should be maintained at the beginning of each firing cycle. Practically,

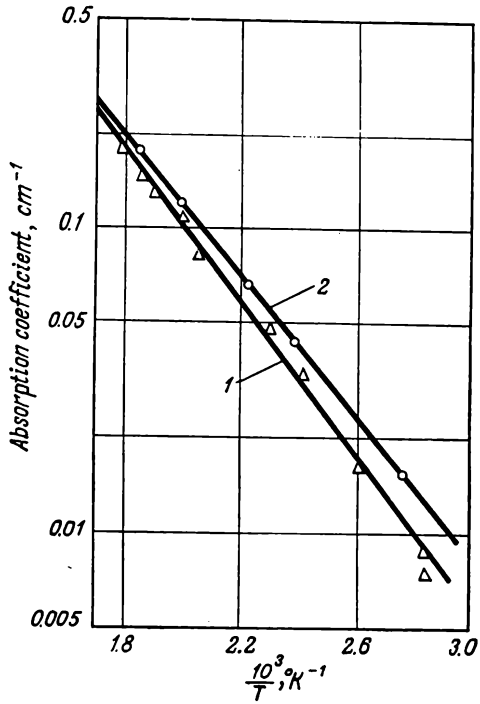

Fig. 4.28. Temperature dependence of the absorption coefficient α for neodymium in silicate glass (*1*) and borate glass (*2*)

the optical element should attain a quasi-stationary state in which the temperature field is fully restored at the instants spaced one period of heat dissipation apart. The time required for the element to attain a steady-state condition and the limit of temperature difference between the centre and surface of the optical element for a specified heat-dissipation period, power output, and boundary conditions may be found from (4.21) and (4.23). If the power dissipation and cooling conditions are such that the time to a steady state is long, the laser may be allowed to operate for a time in-

terval during which the laser-beam distortions remain within safe limits.

With continuous heat dissipation, thermal stabilization consists in that the optical element is allowed a sufficient time to attain a steady-state condition and is maintained at a safe temperature after that. If the cooling conditions and power dissipation are known, the necessary computations can be carried out, using the techniques developed in Sec. 4.1.

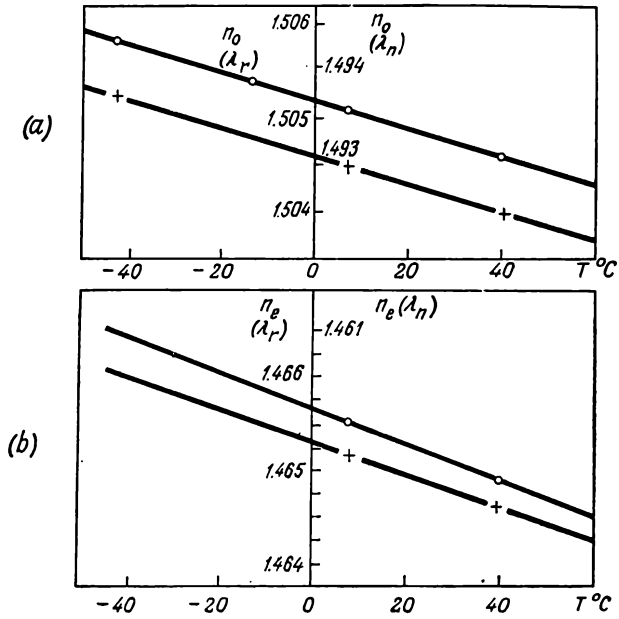

Fig. 4.29. Temperature dependence of (*a*) n_o and (*b*) n_e for KDP crystal at $\lambda = 0{,}69$ μm (λ_r) and $\lambda = 1.06$ μm (λ_n)

In all cases, as is explained in Sec. 4.1, the temperature gradient and temperature transients in a laser component are strongly dependent on the boundary conditions which are in turn determined by the method and rate of cooling. In each specific case, the choice of a cooling method and its efficiency are decided by the functions performed by a given laser component, its design, and by the physico-chemical properties of the material from which it is fabricated. Generally, laser components may be cooled by either the contact or the convective method.

Contact cooling. With contact cooling, heat exchange takes place between a laser component and a heat-sink which is in thermal

contact with that component. In this case, the condition for heat exchange at the interface is described by equation (4.1). The computation of the temperature gradient involves knowledge of the thermal conductivity λ, specific heat at constant pressure C_p, and

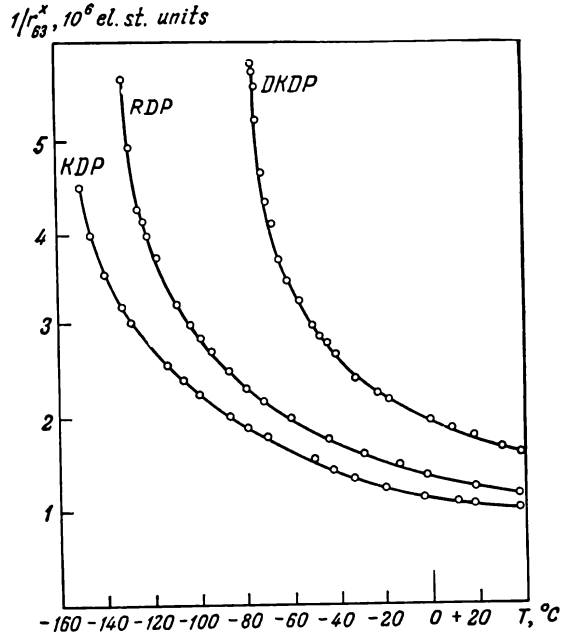

Fig. 4.30. Reciprocal of the electro-optic coefficient, r^*_{63}, as a function of temperature at a wavelength of 0.54 μm

the density of the material γ. Most often, heat-sinks are made from copper, optical glass, quartz, or sealants. The specific heat and density of many optical materials used in laser engineering may

Table 4.2

Nos.	Material	Temperature, °K	Density, g/cm³	Specific heat, J/g·deg
1	Ruby	300	3.99	0.779
2	Glass, type КГСС-7	300	2.95	0.795
3	Garnet, $Y_3Al_5O_{15}$	300	4.2	0.585
4	Copper	273	8.8	0.381
5	Quartz	273	2.5-2.8	0.836

be found in reference handbooks, for example, in [75]. The density and specific heat of some materials are listed in Table 4.2. The thermal conductivity of ruby and copper as a function of temperature is shown in the plot of Fig. 4.31. Already at the temperature of liquid nitrogen, the thermal conductivity of ruby exceeds that of copper. In the temperature range from 20° to 50° K, the thermal conductivity of ruby attains its maximum value and exceeds that of copper by a wide margin.

It should be noted that although ruby is an anisotropic

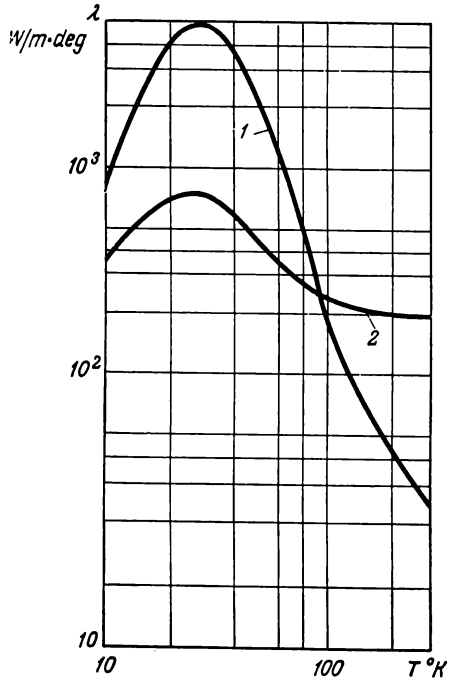

Fig. 4.31. Thermal conductivity of (*1*) ruby and (*2*) copper as a function of temperature

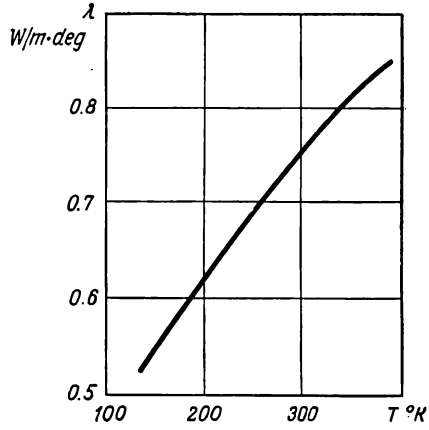

Fig. 4.32. Thermal conductivity of type КГСС glasses as a function of temperature

material, the ratio of its thermal conductivity parallel with and perpendicular to the optical axis is about 1.1 : 1. The thermal conductivity of type КГСС glasses as a function of temperature is shown in Fig. 4.32. The thermal conductivity and specific heat of glass optical elements are markedly dependent on the chemical composition of glasses and are determined by the percentage content of the various oxides [76]. The specific heat of type КГСС glass at 20° K is 0.686 J/g·deg, while for barite crown it is 0.79 J/g·deg. The specific heat of glass increases linearly with increasing temperature.

For YAG crystals, the thermal conductivity is 12.56 W/m·deg. A plot of thermal conductivity as a function of temperature for

crystalline quartz is shown in Fig. 4.33. The thermal conductivity of different sealants ranges from 1 to 2 W/m·deg. With contact cooling, a very important factor is the coefficient of linear expansion of the materials that come in direct contact. The difference in the coefficients of linear expansion may result in the break of contact with changes in temperature at the interface between the cooled and cooling media.

The heat-sink may be cooled either by means of a thermo-pile [77] or by convective cooling, using a liquid or a gas. In sketch form,

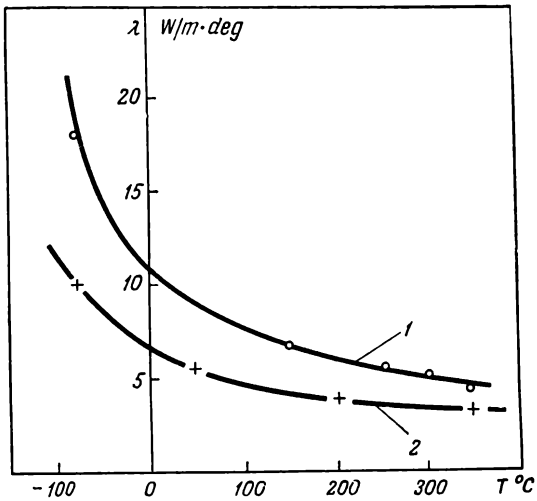

Fig. 4.33. Thermal conductivity of crystalline quartz as a function of temperature
1 — at right angles to the *Z*-axis; *2* — parallel with the *Z*-axis

the arrangement of a contact cooling system for a laser rod is shown in Fig. 4.34. Heat exchange takes place through a small area on the side surface so as not to reduce the efficiency of optical pumping. The heat-sink is cooled by a thermo-pile. This method for cooling the heat-sink may be used in cases where it is desirable to keep the size of the system to a minimum. Figure 4.35 shows a contact cooling system for an electro-optic element. The electro-optic element is set up in a viscous sealant which acts as a heat-sink and is enclosed in a metal jacket cooled by, say, tap water. The ends of the electro-optic element are protected by Brewster glass windows. Although its efficiency is low, this arrangement does not impair the optical and electrical characteristics of the electro-optic element. Besides, it is well adapted to hygroscopic or fragile materials such as KDP crystals.

There may also be other contact-cooling arrangements, for example, those using transparent heat-sinks fabricated from quartz or sapphire. A major disadvantage of contact cooling in comparison with the convective method is the low efficiency of heat abstraction. This is the reason why it is employed on a limited scale in laser engineering.

Convective cooling. With convective cooling, the transport of heat is accomplished through the motion of a suitable convective

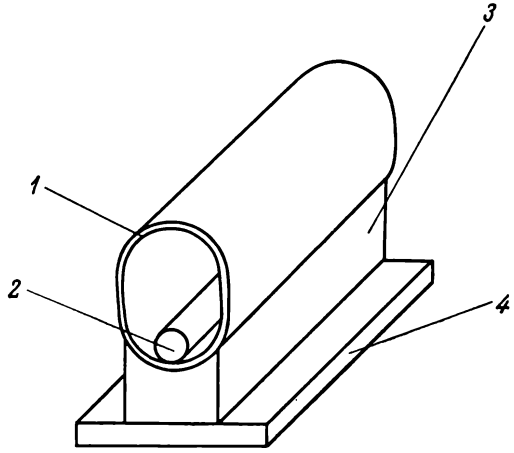

Fig. 4.34. Cooling of the laser rod by the contact method
1—pump unit; *2*—laser rod; *3*—copper heat-sink; *4*—thermo-pile

(cooling) agent which is locally heated upon contact with the element being cooled. The cooling agent may be passed either directly through the flash tube chamber (see Sec. 1.1) or through a separate transparent jacket surrounding the laser rod and along its side surface as shown in Fig. 4.36. The latter arrangement is employed in cases where a high efficiency of heat exchange is essential. In a simple arrangement, the cooling agent may be tap water. Unfortunately, tap water may often impair the optical characteristics of the system because of the impurities lodging on the laser rod or the transparent jacket. This is why, convective cooling systems are usually of the closed-circuit type comprising a heat exchanger, a pump, control valves and alarm or warning devices.

With convective heating, the materials that go into the elements of the cooling circuit must satisfy especially stringent requirements. Among other things, they should not be attacked by, or affect the properties of, the cooling agent, contaminate it with impurities capable of reducing its transparency or lodging on the laser rod or transparent jacket. From the closed circuit, heat is abstracted in the heat exchanger through either natural heat ex-

change with the surroundings, or with a running water line, or with a separate cooling unit having an independent closed cooling circuit, such as a Freon refrigerator. In a simple case, the heat

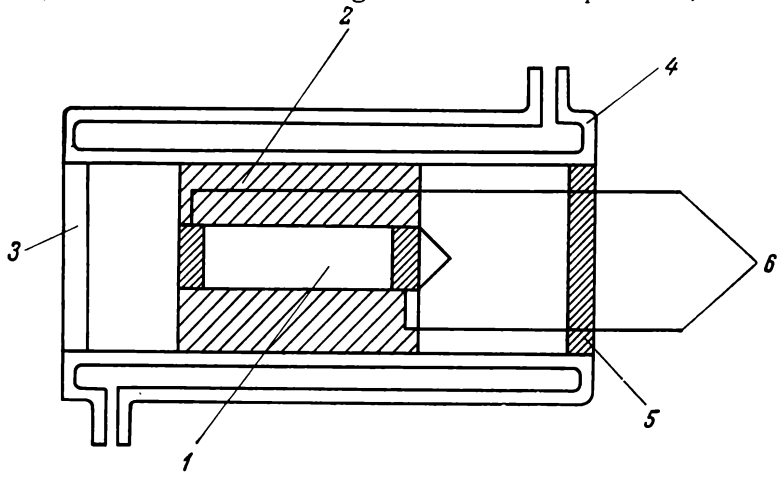

Fig. 4.35. Cooling of an electro-optic shutter by the contact method
1—electro-optic shutter; *2*—H. V. compound; *3*—cover glass; *4*—water-cooled metal housing; *5*—insulator; *6*—leads

exchanger is a stainless-steel coiled tube enclosed in a tank fitted with spiral ducts for tap water flowing through the tank. The coiled tube is connected in the closed cooling circuit of the laser ele-

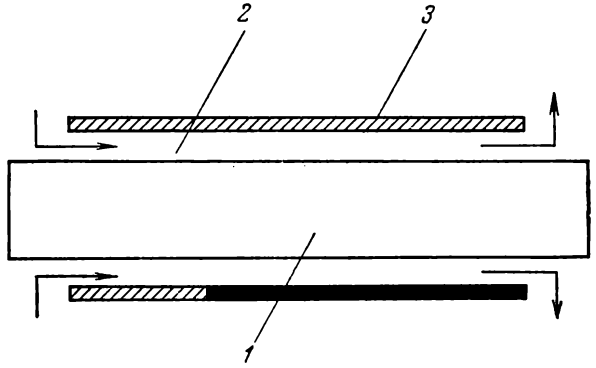

Fig. 4.36. Cooling of the laser rod by the convective method
1—laser rod; *2*—cooling medium; *3*—transparent jacket

ment. Entering the tank, tap water comes in contact with the surface of the coiled tube and cools the liquid inside it to the requisite temperature. The pump (a blower or a compressor, as the case may be) supplies the cooling agent at the requisite flow rate and

maintains an appropriate pressure differential to make up for the hydraulic resistances in the various parts of the circuit and local resistances due to eddies that form at places where the cross-section of the circuit or the direction of flow changes suddenly [78]. The flow rate of the cooling agent determines its velocity near the heat-exchanging surface of the laser element, while the velocity and physical properties of the cooling agent determine the heat

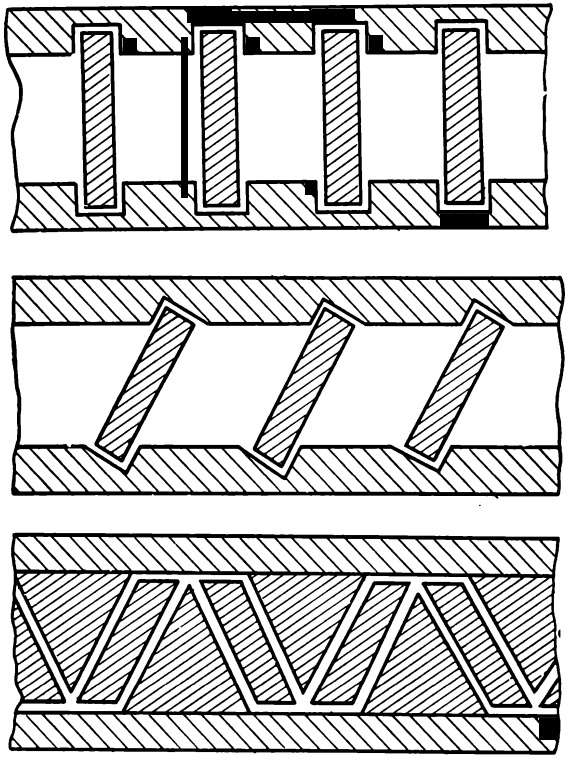

Fig. 4.37. Cooling of laser discs by the convective method (the spaces between discs are filled with a liquid with a refractive index about the same as that of the laser material)

transfer coefficient, α. Most often, the cooling agent is a liquid because liquids have a much higher coefficient of heat transfer than gases. With gas cooling, the heat transfer coefficient ranges between 100 and 150 W/m^2·deg, while with liquid cooling it may be from 2×10^3 to 7×10^3 W/m^2·deg, which is by one or two orders of magnitude greater. This is why preference is usually given to liquid cooling. Besides, the composition of a liquid cooling agent may be chosen such that it will additionally act as a

filter for the pump light, suppressing that part which only causes the harmful heating of the laser rod. For example, in [40], in order to filter the short-wave part out of the pump spectrum, a YAG laser was cooled by an aqueous solution of K_2CrO_4 (with a concentration of 0.2%). In cases where a large laser rod should be cooled at a high rate, either slots may be provided in the rod for the cooling liquid, or the rod may be assembled of discs surrounded by a cooling liquid as shown in Fig. 4.37. In order to minimize reflections from the ends of the laser rod, use is made of liquids with a refractive index equal to that of the laser material. For example, [79] lists several combinations of different cooling liquids giving the requisite refractive index (carbon sulphide-carbon tetrachloride, water-barium bromomercurate, water-potassium bromomercurate, chloroform-bromoform, bromoform-carbon tetrachloride) for a laser rod assembled of neodymium-glass discs.

Apart from the flow rate of the cooling agent, the heat transfer coefficient is affected by its temperature and the characteristics of the cooling circuit. In [80], the heat transfer coefficient is presented as a function of all the above listed factors on the basis of a great number of experimental data.

According to [78, 80], heat transfer in the case of forced convection may be found as follows. With laminar flow, that is, at $Re \leqslant 2200$, the heat exchange coefficient may be found from a criterion of the form

$$Nu_{liquid} = 0.17 Re_{liquid}^{1/3} Gr_{liquid}^{0.1} Pr_{liquid}^{0.43} [Pr_{liquid}/Pr_w]^{0.25} \varepsilon_l \varepsilon_r \quad (4.86)$$

where

$$Nu_{liquid} = \alpha d/\lambda_{liquid}$$
$$Gr = \beta g d^3 \Delta T/\nu^2$$
$$Pr_{liquid} = \nu_{liquid}/a_{liquid}$$
$$Pr_w = \nu_w/a_w$$
$$Re = vd/\nu$$

λ_{liquid}, a_{liquid}, λ_w, a_w = coefficients of thermal conductivity and temperature conductivity at the temperature of the liquid and duct wall

β = coefficient of volume expansion of the liquid

ν_{liquid} = coefficient of kinetic friction of the liquid

d = bore of the cooling circuit

v = velocity of the cooling agent

Since all of these parameters are temperature-dependent, the average temperature, $T_{liquid} = 1/2(T_{in} + T_{out})$ where T_{in} and T_{out} are the inlet and outlet temperatures of the cooling agent, should be chosen as the determining one [80]. The correction factor, ε_r, takes care of the increase in heat transfer in bent ducts

$$\varepsilon_r = 1 + 1.8d/R$$

where R is the radius of bending of the duct.

Variations in the circuit bore are taken care of by the numerical coefficient ε_l tabulated in [80].

With turbulent flow, that is at $Re > 10^4$, the following design equation is recommended in [80]:

$$Nu_{liquid} = 0.021 Re^{0.8}_{liquid} Pr^{0.43}_{liquid} (Pr_{liquid}/Pr_w) \varepsilon_l \varepsilon_r \qquad (4.87)$$

If the cooling agent is a gas, then equations (4.86) and (4.87) respectively reduce to

$$Nu = 0.13 Re^{1/3} Gr^{0.1} \text{ (for air)}$$

$$Nu = 0.018 Re^{0.8} (\varepsilon_l \cdot \varepsilon_r \sim 1)$$

In [81], a criterion is given of the form $Nu = f(Re)$ for a transition case, that is for $2200 \leqslant Re \leqslant 10^4$. Specific recommendations for the use of equations (4.86) and (4.87) will be found in [78, 80, 81].

It should be noted that even when the reverse problem of thermal conductivity is solved and one can determine from it the value of the heat transfer coefficient, α, ensuring the requisite thermal conditions, it cannot be secured in precise agreement with (4.86) and (4.87). This is because the elaborate geometry of the cooling circuit and sudden changes in its cross-section prevent ε_l and ε_r from being found accurately. Besides, the conditions of heat exchange do not remain fixed during operation of a laser since the reflector is gradually heated. It may so happen that there may be a one-way heat exchange when a laser just starts operating, and a two-way heat exchange some time later, with the result that the value of α is changed too. This is why one is forced to use an overrated (or a maximum safe) velocity for the cooling agent in the circuit, the more so that $\alpha > \alpha_{design}$ will not affect operation of the optical element adversely.

REFERENCES

Chapter 1

1. Bykhovskaya L. N., Gurevich I. M., Konova S. V., Neyman I. S., Charnaya F. A. Journal of Applied Spectroscopy (Zhurnal prikladnoy spektroskopii), 1967, vol. 7, No. 1, p. 12.
2. Mak A. A., Ananyev Yu. A., Yermakov B. A., UFN, 1967, vol. 92, issue 3, p. 371.
3. Nelson D. F., Boyle W. S. Appl. Optics, 1962, vol. 1, No. 2, p. 181.
4. Keck P. H., Redmann J. J., White C. E., Bowen D. E., Appl. Optics, 1963, vol. 2, No. 8, p. 833.
5. Kamirio K., Kano T., Matsuzawa H. Trans. of IEEE, 1967, vol. 55, No. 9, p. 101.
6. Kimirio K., Kano T., Matsuzawa H. Japan J. Appl. Phys., 1966, vol. 5, No. 12, p. 1217.
   Hamal Karel, Czechoslovac Journal of Phys. 1968, vol. 18, No. 3, p. 419.
7. Fan G. F., Smoyer G. B., Nunnez J. Appl. Optics, 1964, vol. 3, No. 11, p. 1277.
8. Krylov K. I. *et al.* "Izvestiya vuzov", Instrumentation, 1967, No. 4, p. 9.
9. Ter-Pogosyan A. S., Lantsman A. D. "Izvestiya vuzov", Instrumentation, 1967, vol. 10, No. 12, p. 76.
10. Mitrofanov A. S., Ter-Pogosyan A. S. LITMO Press, 1968, issue 65, pp. 62-65.
11. Kalinin Yu. A., Mak A. A. "Optico-Mechanical Industry" (Optiko-mekhanicheskaya promyshlennost), 1970, No. 2, p. 61.
12. Tsikunov V. N. "Optics and Spectroscopy" (Optika i spektroskopiya), 1964, vol. 16, No. 4, p. 684.
13. Ananyev Yu. A., Buzhinsky I. M., Vanyukov M. P., Dauengauer E. F., Shorokhov O. A. "Optico-Mechanical Industry" (Optiko-mekhanicheskaya promyshlennost), 1968, No. 9, p. 26.
14. Kirsanov V. P., Troshkin S. V. "Light Engineering" (Svetotekhnika), 1967, No. 1, p. 12.
15. Kalinin Yu. A. "Optico-Mechanical Industry" (Optiko-mekhanicheskaya promyshlennost), 1970, No. 1, p. 3.
16. Church C. H., Lesnick J. P. J. Quantum Electronics, 1966, vol. 2, No. 1, p. 16.
17. Khazov L. D., Shestov A. N., Tikhomirova G. P. J. Eng. Phys. (ZhTF), 1968, vol. 38, No. 8, p. 1362.
18. Dianov Ye. M., Prokhorov A. M. Reports of the USSR Academy of Sciences (DAN SSSR), 1970, vol. 192, No. 3, p. 531.
19. Kalinin Yu. A., Mak A. A., Stepanov A. I. J. Eng. Phys. (ZhTF), 1968, vol. 38, No. 8, p. 1108.
20. Swain J. E., Kidder R. E., Pettiriece K., Rainer F., Baird E. D., Loth B. J. of Appl. Phys., 1969, vol. 40, p. 3973.
21. US Patent No. 3, 423, 693.
22. Emmet J. L., Schawlow A. L. J. of Appl. Phys., 1964, vol. 35, No. 9, p. 2601.
23. Lyubavsky Yu. V. Inventor's Certificate No. 251696. Bulletin of Inventions (Byulleten izobreteniy), 1969, No. 28, p. 46.

24. US Patent, No. 3, 521, 178.
25. Methods for the Calculation of Laser Oscillators, vol. 11, ed. by Acad. B. I. Stepanov, Byelorussian Academy of Sciences. "Nauka i tekhnika" Press, 1968.
26. Ananyev Yu. A. "Instrumentation and Techniques of Experiments" (Pribory i tekhnika experimenta), 1964, No. 2, p. 135.
27. Bowness C. Appl. Optics, 1965, vol. 4, No. 1, p. 103.
28. Khazov L. D. "Optiko-Mechanical Industry" (Optiko-mekhanicheskaya promyshlennost), 1967, No. 6, p. 7.
29. Devlin G. E., McKonna J., May L. D., Schawlow A. L. Appl. Opt., 1962, vol. 1, No. 1, p. 11.
30. Tomiyasu K. Appl. Opt., 1967, vol. 6, No. 9, p. 1578.
31. Letokhov V. S., Suchkov A. F. J. Exp. & Eng. Phys. (ZhETF), 1966, vol. 50, No. 4, p. 1148.
32. Ambartsumyan R. V., Basov N. G., Zuev V. S., Kryukov P. G., Letokhov V. S., Shatberashvili O. B. J. Exp. & Eng. Phys. (ZhETF), 1966, vol. 51, No. 2, p. 406.
33. Tomiyasu K. Proc. IRE, 1962, vol. 50, p. 2488.
34. Ananyev Yu. A., Korolev Ye. A. "Optics and Spectroscopy" (Optika i spektroskopiya), 1964, vol. 16, p. 702.
35. Grevtsov N. V., Kutsy A. A., Morozov Yu. F. *et al.* In the collected volume "Exchange of Experience in the Electronics Industry" (Obmen opytom v elektronnoi promyshlennosti), 1968, issue No. 8, p. 23.
36. Gardashian V. M., Libin Yu. V., Lebedinskaya Z. T. *et al.* In the collected volume "Quantum Electronics" (Kvantovaya elektronika), ed. by Acad. N. G. Basov, 1971, No. 3, p. 113.
37. Kaminsky A. A., Osiko V. V., "Inorganic Materials" (Neorganicheskie materialy), 1970, vol. VI, No. 4, p. 29; 1967, vol. III, No. 3, p. 417.
38. Grum-Grzhimailo S. V., Utkina Ye. I. Proceedings of the Crystallography Institute, USSR Academy of Sciences (Trudy instituta kristallografii AN SSSR), 1953, issue 8, p. 99.
39. Ducker J. W., Kellington C. M., Katzmann M., Atwood J. G. Appl. Optics, 1965, vol. 4, p. 109.
40. Akulenok Ye. M., Bagdasarov Kh. S., Papkov V. S., Khaimov-Malkov V. Ya. "Crystallography" (Kristallografiya), 1967, vol. 12, No. 2, p. 286.
41. Nishida K. Japan J. Appl. Phys., 1966, vol. 5, p. 727.
42. Korolev B. A., Bondarchuk V. A., Tikhonova N. P. "Optico-Mechanical Industry" (Optiko-mekhanicheskaya promyshlennost), 1967, No. 3, p. 9.
43. Danileiko Yu. K., Khaimov-Malkov V. Ya., Manenkov A. A., Prokhorov A. M. FTT, 1968, vol. 10, No. 9, p. 2738.
44. Danileiko Yu. K., Khaimov-Malkov V. Ya., Prokhorov A. M. IEEE J. Quant. Electronics, 1969, vol. 5, No. 2, p. 87.
45. Jeppesen M. A. J. Opt. Soc. Amer., 1958, vol. 48, p. 629.
46. Collected volume "Methods and Instruments for the Quality Control of Ruby Crystals" (Metody i pribory dlya kontrolya kachestva kristallov rubina), ed. by S. U. Grum-Grzhimailo and M. V. Klassen-Neklyudov. Nauka Publishers, 1968.
47. Sventsitskaya N. A., Khazov L. D. Journal of Applied Spectroscopy (Zhurnal prikladnoy spektroskopii), 1966, vol. 4, No. 4, p. 345.
48. Rom-Krichevskaya I. A., Ratner A. M., Meshcheryakov A. V. "Optics and Spectroscopy" (Optika i spektroskopiya), 1965, vol. 19, No. 2, p. 264.
49. Pilipovich V. A., Morgun Yu. F. Journal of Applied Spectroscopy (Zhurnal prikladnoy spektroskopii), 1967, vol. 7, No. 5, p. 760.
50. Boiko B. B., Andreyev V. A., Matyushkov V. Ye. Journal of Applied Spectroscopy (Zhurnal prikladnoy spektroskopii), 1969, vol. 10, No. 5, p. 744.
51. Danileiko Yu. K., Khaimov-Malkov V. Ya., Manenkov A. A., Prokhorov A. M. J. Exp. & Eng. Phys. (ZhETF), 1970, vol. 58, No. 1, p. 33.

52. Fersman I. A., Khazov L. D., J. Eng. Phys. (ZhTF), 1968, vol. 40, No. 5, p. 1081.
53. Khazov L. D., Shestov A. N., Tikhomirov G. Ya. J. Exp. & Eng. Phys. (ZhETF), 1968, vol. 38, No. 8, p. 1362.
54. Sviridenkov E. A. FTT, 1967, vol. 9, No. 8, p. 2442.
55. Snitzer E. Appl. Optics, 1966, vol. 5, p. 1487.
56. Kerstes I., Kononkov Ye. A., Kryukov P. G. *et al.* J. Exp. & Eng. Phys. (ZhETF), 1970, vol. 59, No. 4, p. 1115.
57. Lifshits B. L., Tsikunov V. N. Reports of the USSR Academy of Sciences (DAN SSSR), 1965, vol. 163, p. 870.
58. Senatsky Yu. V. "Development and Investigation of a Neodymium-Glass High-Power Laser for High-Temperature Plasma Generation" (Sozdanie i issledovanie moshchnogo lazera na neodimovom stekle dlya vysokotemperaturnogo nagreva plazmy). Resume of a dissertation. Institute of Physics, USSR Academy of Sciences, 1970.
59. Buzhinsky I. M., Mamonov S. K. Journal of Applied Spectroscopy (Zhurnal prikladnoy spektroskopii), 1968, vol. 8, No. 5, p. 731.
60. Marshak I. S. Pulsed Light Sources. Gosenergoizdat, 1963.
61. Volynkin V. M., Mak A. A., Mikhailov Yu. N. *et al.* "Optico-Mechanical Industry" (Optiko-mekhanicheskaya promyshlennost), 1968, No. 3, p. 65. Volynkin V. M., Mikhailov Yu. N., Pogodayev A. K. in the collected volume "Quantum Electronics" (Kvantovaya elektronika) ed. by N. G. Basov, 1971, No. 3, p. 117.
62. Buzhinsky I. M., Yemelyanova N. I., Koryagina Ye. I. Journal of Applied Spectroscopy (Zhurnal prikladnoy spektroskopii), 1970, vol. 12, No. 6, p. 1007.
63. Martinelly I. J. Appl. Phys. 1966, vol. 37, p. 1939.
64. Fersman I. A., Khazov L. D. in the collected volume "Quantum Electronics" (Kvantovaya elektronika), ed. by N. G. Basov, 1971, No. 2, p. 31.
65. Avizonis P. V., Farrington T. Appl. Phys. Lett., 1965, vol. 7, p. 205.
66. Basov N. G., Kryukov P. G., Senatsky Yu. V., Chekalin S. V. J. Exp. & Eng. Phys. (ZhETF), 1969, vol. 57, No. 4, p. 1175.
67. Basov N. G., Zuev V. S., Kryukov P. G. *et al.* J. Exp. & Eng. Phys. (ZhETF), 1968, vol. 54, No. 3, p. 767.
68. Shatilov A. V., Zhulai V. Ya., Smirnov Ye. M. "Optico-Mechanical Industry" (Optiko-mekhanicheskaya promyshlennost), 1969, No. 5, p. 22.
69. Zverev G. M., Maldutis E. K., Pashkov V. N. ZhETF Letters, 1969, vol. 9, p. 108. ZhETF Letters, 1970, vol. 11, p. 177.
70. Geusic J. E., Levinstein H. J., Singh S., Smith R. G., van Uitert L. G. Appl. Phys. Letters, 1968, vol. 12, No. 9, p. 306.
71. Woodbury E. J. IEEE J. Quantum Electronics, 1967, vol. 3, No. 11, p. 509.
72. Electronics, 1969, vol. 42, No. 9, p. 133.
73. Mikaelyan A. L., Ter-Mikaelyan M. L., Turkov Yu. G. Solid-State Lasers (Opticheskie generatory na tverdom tele). "Sovetskoe radio" Publishers, 1967.
74. Electronics, 1969, vol. 42, No. 9, p. 139.
75. Brissot J. J., Raynaud H. J. Phys., 1964, vol. 25, No. 11, p. 199.
76. Zubov V. A. Instrumentation and Techniques of Experiments (Pribory i tekhnika experimenta), 1967, No. 3, p. 205.
77. Buzhinsky I. M., Khomyakova F. T., Danilenko O. P. Journal of Applied Spectroscopy (Zhurnal prikladnoy spektroskopii), 1962, vol. 6, No. 1, p. 120.
78. Furman Sh. A., Fomenko P. N., Skorodumov V. N., Kaznelson L. B. "Optico-Mechanical Industry" (Optiko-mekhanicheskaya promyshlennost), 1970, No. 3, p. 36.
79. Hefft K., Kern R., Nöldeke G., Steudel. Appl. Phys., 1963, vol. 175, No. 4, p. 391.

80. Andryushchenko V. V., Lisitsa M. P. "Quantum Electronics" (Kvantovaya elektronika), issue 2. "Naukova Dumka" Press, Kiev, 1967, pp. 333-355.
81. Lifshits B. L., Nazarov V. P., Sidorenko L. K., Tsikunov V. N. ZhETF Letters, 1965, vol. 1, p. 23.
82. Kuznetsov A. Ya., Poplavsky A. A., Bonch-Bruevich A. M. *et al.* ZhETF, 1970, vol. 40, No. 1, p. 170.
83. Kramarenko N. L., Naboikin Yu. V., Polunov Yu. A. "Quantum Electronics" (Kvantovaya elektronika), issue 3. "Naukova Dumka" Press, Kiev, 1969.
84. Ratner A. M., Soloviev V. S., Tiunova T. I. "Quantum Electronics" (Kvantovaya elektronika), issue 3. "Naukova Dumka" Press, Kiev, 1969.
85. Born N., Wolf E. Principles of Optics, Pergamon Press, London, 1965.
86. Mahlein H. F., Schollmeier G. Appl. Optics, 1969, vol. 8, No. 6, p. 1197.
87. Nikonova Ye. I., Pavlovskaya Ye. N., Startsev G. P. "Optics and Spectroscopy" (Optika i spektroskopiya), 1967, vol. 22, No. 6, p. 984.
88. Mak A. A., Malinin B. G., Stepanov A. I., Fromzel V. A., Perlov D. I. "Optico-Mechanical Industry" (Optiko-mekhanicheskaya promyshlennost), 1970, No. 8, p. 7.
89. Morozova N. G., Startsev G. P., Travina V. G., Travin V. G. "Optico-Mechanical Industry" (Optiko-mekhanicheskaya promyshlennost), 1969, No. 10, p. 38.
90. Meshcheryakov A. V. Spectroscopy. Methods and Applications (Spektroskopiya. Metody i prilozheniya). Proceedings of the 4th Siberian Conference on Spectroscopy, 1965. "Nauka" Publishers, 1969, pp. 336-337.
91. McGeoch M. Opto-Electronics, 1970, vol. 2, p. 85.
92. Farcas G. Optics and Laser Technology, 1970, vol. 2, No. 4, p. 204.
93. Prokhorov A. M. ZhETF, 1958, vol. 34, p. 1658.
Schawlow A. L., Tawnes C. H., Phys. Rev., 1958, vol. 112, p. 1940.
Dicke R. H. US Patent 2, 851, 652, Sept. 9, 1958.
94. "Lasers". Ed. by M. Ye. Zhabotinsky and T. A. Shmaonov, Foreign Literature Publishing House, 1963, p. 325 (Fox L. G., Li T. Bell Syst. Techn. J., 1961, vol. 40, No. 2, p. 453-488).
95. Vainstein L. A. Open Resonators and Waveguides (Otkrytye rezonatory i volnovody), "Sovetskoe Radio" Publishers, 1966.
96. Birnbaum J. Lasers (Russian translation by "Sovetskoe radio" Publishers, 1967).
97. Ratner A. M. Spectral, Spatial and Time Characteristics of Lasers (Spektralnye, prostranstvennye and vremennye kharakteristiki lazera). "Naukova Dumka" Press, Kiev, 1968.
98. Kogelnik H., Li T. Proc. IEEE, 1966, vol. 54, p. 1312.
99. Li T. Bell Syst. Techn. J., 1965, vol. 44, p. 917.
100. Mikaelyan A. L., Turkov Yu. G., Savelyev V. G. ZhETF Letters, 1967, No. 6, p. 675.
101. Siegman A. E. Proc. IEEE, 1965, vol. 53, p. 277.
102. Siegman A. E., Arrathon R. IEEE J. Quantum Electronics, 1967, vol. 3, p. 156.
103. Siegman A. E., Miller H. J., Appl. Optics, 1970, vol. 9, p. 2729.
104. Ananyev Yu. A., Sventsitskaya N. A., Sherstobitov V. Ye., ZhETF, 1968, vol. 56, p. 131.
105. Ananyev Yu. A. UFN, 1971, vol. 103, p. 1.
106. Lifshits B. L., UFN, 1969, vol. 98, No. 2, p. 393.
107. Quelle W. Appl. Optics, 1966, vol. 5, p. 633.
108. Snitzer Proc. IEEE, 1966, vol. 54, p. 1249.
109. Ananyev Yu. A., Mak A. A. "Optics and Spectroscopy" (Optika i spektroskopiya), 1964, vol. 16, p. 1065.
110. Schmidt U. I. J. Appl. Phys., 1964, vol. 35, p. 259.
111. Veduta A. P., Leontovich A. M., Smorchkov V. N. ZhETF, 1965, vol. 48, p. 87.

112. Vanyukov M. P., Isaenko V. I., Luizova L. A., Shorokhov O. A. Journal of Applied Spectroscopy (Zhurnal prikladnoy spektroskopii), 1965, vol. 2, p. 295.
113. Townsend R. I., Stickley C M., Malo A. D. Appl. Phys. Letters, 1965, vol. 7, p. 94.
114. Sims S. D., Stein A., Roth C. Appl. Optics, 1966, vol. 5, p. 621.
115. Bayer E., Schack G. Zs. Naturforsch., 1966, B. 21a, S. 643.
116. Welling H., Bichart C. I. J. Opt. Soc. Am., 1966, vol. 56, p. 611.
117. Ananyev Yu. A., Kozlov N. A., Mak A. A., Stepanov A. I. Journal of Applied Spectroscopy (Zhurnal prikladnoy spektroskopii), 1966, vol. 5, p. 51.
118. Cabezas A. Y., Komai L. G., Treat R. P. Appl. Optics, 1966, vol. 5, p. 647.
119. Riedel E. P., Baldwin G. D. J. Appl. Phys., 1967, vol. 38, p. 2720.
120. Grishmanova N. I., Sventsitskaya N. A., Khazov L. D. Journal of Applied Spectroscopy (Zhurnal prikladnoy spektroskopii), 1967, vol. 7, p. 340.
121. Veduta A. P., Leontovich A. M., Matyushin G. A. Journal of Applied Spectroscopy (Zhurnal prikladnoy spektroskopii), 1968, vol. 8, p. 238.
122. Ananyev Yu. A., Grishmanova N. I. Journal of Applied Spectroscopy (Zhurnal prikladnoy spektroskopii), 1970, vol. 12, p. 668.
123. White D., Gregg D. Appl. Optics, 1965, vol. 4, p. 1034.
124. Roess D. J. Appl. Phys., 1966, vol. 37, p. 3587.
125. Lifshits B. L., Tsikunov V. N. ZhETF, 1965, vol. 49, p. 1843.
126. Skinner I. G. Appl. Optics, 1964, vol. 3, p. 963.
127. Li T., Skinner I. G. J. Appl. Phys., 1965, vol. 36, p. 2595.
128. Ananyev Yu. A., ZhTF, 1967, vol. 37, p. 139.
129. McAllister G. I., Mann M. M., De Shazer L. G. IEEE J. of Quantum Electronics, 1970, vol. 6, p. 44.
130. Tang C. L., Statz H., De Mars G. J. Appl. Phys., 1963, vol. 34, p. 2289.
131. Collins S. A., White G. R. Appl. Optics, 1963, vol. 2, No. 4, p. 448.
132. Hercher M. Appl. Phys. Letters, 1965, vol. 7, p. 39.
133. Antsiferov V. V., Krivoshchekov G. V., Folin K. G. "Izvestiya vuzov", Radio Physics (Radiofizika), 1967, vol. 10, No. 6, p. 879.
134. Snitzer E. Appl. Optics, 1966, vol. 5, p. 121.
135. Rigrod W. W. IEEE J. of Quantum Electronics, 1970, vol. 6, p. 9.
136. Genkin R. O., Isyanova Ye. D., Marugin A. M., Ovchinnikov V. M. Journal of Applied Spectroscopy (Zhurnal prikladnoy spektroskopii), 1970, vol. 12, p. 227.
137. Tang C. L., Statz H., De Mars G. A., Willson D. T., Phys. Rev., 1964, vol. 136 A, p. 1.
138. Bjorkholm J. E., Stolen R. H. J. Appl. Phys., 1968, vol. 39, p. 4043.
139. Marugin A. M., Ovchinnikov V. M. In the collected volume "Quantum Electronics" (Kvantovaya elektronika), ed. by N. G. Basov. "Sovetskoe radio" Publishers, 1972, No. 4.
140. Baker J. A., Peters C. W., Appl. Optics, 1962, vol. 1, p. 674.
141. Hagen W. F. J. Appl. Phys., 1969, vol. 40, p. 511.
142. Stein A. Appl. Optics, 1967, vol. 6, p. 2193.
143. Evtuhov U., Neeland J. K. Appl. Optics, 1962, vol. 1, p. 517.
144. Giordmaine J. A., Kaiser W. J. Appl. Phys., 1964, vol. 35, p. 3446.
145. De Shazer L. J., Maunder E. A. Appl. Optics, 1967, vol. 6, p. 431.
146. Boiko B. B., Petrov I. S., Valyavko V. V., Vashkevich I. M. "Optics and Spectroscopy" (Optika i spektroskopiya), 1967, vol. 22, p. 119.
147. Yevtuhov V., Neeland J. K. IEEE J. of Quantum Electronics, 1965, vol. 1, p. 7.
148. Mak A. A., Malinin B. G., Stepanov A. I. *et al.* "Optico-Mechanical Industry" (Optiko-mekhanicheskaya promyshlennost), 1970, No. 8.
149. Balashov I. F., Blagoveshchensky V. V., Dovger L. S. *et al.*, ZhTF, 1970, vol. 40, p. 1428.

150. Ananyev Yu. A., Sventsitskaya N S., Sherstobitov V. Ye., ZhTF, 1969, vol. 39, p. 1385.
151. Basov N. G., Zuev V. S., Kryukov P. G. ZhETF, 1962, vol. 43, No. 1, p. 353.
152. Collins R. I., Kisliuk P. J. Appl. Phys., 1962, vol. 33, No. 6, p. 2009.
153. Court F. K., Von Willisen. Appl. Optics, 1964, vol. 3, p. 719.
154. Buchman W., Koecher W., Rice D. IEEE J. of Quantum Electronics, 1970, vol. 6, No. 11, p. 747.
155. Theory and Design of Balancing Machines (Teoriya i konstruktsiya balansirovochnykh mashin), ed. by V. A. Shchepetilnikov. Mashgiz, 1963.
156. Military Application of the Laser. Collection of translations. Voenizdat, USSR Ministry of Defence, 1966, p. 47.
157. Balashov I. F., Berezin B. G. Yermakov B. A., Konyshev V. V. Journal of Applied Spectroscopy (Zhurnal prikladnoy spektroskopii), 1967, vol. 7, No. 3, p. 354.
158. Chesler R. B., Geusic J. E., Karı M. A. IEEE J. of Quantum Electronics, 1969, vol. 5, No. 6, p. 345.
159. Chesler R. B., Karr M A., Geusic J. E. Proc. IEEE, 1970, vol. 58, No. 12, p. 27.
160. Deutch I. Appl. Phys. Lett., 1965, vol. 7, p. 80.
161. Kryukov O. N., Letokhov V. S. UFN, 1969, vol. 99, No. 2, p. 169.
162. Terenin A. N. Photonics of Molecules (Fotonika molekul). "Nauka" Publishers, 1967.
163. Gurinovich G. P., Sevchenko A. N., Solovyev K. N. UFN, vol. 79, issue 2, p. 173.
164. Gurinovich G. P., Sevchenko A. N., Solovyev K. N. Spectroscopy of Chlorophyll and Related Compounds (Spektroskopiya khlorofilla i rodstvennykh soedineniy). "Science and Technology" (Nauka i tekhnika), Minsk, 1968.
165. Sharlai S. F. Investigation of Laser Performance with Passive Q-switching (Issledovanie protsessov v kvantovom generatore s passivnoy modulyatsiey dobrotnosti). Resume of a dissertation. LITMO Press, 1968.
166. Akhmanov S. A., Sukhorukov A. P., Khokhlov R. V., UFN, 1967, vol. 93, issue 1, p. 19.
167. Maier M., Kaiser W. Physics Letters, 1966, vol. 21, No. 5, p. 529.
168. Blombergen N., Lallemand P., Pine A. IEEE J. Quantum Electronics, 1966, vol. 2, No. 8, p. 246.
169. Avdeeva V. I., Alperovich M. A., Vanyukov M. P. *et al.* In the collected volume "Quantum Electronics" (Kvantovaya elektronika), ed. by N. G. Basov, 1971, No. 2, p. 69.
170. Kogan B. Ya., Churkin V. L. "Optics and Spectroscopy" (Optika i spektroskopiya), 1969, vol. 27, No. 3, p. 530.
171. Lisitsa M. P., Kulish N. R., Koval P. N., Geets V. I. "Optics and Spectroscopy" (Optika i spektroskopiya), 1967, vol. 23, issue 6, p. 981.
172. Smith W. V., Sorokin P. P., Lasers. McGraw-Hill, New York, 1966.
173. Ovchinnikov V. M., Khartsiev V. E., ZhETF, 1965, vol. 49, p. 315.
174. Khartsiev V. Ye. "Optics and Spectroscopy" (Optika i spektroskopiya), 1966, vol. 20, No. 3, p. 514.
175. Zuev V. S., Shcheglov V. A. Journal of Applied Spectroscopy (Zhurnal prikladnoy spektroskopii), 1966, vol. 5, No. 5, p. 604.
176. Ovchinnikov V. M., Khartsiev V. Ye. Journal of Applied Spectroscopy (Zhurnal prikladnoy spektroskopii), 1966, vol. 4, p. 509.
177. Stepanov B. I., Lashitskaya R. K. Journal of Applied Spectroscopy (Zhurnal prikladnoy spektroskopii), 1966, vol. 5, No. 5, p. 595.
178. Khartsiev V. Ye., Staselko D. N., Ovchinnikov V. M. ZhETF, 1967, vol. 52, No. 6, p. 1457.
179. Khartsiev V. Ye. Physica, 1967, vol. 3, No. 3, p. 143.

180. Macomber J. D. J. Appl. Phys., 1967, vol. 38, No. 9, p. 3525.
Selden A. C., Brit. J. Appl. Phys., 1967, vol. 18, No. 6, p. 743.
181. Lower S, El-Sayed M. UFN, 1968, vol. 94, p. 289.
182. Yermolayev V L. UFN, 1968, No. 80, p. 3.
183. Letokhov V. S. ZhTF, 1968, vol 55, No. 9, p. 11.
184. West C. D. US Patent 2, 788, 710, 1957.
185. Kerr J. Phyl. Mag., 1875, vol 4, p. 337.
186. Nye J. F. Physical Properties of Crystals. Their Representation by Tensors and Matrices. Oxford, Claredon press, 1957.
187. Zheludev I. S. Physics of Crystalline Dielectrics (Fizika kristallicheskikh dielektrikov), "Nauka" Publishers, 1968.
188. Katys G. P., Kravtsov N. V., Chirkov L. Ye., Konovalov S. M. Modulation and Deflection of Optical Emission (Modulyatsiya i otklonenie opticheskogo izlucheniya). "Nauka" Publishers, 1967.
189. Mustel Ye. A, Parygin V. N. Light Modulation and Scanning Techniques (Metody modulyatsii i skanirovaniya sveta). "Nauka" Publishers, 1970.
190. Cady, Walter Guyton. Piezoelectricity. An Introduction to the Theory and Applications of Electromechanical Phenomena in Crystals. McGraw-Hill Book co., 1946.
191. Rez I. S. UFN, 1967, vol. 93, issue 4, p. 633.
192. Stephany J. F. Josa. 1965, vol. 55, No. 2, p. 136.
193. Marugin A. M., Ovchinnikov V. M. "Optico-Mechanical Industry" (Optiko-mekhanicheskaya promyshlennost), 1970, No. 2, p. 79.
194. Kaminow. Appl. Optics, 1964, vol. 3, No. 4, p. 511.
195. Davies M. B., Sarkies P. H., Wright J. K. IEEE J. of Quantum Electronics, 1968, vol. 4, No. 9, p. 533.
196. Kulevsky L. A., Prokhorov A. M., Smirnov V. V. ZhETF, 1968, vol. 54, p. 8.
197. Statz H., De Mars G. A., Wilson P. T. J. Appl. Phys., 1965, vol. 36, No. 5, p. 1510.
198. Thomas C. H., Price Ye. V. IEEE J. of Quantum Electronics, 1966, vol. 2, No. 9, p. 617.
199. Ditchburn P. Physical Optics, "Nauka" Publishers, 1965.
200. Shurkliff, William A. Polarized Light, Production and Use. Harvard University Press, Cambridge, Massachusetts, 1962.
201. Archard J. E., Taylor A. M. J. Sci. Instr., 1948, vol. 25, p. 407.
202. Kamach Yu. E., Kozlovsky Ye. N., Ovchinnikov V. M., Solomatnikova T. M. "An Electro-Optic Shutter-Reflector as a Q-switch for a Polarized-Light Laser Oscillator" (Elektro-opticheskiy zatvor-otrazhatel dlya modulyatsii dobrotnosty rezonatora OKG s polyarizovannym izlucheniem). Inventor's Certificate No. 257,066. "Bulletin of Inventions" (Bulleten izobreteniy), 1969, No. 35.
203 Gostev V. I., Gruzdev V. V., Lavrov V. I., Shamburov V. A. "Optico-Mechanical Industry" (Optiko-mekhanicheskaya promyshlennost), 1970, No. 5, p. 30.
204. Zharkov A. P., Kamach Yu. E., Kozlovsky Ye. N., Ovchinnikov V. M. "Optico-Mechanical Industry" (Optiko-mekhanicheskaya promyshlennost), 1968, No. 3, p. 5.
205. Shubnikov A. V. Optical Crystallography (Opticheskaya kristallografiya). USSR Academy of Sciences Press, 1950.
206. Zharkov A. P., Kamach Yu. E., Kozlovsky Ye. N., Lyubavsky Yu. V., Ovchinnikov V. M. "Optico-Mechanical Industry" (Optiko-mekhanicheskaya promyshlennost), 1970, No. 9, p. 30.
207. Kamach Yu. E., Kozlovsky Je. N., Ovchinnikov V. M., Solomatnikova T. M. "Electro-Optic Shutter-Reflector as a Q-switch for a Laser". Inventor's certificate No. 273,023, Application No. 1.218, 194/26-25, Feb. 7, 1968.
208. Kamach Yu. E., Kozlovsky Ye. N., Ovchinnikov V. M., Solomatnikova T. M.

"Optical Quantum-Mechanical Oscillator", Inventor's Certificate No. 270, 920, Application No. 1, 190 254/26-25, Feb. 16, 1968.
209. Isyanova Ye. D., Kamach Yu. E., Kozlovsky Ye. N., Ovchinnikov V. M. "Optico-Mechanical Industry" (Optiko-mekhanicheskaya promyshlennost), 1970, No. 2, p. 80.
210. Vishnevsky V. N., Stefansky I. V., "Optics and Spectroscopy" (Optika i spektroskopiya), 1966, vol. XX, p. 357.
211. Belostotsky B. R., Kamach Yu. E., Kozlovsky Ye. N., Ovchinnikov V. M. Journal of Applied Spectroscopy (Zhurnal prikladnoy spektroskopii), 1969, vol. XI, No. 2, p. 257.
212. Masters J. I. J. Sci. Instr., 1963, vol. 34, p. 362.
213. Masters J. I., Murray E. M. E. Proc. IEEE, 1965, vol. 53, p. 73.
214. Kalinin Yu. A., Stepanov A. I. Optico-Mechanical Industry (Optiko-mekhanicheskaya promyshlennost), 1968, No. 7, p. 59.
215. Exploding Wires. Collected volume ed. by A. A. Rukhadze. Foreign Literature Publishing House, 1963.
216. Electric Wire Explosion (Elektricheskiy vzryv provodnikov). Collection of translated articles. "MIR" Publishers, 1965.
217. Kulgavchuk V. M., Novoskoltseva G. A. ZhTF, 1966, vol. 36, issue 3, p. 549.
218. Protopopov N. A., Kulgavchuk V. M. ZhTF, 1961, vol. 31, issue 5, p. 557.
219. Petrosyan V. I., Datman E. I. ZhTF, 1969, vol. 39, issue 11, p. 2084.
220. Gorlanov A. V., Lyubimov V. V., Petrov V. F. PTE, 1969, No. 6, p. 176.
221. Geusik J. E., Scovil H. E. D. Bell System Techn. J., July 1962, vol. 41, p. 1371.
222. De Shazer L. G., Maunders E. A. Rev. Sci. Instrum., 1967, vol. 38, No. 2, p. 248.
223. Bird G. R., Shurcliff W. A. J. Opt. Soc. Am., 1959, vol. 49, p. 235.
224. Fong P. K Rev. Sci. Instrum. 1970, vol. 41, No. 10, p. 1434.
225. Robinson C. C. Appl. Optics, 1964, vol. 3, p. 1163.
226. Padula C. F., Young C. G. IEEE J. of Quantum Electronics, 1967, vol. QE-3, p. 493.
227. Watts J. K. Appl. Optics, 1968, vol. 7, No. 8, p. 1621.
228. Lyubimov V. V., Fersman I. A., Khazov L. D. In the collected volume "Quantum Electronics" (Kvantovaya elektronika), ed. by N. G. Basov, 1971, issue 2, p. 119.
229. Boiko B. B., Petrov N. S., Valyavko V. V., Vashkevich I. M. "Optics and Spectroscopy" (Optika i spektroskopiya), 1967, vol. 22, No. 1, p. 119.
230. Ritus A. I., Manenkov A. A. ZhETF Letters, 1967, vol. 6, No. 11, p. 927.
231. Cullom J. H., Waynant R. W. Appl. Optics, 1964, vol. 3, No. 8, p. 989.
232. Martinelli J. A. J. Appl. Phys., 1966, vol. 37, No. 4, p. 1939.
233. Feofilov P. P. "Izvestiya AN SSSR", 1962, vol. 26, p. 435.
234. Gerlich P., Karras H., Ketitz G., Lehmann R. Spectroscopic Properties of Activated Laser Crystals (Russian translation), "Nauka" Publishing House, 1966.

Chapter 2

1. Prokhorov A. M. "Radio Engineering and Electronics" (Radiotekhnika i elektronika), 1963, vol. 8, No. 6, p. 1073.
2. Arecchi F. T., Potenza G., Sona A. Nuovo Cimento, 1964, vol. 34, No. 6, p. 1458.
3. Methods for the Calculation of Lasers (Metody rascheta opticheskikh kvantovykh generatorov), vol. II, ed. by B. I. Stepanov. "Science and Technology" (Nauka i tekhnika), 1968.
4. Misso D. V., Sieber K. N. Alta Frequenza, 1965, vol. 34, No. 5, p. 323.
5. Bespalov V. I., Freidman G. I. "Izvestiya vuzov", Radio Physics (Radiofizika), 1966, vol. 9, No. 3, p. 513.

6. Mikaelyan A. L., Ter-Mikaelyan M. L., Turkov Yu. G. Solid-State Lasers (Opticheskie kvantovye generatory na tverdom tele). "Sovetskoe radio" Publishers, 1967.
7. Pilipovich V. A., Morgun Yu. F. Journal of Applied Spectroscopy (Zhurnal prikladnoy spektroskopii), 1967, vol. 7, No. 5, p. 760.
8. Baiborodin Yu. V., Garazha S. A., Kravchenko V. I., Spizhava N. I. Ukrainian Physics Journal (UFN), 1965, vol. 10, No. 8, p. 919.
9. Basov H. G., Zuev V. S., Senatsky Yu. V. ZhETF, 1965, vol. 48, No. 6, p. 1562.
10. Daly R., Sims S. D. Appl. Optics, 1964, vol. 3, No. 9, p. 1063.
11. Lyubimov V. V., Nilov Ye. V. "Optico-Mechanical Industry" (Optiko-mekhanicheskaya promyshlennost), 1967, No. 7, p. 32.
12. Balashov I. F., Berezin B. G., Yermakov B. A., Konyshev V.V. Journal of Applied Spectroscopy (Zhurnal prikladnoy spektroskopii), 1967, vol. 7, No. 3, p 354.
13. Ishchenko V. N., Starinsky V. N. "Izvestiya vuzov", Radio Physics (Radiofizika), 1967, vol. 10, No. 8, p. 1189.
14. Gates J. W., Hall R. S. N. Nature, 1965, No. 34, p. 1141.
15. Starunov M. G., Yeremka V. D., Bonchkovsky V. I. Ukrainian Physics Journal (UFN), 1966, vol. 2, No. 2, p. 217.
16. Lyubavsky Yu. V., Gavrilov N. I. Multi-Position Laser (Mnogopositsionny OKG), Inventor's Certificate No. 291, 644, Application No. 134,876/26-25 of July 14, 1969.
17. Duf L. E., Pereff R., Dupeyrat R. Physical Rev., Applied, 1966, vol. 11, No. 2, p. 117.
18. Hull D. Applied Optics, 1966, vol 5, No. 8, p. 1342. Sorokin P. P., Luzzi J. J., Lankard J. R., Pettit G. D. IBM J., 1964, vol. 8, No. 2, p. 182.
19. Borovich B. L., Zuev V. S., Shchetkov V. A., ZhETF, 1965, vol. 49, No. 4, p. 1009.
20. Szabo A., Stein R. A. J. Appl. Phys., 1965, vol. 36, p. 1562.
21. Korobkin V. V., Leontovich A. M., Popova M. N., Shchelev M. Ya. ZhETF Letters, 1966, vol. 3, No. 7, p. 301.
22. Sooy W. R. J. Appl. Phys., 1965, vol. 7, No. 2, p. 36.
23. Daneu V., Sacchi C. A., Svelto O. IEEE J. of Quantum Electronics, 1966, vol. QE-2, No. 8, p. 290.
24. Hanna D. C. Optics and Laser Technology, 1970, vol. 2, No. 4, p. 173.
25. Mikaelyan A. L., Turkov Yu. G., Savelyev V. G., ZhETF Letters, 1967, vol. 6, No. 6, p. 675.
26. Bjorkholm J. E., Stolen R. N. J. Appl. Phys., 1968, vol. 39, No. 8, p. 4043.
27. Balashov I. F., Blagoveshchensky V. V., Dovger L. S. *et al.* ZhTF, 1970, vol. 40, No. 7, p. 1428.
28. Ananyev Yu. A., Sventsitskaya N. S., Sherstobitov V. Ye. ZhTF, 1969, vol. 39, No. 7, p. 1325.
29. De Maria A. J., Stetser D. A., Heynau N. A., Appl. Phys. Letters, 1966, vol. 8, No. 7, p. 174.
30. Belenov E. M., Morozov V. N., Oraevsky L. N. Quantum Radio Physics (Kvantovaya radiofizika). "Nauka" Publishers, 1970, vol. 52, p. 237.
31. Markin A. C. Transactions of the USSR Academy of Sciences' Institute of Physics. "Nauka" Publishers, 1971, vol. 56, p. 3.
32. Krasyuk I. K., Pashinin P. P., Prokhorov A. M. ZhETF Letters, 1968, vol. 7, issue 4, p. 117.
33. Hellwarth R. W. Advances in Quantum Electronics. Columb. Univ. Press, N. Y., 1961, p. 334.
34. Vuylsteke A. A. J. Appl. Phys., 1963, vol. 34, No. 6, p. 1615.
35. Deutcsh T. Appl. Phys. Lett., 1965, vol. 7, p. 80.
36. Statz H., De Mars G. A., Wilson D. T., Tang C. L. J. Appl. Phys., 1965, vol. 36 No 5, p. 1510.

37. Thomas C. H., Price E. V. IEEE J. of Quantum Electronics, 1966, vol. QE-2, No. 9, p. 617. Pheneger P. W., Panfell R. H. IEEE J. of Quantum Electronics, 1966, vol. QE-2, No. 9, p. 645.
Lengyel B. A. Introduction of Laser Physics. J. Willey and Sons, Inc., 1966, vol. 14, No. 128, p. 428.
38. Bespalov V. I., Gostev V. I., Gruzdev V. V., Katsman V. I. *et al.* "Optico-Mechanical Industry" (Optiko-mekhanicheskaya promyshlennost), 1970, No. 6, p. 11.
39. Kamach Yu. E., Kozlovsky Ye. N., Ovchinnikov V. M. "Optical Quantum-Mechanical Oscillator" (Opticheskiy kvantovy generator). Inventor's Certificate No. 291,644, Application No. 1,190,254/26-25, Oct. 16, 1967.
40. Isyanova Ye. D., Kamach Yu. E., Kapitsa M. L. *et al.* "Optics and Spectroscopy", 1969, vol. 27, No. 4, p. 686.
41. Isyanova Ye. D., Marugin A. M., Ovchinnikov V. M. Journal of Applied Spectroscopy (Zhurnal prikladnoy spektroskopii), 1970, vol. 12, No. 5, p. 834.
42. De Maria A. J., Ferrar C. M., Danielson G. E. Appl. Phys. Lett., 1966, vol. 8, No. 1, p. 22.
43. Letokhov V. S. ZhETF, 1968, vol. 54, No. 5, p. 1392.
44. Marugin A. M., Ovchinnikov V. M. Quantum Electronics (Kvantovaya elektronika), a collected volume (in press).
45. Kobayashi T., Cho Y., Matsuo Y. Japanese J. of Appl. Phys., 1970, vol. 9, No. 3, p. 318.
46. Frantz L. M., Nodvik J. S. J. Appl. Phys., 1963, vol. 34, p. 2346.
47. Bellman R., Birnbaum G., Wagner W. J. Appl. Phys., 1963, vol. 34, p. 780. Davis J. I., Sooy W. R., Applied Optics, 1964, vol. 3, p. 715.
48. Avizonis P. V., Grotbeck R. L. J. Appl. Phys., 1966, vol. 37, p. 687.
49. Zverev V. A., Kulikov V. Ye *et al.* "Optico-Mechanical Industry" (Optiko-mekhanicheskaya promyshlennost), 1973, No. 6.
50. Ralston A., Herbert W. S. Mathematical Methods for Digital Computers. John Wiley & Sons., Inc., New York, 1960.
Gill S.Proc. Cambridge Phil. Soc., 1951, vol. 47, p. 96.
51. Avizonis P. V., Farrington E. Appl. Phys. Letters, 1965, vol. 7, p. 20, No. 8, p. 205.
52. Senatsky Yu. V. Development and Investigation of a High-Power Neodymium-Glass Laser for High-Temperature Plasma Generation. (Sozdanie i issledovanie moshchnogo lazera na neodimovom stekle dlya vysokotemperaturnogo nagreva plazmy.) Resume of a dissertation. USSR Academy of Sciences' Institute of Physics, 1970.
53. Roess D. Proc. IEEE, 1964, vol. 52, p. 853.
54. Young C. G., Kantorski I. W. Appl. Optics, 1965, vol. 4, No. 12, p. 1675.
55. Zuev V. S., Letokhov V. S., Senatsky Yu. V. ZhETF Letters, 1966, vol. 4, No. 5, p. 182.
56. Young C. G., Kantorsky I. W., Dixon E. O. J. Appl. Phys., 1966, vol. 37, No. 12, p. 4319.
57. Ambartsumyan R. V., Basov N. G., Kryukov P. G., Letokhov V. S. ZhETF Letters, 1966, vol. 3, No. 6, p. 262.
58. Sooy W. R., Gongleton R. S., Dobratz B. E. WK. Ng. Proceedings of the 3rd Intern. Conf. on Quantum Electronics, p. 1103. Columbia Univ. Press, Paris, N. Y., 1964.
59. Avdeev O. I., Venchikov V. A., Zhulai V. Ya., Lyubimov V. V. "Optico-Mechanical Industry" (Optiko-mekhanicheskaya promyshlennost), 1967, No. 10, p. 64.
60. Bonch-Bruyevich A. M., Imas Ya. A., Sokolov N. I. Journal of Applied Spectroscopy (Zhurnal prikladnoy spektroskopii), 1964, vol. 1, No. 1, p. 1.
61. Maiman T. US Patent No. 3,353,115, Nov. 14, 1967.

62. Basov N. G., Zuev V. S., Senatsky Yu. V. ZhETF, 1965, vol. 48, p. 1562. ZhETF Letters, 1965, vol. 2, No. 2, p. 57.
63. Basov N. G., Ambartsumyan R. V., Zuev V. S. *et al.* ZhETF, 1966, vol. 51, p. 23. ZhETF Letters, 1966, vol. 4, p. 19.
64. Basov N. G., Zuev V. S., Kryukov P. G. *et al.* ZhETF, 1968, vol. 54, No. 3, p. 767.
65. Robieux I., Riffard I., Ernest I., Sturel B. IEEE J. of Quantum Electronics, 1968, vol. QE-4(5), p. 46.
66. Basov N. G., Kryukov P. G., Senatsky Yu. V., Chekalin S. V. ZhETF, 1969, vol. 57, No. 4, p. 1175.
67. Hagen W. F. J. Appl. Phys., 1969, vol. 40, No. 2, p. 511.
68. Gebelt G. Electronics News, 1969, vol. 14, p. 72. Laser Focus, 1969, vol. 4, p. 24.
69. Basov N. G., Zakharov S. L., Kryukov P. G., Senatsky Yu. V. Report at the International Conference on Lasers and Their Applications. Dresden, June, 1970.
70. Basov N. G., Zakharov S. L., Kryukov P. G., *et al.* Preprint of the FIAN, No. 63, 1968. ZhETF Letters, 1968, vol. 8 (1), p. 26.
71. Vanyukov M. P., Lyubimov V. V. *et al.* In the collected volume "Quantum Electronics" (Kvantovaya elektronika), ed by N. G. Basov, 1971, issue 4.
72. Design News (USA), 1971, vol. 26, No. 8, p. 11.
73. Huggett G. R. Appl. Phys. Letters, 1968, vol. 13, p. 186.
74. Balashov I. F., Berenberg V. A., Blagoveshchensky V. V. ZhTF, 1969, vol. 39, issue 5, p. 926.
75. Michon M., Auffret R., Dumanchin R. J. Appl. Phys. 1970, vol. 41, No. 6, p. 2739.
76. Basov N. G., Grasyuk A. Z., Zubarev I. G. Reports of the USSR Academy of Sciences (DAN SSSR), 1964, vol. 157, p. 1084.
77. Basov N. G., Grasyuk A. Z., Zubarev I. G., Tevelev L. V. Quantum Radio Physics (Kvantovaya radiofizika). Transactions of the USSR Academy of Sciences' Institute of Physics (Trudy FIAN SSSR), 1965, vol. 31, p. 74.
78. Ananyev Yu. A., Sventsitskaya N. A., Sherstobitov V. Ye. ZhETF, 1968, vol. 55, No. 1, p. 130.
Ananyev Yu. A., Vinokurov G. N., Kovalchuk L. V. *et al.* ZhTF, 1970, vol. 58, p. 786.
79. Bondarenko A. N., Folin K. G., Smirnov V. A., Antsiferov V. V. ZhETF Letters, 1967, vol. 6, issue 6, p. 692.
80. Bondarenko A. N., Krivoshchekov G. V., Smirnov V. A. ZhETF Letters, 1969, vol. 9, issue 2, p. 100.
81. Swain J. E., Rainer F. IEEE Quantum Electronics, 1967, vol. QE-5, No. 7, p. 385.
82. Blombergen N. Non-Linear Optics. "Mir" Publishers, 1966.
83. Akhmanov S. A., Khokhlov R. V. Problems of Non-Linear Optics (Problemy nelineinoy optiki). Institute of Scientific Information, USSR Academy of Sciences. Moscow, 1964.
84. Kleinman D. A. Phys. Rev., 1962, vol. 128, No. 4, p. 1161.
85. Giordmaine J. A. Phys. Rev. Lett., 1962, vol. 8, No. 1, p. 19.
86. Maker P. D., Terhune R. W., Nisenhoef M., Savage G. M. Phys. Rev. Letters, 1962, vol. 8, No. 1, p. 21.
Weber H. P., Mathieu E., Mayer K. P. J. Appl. Phys., 1966, vol. 37, No. 9, p. 3584.
87. Terhune R. W., Maker P. D., Savage C. Phys. Rev. Lett., 1962, vol. 8, p. 404.
88. Bokut B. V., Zharkov A. P., Ovchinnikov V. M. *et al.* Inventor's Certificate No. 200,010, Jan. 7, 1965. Bulletin of Inventions (Byulleten izobreteniy), 1967, No. 16, p. 55.

89. Bokut B. V., Khatkevich A. G. Reports of the BSSR Academy of Sciences (DAN BSSR), 1965, vol. 9, No. 6, p. 357.
90. Vanyukov M. P., Volosov V. D., Rashchektaeva M. I. "Optics and Spectroscopy" (Optika i spektroskopiya), 1968, vol. 25, No. 5, p. 735.
91. Volosov V. D., Rashchektaeva M. I. "Optics and Spectroscopy" (Optika i spektroskopiya), 1970, vol. 28, No. 1, p. 105.
92. Volosov V. D., Kamach Yu. E., Kozlovsky Ye. N., Ovchinnikov V. M. "Optico-Mechanical Industry" (Optiko-mekhanicheskaya promyshlennost), 1969, No. 10, p. 3.
93. Volosov V. D. ZhTF, 1969, vol. 39, No. 12, p. 2188.
94. Polloni R., Svelto O. IEEE J. of Quantum Electronics, 1968, vol. 4, No. 9, p. 528.
95. Geusic J. E., Levinstein H. J., Singh S., Smith R. G., Van Vitert L. G. Appl. Phys. Letters, 1968, vol. 12, p. 306.
96. Murray J. E., Harris S. E. J. Appl. Phys., 1970, vol. 41, No. 2, p. 609.
97. Isyanova Ye. D., Ovchinnikov V. M. "Optics and Spectroscopy" (Optika i spektroskopiya), 1972, vol. 31, No. 1, p. 71.
98. Deserno V., Nath G. Phys. Lett., 1969, vol. 30A, No. 8, p. 483.
99. Genkin R. O., Isyanova Ye. D., Kamach Yu. E., Kozlovsky Ye. N., Ovchinnikov V. M. "Optics and Spectroscopy" (Optika i spektroskopiya), 1971, vol. 30, No. 1, p. 137.
100. Prokhorov A. M. ZhETF, 1958, vol. 34, p. 1658.
101. Kotik J., Newstein M. C. J. Appl. Phys., 1961, vol. 32, No. 2, p. 178.
102. Basov N. G., Krokhin O. N., Popov Yu. M. UFN, 1960, vol. 72, No. 2, p. 161.
103. Mikaelyan A. L., Gardashyan V. M., Sakharova N. A., Turkov Yu. G. "Radio Engineering and Electronics" (Radiotekhnika i elektronika), 1964, vol. 9, No. 8, p. 1542.
104. Vanyukov M. P., Isayenko V. I., Luizova L. A., Shorokhov O. A. Journal of Applied Spectroscopy (Zhurnal prikladnoy spektroskopii), 1965, vol. 2, No. 5, p. 415.
105. Kravchenko V. I., Soskin M. S. "Quantum Electronics" (Kvantovaya elektronika), 1969, issue 4. "Naukova Dumka" Publishers, Kiev.
106. Leontovich A. M., Veduta A. P. ZhETF, 1964, vol. 46, No. 1, p. 71.
107. Veduta A. P., Leontovich A. M., Smorchkov V. N. ZhETF, 1964, vol. 47, No. 3, p. 1050.
108. Kalinin V. P., Lyubimov V. V. "Optics and Spectroscopy" (Optika i spektroskopiya), 1967, vol. 22, No. 1, p. 123.
109. Collins R. J., Nelson D. F. Proc. of the Conference on Optical Instruments and Techniques. London, 1961, p. 441.
110. Rochlicek F. R. Jemna Mechanika a Optika, 12/68, p. 383.
111. Guintoft R. I., Sartevsky A. M. Journal of Applied Spectroscopy (Zhurnal prikladnoy spektroskopii), 1966, vol. 5, No. 2, p. 259.
112. Everett. Instruments for Scientific Research (Russian translation), 1966, vol. 37, No. 3, p. 128.
113. Bergmann T. G., Thompson J. L. Applied Optics, 1968, vol. 7, No. 5, p. 923.
114. Gryaznov Yu. M., Chastov A. A. "Measurement Techniques" (Izmeritelnaya tekhnika), 1966, No. 3, p. 90
115. Lyubavsky Yu. V. "Arrangement for the Alignment of Mirrors" (Ustroystvo dlya yustirovki zerkal). Inventor's Certificate No. 337,747, Application No. 1,347,887/18-10, July 14, 1969.
116. McMahon J. M. IEEE J. of Quant. Electr., 1969, vol. 5, No. 10, p. 389.
117. Letokhov V. S., Suchkov A. F. ZhETF, 1965, vol. 50, p. 1148, ZhETF, 1966, vol. 51, No. 1.
118. Malyshev V. I., Markin A. S., Sychev A. A. Journal of Applied Spectroscopy (Zhurnal prikladnoy spektroskopii), 1969, vol. 10, No. 2, p. 248.

119. Marugin A. M., Ovchinnikov V. M. "Optico-Mechanical Industry" (Optiko-mekhanicheskaya promyshlennost), 1970, No. 2, p. 79.
120. Marshall F. R., Roberts D. L. Proc. IRE, 1962, vol. 50, No. 10, p. 2108.
121. Soffer B. H. J. Appl. Phys., 1964, vol. 35, p. 2551.
122. Statz H., de Mars G. A., Wilson D. T., Tang C. L. J. Appl. Phys., 1965, vol. 36, No. 5, p. 1510.
123. Agabekyin A. S., Grasyuk A. Z., Zubarev N. G. *et al.* "Radio Engineering and Electronics" (Radiotekhnika i elektronika), 1964, vol. 9, No. 13, p. 2156.
124. Thomas C. H., Price E. V. IEEE J. of Quant. Electronics, 1966, vol. 2, No. 9, p. 617.
125. Goldstein I., Chabot A. IEEE J. of Quant. Electronics, 1966, vol. 2, No. 9, p. 519.
126. Keller D. V., Davis B. I. J. of Quantum Electronics, 1966, vol. 2, No. 7, p. 179.
127. Morozov V. N., Orayevsky A. N. ZhTF, 1967, vol. 37, No. 5, p. 947.
128. Samson A. M., Rybakov V. A., Journal of Applied Spectroscopy (Zhurnal prikladnoy spektroskopii), 1968, vol. 8, No. 6, p. 949.
129. Chang I. C., Lean E. G. H., Powell C. G. IEEE J. of Quant. Electronics, 1970, vol. 2, No. 7, p. 436.
130. Mishin V. I. "Instruments and Techniques of Experiments" (Pribory i tekhnika experimenta), 1971, No. 4, p. 181.
131. Gorlanov A. V., Lyubimov V. V., Petrov V. F. "Instruments and Techniques of Experiments" (Pribory i tekhnika experimenta), 1969, No. 6, p. 176.

Chapter 3

1. Kirsanov V. P., Troshkin S. V., Semenova G. N. "Limiting and Safe Load Characteristics of Tubular Quartz Flash Tubes" (Predelnye i dopustimye nagruzochnye kharakteristiki impulsnykh kvartsevykh lamp trubchatogo tipa). Electronic Engineering (Elektronnaya tekhnika), Series 3, Gas Discharge Devices (Gazorazryadnye pribory), 1966, No. 2.
2. Marshak I. S. Pulsed Light Sources (Impulsnye istochniki sveta). PTE, 1962, No. 3.
3. Studer F. J., van Burs R. F. J. Opt. Soc. Amer., 1964, vol. 54, p. 945.
4. Levikov S. I. Laser Pumping Tubes (a review). "Optico-Mechanical Industry" (Optiko-mekhanicheskaya promyshlennost), 1969, No. 8.
5. Emmet J. L., Schawlow A. L. J. Appl. Phys., 1964, vol. 35, p. 260.
6. Newell *et al.* IEEE J. of Quantum Electronics, vol. QE-4, 1968, No. 5, p. 291.
7. Fountain W. D., Osterink Z. N., Foster I. D. A. Comparison of Kr- and Xe-Flashlamps for Nd : YAG Lasers. IEEE J. of Quantum Electronics. 1970, vol. QE-6, No. 11.
8. Galaktionova N. M., Yegorova V. F., Mak A. A. Non-Spiking Mode of Operation and Mode Width of a CW Laser (Bespichkovy rezhim i shirina mody lazera nepreryvnogo deystviya). "Optics and Spectroscopy" (Optika i spektroskopiya), 1968, vol. 25, No. 2.
9. Liberman L. *et al.* IEEE J. of Quantum Electronics, 1969, vol. QE-5, No. 5, p. 238.
10. Marshak I. S. Pulsed Light Sources. Gosenergoizdat, 1963.
11. Gonez J. H. J. Appl. Phys., 1965, vol. 36, p. 742.
12. Perlman D. E. Rev. Sci. Instr., 1966, vol. 37, No. 3, p. 92.
13. Perlman D. E. Rev. Sci. Instr., 1967, vol. 38, No. 1, p. 68.
14. Sims S. D., Waszak Z. Electronics, 1968, vol. 41, No. 17.
15. Konyukhov V. K., Kulevsky L. A., Prokhorov A. M. Energy and Spectral Characteristics of the ИФП-5000 Xenon Flash Tube (Energeticheskie i spektralnye kharakteristiki impulsnoy ksenonovoy lampy ИФП-5000). Journal

of Applied Spectroscopy (Zhurnal prikladnoy spektroskopii), 1964, vol. 1, No. 1.
16. Andreyev S. I., Vanyukov M. P., Gavrilov V. Ye. Comparative Study of Light and Electrical Characteristics of Neon and Xenon Tubular Flash Tubes (Sravnitelnye issledovaniya svetovykh i elektricheskikh kharakteristik trubchatykh impulsnykh lamp s neonovym i ksenonovym zapolneniem). Journal of Applied Spectroscopy (Zhurnal prikladnoy spektroskopii), 1967, vol. 6, No. 1.
17. Korolev Ye. A., Khazov L. D. Calculation of Power Supplies for Solid-State Laser Flash Tubes (Raschet skhem pitaniya impulsnykh lamp dlya nakachki tverdotelnykh OKG). Journal of Applied Spectroscopy (Zhurnal prikladnoy spektroskopii), 1967, vol. 6, No. 4.
18. Lebedev L. F. A Charge Circuit with a Ballast Choke for Pulsed Light Sources (Zaryadnoe ustroystvo s ballastnym drosselem dlya impulsnykh istochnikov sveta). Light Engineering (Svetotekhnika), 1969, No. 3, p. 10.
19. Mayevsky O. A. *et al.* The Charging of a Capacitor from a Rectifier with an Inductive Current Limiter (Zaryad kondensatora ot vypryamitelya s induktivnym ogranichitelem toka). Electromechanics (Elektromekhanika), 1969, No. 11, p. 31.
20. Gardatyan V. M. *et al.* Efficient Transformerless Power Supplies for Solid-State Pulsed Lasers (Effektivnye bestransformatornye sistemy pitaniya impulsnykh opticheskikh kvantovykh generatorov na tverdom tele). "Problems of Radio Engineering" (Voprosy radiotekhniki), Series OT, 1968, No. 5.
21. Vakulenko V. M. Some Aspects of the Oscillatory Charge of a Capacitive Energy Storing Circuit (Nekotorye osobennosti kolebatelnogo zaryada yemkostnogo nakopitelya energii). Journal of Applied Spectroscopy (Zhurnal prikladnoy spektroskopii), 1969, vol. 11, No. 4.
22. Garber I. S. Magnetic Pulse Modulators. "Sovetskoe radio" Publishers, 1964.
23. Milyakh A. N., Kubyshin B. Ye., Volkov I. V. Inductive-Capacitive Voltage-to-Current Converters. "Naukova Dumka" Publishers, Kiev, 1964.
24. Volkova G. A., Smolyar T. Ya. The Effect of Firing on the Emission of Flash Tubes. (Vliyanie podzhiga na izluchenie impulsnykh lamp). Journal of Applied Spectroscopy (Zhurnal prikladnoy spektroskopii), 1971, vol. XIV, issue 4, pp. 717-719.
25. Korolev Yu. N. Thyristors. "Znanie" Publishers, Moscow, 1968.

Chapter 4

1. Methods for the Calculation of Lasers (Metody rascheta opticheskikh kvantovykh generatorov). Ed. by B. I. Stepanov, vol. 2, "Nauka i tekhnika" Publishers, Minsk, 1968.
2. Lykov A. V. Theory of Thermal Conduction. "Higher school" Publishing House, 1967.
3. Ivanov V. A., Lebedev V. I. Journal of Applied Spectroscopy (Zhurnal prikladnoy spektroskopii), 1970, vol. 13, No. 1, p. 40.
4. Belostotsky B. R., Rubanov A. S. The Thermal Conditions of Laser Active Elements (Teplovoy rezhim aktivnykh elementov opticheskikh kvantovykh generatorov). "Energiya" Publishers, 1973.
5. Belostotsky B. R. Thermal Conditions of Solid-State Pulsed Lasers (Teplovoy rezhim tverdotelnykh impulsnykh opticheskikh kvantovykh generatorov). LDNTP Press, 1970.
6. Stepanov B. I., Rubanov A. S., Chaley A. V. Journal of Applied Spectroscopy (Zhurnal prikladnoy spektroskopii), 1966, vol. 4, No. 4, p. 348.
7. Khromov A. B., Libin Yu. V. Engineering Physics Journal (Inzhenernofizicheskiy zhurnal), 1966, vol. 11, No. 4, p. 526.

8. Yushkov P. P. On the Numerical Integration of the Thermal Conductivity, Equation in Polar Grids (O chislennom integrirovanii uravneniya teploprovodnosti v polyarnykh setkakh). Transactions of the Leningrad Technological Institute of the Refrigerating Industry, vol. 14, 1956.
9. Leibenzon L. S. Collected Works. USSR Academy of Sciences' Press, 1955, vol. 3, pp. 215-274.
10. Kudryashev L. I., Belostotsky B. R. Journal of Applied Spectroscopy (Zhurnal prikladnoy spektroskopii), 1967, vol. 7, No. 5, p. 763.
11. Kudryashev L. I., Belostotsky B. R., Kudryasheva N. L. Journal of Applied Spectroscopy (Zhurnal prikladnoy spektroskopii), 1967, vol. 6, No. 5, p. 614.
12. Mitskevich N. S. ZhETF, 1954, vol. 26, No. 5, p. 557.
13. Kurosh A. G. A Course in Higher Algebra. "Nauka" Publishers, 1965.
14. Carslow H. S. and Jaeger J. C. Conduction of Heat in Solids. 2nd ed. Oxford, Clarendon Press, 1959.
15. Delvin G. E., McKenna J., May A. O., Schawlow A. L. Appl. Optics, 1962, vol. 1, No. 1, p. 11.
16. Tomiyasu K. Proc. IRE, 1962, vol. 50, p. 2488.
17. Soures J. M., Goldman L. M., Lubin M. J. Appl. Optics, 1973, vol. 12, No. 5, p. 927.
18. Kogelnic H. Appl. Optics, 1965, vol. 4, No. 12, p. 1562.
19. Casperson L., Yariv A. Appl. Physics, Letters, 1968, vol. 12, No. 10, p. 355.
20. Riedel E. P., Baldwin G. D. J. Appl. Phys., 1967, vol. 38, No. 7, p. 2720.
21. Boley, Bruno A. and Weiner, Jerome H. Theory of Thermal Stresses. New York-London, Wiley, 1960.
22. Nye J. F. Physical Properties of Crystals. Their Representation by Tensors and Matrices. Oxford, Claredon Press, 1, 1957.
23. Qwuelly F. W. Appl. Optics, 1966, vol. 5, No. 4, p. 633.
24. Dianov Ye. N., Prokhorov A. M. Reports of the USSR Academy of Sciences (DAN SSSR), 1970, vol. 192, No. 3, p. 531.
25. Snitzer E. Proc. IEEE, 1966, vol. 54, No. 10, p. 1249.
26. Foster J. D., Osternik L. M. J. Appl. Phys., 1970, vol. 41, No. 9, p. 3656.
27. Koechner W., Rice D. K. IEEE J. of Quantum Electronics, 1970, vol. 6, No. 9, p. 557.
28. Koechner W. Appl. Optics, 1970, vol. 9, No. 11, p. 2548.
29. Bubnov N. M., Buzhinsky I. M., Dianov Ye. N., Mamonov S. K., Mikhailova L. I., Prokhorov A. M. Reports of the USSR Academy of Sciences (DAN SSSR), 1972, vol. 205, No. 3, p. 556.
30. Courant R. A Course in Differential and Integral Calculus, vol. 2, "Nauka" Publishers, 1970.
31. Born M., Wolf E. The Fundamentals of Optics. "Nauka" Publishers, 1970.
32. Kogelnic H. Bell System. Techn. J., 1965, vol. 44, No. 3, p. 455.
33. Neumann F. E. Ann. Physik, 1841, vol. 54, p. 449.
34. Tien R. K. *et al.* IEEE, 1965, vol. 53, No. 8, p. 129.
35. Goncharenko A. M. Reports of the Belorussian Academy of Sciences (DAN BSSR), 1971, vol. XV, No. 1, p. 22, No. 7, p. 587.
36. Goncharenko A. M. Reports of the Belorussian Academy of Sciences (DAN BSSR), 1973, vol. XVI, No. 10, p. 807.
37. Afanasyev V. A. Optical Measurements (Opticheskie izmereniya). "Nedra" Publishers, 1968, Moscow.
38. Burnham D. C. Appl. Optics, 1970, vol. 9, No. 7, p. 1727.
39. Mak A. A., Soms L. N., Stepanov A. I. *et al.* Optics and Spectroscopy (Optika i spektroskopiya), 1971, vol. 30, No. 6, p. 1081.
40. Dmitriev V. G., Umansky B. M., Shkunov N. V. In the collected volume "Quantum Electronics" (Kvantovaya elektronika) ed. by Acad. N .G. Basov, 1971, No. 2, p. 80.
41. Baldwin G. D., Riedel E. P. J. Appl. Phys., 1967, vol. 38, No. 7, p. 2726.

42. Buzhinsky I. M., Dianov Ye. M., Mamonov S. K., Mikhailova L. I., Prokhorov A. M. Reports of the USSR Academy of Sciences (DAN SSSR), 1970, vol. 190, No. 3, p. 558.
43. Senatsky Yu. V. Development and Investigations of a High-Power Neodymium-Glass Laser for High-Temperature Plasma Generation (Sozdanie i issledovaniya moshchnogo lazera na neodimovom stekle dlya vysokotemperaturnogo nagreva plazmy). Resume of a dissertation. USSR Academy of Sciences' Institute of Physics, 1970.
44. Funkhouser A. T., Mielenz K. D. Appl. Optics, 1970, vol. 9, No. 5, p. 1215
45. Reynolds J. and de Wellis J. Holography, Voenizdat, 1970 (Russian translation).
46. Sonin A. S., Vasilevskaya A. S. Electro-Optic Crystals (Elektroopticheskie kristally). Atomizdat, 1971.
47. Kertes I., Kononkov Ye. A., Kryukov P. G., Senatsky Yu. V., Chekalin S. V. ZhETF, vol. 59, No. 10, p. 1115.
48. Welling H., Bickart C. J J. Opt. Soc. Am., 1966, vol. 56, No. 5, p. 611.
49. Dishington R. H., Hook W. R., Hilbert R. P. Proc. IEEE, 1967, vol. 55, p. 2038.
50. Chun M K., Bischoff J. T. IEEE J. of Quantum Electronics, 1971, vol. 7, No. 5, p. 200.
51. Swedish Patent No. 342.807.
52. Bubnov M. M., Buzhinsky I. M., Dianov Ye. M. *et al.* Reports of the USSR Academy of Sciences (DAN SSSR), 1972, vol. 205, No. 3, p. 556.
Bubnov M. M., Buzhinsky I. M., Dianov Ye. M. *et. al.* Quantum Electronics (Kvantovaya elektronika), 1973, No. 16, p. 113.
53. Bubnov M. M., Buzhinsky I. M., Dianov Ye. M. *et al.* Brief Reports on Physics (Kratkie soobshcheniya po fizike), 1971, No. 3, p. 7, USSR Academy of Sciences' Institute of Physics Press.
54. US Patent No. 3,699,472.
55. US Patent No. 3,660,779.
56. US Patent No. 3,629,723; US Patent No. 3,484,714. Snitzer E. Appl. Optics, 1966, vol. 5, No. 10, p. 1487.
57. Koechner W., Rice D. K. America, 1971, vol. 61, No. 6, p. 758.
US Patent No. 3,702,974.
58. Dianov Ye. M. In the collected volume "Brief Reports on Physics" (Kratkie soobshcheniya po fizike), 1971, No. 8. USSR Academy of Sciences' Institute of Physics Press, Minsk.
59. Roess D. J. Appl. Phys. 1966, vol. 37, No. 9, p. 3587. Voronko O. M., Kozlov N. A., Mak A. A., Malinin B. G., Stepanov A. I., Reports of the USSR Academy of Sciences (DAN SSSR), 1967, vol. 173, No. 3, p. 542.
60. Jego T. M. Appl. Optics, 1970, vol. 9, No. 1, p. 225.
61. US Patent No. 3,577,098.
62. US Patent No. 3,665,335.
63. Swain J. E., Kidder R. E., Pettipiece K., Rainer F., Baird E. D., Loth B. J. Appl. Phys, 1969, vol. 40, No. 10, p. 3973.
64. Lubin M. I., Fraas A. P. Scientific American, 1971, vol. 234, No. 6, p. 21.
65. McMahon J. M., Emmett J. L. Naval Research Lab., Preprint, May 11, 1971.
66. US Patent No. 3,609,584.
67. US Patent No. 3,662,823.
68. Lenguel B. A. Introduction to Laser Physics. Wiley & Sons, Inc., New York, London, Sydney, 1966.
69. Mikaelyan A. L., Ter-Mikaelyan M. L., Turkov Yu. G. Solid-State Lasers (Opticheskie generatory na tverdom tele). "Sovetskoe radio" Publishers, 1967.
70. Bokks Ye. Ye., Morgenstern Z. L., "Optics and Spectroscopy" (Optika i spektroskopiya), 1963, vol. 14, No. 5, p. 687.
71. Karapetyan G. O., Karris Ya. E., Lupter S. K. *et al.* Journal of Applied Spectroscopy (Zhurnal prikladnoy spektroskopii), 1964, vol. 1, No. 3, p. 193.

72. Tornton J. R., Fountain W. D. Flint G. W. *et al.* Appl. Optics, 1969, vol. 8, No. 6, p. 1087.
73. Mauer P. Appl. Optics, 1964, vol. 3, No. 3, p. 433.
74. Heard, Hary G. Laser Parameters Measurements Handbook, New York, 1968, Wiley Ser. in Pure and Appl. Optics.
75. Voronkov Ye. M., Grechushnikov B. N., Distler G. I. *et al* Optical Materials for Infrared Applications. "Nauka" Publishers, 1965.
76. Handbook for the Manufacture of Glass (Spravochnik po proizvodstvu stekla), GSI, Moscow, 1963.
77. Kolenko Ye. A. Thermo-Electric Cooling Devices (Termoelektricheskie okhlazhdayushchie pribory), USSR Academy of Sciences' Press, 1963.
78. Kutateladze S. S., Borishansky V. M. Heat Transfer Handbook (Spravochnik po teploperedache), Gosenergoizdat, 1959.
79. US Patent No. 3, 711, 790.
80. Mikheyev M. A. Principles of Heat Transfer (Osnovy teploperedachi), Gosenergoizdat, 1956.
81. Dulnev G. N., Semyashkin E. M. Heat Exchange in Radio and Electronic Equipment. "Energiya" Publishers, 1968.

INDEX

Absorbers, resonant, 79
  saturable optical, 84
Alignment of optical systems, 171
Aperture stops, 53

Beam coherence, 12
Beam spread, 12
Birefringence, 220
  investigation of, by the polarization method, 233

Centres, active, 11
Cooling, contact, 253
  convective, 257
Current source, rectifier, type, 193

Distortions of laser light, 235
  caused by birefringence, 245
  correction of, 235, 241
  of wavefront, 218

Efficiency, light-trapping, 27
Energy storage circuits for laser pumps, 188

Fabry-Perot cavity, 68
Fabry-Perot etalon, 68, 71
Faraday rotator, non-reciprocal, 112-117
Feedback in pulse control, 139
Flash tubes, 13
Flash tubes, trigger circuits for, 194
Fluorite, Soviet-made grades, 42-3

Garnet, yttrium-aluminium, 43
Glasses for lasers, classification, 47
  neodymium-doped, 39-42

Harmonic generation, 17

Interferometer, Mach-Zehnder, 229
  Michelson, 229
Isolators, optical, 115-19

Kerr cells, 90, 95-8

Laser adjustment, autocollimation method for, 176
  optical-lever method for, 177
Laser alignment, interference method, 178
Laser amplifiers, basic theory, 150
  controlled-cavity, 15, 16
  multi-pass, 15, 16, 157
  regenerative, 15, 16, 159
  single-pass, travelling-wave, 15, 16, 155
  switched-gain, 160
Laser beam, Gaussian, 223
Laser beam amplification, 15
Laser cavities, 54-72
  electro-optic control of, 132-40
  for oscillators, 65-8
  stable, 58-61
  unstable, 62-5
Laser components, optical distortions in, 211
Laser elements, thermal distortions in, 226
  measurement of, 226
Laser frequency control, 17
Laser light, distortions of, 235
  caused by birefringence, 245
Laser materials, effect of temperature on, 246
Laser oscillators, temperature stability of, 246, 250
Laser pumps, 13, 19-34
  classification of, 20
  with condencers, 18
  for cylindrical laser rods, 19
  for rectangular laser rods, 25
Laser systems, disc, 25
Lasers, distortions in, 200
  dye, 18
  electrical components of, 181
  instabilities of, 200
  physical basis of, 11
  pulsed, optical systems of, 120
  Raman, 18
  solid-state, 11
    materials for, 34
Lasing action control, 14
Lasing action threshold, 12
Liquid, cladding, 30
  immersion, 30

Michelson interferometer, 69
Mirrors, 43
  dielectric-coated, 43-5
  metal-coated, 43
Mode control, 13
Mode locking, 12
  in generation of picosecond pulses, 137
Mode selection, angular, 71
  axial, 68-70
  by CIR technique, 71
  in lasers electro optically Q-switched, 145

in lasers with phototropic shutters, 142
transverse
Mode selection systems, 141-49
Modes, axial, selection of, 68-70
cavity, 11
resonator, 11
transverse, selection of, 70-1

Optical elements, analysis of temperature fields in, 203
anisotropic, 209
heat exchange on the surface of, 202
thermal processes in, 200
Optical path length, change of, 220
Optical pumping, 11, 13
Optical pumping tubes, 181
Optical systems, alignment of, 171
Output coupling, diffraction, 63

Pockels effect, 90
Polarizers, 98-100
Population inversion, 11
effect of refractive index on, 212
for light amplification, 152
in solid-state lasers, 13
Prisms, 49
Archard-Taylor, 98-9
Arens, 98
Brewster-angled, 50
Glan-Foucault, 98
Nicol, 98
roof, 49
TIR, 52
Wollaston, 98
Pulse control by feedback, 139
Pulse generator, high-voltage, 198
Pulsed power supply, 191
Pulses, nanosecond, generation of, 126, 136
picosecond, generation of, 129
by mode locking, 137
Pump tubes, continuous, 181
flash, 186
Pumping energy distribution, 31

Q-spoiling, 12
Q-switches, 14, 74
Q-switching, 12, 15
fast, 132

Raman scattering, 13
stimulated (SRS), 17
Reflection, total internal (TIR), 105
Reflectors, electro-optic, 15, 107
controlled, 105-111
mirror, 32
resonant, 45
temperature distortion of, 109
Refractive index, dependence on population inversion, 212
dependence on temperature gradient, 214
Ruby, Soviet-made grades, 35-9

Second harmonic generation (SHG), 13, 17
optical systems for, 162-71
Shutters, alignment of, 100-02
bleachable, 14, 79-90
electrically exploded film, 15, 112-15, 140
electro-optic, 15, 90-105
mechanical construction of, 102-05
optical systems of, 102
optico-acoustical, 79
optico-mechanical, 72, 120
as Q-switches, 77
phototropic, 14, 79-90, 126
construction of, 88-90
Pockels, 90
spinning-mirror, 74
spinning-prism, 74
Switching, regenerative, 136
Synchronization, shutter and flash tube, 77

Temperature gradients, investigation by the polarizer method, 233
Trigger circuits for flash tubes, 233
Tubes, optical-pumping, 181

Wavefront distortion, 218

Printed in the Union of Soviet Socialist Republics